AN EVALUATION OF SEISMIC FLAT DILATOMETER AND LATERAL STRESS SEISMIC PIEZOCONE

by

Ivan Rivera Cruz

Civil Engineering, Instituto Politécnico Nacional, México, 2004

B.Sc., Instituto Politécnico Nacional, México, 2002

A THESIS SUBMITTED IN PARTIAL FULFILLMENT OF
THE REQUIREMENTS FOR THE DEGREE OF

MASTER OF APPLIED SCIENCE

in

THE FACULTY OF GRADUATE STUDIES
(Civil Engineering)

THE UNIVERSITY OF BRITISH COLUMBIA
(Vancouver)

January 2009

ABSTRACT

The flat dilatometer (DMT) and piezocone penetration (CPTU) tests are likely to be among the most widely used in situ testing methods for soil characterization and indirect determination of geotechnical design parameters such as: strength, stiffness, permeability and compressibility. The flat dilatometer has proved to be a reliable, robust and adaptable tool, and the data obtained with this instrument is very repeatable, and easy to reduce and process. Furthermore, the addition of a seismic module to the standard flat dilatometer (SDMT) to measure the shear wave velocity (V_s) significantly complements the set of data typically obtained with a standard DMT test. Nonetheless, the experience in interpreting the combination between V_s and DMT data is fairly limited due to the recent introduction of the SDMT for commercial applications. Additionally, the estimation of the coefficient of earth pressure at rest (K_0) has been the most important application of the DMT since its introduction. However, a potential weakness of the DMT is that the derivation of K_0 is based upon empirical correlations developed some time ago and neither improvement work nor upgrade of these approaches has been performed in the last 10 years.

Throughout the years several additional sensors have been developed in order to supplement the data collected with the CPTU test. Among the wide variety of sensor developed, the lateral stress module mounted behind a piezocone represents a promising tool for estimation of in situ lateral stress conditions from the interpretation of lateral stress penetration data. However, the popularity of the so called lateral stress cone has declined over the years due to constraints in both the instrumentation and the interpretation of measured data. Also, the application of this instrument remains limited to specific soils conditions and specific projects. However, the valuable experience gained throughout the years in the development and application of several lateral stress cones in combination with developments in electronics and understanding of soil behaviour allow the improvement of this type of technology.

This thesis presents the results of a comprehensive laboratory and field testing programs performed by the author at several research sites located in the Lower Mainland of BC, undertaken in order to assess the performance of the seismic flat dilatometer and lateral stress seismic piezocone (LSSCPTU), built and develop at UBC. Firstly, the analysis of field measurements with the SDMT collected at several sites have demonstrated the potential for an improved soil characterization through the combination of DMT parameters and the small strain shear modulus (G_0). Additionally the usefulness of the DMT-C closing pressure for soil identification is shown. On the basis of several relationships identified from this data, a new soil type behaviour system based upon SDMT measurements is proposed. Furthermore, empirical correlations based upon fairly large and updated databases have been developed to estimate K_0 and V_s values from DMT parameters.

On the other hand, results of laboratory calibrations and field tests have demonstrated a good performance of the LSSCPTU. It was also found that the configuration of this instrument is less sensitive to temperature and cross-talk effects due to axial loading than previous designs of lateral stress modules. The good performance of the design and instrumentation of the new lateral stress module represents a substantial contribution to the development of this type and technology. Also, penetration and dissipation data recorded in fine grained soils, with the LSSCPTU, clearly show that the change in effective lateral stresses induced by a full displacement probe is a function of soil type and probe geometry.

TABLE OF CONTENTS

LIST OF TABLES

LIST OF FIGURES

LIST OF SYMBOLS

A	DMT pressure required to just move the membrane against the soil ("lift-off" pressure)
A_{LS}	Amplification factor, $A_{LS} = \sigma_{LS}' / \sigma_{h0}'$
a	DMT constant for a particular clay
a_n	Piezocone net area ratio
B	DMT pressure required to move the centre of the DMT membrane 1.1 mm against the soil
B_q	Pore pressure parameter, $B_q = \Delta u/(q_t - \sigma_{v0})$
B_t	Temperature coefficient
b	DMT constant for a particular clay
β_k	DMT empirical factor (Mayne & Kulhawy, 1990)
C	DMT external pressure required to push back the membrane until contact with the blade is re-established
CC	Calibration chamber test
COV	Coefficient of variation
CPM	Cone-pressuremeter test
C_c	Virgin compression index
C_s	Swelling index
c_h	Horizontal coefficient of consolidation
D	Diameter of the cone
D_1, D_2, D_3	DMT empirical fitting parameters (Baldi et al., 1986)
D_r	Relative density
D_{50}	Grain size corresponding to 50% fine
DMT	Flat dilatometer test
ΔA	Required suction pressure to overcome the stiffness of the membrane in free air
ΔB	External pressure required to lift the centre of the membrane above its support
Δp	Increment in pressure

Δt	Delay of the arrival time of the impulse from the first to the second sensor
Δu	Excess pore-water pressure
$\Delta V/V$	Change in volume of the cavity
$\Delta\sigma_h$	Increase in total lateral stress
E	Young's modulus
E_D	Dilatometer modulus
ϵ	Cavity strain
ϵ_v	Vertical strain
ϵ_h	Horizontal strain
FS	Full scale
FVT	Field vane test
f_s	Friction sleeve resistance
ϕ'	Effective friction angle
ϕ_{ax}'	Angle of shearing resistance as determined by standard triaxial compression tests
G	Shear modulus
G_0	Small strain shear modulus
γ	Total unit weight of the soil
HF	Hydraulic fracture test
I_D	Material index
I_r	Rigidity index
J-FLSC	Japanese friction lateral stress cone
J-LSC	Japanese lateral stress cone
K	Earth pressure coefficient
K_c	Reconsolidation coefficient of lateral stress
K_D	Horizontal stress index
$K_{(NC)}$	Coefficient of lateral stress pressure measured under NC conditions

K_0	Coefficient of earth pressure at rest
$K_{(OC)}$	Coefficient of lateral stress pressure measured under overconsolidated conditions
k_h	Horizontal hydraulic conductivity
L_1, L_2	Slant distances between each receiver in the SDMT probe and the source beam
LI	Liquidity index
LSCPTU	Lateral stress piezocone
LSSCPTU	Lateral stress seismic piezocone
LSSCP	Lateral stress sensing cone
LSM	Lateral stress module
Λ	Plastic volumetric stress ratio
M_{DMT}	Constrained dilatometer modulus
m	DMT constant for a particular clay
μ	Coefficient of friction
N_{60}	N values corrected to a standard dynamic energy of 60% of the hammer potential energy (475 J)
n	Number of data points
ν	Poisson ratio
OCR	Overconsolidation ratio
PI	Plasticity index
p	Mean total stress
p’	Mean effective stress
p_0	Corrected DMT “lift-off” pressure
p_1	Corrected DMT expansion pressure
p_2	Corrected DMT closing pressure
q_c	Cone total tip resistance
$q_{c(NC)}$	Cone tip resistance measured under normally consolidated conditions

$q_{c(OC)}$	Cone tip resistance measured under overconsolidated conditions
q_D	Dilatometer tip resistance
q_t	Corrected total cone tip resistance, $q_t=q_c+u_2(1-a)$
R	Correlation coefficient
R^2	Square of the correlation coefficient
R_f	Friction ratio, $R_f = (f_s/q_t)\times 100$
r	Radius of the penetrometer at where total lateral stress measured
r_0	Cone radius
ρ	Bulk density of the soil
SBP	Self-boring pressuremeter
SCPTU	Seismic piezocone test
SD	Standard deviation
SE	Standard error
SDMT	Seismic flat dilatometer
S_t	Sensitivity
S_0	Settlement at the centre of a circular area
s_r	Stress relaxation gradient
s_u	Undrained shear strength
$s_{u(FVT)}$	Undrained shear strength from result of field vane tests
σ_c	Reconsolidated total lateral stress
σ_h	Horizontal total stress
σ_{h0}'	Effective horizontal geostatic stress
σ_n'	Normal effective stress
σ_v	Vertical total stress
σ_{vo}'	Effective vertical geostatic stress
σ_{LS}	Total lateral stress acting on the shaft of the penetrometer

$\sigma_{LS(m)}$	Total lateral stress uncorrected for cross talk effects
σ_{LS}'	Effective lateral stress acting on the shaft of the penetrometer
σ_{LS-f}'	Effective lateral stress acting on the shaft of the penetrometer after consolidation
σ_p'	Preconsolidation pressure
TSC	Total stress cell (also known as push-in spade cell)
U	Degree of dissipation (%)
U_D	Pore pressure index
u_0	In situ pore water pressure
u_1	Pore pressure measured on the face of the cone
u_2	Pore pressure measured behind the cone tip
u_3	Pore pressure measured behind the friction sleeve
u_{LS}	Pore pressure measured with lateral stress module
V_p	Compression wave
V_s	Shear wave velocity
w_{LL}	Liquid limit
w_N	Natural moisture content
w_P	Plastic limit
Z_M	Gauge zero offset (gauge reading when vented to atmospheric pressure)
z	Distance behind the cone tip
ζ	State parameter

ACKNOWLEDGMENTS

I wish to express my most sincere gratitude to my supervisor Dr. John Howie for his guidance, support and encouragement throughout the period of this research. I would also like to thank Scott Jackson and Harald Schremp for their suggestions, assistance and more important their time and patience during this research; their contribution to the design, instrumentation and repair expertise for the lateral stress seismic piezocone is gratefully acknowledge. Special thanks to Mark Styler for donating valuable time and effort to carry out the in situ testing program, where without his assistance this research would not have been possible.

I would like to thank ConeTec Investigations Ltd for their financial support and for unconditionally providing personnel and equipment to assist in performing the field testing program. Also, I am very grateful to David Woeller, Jim Greig, Jamie Sharp and Jeff Schaeffers for their trust and encouragement.

I would also like to thank Enrique Santoyo, Rene Contreras and Octavio Zaldivar from TGC Geotecnia S.A. de C.V., for providing access to DMT data collected in Mexico City. I also wish to express my gratitude to Armando Pantoja and Oscar Luna, at Comisión Federal de Electricidad, for their contribution to the data presented in this thesis. Similarly, I would like to thank Chris Hendry (Golder Associates), Mustapha Zergoun (Thurber Engineering) and Diego Marchetti for providing access to complementary DMT and SDMT data.

I would like to thank Pierre Choquet (RST Instruments) for his useful comments and suggestions. Also, special thanks to my colleagues and friends in the UBC geotechnical group; Pascale Rouse, Mavi Sanin and Anton Dabeet for their interesting discussion and constructive feedback. Finally, I would also like to thank Youngju for her total support and unconditional love during this process.

Con amor para mis padres, Elia y Oscar

El fruto de mi trabajo es una humilde muestra de agradecimiento a su apoyo, consejos, confianza, y sobre todo amor incondicional

Gracias

Chapter 1 INTRODUCTION

1.1 Purpose of study

Over the last few decades the popularity of in situ testing in geotechnical engineering has increased significantly. The soil response to in situ testing can be interpreted to indicate soil stratigraphy and to allow estimates of soil properties. The advantage of in situ testing over conventional drilling and sampling approaches is that the effects of sample disturbance on conventional laboratory testing are avoided (Eslami & Fellenius, 1997). However, Yu (2004) points out that in situ testing is generally an indirect technique since soil properties can only be obtained from measured responses to in situ tests by solving a boundary value problem.

The piezocone penetration test (CPTU) and flat dilatometer test (DMT) are nowadays among the most popular tools used in geotechnical practice for site characterization and estimation of geotechnical soil parameters. Additionally, several direct foundation design methods have been developed from correlation to CPTU and DMT parameters (e.g. Bustamante & Gianeselli, 1982; Eslami & Fellenius, 1997; Powell et al., 2001). Both tests offer the advantage of a continuous profile of measured parameters which allow interpretation of stratigraphy as well as estimates of geotechnical parameters such as (i) shear strength, (ii) stiffness, (iii) permeability and (iv) compressibility. With advances in instrumentation, additional sensors and modules have been incorporated into the CPTU to allow the additional parameters such as total lateral stress (σ_{LS}) during penetration and shear wave velocity (V_s) to be gathered in the same sounding. The importance of the in situ lateral stress in both site investigation and geotechnical analysis is well known and consequently much research has been determining its value from in situ measurements with a variety of tools. Indeed, Schmertmann (1985) argues that failure to measure and use the in situ lateral stress can easily result in conservative or uneconomical design.

Since its development in 1975 in Italy (Marchetti, 1975), the flat dilatometer has proved to be a very reliable, adaptable and robust tool for soil characterization and derivation of geotechnical design parameters but, it has not found as wide acceptance as the CPTU. Long (2008) points out that a possible weakness of the DMT is that derivation of geotechnical parameters is based on empirical correlations developed some time ago. Instead, most research on the DMT has been focused on a better understanding of the fundamental mechanics of the DMT by using theoretical and numerical approaches. Recently, however, there has been increased interest in the use of additional sensors such as geophones (Foti, et al., 2006; Bang, et al., 2008) and a resistivity module (Bang, et al, 2008) mounted above the DMT. The addition of shear wave velocity (V_s) measurements to the standard DMT provides an opportunity to improve on the existing DMT interpretation procedures, and the potential to identify unusual soil conditions such as sensitivity, ageing or cementation. The new tool is referred to as the Seismic DMT or SDMT. In addition, the small strain shear modulus, G_0, obtained from $G_0=\rho V_s^2$ where ρ is the bulk density is now recognized as an important parameter in geotechnical engineering. Recent attempts have been made to use combinations of CPTU tip resistance and G_0 to identify soil characteristics such as cementation and compressibility (Robertson, et al., 1995; Schnaid, et al., 2004).

The idea of mounting a lateral stress sensor behind the tip of the penetrometer was first introduced in the mid 1980's. Indeed, the development of cones capable of measuring lateral stress originated from the idea that the sleeve friction measured during penetration in sand should be related to the pre-penetration lateral stress (Robertson, 1982; Hughes & Robertson, 1984). Because of the shape of the cone, researchers have explored the interpretation of lateral stress cone data by cylindrical cavity expansion approaches in the search for a more fundamental method to estimate the in situ lateral stress from penetration measurements (Sully 1991; and Takesue & Isano 2001). Unfortunately, due to several problems with the instrumentation and the interpretation of measured data, the lateral stress cone has not found practical use yet and it remains constrained to research activities or application to special projects.

This thesis will investigate the performance of the SDMT and a new version of the UBC Lateral Stress Module in soils of the Lower Mainland soils as follows:

- Assess the capabilities of the SDMT at well-documented research sites in the Lower Mainland of B.C. This includes an attempt to identify relationships between DMT parameters and G_0 in order to develop an improved DMT soil behaviour type classification system.

- Describe developments undertaken to improve the quality of lateral stress measurements using the lateral stress piezocone developed at UBC and described by Sully (1991). This includes an assessment of the performance of the redesigned UBC lateral stress module (LSM-II) in the laboratory and in the field.

The thesis also explores the potential for improved site characterization using the additional information provided by the seismic flat dilatometer (SDMT). In order to achieve these objectives an extensive field testing program, using the SDMT has been performed by the author at several research sites located in the Lower Mainland of BC. Also, the corresponding SDMT database established has been complemented with additional SDMT and DMT data collected by others at sites located in western Canada, Mexico and Italy.

1.2 Thesis organization

Chapter 2 presents a comprehensive review of the seismic flat dilatometer (SDMT) and developments in lateral stress cone technology. The first section of this chapter provides a description of the SDMT in term of equipment description and the reduction of field measurements. This section is followed by a description of several empirical and semi-empirical approaches for estimation of in situ lateral stress conditions in clay and sand from DMT measurements. The second section presents a critical review of research performed throughout the years on the development of lateral stress cone technology. The theoretical framework for the development of instruments capable of measuring the lateral stress acting on the shaft of and advancing penetrometer is described. Then, the development of lateral stress measuring sensors over the years is described in chronological order.

Chapter 3 presents an overview of the geology of the Fraser River Delta and the Serpentine River lowland. Additionally, a complete description of research sites is presented. This includes the location of the test site and a detailed soil stratigraphy based upon data from several in situ test methods as well as results of laboratory tests performed on relatively undisturbed and disturbed soil samples.

Chapter 4 presents an assessment of the seismic dilatometer (SDMT) and describes the results of several SDMT tests performed at research sites. The first section describes the performance in the field of the SDMT and the problems encountered when performing shear wave velocity (V_s) measurements. The profiles of shear wave velocities obtained from SDMT test are compared to results of other in situ techniques in common use and conclusions are drawn. The second section presents a detailed description, analysis and discussion of field measurements obtained with the seismic dilatometer (SDMT) at several research sites. Also, several relationships between DMT parameters and the small strain shear modulus (G_0) are identified and discussed. Then based upon these relationships and a thorough review of SDMT data collected at research and additional sites a new SDMT soil behaviour type chart is proposed. Additionally, based upon the identified relationships an empirical correlation to estimate the shear wave velocity (V_s) from DMT data is proposed. The last section presents the development and assessment of proposed empirical correlations to estimate the coefficient of earth pressure at rest, in fine and coarse grained soils. The rationale behind the development of each correlation is described and estimates from these new methods are discussed.

Chapter 5 presents a detailed description of the lateral stress module Model II (LSM-II) built and developed at UBC. Also, results of laboratory calibrations of the LSM-II are discussed and its performance is compared to that of similar designs of lateral stress modules reported in the literature. Also, the testing procedures adopted in this thesis for the execution of field tests with the lateral stress seismic piezocone are outlined. The next section presents the review of field measurements, recorded at one research site, aimed at assessing the performance of the instrumentation of the new design during penetration and in dissipation mode. Based upon a comprehensive review of laboratory and field measurements, minor drawbacks with the current design of the LSM-II were identified. The second section of this chapter describes the results of dissipation tests performed with the lateral stress seismic piezocone (LSSCPTU) in fine grained soils.

Chapter 6 presents a summary of major findings, conclusion and recommendations for further research.

Chapter 2 LITERATURE REVIEW

2.1 In situ testing using full displacement probes

2.1.1 Stress and pore pressure distribution around full-displacement probes

Sully (1991) presents a comprehensive review of stress and pore pressure distribution around full-displacement probes and their application for in situ measurement of lateral stresses. He argues that it is important to identify factors which affect the measured values with these methods so that a meaningful interpretation can be performed. Full displacement probes (e.g. total stress cell, piezocone, flat dilatometer) were developed to introduce repeatable degrees of disturbance; the problem then becomes one of relating the measured stress to the pre-penetration values as opposed to evaluating whether or not the soil had been disturbed as in the ideal case during installation of a self-boring pressuremeter (SBP). In the ideal case for undrained penetration, the penetration lateral stress, σ_{LS} measured by a full displacement probe results of two components:

$$\sigma_{LS} = \sigma_{h0} + \Delta\sigma_h \qquad \text{Equation 2.1}$$

where σ_{h0} is the in situ total lateral stress and $\Delta\sigma_h$ is the total stress increment due to insertion of the probe. In any particular soil, the magnitude of $\Delta\sigma_h$ caused by insertion is made up of both stress and pore pressure components and can be expected to be related to the displacement caused during penetration of a probe. Figure 2.1 shows the idealized change in the lateral stress coefficient (K) for various in situ testing probes. Sully (1991) points out that this simplified representation is instructive but complicated due to the fact that for each test method the stress/strain paths are very different and even under undrained conditions a single curve does not exist.

The insertion of a full displacement probe in clay gives rise to excess pore pressure (Δu) as the probe advances and the soil is displaced both vertically and horizontally. Cavity expansion methods indicate that the magnitude of Δu depends upon the location of the pore pressure measurement and upon soil parameters such as: shear modulus (G), in situ horizontal effective stress (σ_{h0}'), undrained shear strength (s_u), sensitivity (S_t) and overconsolidation ratio (OCR), etc. In terms of soil response to undrained loading, the excess pore pressure components close to the probe, i.e. within the plastic zone, are:

$$\Delta u = \Delta u_{oct} + \Delta u_s \qquad \text{Equation 2.2}$$

where Δu_{oct} is the excess pore pressure caused by changes in the octahedral normal stress and Δu_s is the excess pore pressure resulting from changes in the octahedral shear stress.

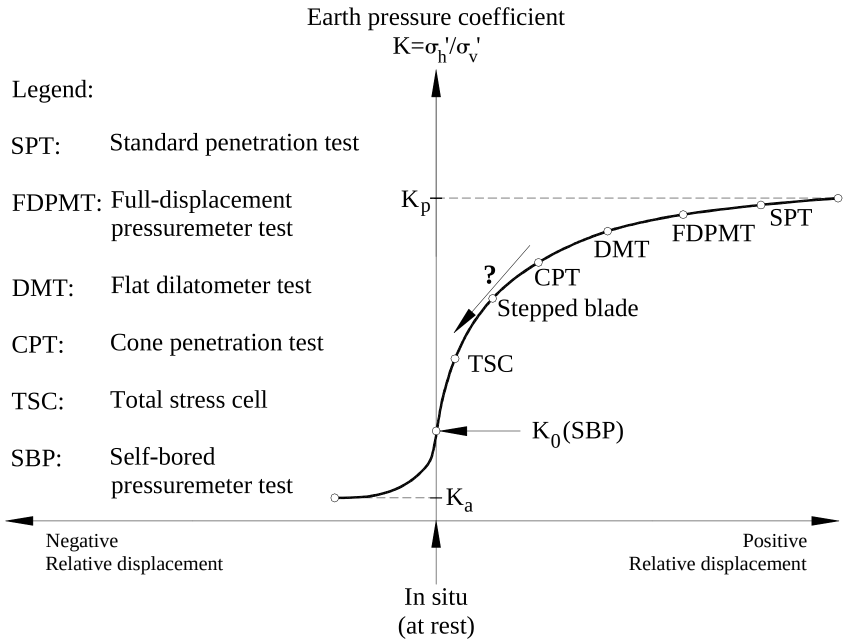

Figure 2.1 Idealized change of lateral stress coefficient (K) caused by full displacement probes (adapted from Sully 1991).

Under the cone tip, the largest effect on the magnitude of the pore-water pressure is created by changes in the mean normal stress. However, along the shaft of the penetrometer, the shear stresses induce a significant portion of the excess pore pressure because the octahedral normal stresses acting on the cone tip experience stress relief (Kim, et al., 2007). Cavity expansion methods consider both the octahedral and shear induced pore pressure components in an empirical manner (Vesic, 1972; Mayne & Chen 1994).

It has also been established that a gradient of pore pressure exists around a penetrating cone (Robertson et al., 1986) and that this gradient can be qualitatively related to changes in normal and shear stresses as the soil moves around the cone tip. Figure 2.2 suggests that measurement of the gradient around a penetrating cone should provide information related to the stress distribution during undrained penetration in clay. The data shown in this figure indicate that the soil is unloaded and intensively sheared as it passes the cone tip and that the effect of unloading is more pronounced as the stiffness of the soil increases.

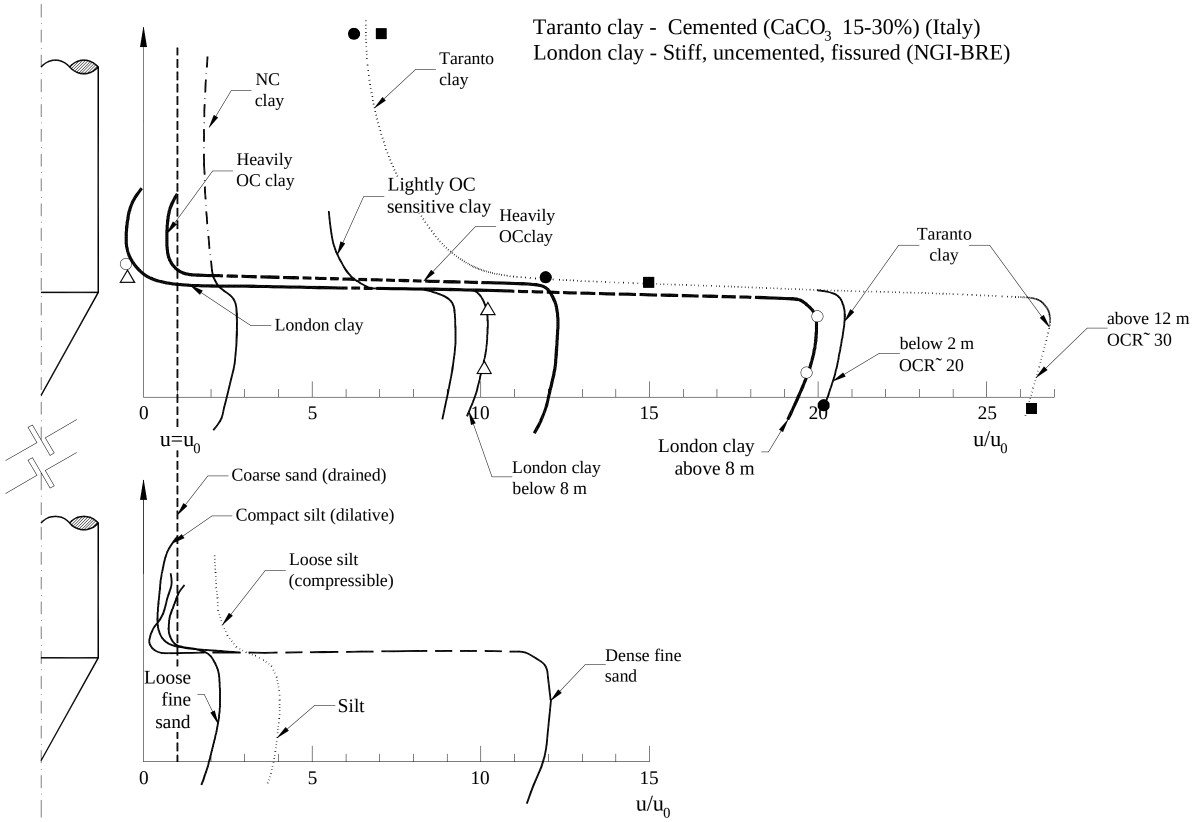

Figure 2.2 Conceptual pore pressure distribution in saturated soil during CPT based on field measurements (adapted from Robertson et al. 1986)

On the other hand, in clean sands the penetration process of full displacement probes can be considered as drained and therefore no large excess pore pressure are generated. Gillespie (1990) demonstrates that, irrespective of relative density (D_r), for σ_v' <200 kPa, the excess pore pressures behind the tip are zero or negative of static equilibrium from the rapid unloading that occurs due to the cone geometry in this region. Furthermore, pore pressures on the face of the cone are approximately equal to hydrostatic if filter compressibility effects do not occur. As a result, penetration pore pressures provide little information in terms of stress changes along the probe in coarse grained soils.

Campanella & Robertson (1981) and Hughes & Robertson (1984) examined the possible variation of lateral stress around a penetrating cone with respect to changes in measured sleeve friction (f_s). The results of CPT tests performed in sands indicate a marked increase in f_s between 10 cm and 25 cm behind the cone tip, whereas for larger distances (greater than 25 cm, or 7*D*, where *D* is the cone diameter), f_s is essentially constant. Hughes & Robertson (1984) suggested the existence of high stress gradients, similar to the pore pressure gradients for clays, as the cone tip approaches and passes a soil element. In other words, soil is unloaded but intensively sheared as it passes the tip of the penetrometer. This is reviewed further in section 2.4 of this chapter.

Marchetti (1979) suggests that the disturbance caused during flat plate penetration (i.e. flat dilatometer) is less than that associated with a cone, simply based on the lower apex angle at the tip (20° for the DMT as opposed to 60° for the CPT). Studies on the penetration of long wedges by Baligh (1975) confirm this observation. However, Sully (1991) points out that the model tests reported by Baligh (1975) are 2D in nature and are misleading since the 3D effect of cone penetration are not considered. He also argues that the generally available flat penetrometers cannot be considered as infinitely long and hence the deformation may lie somewhere between the 2D and 3D idealizations. Results of 3D strain path analysis performed by Huang (1989) demonstrate that the difference between the strain fields for cone and plate penetrometers are more than expected solely from apex angle variations. The results of this analysis also suggest that the stress behind the cone tip should be higher than that behind a DMT tip due to the larger disturbance caused by insertion of the probe. Sully (1991) concludes that several methods exist to evaluate the stress distribution around full displacement probes (e.g. cavity expansion, strain path). The validity of each approach depends upon both soil properties and probe geometry.

2.2 Seismic piezocone (SCPTU)

2.2.1 Equipment

The standard piezocone has a conical tip with a 60˚ apex angle, is 10 cm^2 in cross-section, has a 150 cm^2 friction sleeve and pore pressure can be measured during penetration at one or more locations on or near the cone tip. A seismic module containing an accelerometer is mounted just behind the piezocone unit. For the work described herein, the pore pressure was measured at the u_2 position just behind the shoulder of the cone and the u_3 position, just above the friction sleeve. The u_2 position is the optimum measurement location to allow correction of the measured value of tip resistance (q_c) for the effects of water pressure on unequal end areas of the cone tip using the expression:

$$q_t = q_c + u_2(1 - a_n) \qquad \text{Equation 2.3}$$

In Equation 2.3 a_n is the area ratio for the particular cone used. Campanella & Howie (2005) point out that this correction is especially significant in soft clays, where high-values of pore pressure (u_2) and low cone tip resistance (q_c) may lead to the physically incorrect situation of $u_2 > q_c$. In clean sand, where no excess pore pressure is generated, the pore pressures are relatively small to the cone tip resistance and hence the effect of pore water pressure correction on q_c is relatively small, i.e., $q_c \approx q_t$.

2.2.2 Testing procedure

The cone is pushed into the ground at a standard rate of 2 cm/sec and tip resistance, q_c, sleeve friction, f_s, and pore pressure, u_2, are recorded at typical intervals of 2.5 or 5 cm. At this standard rate of penetration, the soil response tends to be drained in sands, undrained in clays and clayey silts, and partially drained in soils of intermediate grain size. At selected depth intervals, the penetration is stopped and the rod string is unloaded. Seismic waves are generated at the surface using a sledge hammer to strike the end of a steel beam which is anchored using the stabilizers of the cone truck or drill rig as shown in Figure 2.3. The contact between steel hammer and steel pad triggers the data acquisition system, which records the horizontal particle motion that arrives at the seismometer in the seismic module. The signal is displayed against time since triggering on a computer screen. The same procedure is repeated by hitting the other end of the pad, which generates shear waves with inverse polarity and produces a mirror image response at the sensor as schematically shown in Figure 2.3.

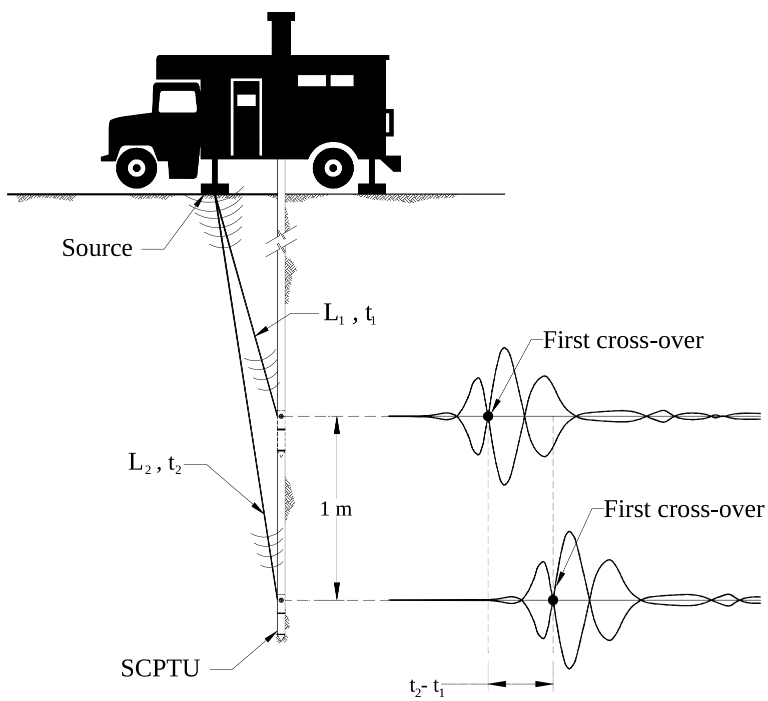

Figure 2.3 Seismic piezocone penetration test.

Two or more blows on each end of the pad are recorded to ensure repeatability of the signals. The cone is then advanced to the next depth interval and the procedure is repeated. Then, the average V_s over a given depth interval can be calculated by an interval technique using Equation 2.4.

$$V_s = \frac{(L_1 - L_2)}{(t_2 - t_1)} \quad \text{Equation 2.4}$$

L_2 and L_1 are the slant distances between the sensor in the cone and the source beam taking account of the offset between the vertical axis of the cone string and the source beam. The time interval, $\Delta t = (t_2 - t_1)$, is the difference between the arrival times of shear waves at two successive depths intervals. Since it is hard to accurately pick out the initial arrival of shear waves from the signals, different approaches have been developed for definition of the time interval.

The simplest approach, termed the cross-over method, uses the mirror image wave traces plotted over one another to identify a consistent reference time or time marker. The difference in arrival time of any time markers at two successive depth intervals can be used as Δt in Equation 2.4. Usually the first cross-over schematically illustrated in Figure 2.3 or the next peak is the selected time marker. A more elaborate approach uses cross-correlation of the signals by shifting one signal by small time steps relative to the other signal. At each shift the sum of the product of the signal amplitudes is calculated. The time shift corresponding to the maximum cross-correlation is taken as the Δt between the two depths. The entire signal or only a part of the signal may be used for the cross-correlation.

2.2.3 Estimation of soil stratigraphy from SCPTU data

The profiles of q_t, f_s and u_2 versus depth are interpreted to obtain soil stratigraphy and estimates of stress history and engineering parameters through empirical correlations or semi-empirical approaches. Prior to the interpretation and analysis of SCPTU data it is important to visually inspect the profiles of SCPTU field measurements, i.e. q_t, f_s and u_2, in order to identify trends and layer interfaces. Campanella & Howie (2005) provide useful guidelines for a qualitative assessment of profiles of SCPTU field data.

The soil behaviour type classification system (SBT) is a soil classification system based upon observed behaviour during penetration of the SCPTU rather than grain size or plasticity. Several soil classification or soil behaviour charts have been proposed by researchers throughout the years (e.g. Schmertmann 1978, Robertson et al., 1986; Robertson, 1990; Robertson et al., 1995; Schnaid, 2004; Schneider et al. 2008). Generally these charts use a combination of corrected piezocone tip resistance (q_t), sleeve friction (f_s) and pore water pressure (u_2) data or intermediate parameters such as friction ratio (R_f) or pore pressure parameter (B_q).

Mollé (2005) carried out a comprehensive review of the reliability of the CPT/CPTU based charts. He concluded that the Robertson et al. (1986) and Robertson (1990) charts yield reasonable to good results.

Long (2008) confirms the reliability of these charts for characterization of uniform soft to medium stiff clay and uniform sand deposits. Similarly, for intermediate soils such as silty clay or clayey silt and sandy silt, the Robertson et al. (1986) charts also work fairly well. However, Long (2008) argues that there seem to be difficulties with the use of these CPTU based charts for characterizing peat, organic clay and laminated soils. Figure 2.4 presents the CPTU based soil behaviour type charts proposed by Robertson et al. (1986).

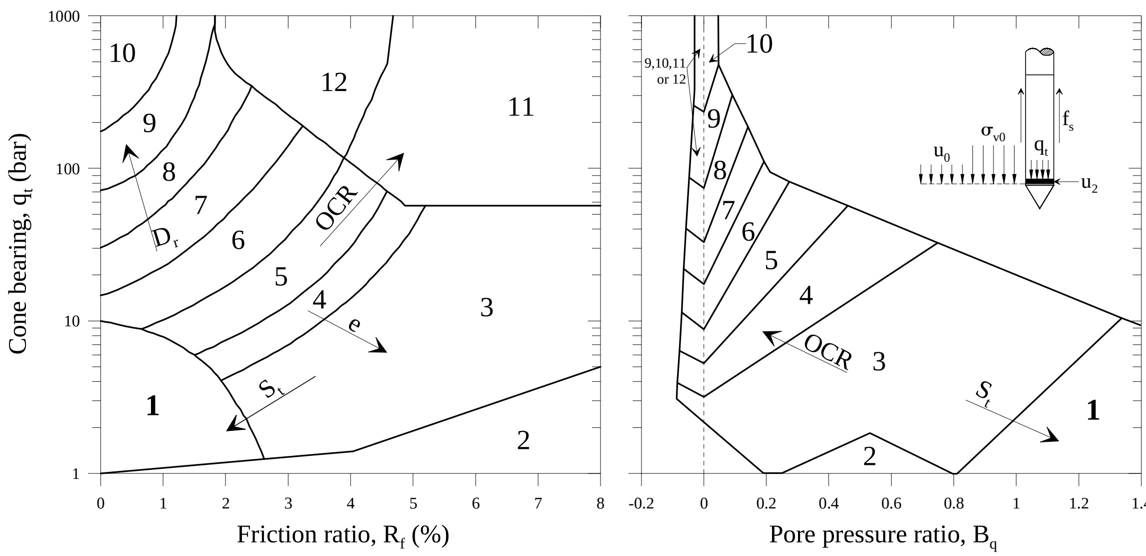

Zone	Soil behaviour type	Zone	Soil behaviour type
1	Sensitive fine grained	7	Silty sand to sandy silt
2	Organic material	8	Sand to silty sand
3	Clay	9	Sand
4	Silty clay to clay	10	Gravelly sand to sand
5	Clayey silt to silty clay	11	Very stiff fine grained*
6	Sandy silt to clayey silt	12	Sand to clayey sand*

$$R_f = \left(\frac{f_s}{q_t}\right) \times 100$$

$$B_q = \frac{u_2 - u_0}{q_t - \sigma_{v0}}$$

*Overconsolidated or cemented

Figure 2.4 Soil behaviour type classification system from CPTU data (adapted from Robertson et al., 1986).

Additionally, there has been a considerable increase in interest in using V_s in combination with parameters such as q_t from the SCPTU to identify unusual soil conditions such as: highly compressible sands, cemented or aged soils and clays with either high or low void ratio (Robertson, et al., 1995; Schnaid et al. 2004). More recently, Schneider et al. (2008) proposed new soil type classification charts based on normalized CPTU data. These charts were developed from a combination of large strain finite element analyses of undrained cone penetration and cavity expansion modelling of pore pressure generation. The proposed charts have been used successfully but only by the authors themselves.

2.3 Seismic flat dilatometer (SDMT)

2.3.1 Introduction

The flat dilatometer (DMT) is a site investigation tool commonly used in practice to obtain geotechnical design parameters. After the standard penetration (SPT) and piezocone penetration (CPTU) tests, the DMT test is perhaps the third most widely used in situ test method for soil characterization and determination of soil parameters (Long, 2008). The DMT was introduced as a new in situ test method to investigate the values of soil modulus for the design of laterally loaded piles (Marchetti, 1975). Marchetti (1980) described the application of the flat dilatometer for in situ investigation of soil properties.

He also presented a series of empirical correlations between DMT measurements and several geotechnical soil parameters such as: (i) coefficient of earth pressure at rest, K_0, (ii) overconsolidation ratio, OCR, (iii) undrained shear strength, s_u, and (iv) constrained dilatometer modulus, M_{DMT}. These were developed mainly for Italian soils. Marchetti (2006) describes the evolution of the DMT from its original concept, manufactured in 1974 by S. Marchetti at L'Aquila University in Italy, to the current version which has been used in its present format since 1980.

2.3.2 Equipment description

2.3.2.1 Standard flat dilatometer

The current design consists of a streamlined stainless steel blade 15 mm thick, 95 mm wide by 240 mm in length, and a curved cutting edge with an apex angle between 24° and 32°. A flexible and expandable circular thin stainless steel membrane 60 mm in diameter is mounted flush on one face of the blade (see Figure 2.5).

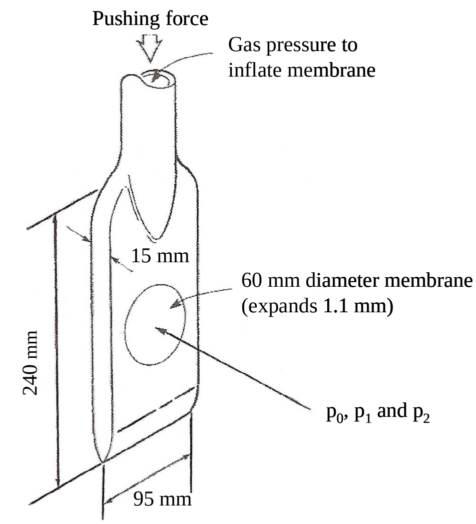

Figure 2.5 Geometry of the flat dilatometer (adapted from Powell et al., 1988a).

The DMT blade is connected to a control unit located at ground surface by a pneumatic tube, pre-threaded through the steel push rods. A wire conductor is contained within the gas line. The plastic tube allows passage of gas pressure and wire threaded through the plastic tube provides electrical continuity from the control unit. This unit is equipped with high and low pressure gauges, a buzzer and vent valves. A gas tank connected to the control unit supplies the gas pressure required to expand the membrane. The working principle of the DMT is illustrated in Figure 2.6.

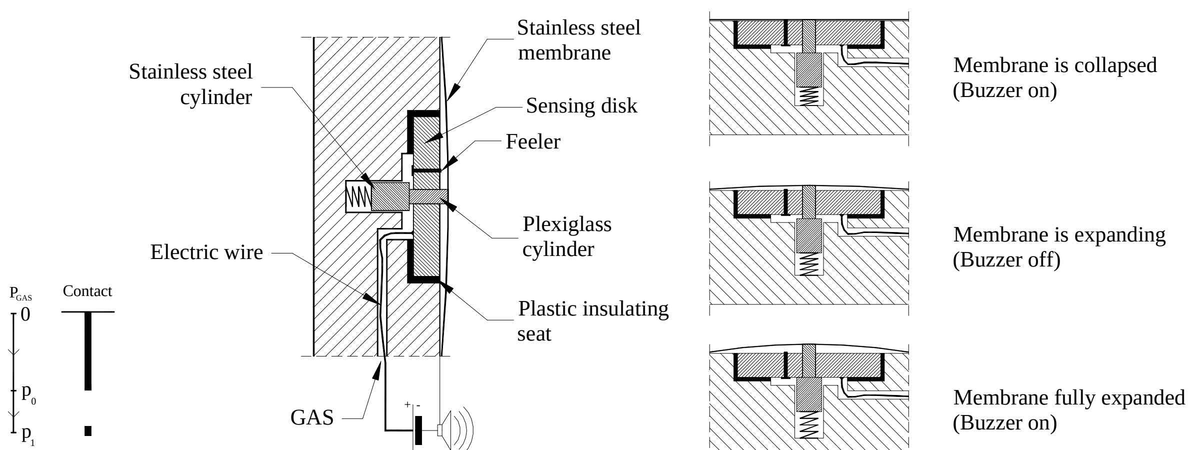

Figure 2.6 Working principle of DMT (adapted from Marchetti et al., 2001).

The insulating seat avoids electrical contact between the sensing disc and the underlying steel body of the blade. Since the sensing disc is grounded, the control unit emits an audio/visual signal when the membrane is in contact with the sensing disc and when the spring loaded stainless steel cylinder makes contact with the sensing disc when the centre of the membrane has moved 1.1 mm into the soil.

The blade is pushed into the ground at a constant rate of 2 cm/s using a hydraulic ram. At each test level (generally 20 to 30 cm depth intervals) penetration is halted and regulated gas pressure is applied to displace the membrane into the soil.

The basic DMT test consists of recording two pressures (A and B readings) with an optional third pressure known as the C-reading. The A-reading corresponds to the pressure required to overcome the soil resistance and move the membrane into the surrounding soil. At this stage of the test, the membrane is flush with the blade. Expansion continues until the centre of the membrane has moved 1.1 mm against the soil. At this point, the stainless steel cylinder makes contact with the sensing disk, completes the circuit and the sound starts again (B-reading). Immediately after B is reached the membrane is deflated and the sound stops. The C-reading is taken by slowly deflating the membrane immediately after B is reached. The membrane is pushed back by the external pressure until contact with the blade is re-established , i.e. flush with the blade, and the C-reading is recorded when the sound starts again.

2.3.2.2 Performing the test

The blade is pushed into the ground at a constant rate of 2 cm/s using a hydraulic ram. At each test level (generally 20 to 30 cm depth intervals) penetration is halted and regulated gas pressure is applied to displace the membrane into the soil. The basic DMT test consists of recording two pressures (A and B readings). The C-reading is not in widespread use but can also be recorded at each depth. The DMT is then pushed to the next test depth.

2.3.2.3 Data processing

Prior to interpretation, all field readings, i.e. A, B and C pressures, must be corrected to obtain the corrected pressures p_0, p_1 and p_2. The correction is applied to account for the effect of membrane stiffness (ΔA and ΔB), and the gauge pressure deviation from zero (Z_M) when vented to atmospheric pressure. The following expressions are used (Marchetti, 1980):

$$p_0 = A - Z_M + \Delta A \qquad \text{Equation 2.5}$$

$$p_1 = B - Z_M - \Delta B \qquad \text{Equation 2.6}$$

$$p_2 = C - Z_M + \Delta A \qquad \text{Equation 2.7}$$

Z_M is the gauge pressure deviation from zero when vented to atmospheric pressure, ΔA is the required suction pressure to overcome the stiffness of the membrane in free air, i.e. atmospheric pressure, and bring it in contact with the sensing disc (0.05<ΔA<0.30 bar), and ΔB is the external pressure required to lift the centre of the membrane above its support and move it outwards 1.1 mm against only the atmospheric pressure (0.05<ΔB<0.80 bar). The corrected A-pressure, is the gas pressure required to move the centre of the membrane horizontally 0.05 mm into the soil (p_0). Schmertmann (1988) suggested extrapolating p_0 to zero displacement to find the soil pressure against the membrane before the start of expansion. This extrapolation assumes a linear stress-strain soil response during the test up to the corrected B-pressure, p_1. Thus the extrapolated p_0 pressure at zero displacement is given by

$$p_0 = 1.05(A - Z_M + \Delta A) - 0.05(B - Z_M - \Delta B) \qquad \text{Equation 2.8}$$

Schmertmann (1988) argued that research by Campanella et al. (1985) using a specially instrumented DMT blade confirmed that, for the low strain involved, the assumption of linear extrapolation is accurate. It is evident that the pressure at zero displacement computed with Equation 2.8 results in lower pressure values, since the expansion curve in reality is nonlinear. Sully (1991) points out that while the curve between p_0 and p_1 may closely approximate a linear response, it is not probably the case for the initial pressure increase from 0 to 0.05 mm displacement but also argues that the effect may not be important due to the fact that interpretation of soil parameters from DMT data is based on empirical correlations. Equation 2.8 is now the standard approach to determination of p_0.

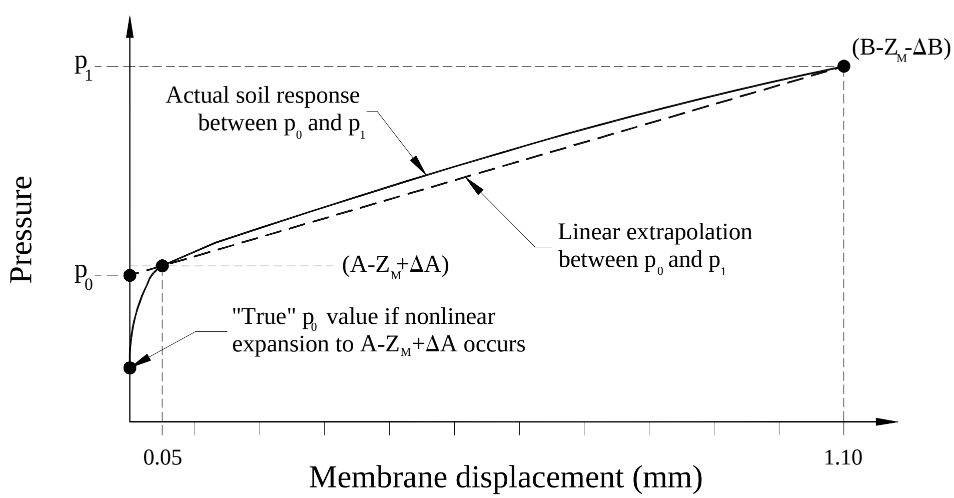

Figure 2.7 Linear extrapolation to estimate pressure p_0 at zero displacement (adapted from Sully, 1991).

2.3.2.4 Seismic DMT

The seismic flat dilatometer (SDMT) is a combination of the standard flat dilatometer (DMT) equipment with a seismic module for used for downhole measurement of the shear wave velocity (V_s). The test is conceptually similar to the seismic cone introduced by Campanella & Robertson (1984). The SDMT was first introduced by Hepton (1988), and significant improvements to the equipment were made at Georgia Tech as described by Martin & Mayne (1997, 1998) and Mayne et al. (1999). The current design of the seismic probe consists of a cylindrical element placed above the DMT blade with two built-in receivers separated by 0.5 m and so allows determination of V_s by a true interval technique. Foti et al. (2006) argues that the true-interval test configuration with two receivers avoids the possible inaccuracy in the determination of the zero time at the hammer impact that sometimes is observed in the pseudo-interval one-receiver configuration.

The data acquisition system can be triggered automatically when the hammer blow is sensed at the upper geophone or externally by contact between the hammer and the beam. A third option called immediate triggerring is only used to check the equipment and the system is automatically triggered from the computer. A detailed description of these options can be found in the SDMT software manual provided by the manufacturer (Studio Prof. Marchetti). The signal is amplified and digitized at depth before transmission to the surface, and it is automatically processed with the software provided by the manufacturer (SDMT Elab). The shear wave velocity (V_s) is displayed on the computer screen immediately upon data acquisition. The average shear wave velocity over a 0.50 m depth interval can be calculated by an interval technique using the following expression:

$$V_s = \frac{(L_1 - L_2)}{(t_2 - t_1)} \qquad \text{Equation 2.9}$$

where L_2 and L_1 are the slant distances between each receiver in the probe and the source beam taking account of the offset between the vertical axis of the DMT and the source beam. The time interval, $\Delta t = (t_2 - t_1)$, is the delay of the arrival time of the impulse from the first to the second sensor. The time interval (Δt), is computed by an interpretation algorithm developed by the manufacturer. A schematic arrangement of the system is shown in Figure 2.8.

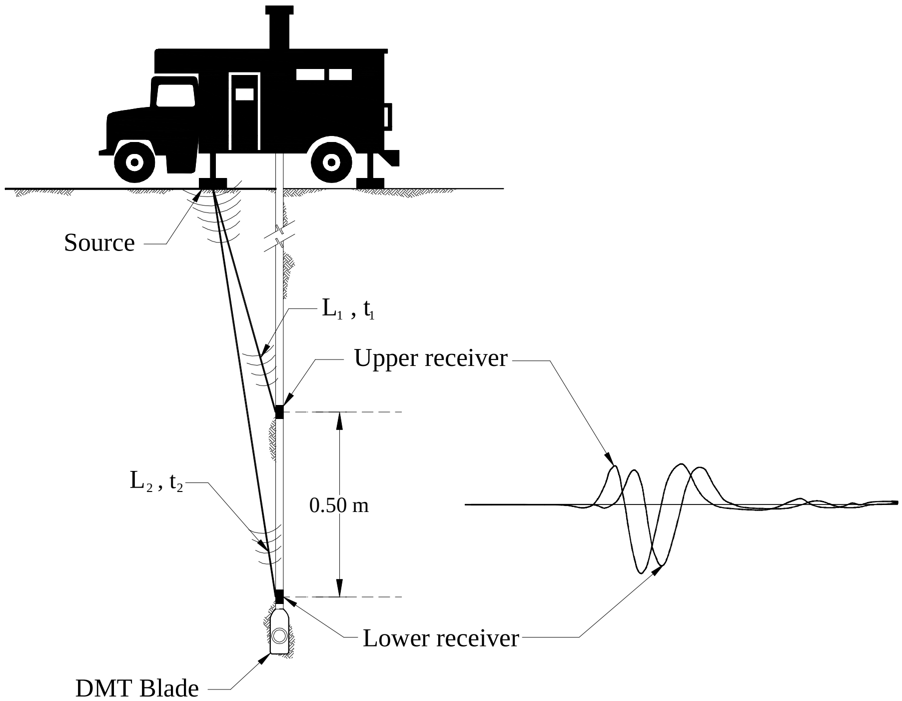

Figure 2.8 Seismic flat dilatometer test.

2.3.3 Interpretation of SDMT data

Marchetti (1980) used the measured p_0 and p_1 to derive intermediate DMT parameters which he then used as indicators of soil behaviour type and of engineering properties. Since Marchetti's initial publications, various investigators have suggested additional parameters and procedures designed to improve the capabilities of the DMT. (e.g. Schmertmann 1988, Lacasse & Lunne 1988, Mayne & Kulhawy 1990, Marchettti, et al. 2001). In fact, since its introduction in 1980 two international conferences have been devoted to dilatometer testing in the intervening 3 decades (Edmonton 1983 and Washington 2006) and substantial contributions, in terms of equipment development and data interpretation, have been published in several journals as well as national and international conferences.

The corrected pressures p_0, p_1 and $p_{2,}$ are combined to calculate the intermediate DMT parameters: (i) material Index (I_D), (ii) horizontal stress index (K_D), (iii) dilatometer modulus (E_D), and (iv) pore pressure index (U_D) (Lutenegger & Kabir, 1988) using the following expressions:

$$I_D = \frac{(p_1 - p_0)}{(p_0 - u_0)} \qquad \text{Equation 2.10}$$

$$K_D = \frac{(p_0 - u_0)}{\sigma_{vo}'} \qquad \text{Equation 2.11}$$

$$E_D = 34.7(p_1 - p_0) \qquad \text{Equation 2.12}$$

$$U_D = \frac{(p_2 - u_0)}{(p_0 - u_0)} \qquad \text{Equation 2.13}$$

in which u_o is the estimated equilibrium pore water pressure, and σ_{vo}' is the estimated effective vertical stress.

2.3.3.1 Estimation of soil type

I_D and U_D can assist in identification of soil type. Marchetti (1980) suggested that the soil type can be identified as a function of the material index (I_D) as summarized in Table 2.1. Marchetti et al. (2001) point out that I_D tends to indicate silt as clay and vice versa, and a mixture of clay and sand will generally be described as silt. They also argue that the pore pressure index (U_D) seems to be a parameter that can be interpreted to detect the difference between those soils. For instance, Marchetti et al. (2001) suggested a value of $U_D \approx 0$ for permeable soils (sands), U_D=0.7 for impermeable layers (clays) and U_D between 0 and 0.7 for soils within the silts region ($0.6<I_D<1.8$).

Table 2.1 Soil behaviour type based on I_D (Marchetti, 1980)

Soil Type	Material Index (I_D)
Peat or sensitive clays	$I_D<0.1$
Clay	$0.1<I_D<0.35$
Silty clay	$0.35<I_D<0.6$
Clayey silt	$0.6<I_D<0.9$
Silt	$0.9<I_D<1.2$
Sandy silt	$1.2<I_D<1.8$
Silty sand	$1.8<I_D<3.3$
Sand	$I_D>3.3$

2.3.3.2 Interpretation of soil state and engineering properties

The flat dilatometer can also be used to estimate geotechnical parameters such as: undrained shear strength, s_u, overconsolidation ratio, OCR, and coefficient of earth pressure at rest, K_0. Mayne & Martin (1998) present a comprehensive review of several comparative studies, modified relationships, and new DMT correlations for estimation of several geotechnical parameters. The paper of Mayne & Martin (1998) is widely recommended as an excellent reference document. Alternatively, the report by Marchetti et al. (2001) on the DMT provides general guidelines on the interpretation and derivation of DMT data using the original correlations proposed by Marchetti (1980).

The horizontal stress index K_D, is empirically related to the coefficient of earth pressure at rest (K_0) and it is also used in the estimation of the overconsolidation ratio (OCR) and the undrained shear strength (s_u). In normally consolidated (NC) clays without ageing, structure or cementation, K_D will be in the range of 1.8 to 2.3. Higher values of K_D suggest higher overconsolidation in fine grained soils.

The dilatometer modulus E_D is used to determine the constrained modulus M_{DMT}, which is the vertical drained confined (one-dimensional) tangent modulus at σ_{v0}'. This modulus is the inverse of the coefficient of volume change (m_v), which is used to estimate the one-dimensional deformation due to consolidation settlement. M_{DMT} is calculated by applying to E_D the correction factor R_M, which is a function of the material index (I_D) and horizontal stress index (K_D). Marchetti et al. (2001) point out that R_M varies mostly in the range of 1 to 3. The use of I_D and K_D to determine R_M recognises the influence of soil type and stress level on M_{DMT} and the use of E_D recognises the different stress-strain characteristics of different soils (McPherson, 1985).

Finally, the pore pressure index parameter, U_D, provides insight into the drainage conditions of the soil. For free-draining layers, such as clean sands, the DMT test is performed under perfectly drained conditions and the excess pore pressure (Δu) is practically zero throughout the test. Hence, $p_2 \approx u_0$. However, in layers that are not free-draining, i.e. clays, the test is undrained. The excess pore pressure generated during DMT insertion will partially dissipate before membrane expansion begins. Additional excess pore pressures will be generated during membrane expansion and contraction resulting in excess Δu when the C-reading is taken, and consequently, $p_2>u_0$.

2.3.4 Estimation of in situ lateral stresses from SDMT measurements

The flat dilatometer has been widely used to estimate the coefficient of earth pressure at rest (K_0), though estimates are based upon empirical correlations developed some time ago. Mayne & Martin (1998) point out that the original empirical correlations proposed by Marchetti (1980) have proved useful but that the statistical trends used for its development were derived from fairly limited databases with information mainly on Italian soils. Several researchers have assessed the validity of the original correlations of Marchetti in different soils and have proposed new empirical approaches for estimation of K_0 from DMT data. This section provides the reader with a summary of the most common empirical and semi-empirical approaches for estimation of K_0 from DMT data. The description of these approaches has been divided into interpretation of DMT data in clays and sands.

2.3.4.1 Interpretation of lateral stress in clay

2.3.4.1.1 Empirical approaches

The first DMT correlation for estimation of the coefficient of earth pressure (K_0) was proposed by Marchetti (1980). The horizontal stress index K_D is related to K_0 through the empirical correlation given by

$$K_0 = \left(\frac{K_D}{1.5}\right)^{0.47} - 0.6 \qquad \text{Equation 2.14}$$

The basis for this correlation was a direct comparison between pairs of values of K_D and K_0 from experimental results from nine clay sites in Italy, and two sand sites in Italy and Saudi Arabia. K_0 values in clays were empirically obtained from the overconsolidation ratio (OCR) and the plasticity index (PI) using the empirical correlation suggested by Brooker & Ireland (1965). Additionally, results of calibration chamber (CC) tests on sands were used as reference values. Since reference K_0 values were not measured directly in the field, the reference values may not represent the true in situ lateral stress state. This correlation is based mainly upon experimental data on uncemented, insensitive soils that have not experienced aging, thixotropic hardening or cementation. Marchetti (1980) concludes that Equation 2.14 can be used for quantitative estimates of K_0 in soils within the limitations above mentioned.

Throughout the years several researchers (e.g. Lacasse & Lunne 1988; Powell & Uglow 1988a, 1988b; Lunne et al. 1990; Mayne & Kulhawy 1990) have assessed the validity of Marchetti's correlation and have proposed slightly modified versions of Equation 2.14 based on empirical or semi-empirical reasoning (see Figure 2.9 to Figure 2.11). In all cases, the relationships take the same general format

$$K_0 = aK_D{}^m + b \qquad \text{Equation 2.15}$$

Table 2.2 summarizes the a, b and m parameters for these studies. However, Marchetti et al. (2001) argue that the original K_D-K_0 correlation (Equation 2.14) gives reasonable estimates of K_0, especially considering the inherent difficulty of precisely measuring this parameter and that, in many applications, even an approximate estimate of K_0 may be sufficient.

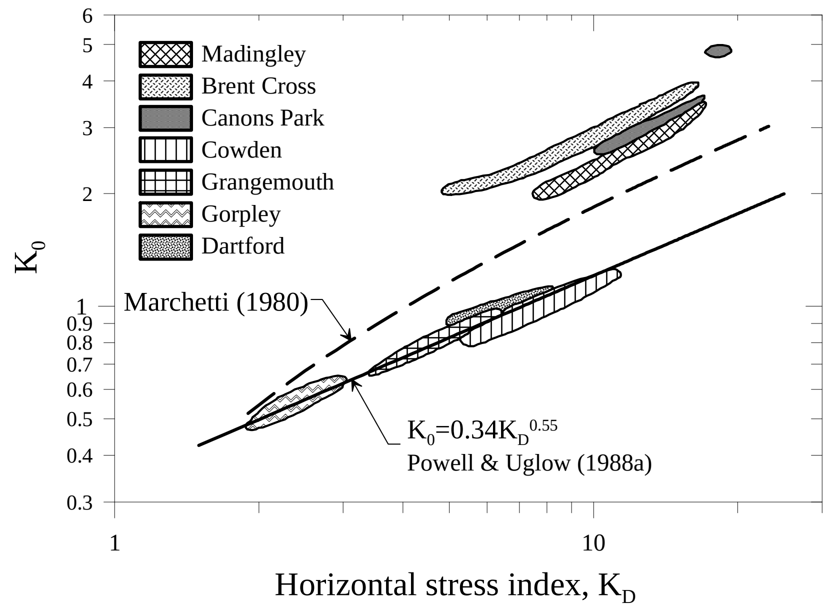

Figure 2.9 Relationship between K_D and K_0 for old U.K. clays (adapted from Powell & Uglow, 1988a).

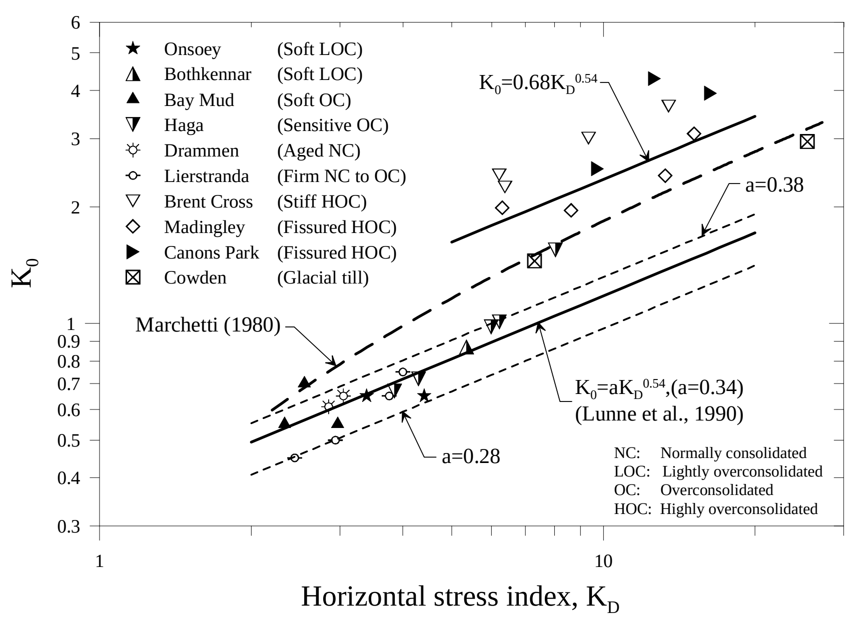

Figure 2.10 Relationships between K_D and K_0 for “young” and “old” clays

(adapted from Lunne et al. 1990).

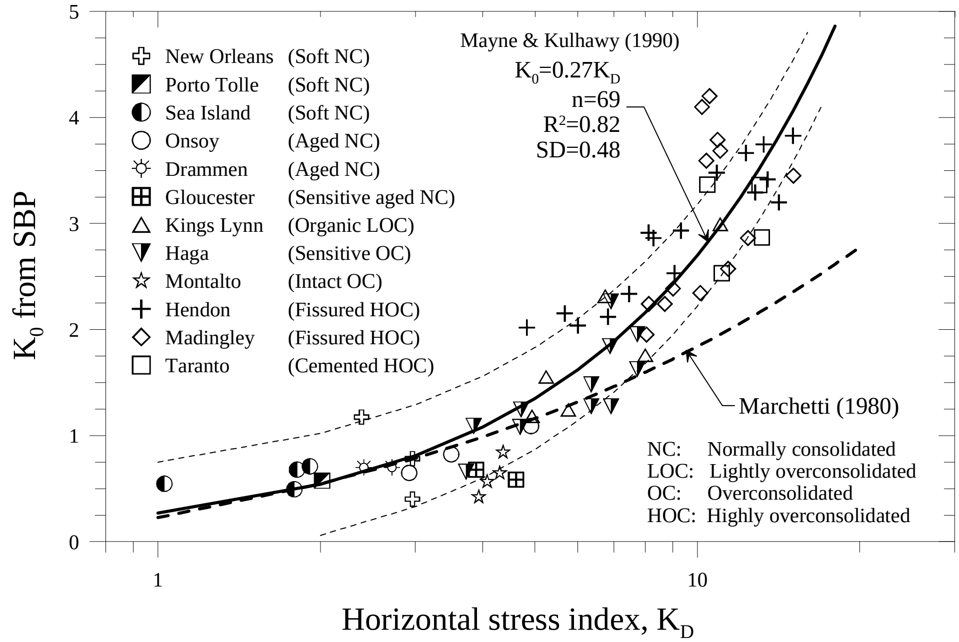

Figure 2.11 Empirical relationship between K_D and K_0 (adapted from Mayne & Kulhawy, 1990).

Table 2.2 Summary of empirical and semi empirical approaches to estimate K_0 from K_D in clay

Reference	a	m	b	Notes
Marchetti (1980)	0.8	0.47	-0.6	K_0 reference values derived from the empirical correlation of Brooker & Ireland (1965)
Lacasse & Lunne (1988)	0.34	0.44 to 0.64	N/A	K_0 reference values derived from TSC, HF, SBP and FVT m=0.44 high plasticity clays m=0.64 low plasticity clays
Powell & Uglow (1988a, 1988b)	0.34	0.55	N/A	for "young" U.K. clays, less than 70 000 years old
Mayne & Kulhawy (1990)	0.27	1	N/A	Statistical relationship based upon SBP data collected in Europe and North America
	$\frac{1}{(\beta_k)^{0.47}}$	0.47	-0.6	Fissured clay - $\beta_k = 0.9$ Insensitive clay - $\beta_k = 1.5$ Sensitive clay - $\beta_k = 2$ Glacial till - $\beta_k = 3$
Lunne et al. (1990)	0.34 to 0.68	0.54	N/A	"young" clay - a=0.34 $s_u/\sigma_{vo}'<0.7$ "old" clay - a=0.68 $s_u/\sigma_{vo}'>0.7$
Sully (1991)	0.34	0.55	$\left[\left(\frac{15-PI}{PI}\right)\left(\frac{0.5s_u}{\sigma_{vo}'}\right)_{DMT}\right]$	s_u values determined from DMT correlations
Semi empirical method				
Mayne & Kulhawy (1990)	$K_0 = (1-\sin\phi')\left[\frac{2K_D}{\sin\phi'(\ln I_r + 1)}\right]^{\frac{\sin\phi'}{\Lambda}}$			Λ=1-(C_s/C_c) is plastic volumetric strain ratio C_s, C_c = swelling and compression indexes I_r= rigidity index ($I_r=G/s_u$) $\Lambda \approx 0.8$ for low to medium sensitivity clays $\Lambda \approx 0.9$ for highly structured or cemented clays

HOC =	Highly overconsolidated	HF =	Hydraulic fracture test	ϕ'=	Effective peak friction angle
PI =	Plasticity Index	FVT =	Field vane tests		
SBP =	Self-boring pressuremeter	σ_{vo}'=	Effective vertical stress		
TSC =	Total stress cell	s_u=	Undrained shear strength		

2.3.4.1.2 DMT dissipation tests

It has been argued that it is also possible to carry out pore pressure dissipation tests with the DMT, in low permeability soils, i.e. clays and silts. The excess pore pressure generated by the blade insertion dissipates over a longer period of time than that of a standard DMT test, which is approximately 1 minute. The results and interpretation of a DMT dissipation test are aimed at estimating the magnitude of the in situ coefficient of consolidation (c_h) and hydraulic conductivity (k_h) of a soil deposit in the horizontal plane. Overall, the test consists of stopping the blade at a specific depth, then monitoring over time the decay of the contact total horizontal stress acting on the membrane. Upon achieving the desired test depth and depending upon the test method, either the decay of the A-reading or "lift off" pressure, or the C-reading is monitored over time until constant values are obtained. Also, the pressures A, B and C recorded in the field are corrected to account for the effect of membrane stiffness, and zero gauge offset when vented to atmospheric pressure.

The DMT-A method consists of taking a time sequence of A-readings avoiding the expansion required for the B-reading. Upon execution of the test the decay of the A-reading is plotted against the logarithm of time. Marchetti et al. (2001) recommend stopping the test once the curve has flattened sufficiently so that the contraflexure point is clearly identified. The time at this point is used for interpretation of the tests. On the contrary, the DMT-C method consists of performing, at different times, one cycle of readings A-B-C and plotting the decay curve of the C-readings taken at the end of each cycle. Marchetti et al. (2001) point out that the method relies upon the assumption that the corrected C-pressure is approximately equal to the pore pressure in the soil facing the membrane. The DMT-A_2 method is very similar to the former. The decay curve of the A-readings is plotted rather than the C-readings, and the test is stopped after 50% dissipation of the A-reading is achieved. However, if time is not a constraint is recommended that the test should be continued until 100% dissipation.

Marchetti et al., (1986) suggest the possibility of recording the A-pressure with time during a stop in penetration and plotting this value versus log time. The method is aimed at estimating the effective lateral stress acting on the shaft of vertical driven piles in clay after dissipation of the excess pore pressure due to installation. The time-dependent decay of the corrected A-reading may be used to estimate the reconsolidated horizontal effective stress after penetration, which can be useful for an effective stress analysis for vertical driven pile design. The test described by Marchetti et al. (1986), later named as the DMT-A dissipation test, consists of monitoring the decay of the A-reading until equilibrium is reached. Results of several DMT-A tests reported by Marchetti et al., (1986), Powell & Uglow (1988b), Lutenegger & Miller (1993) and Lutenegger (2006) indicate that the time required to achieve 100% dissipation depends upon the soil type and may be on the order of several hours up to a few days.

Furthermore, Lutenegger (1990, 2006) suggests that the DMT can be used as a push-in total pressure cell to obtain a measure of the reconsolidated lateral stress (σ_c) after dissipation of excess pore pressures due to blade penetration. Results of several DMT-A tests performed at several sites in very soft to very stiff fine grained soils indicate that the reconsolidation coefficient of lateral stress $K_c = (\sigma_c - u_0)/ \sigma_{vo}'$ obtained after σ_c reaches equilibrium is very close to reference K_0 values. The results of several DMT-A tests described by Lutenegger (1990, 2006) and Lutenegger & Miller (1993) are encouraging and seem to demonstrate the usefulness of this method to estimate the coefficient of earth pressure at rest in soft to medium clays. Nonetheless, the writer is not aware of any recent assessment of this method, which is an area that well warrants research.

2.3.4.2 Lateral stress in sand

2.3.4.2.1 Empirical approaches

The correlation by Marchetti (1980) between the coefficient of earth pressure at rest (K_0) and the horizontal stress index (K_D) is mainly based upon data obtained in clay soils. Therefore, it is not surprising that estimates of K_0 with this method are not representative of those of sandy soils. In an attempt to improve the estimation of K_0 in sandy soils, Schmertmann (1982, 1983) proposed an analytical approach to estimate this parameter in uncemented sands based on results of a limited number of calibration chamber tests. The proposed relationship between K_0, K_D and the effective friction angle (ϕ') is given by the following expression

$$K_0 = \frac{40 + 23K_D - 86K_D(1 - \sin\phi_{ax}') + 152(1 - \sin\phi_{ax}') - 717(1 - \sin\phi_{ax}')}{192 - 717(1 - \sin\phi_{ax}')} \qquad \text{Equation 2.16}$$

where ϕ_{ax}' is the angle of shearing resistance as determined by standard triaxial compression tests (also referred to as ϕ'). The method by Schmertmann (1982, 1983) is ill conditioned due to the sensitivity to different values of ϕ'. Also, in Equation 2.16 previous knowledge of ϕ' is required but the magnitude of this parameter is usually unknown a priori. Schmertmann (1983) and Marchetti (1985) developed this idea and introduced the idea of incorporating q_c as a function of K_0 and ϕ' into the correlation equation. Marchetti (1985) concludes that the K_0-q_c-K_D correlation still requires further verification with results from CC tests and field data.

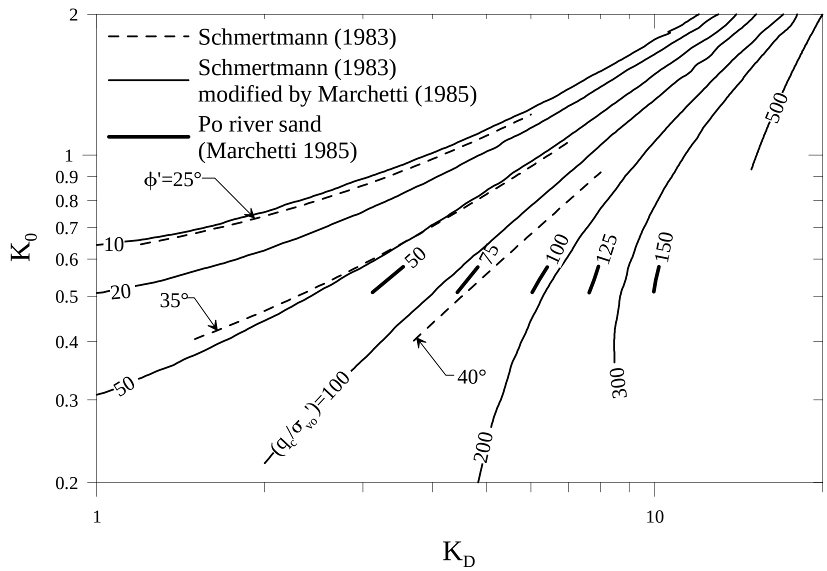

Figure 2.12 Comparison between Schmertmann's and Marchetti's correlations for estimation of K_0 in sands (adapted from Marchetti 1985).

Baldi et al. (1986) made further adjustments to the approach based on a function of K_0, K_D, and q_c/σ_{vo}' of the form:

$$K_0 = D_1 + D_2 K_D + D_3 \left(\frac{q_c}{\sigma_{vo}'} \right) \qquad \text{Equation 2.17}$$

Table 2.3 presents a summary of the correlations proposed by Baldi et al. (1986) to estimate K_0 from DMT data in natural uncemented predominantly quartz sand. Jamiolkowski & Robertson (1988) continued this line of research. All of the derived relationships proved extremely sensitive to small changes in the input parameters. Marchetti et al. (2001) recommend the use of Equation 2.17 with the fitting parameters used to fit the results of CC tests run under BC1 conditions and the Po river data, and with q_c/σ_{vo}'= -0.005 in "seasoned" sand, and -0.002 in "freshly deposited" sand. The uncertainty in estimates of K_0 from these empirical approaches is significantly increased when the soil explored has experienced cementation and/or ageing, which results in a more complex soil structure that can not be mimicked in CC tests.

Table 2.3 Empirical relationships between K_0 and K_D in sand proposed by Baldi et al. (1986).

Database	D_1	D_2	D_3	R^2	Notes
All CC data (BC1, BC2, BC3 and BC4)	0.359	0.071	-0.00093	0.746	Overestimates K_0 values from CC tests performed under BC3 boundary conditions
CC data (BC-1)	0.376	0.095	-0.00172	0.802	Adjusted to fit results of CC tests performed under BC1 boundary conditions, but overestimates K_0 for Po river sand
Field data	0.376	0.095	-0.00461	N/A	Field calibrated using K_0 reference values derived from the interpretation of SBP tests performed in Po river sand

BC-1 = σ_v=constant, σ_h =constant $\quad$ σ_v= Vertical stress

BC-2 = $\epsilon_v = \epsilon_h$=0 $\quad$ σ_h = Horizontal stress

BC-3 = σ_v=constant, ϵ_h=0 $\quad$ ϵ_v= Vertical strain

BC-4 = ϵ_v=0, σ_h =constant $\quad$ ϵ_h= Horizontal strain

2.4 Lateral stress modules mounted behind cones

2.4.1 Introduction

There have been several attempts to estimate the in situ lateral stress by measuring and interpreting the lateral stress acting on an advancing cone (Huntsman, 1985; Bayne & Tjelta, 1987; Tseng, 1989; Masood, 1990; Sully, 1991; Takesue & Isano, 2001). The different designs of lateral stress cones can be divided into two categories: (a) instrumented friction sleeves and (b) passive sensing elements. Both approaches have been attempted at UBC. The location of the lateral stress measuring section with respect to the tip of the cone has varied from one design to another. This section provides the reader with an overview of the development of different lateral stress cones that are considered to represent landmarks in the progress of this type of device.

2.4.2 Background and theoretical framework

The friction sleeve measurement on the cone, f_s, is obtained by dividing the load registered on the friction sleeve load cell by the surface area of the friction sleeve (150 cm^2 on a standard 10 cm^2 cone) and represents the average shear stress acting on the sleeve. The average stress, f_s, should be related to the normal effective stress on the friction sleeve, σ_n' through the relationship:

$$f_s = \sigma_n' \tan \delta \qquad \text{Equation 2.18}$$

where δ is the angle of friction between the friction sleeve and the soil. However, the zone immediately behind the cone tip is known to be one in which there are high gradients of stress and pore pressure and so the true stress distribution on the sleeve is unlikely to be uniform.

The lateral stress at the surface of a cone penetrometer is not constant with respect to distance behind the tip. Indeed, Campanella & Robertson (1981) showed that the friction sleeve resistance in medium (D_r=60%) to very dense sand (D_r=80%) varies as a function of the distance behind the cone tip. Their field measurements using friction sleeves located at varying distances behind the cone tip indicated a significant increase in f_s between 10 and 25 cm behind the tip as shown in Figure 2.13. However, beyond about 40 cm or about 10 to 11 cone diameters (*D*) behind the tip, the magnitude of f_s is fairly constant regardless of the density of the sand. This suggests that instrumentation designed to monitor lateral stress during penetration should be placed at least 10*D* behind the cone tip.

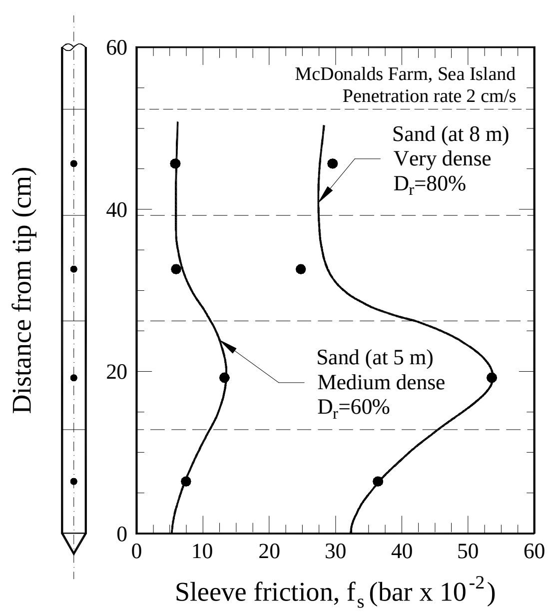

Figure 2.13 Friction along shaft during cone penetration in sand (adapted from Campanella & Robertson, 1981).

Campanella & Robertson (1981) suggest that the lateral stress on the cone rods remains constant for any particular relative density beyond a distance of about 12*D* (*D*=diameter of the cone) behind the tip.

Between the cone tip and 12*D* behind the tip, the friction sleeve measurement would be recorded in an area of highly variable stresses. Also, at this location dimensional tolerances of the components of the cone may have unacceptable effects on the measured values, i.e., a slightly undersized friction sleeve may promote a larger stress reduction while an oversized sleeve may reduce the unloading effect. Also strain rate effects near the tip and rotation of principal stresses may be important.

Robertson (1982) reviewed the calibration chamber data of Baldi et al. (1982) and attempted to estimate with Equation 2.18 the average effective lateral stress over the length of the cone friction sleeve. The results of these analyses indicate that the magnitude of the estimated lateral stress measured during penetration varies from 1 to 7 times the pre-penetration lateral stress.

Furthermore, the first attempt to directly measure the lateral stress during cone penetration was made by Huntsman (1985) at University of California at Berkeley (UCB). Huntsman (1985) assessed the effect of increased lateral stress on q_c through a review of results of calibration chamber (CC) tests performed by Villet (1981), Jamiolkowski (1982) and Schmertmann (1978). Figure 2.14 shows the relationship between the ratios of the cone tip resistance measured under high lateral stress conditions, i.e. overconsolidated, to that measured under normally consolidated (NC) conditions ($q_{c(OC)}/q_{c(NC)}$), versus the ratio of the corresponding lateral stress coefficients for these two conditions (K_{OC}/K_{NC}).

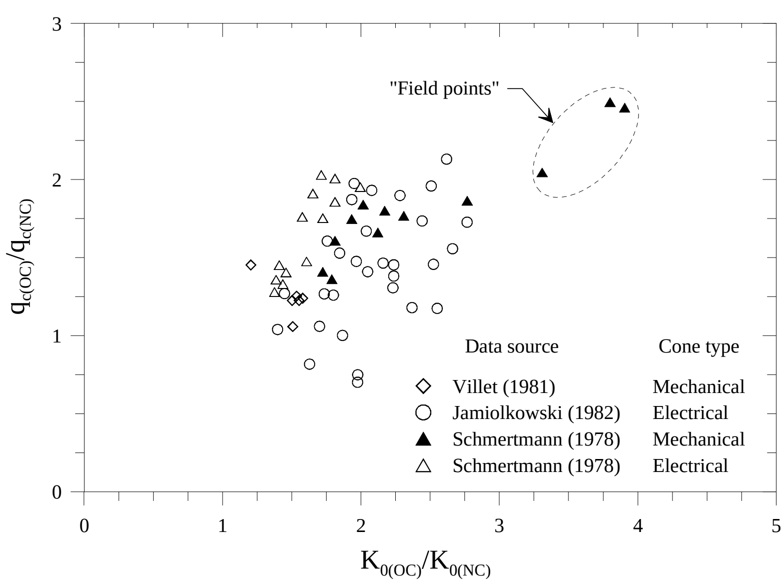

Figure 2.14 Effect of increased lateral stress on tip resistance (adapted from Huntsman, 1985).

Huntsman (1985) noted that the data shown in Figure 2.14 indicate that a unique relationship between the lateral stress and tip resistance is not feasible. On this basis, he concludes that reliable and direct estimates of the effective lateral stress from the cone tip resistance are not possible. As an alternative, he explored the possibility of using f_s for the same purpose. The relationship between the sleeve friction and imposed horizontal boundary stress for laboratory calibration chamber tests reported by Jamiolkowski (1982) is presented in Figure 2.15. Huntsman (1985) argues that the dashed lines on Figure 2.15 suggest that there is a relationship between friction sleeve measurements and horizontal stress boundary conditions at different relative densities. Indeed, Campanella et al. (1990) suggest that the true correlation representing “in ground” conditions probably lies somewhere between the two data sets.

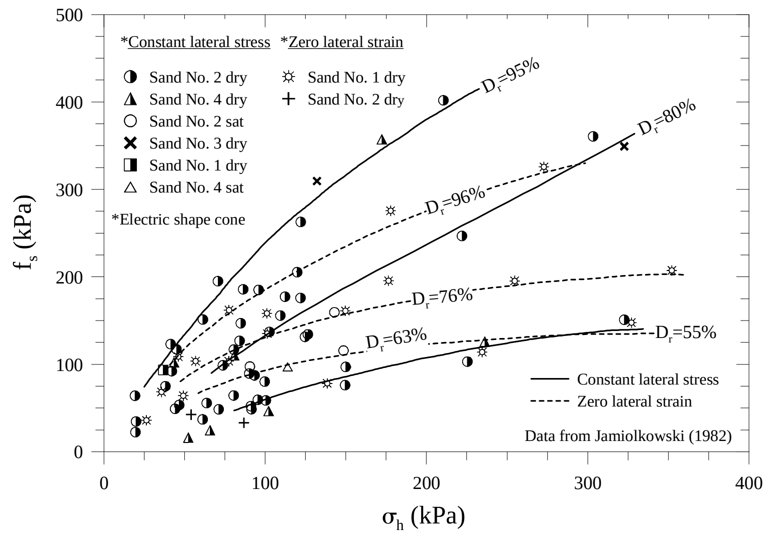

Figure 2.15 Influence of relative density on f_s-σ_h relationship from CC test data (adapted from Huntsman, 1985).

Huntsman (1985) and Huntsman et al. (1986) conclude that the data shown in Figure 2.14 and Figure 2.15 demonstrate that the friction sleeve measurement is more sensitive to lateral stress than the cone tip resistance. They also suggest that a measurement of the normal stress will offer a better correlation to lateral stress than the cone friction sleeve alone. This assumption relies on the dependence of the friction resistance upon the coefficient of friction (μ) at the interface between the sleeve surface and the soil. This is for a cone of constant diameter.

Several studies into soil behaviour around a penetrating cone (e.g. Gillespie 1981, 1990; Hughes & Robertson 1984) have demonstrated the existence of large gradients of both stresses and pore pressures in the vicinity of the cone tip. These gradients are primarily related to the geometry of the equipment since the change in geometry at the base of the tip causes a large normal stress reduction as the soil passes the cone shoulder. The qualitative evaluation of stress distribution around a penetrating cone in sand proposed by Hughes & Robertson (1984) showed that at the base of the cone tip a large normal stress reduction occurs as the soil passes the shoulder (see Figure 2.16).

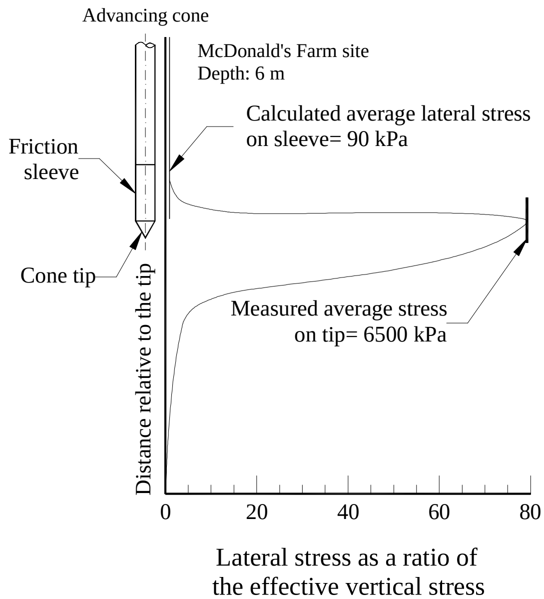

Figure 2.16 Qualitative evaluation of stress distribution around an advancing cone in sand (adapted from Hughes & Robertson, 1984).

The amount of this reduction with respect to pore pressures was first experimentally evaluated by Gillespie (1981). He concluded that in saturated fine grained soils, the decrease in pore pressure up the shaft is due to changes in total stresses, and that these changes represent the transition from a spherical to a cylindrical cavity expansion. Similarly, Salgado (1993) points out that a stress rotation takes place in the neighbourhood of the tip of the penetrometer. Furthermore, Campanella et al. (1990) pointed out that the lateral stress measured at a location away from the tip may more closely represent conditions of cylindrical cavity expansion, whereas stress changes near the tip may cause significant deviation from the cylindrical cavity expansion condition.

The insertion of a cone into the ground generates stresses and/or pore pressure increments in the surrounding soil due to the imposed strains. The magnitude of these increments will depend upon the soil characteristics, probe geometry and penetration rate. Also, the nature of those increments will depend upon whether the penetration process is drained, undrained, or partially drained. The magnitude of lateral stress acting on the shaft of an advancing cone (σ_{LS}) represents the pre- and post-penetration state of stresses. The relationship between the pre and post penetration lateral stresses is

$$\sigma_{LS} = \sigma_{h0}' + \Delta\sigma_h' + u_0 + \Delta u = \sigma_{h0} + \Delta\sigma_h \qquad \text{Equation 2.19}$$

In Equation 2.19 σ_{LS} is the total lateral stress measured by the cone, σ_{ho}' is the initial in situ effective lateral stress, $\Delta\sigma'_h$ is the increase in effective lateral stress, u_o is the equilibrium pore pressure and Δu is the change in pore pressure caused by undrained or partially drained deformation of the soil. For drained penetration, $\Delta\sigma_h = \Delta\sigma_h'$, whereas for undrained penetration $\Delta\sigma_h = \Delta\sigma_h' + \Delta u$. Sully (1991) points out that it is generally assumed that no change in effective stress occurs but this neglects the effect of shear induced pore pressure. He indicated that the ratio of final to initial lateral stress could be considered to an amplification factor (A_{LS}), i.e. $A_{LS} = \sigma_{LS}'/\sigma_{h0}'$. He demonstrated that the magnitude and variation of the amplification factor depend upon both probe geometry and soil characteristics.

2.4.3 Lateral stress modules

The original UBC lateral stress module was an instrumented friction sleeve comprising a friction sleeve with a reduced wall thickness, instrumented with strain gauges bonded to its inside so that the circumferential or hoop strain of that section was measured. Instruments have also been developed which measure the stress using a passive sensing element. These typically consist of an external pressure-receiving plate that is flush with the body of the cone and transfers the normal stress acting on the shaft of the penetrometer to an internal sensor. This section provides an overview of the development of instrumentation developed for measurement of the lateral stress acting on the shaft of an advancing cone. The basic characteristics of lateral stress modules designed to be mounted behind cones that have been reported in the technical literature are summarized in Table 2.4.

2.4.3.1 Instrumented friction sleeves

Huntsman (1985) describes the laboratory and field lateral stress sensing penetrometers (LSSCP) used for his research. The laboratory model (LSSCP-I) was a modified version of the acoustically damped electric cone penetrometer designed and used by Tringale (1983). The seven-channel laboratory cone had a tip area of 10 cm^2, a friction sleeve area of 150 cm^2 and was designed to independently measure: tip resistance (q_c), friction resistance (f_s), acoustic emissions near the tip, lateral stress approximately 1 diameter behind the tip, pore pressure immediately behind the tip (u_2), lateral stress around 9 diameters behind the tip, and pore pressure at about 10 diameters behind the tip.

The lower lateral stress measuring section which was located approximately one diameter behind the cone tip, consisted of a section of the friction sleeve machined (from the inside) to a wall thickness of 0.25 mm. The circumferential strain of this section was measured by means of electric resistance strain gauges bonded to the inside of the machined friction sleeve. This measurement was calibrated against hydrostatic pressure acting on the exterior surface of the friction sleeve. The upper lateral stress measuring section contained a thin-walled section with circumferentially oriented strain gages similar to that in the lower section of the friction sleeve. Also, a pore pressure transducer, which was similar to the one behind the tip, was mounted just above the upper lateral stress section. Figure 2.17 shows a schematic diagram of the laboratory LSSCP-I.

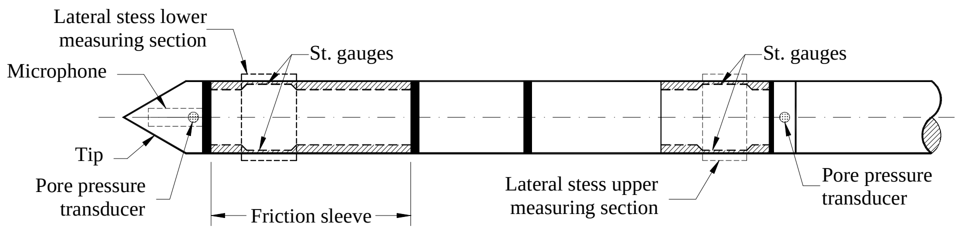

Figure 2.17 Schematic diagram of laboratory lateral stress sensing cone penetrometer (LSSCP-I) (adapted from Huntsman, 1985).

The field penetrometer (LSSCP-II) was a modification of the design used for the laboratory cone. The principal changes in the second design were:

- The capacity of the load cells for measuring tip and friction resistance was increased.
- The microphone and acoustic dampening elements were omitted.
- A thermistor was mounted on the friction sleeve and adjacent to the lateral stress sensing strain gages to monitor the effect of temperature on this array.
- In both lateral stress measurement sections, the strain gages were connected to form a half Wheatstone bridge. This configuration allowed the instrument to be less temperature sensitive.
- The upper pore pressure sensor was removed.
- The radial orientation of the lower pore pressure sensor was moved to an axial orientation.
- An electronics section was mounted immediately above the upper lateral stress measurement section.

The six-channel field cone allowed simultaneous measurement of: tip resistance (q_c), friction resistance (f_s), pore pressure immediately behind de tip (u_2), lateral stress and temperature approximately 1 diameter behind the tip, and lateral stress at about 9 diameters behind the tip. The LSSCP-II is shown in Figure 2.18.

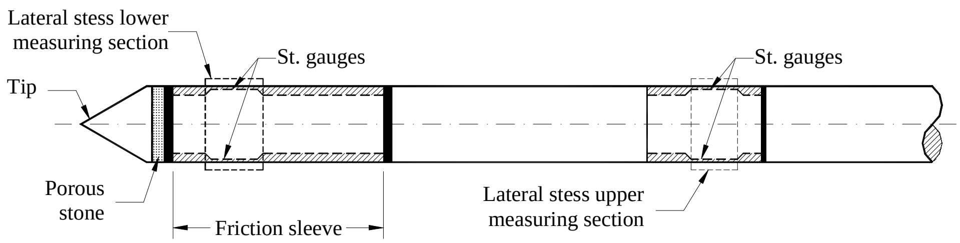

Figure 2.18 Schematic diagram of field lateral stress sensing cone penetrometer (LSSCP-II) (adapted from Huntsman, 1985).

The design of the LSSCP-II was sensitive to cross-talk effects on the friction sleeve, and susceptible to damage under high hydrostatic pressure or gravel encountered during penetration. In an attempt to overcome these problems the lateral stress sections of the LSSCP- II were redesigned by Tseng (1989). The improvements in the design resulted in an instrument with insignificant cross-talk effects and a more robust design less susceptible to damage (Masood, 1990). Furthermore, the new design allowed the lateral stress to be measured in a different manner from that used by Huntsman (1985), and therefore falls into the category of passive sensing elements. A complete description of the measurement principle of the LSSCP-III is given in section 2.4.3.2.

Campanella, et al. (1990) described the first model of the lateral stress piezocone (LSCPTU-I) developed and built at the University of British Columbia. The instrument consisted of two separate measuring systems: a standard UBC piezocone unit (CPTU) and a lateral stress module (LSM-I). The eight-channel piezocone had a tip area of 15 cm^2, a friction sleeve area of 225 cm^2 and allowed simultaneous measurement of the following parameters: tip resistance (q_c), pore pressure on the face (u_1) or behind the tip (u_2), sleeve friction (f_s), pore pressure behind the friction sleeve (u_3) and temperature. The lateral stress module consisted of an instrumented friction sleeve located 69.9 cm behind the tip. This section was designed to independently measure lateral stress, sleeve friction, pore pressure, and temperature. Despite the fact that two temperature sensors were located in the LSCPTU-I only the temperature at the position of the lateral stress module was recorded when the cone was in this configuration. The transducer ranges were 7.5 V for all the channels with the exemption of the lateral stress channel, which operated on 1 V full scale. The geometry of the LSCPTU-I cone is shown in Figure 2.19.

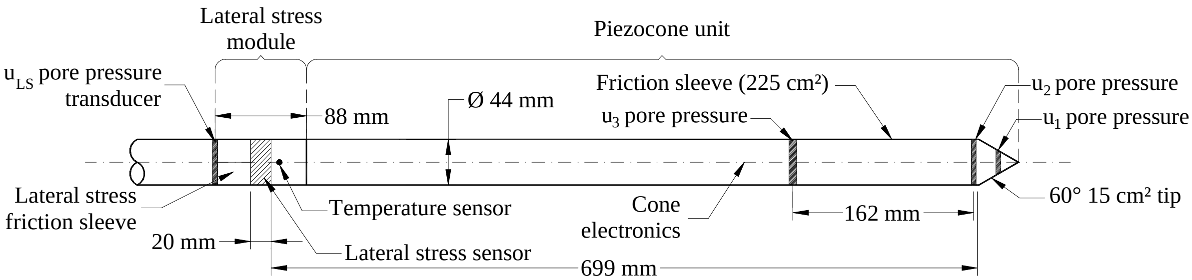

Figure 2.19 UBC lateral stress piezocone (LSCPTU-I)
(adapted from Campanella et al, 1990).

Results of laboratory calibrations of the LSCPTU-I reported by Campanella et al. (1990) indicated that lateral stress measurements were sensitive to both axial loads on the friction sleeve and on temperature. However, they argued that these effects can be calibrated out by making appropriate corrections to measured data. For example, a temperature sensor installed in the sleeve allowed for temperature compensation to both lateral stress and friction sleeve measurements. Also, Sully (1991) suggested using a thinner instrumented section in order to increase the sensitivity. However, the use of a thinner section may result in an instrument more sensitive to cross-talk effects and temperature variations, and reduces the robustness of the equipment. Finally, Campanella et al. (1990) suggested that the actual ±7 kPa resolution of the lateral stress channel could be improved by refining signal processing.

2.4.3.2 Passive sensing element approach

Bayne & Tjelta (1987) describe the development and application of different multi-element piezocones for investigation of a site located at the North Sea. The lateral stress piezocone (LSCPTU) described consisted of a module designed to measure simultaneously the total lateral stress acting on the shaft of the penetrometer, and pore pressure and sleeve friction at 27 mm and 140 mm above the lateral stress sensor, respectively. This module was attached to a 3 channel, 15 cm^2 piezocone unit capable of measuring tip resistance (q_c), pore pressure at the tip (u_1) and sleeve friction (f_s). The lateral stress module was placed at distances between 1 and 3 m behind the piezocone unit. The total lateral stress was measured by a load cell with two active faces set on opposite sides of the element and flush with its face. Each active face was circular with a projected area of 403 mm^2, i.e. approximately 11.3 mm in diameter. The load cell was a spool shaped post instrumented with foil gauges.

Tseng (1989) redesigned the lateral stress sections of the cone developed by Huntsman (1985) in an attempt to overcome the weaknesses of the previous instrumented friction sleeve approach. The improvements in the design resulted in an instrument with insignificant cross-talk effects and a more robust design less susceptible to damage. The new design measured the lateral stress using two lateral stress sensors located 1*D* and 7.5*D* behind the tip, where *D* is the cone diameter. The lower pore pressure sensor was located immediately behind the tip (u_2) and the upper sensor was located 6.3*D* behind the tip. A schematic diagram of the lateral stress sensor of the LSSCP-III is shown in Figure 2.20.

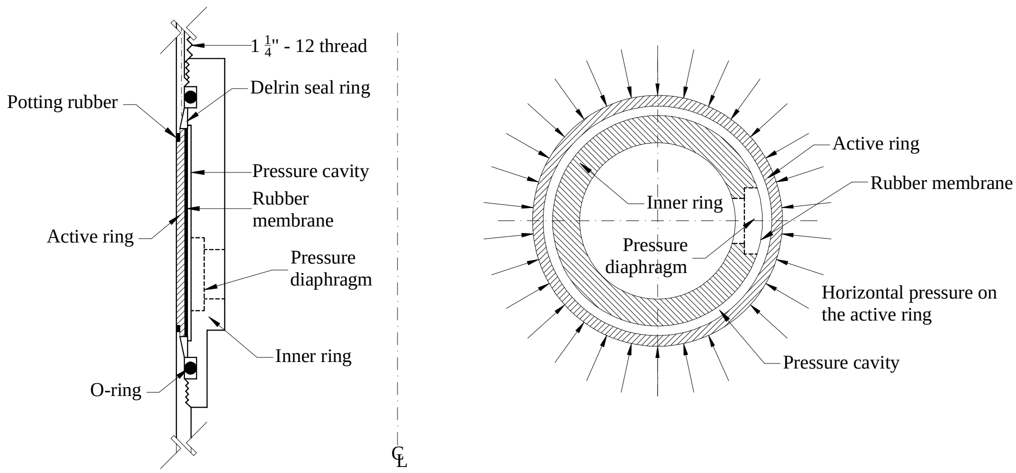

Figure 2.20 Schematic illustration of the lateral stress measuring system of the LSSCP-III (adapted from Tseng, 1989).

As shown in Figure 2.20, the lateral stress section consisted of a double stainless steel ring configuration comprising an outer active ring and an inner passive ring. Four identical steel curved pieces, 1.3 mm thick, were joined together with a polyurethane compound to form the outer flexible ring. The cavity created between the active ring and the inner ring was covered with a rubber membrane and sealed at both ends by two sealing rings. A strain gauged stainless steel diaphragm, 6.3 mm in diameter, was installed on the inner ring and functioned as a pressure transducer. The cavity formed between the membrane and the inner ring was filled with de-aired water. Saturation of the fluid was critical to the performance of the measuring system. Masood (1990) suggested modifications to the above design but no further work appears to have been done on it.

Takei & Isano (199) and Takesue & Isano (2000, 2001) described a lateral stress cone exclusively designed to measure the lateral stress acting on the shaft of a cone during penetration. The cone was developed with a relatively simple structure and with particular attention to ease of field use. The Japanese lateral stress cone (J-LSC) consisted of a probe with the same diameter and tip shape as a standard penetrometer, i.e. apex angle of 60° and tip area of 10 cm^2. The J-LSC was equipped with a lateral stress sensor, two pore pressure transducers and one biaxial inclinometer (Figure 2.21). The five channel configuration of this equipment allowed simultaneous measurements of: (i) pore pressure behind the tip, (ii) lateral stress 2.1*D* behind the tip, pore pressure 2.6*D* behind the tip, and inclination in the x and y directions. The lateral stress acting on the cone was transferred to an internal load cell through an external curved pressure-receiving plate in direct contact with the soil. As shown in Figure 2.21, the plate was located 2.14D behind the tip.

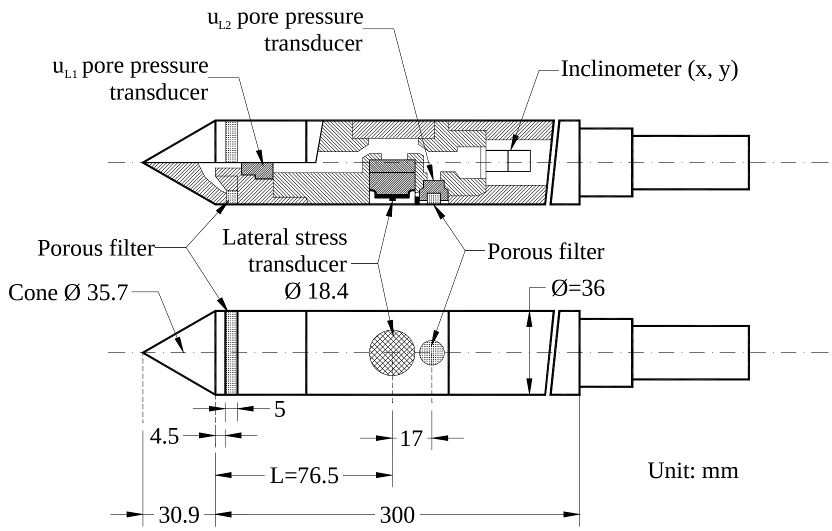

Figure 2.21 Japanese lateral stress cone (J-LSC) (adapted from Takesue & Isano, 2001).

A second model of lateral stress cone, termed a friction-lateral stress cone (J-FLSC), was described by Takesue (2001). The new device was capable of measuring the lateral stress acting on the penetrometer shaft and the pore pressure behind the lateral stress sensor at two different locations along the cone shaft. Also, the friction between the penetrometer and soil was measured by an instrumented friction sleeve located between the two lateral stress sections, and the inclination of the probe was monitored with a built in inclinometer. The diameter of the J-FLSC was constant along the probe. Instruments of 36 mm and 44 mm diameter were developed. A schematic diagram of the Japanese friction-lateral stress cone is shown in Figure 2.22.

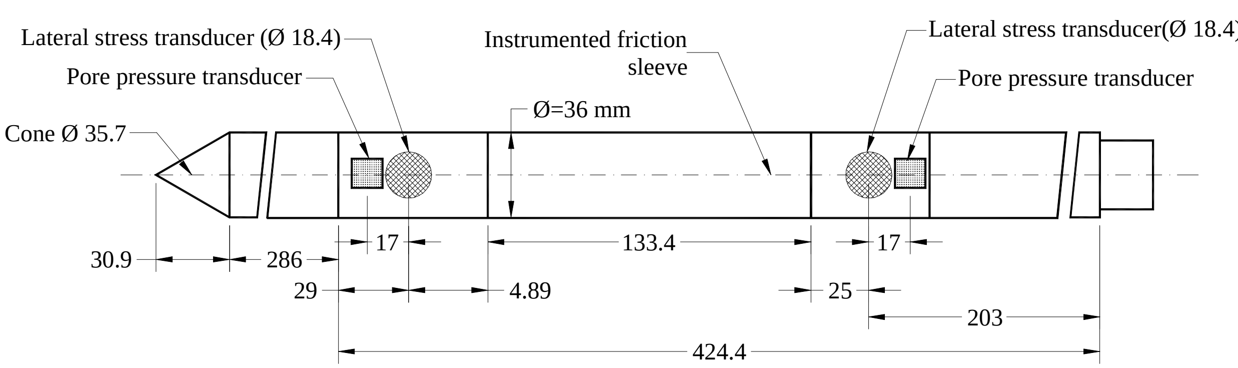

Figure 2.22 Japanese friction-lateral stress cone (J-FLSC) (adapted from Takesue, 2001).

2.4.3.3 Review of instrumentation

The principle of measurement of lateral stress modules developed by Huntsman (1985) and Campanella, et al. (1990) was based upon measurement of the hoop strain generated in instrumented sections of the cone that are in direct contact with the soil. Results of laboratory calibrations and field experience demonstrated that this type of design was sensitive to both cross talk effects on the sleeve and to temperature effects, and was susceptible to physical damage. Takesue & Isano (2001) argued that with this type of instrument, damage to the instrumented section directly affects lateral stress measurement. Masood (1990) reported fairly good performance in the field of the double ringed design by Tseng (1989). However, the main drawback in that design was the damage to the membrane when soil particles penetrated between it and the active ring.

The lateral stress module described by Takesue & Isano (2000, 2001) consisted of a measuring system that was not in direct contact with the soil. An external circular receiving plate transferred the external pressure to an internal load sensor. Results of hydrostatic and temperature calibrations reported by them indicated good performance of the lateral stress sensor. A nonlinearity and hysteresis of about 0.49 % of full scale (FS) and a temperature coefficient (B_t) of 0.056% FS/°C were obtained for the lateral stress sensor respectively. Results of laboratory calibrations confirmed that axial and frictional loads acting on the lateral stress module did not affect measurements of either lateral stress or pore pressure. The configuration of this type of sensor reduces the risk of damage to the instrument.

2.5 Summary

2.5.1 Seismic flat dilatometer (SDMT)

The SDMT is a conventional flat DMT with an added module to allow measurement of shear wave velocity (V_s). This capability was added in response to demand from industry and due to advances in understanding of the importance of small strain shear modulus in geotechnical engineering and, in particular, in geotechnical earthquake engineering. There are still few data available to allow assessment of possible improvements in site characterization with the DMT due to this added capability. This thesis explores if the addition of shear wave velocity to standard DMT data can provide additional useful information for an improved site characterization

The DMT expands the soil in a horizontal direction and so is likely to be greatly influenced by the in situ lateral stress. The information reviewed indicates that estimation of the lateral stress or the coefficient of earth pressure at rest (K_0) from DMT data in both clay and sand is mainly based upon empirical correlations to DMT parameters such as K_D. Alternatively, K_0 can be estimated in sand by combining DMT and CPT parameters, i.e. K_D and q_c, however the successful application of this approach requires and accurate match between results of both tests. In addition, by performing DMT-A dissipation tests in clay is it possible to estimate directly the total lateral stress in the field, rather than through empirical correlations to DMT data. Nonetheless, this approach is not very practical since long testing periods are required, and therefore its application still remains constrained to special projects. This thesis will revisit some of existing correlations to estimate K_0 from DMT parameters in an attempt to assess estimates with these approaches.

2.5.1 Lateral stress cone

The development of cones capable of measuring lateral stress originated from the idea that the sleeve friction measured during penetration in sand should be related to the pre-penetration lateral stress (Campanella, et al., 1990). There have been several attempts to estimate the in situ lateral stress by measuring and interpreting the lateral stress acting on the shaft of an advancing cone (Huntsman, 1985; Bayne & Tjelta, 1987; Tseng, 1989; Masood, 1990; Sully, 1991; Takesue & Isano, 2001). The different designs of lateral stress cones developed can be divided into two categories: (a) instrumented friction sleeves and (b) passive sensing elements. The principle of measurement of the former is based upon the strain generated in an external part that is in direct contact with the soil, whereas in a passive sensing element the measuring element consists of a system with an internal load transducer and an external pressure receiving plate in direct contact with the soil. Both approaches have been attempted at UBC.

The information reviewed indicates that lateral stress measuring sections based upon instrumented friction sleeves are more susceptible to physical damage than passive sensing elements. In addition, laboratory and field data have shown that instrumented friction sleeves are more sensitive to both axial loads on the friction sleeve (cross-talk effect) and to temperature than passive sensing elements. This thesis describes a new lateral stress cone built and developed at UBC. The lateral stress sensor consists of a passive sensing element similar to that described by Bayne & Tjelta (1987) and Takesue & Isano (2001). The performance of the new instrument is assessed through a comprehensive laboratory and field testing program.

Table 2.4 Main characteristics of lateral stress cones reviewed

Cone	Principle of measurement	Diameter of the probe (mm)	Location of lateral stress sensor behind the cone tip	Pore pressure sensor	Reference
LSSCP-I	Friction sleeve with strain gauges	35.7	1*D* and 9*D*	u_2 and u_{LS} at 10*D* behind the cone tip	Huntsman (1985)
LSSCP-II	Friction sleeve with strain gauges	35.7	1*D* and 9*D*	u_2	Huntsman (1985)
LSSCP-III	Double steel ring configuration with strain gauged diaphragm	35.7	1*D* and 7.5*D*	u_2 and u_{LS} at 6.3*D* behind the cone tip	Tseng (1989) Masood (1990)
LSCPTU-I	Friction sleeve with strain gauges	44	15.9*D*	u_1 or u_2 and u_{LS} at 16.7*D* behind the cone tip	Campanella, et al. (1990)
LSCPTU	Internal load cells with external circular active faces	44	Variable from 31.5*D* to 77*D*	u_1 and u_{LS} – variable from 32.1*D* to 77.6*D*	Bayne & Tjelta, (1987)
J-LSC	Internal load cell with an external pressure plate	35.7	2.1*D*	u_2 and u_{LS} at 2.6*D* behind the cone tip	Takesue & Isano (2000, 2001)
J-FLSC	Internal load cell with an external pressure plate	36	8.8*D* and 14.1*D*	u_2 and u_{LS} at 8.3*D* and 14.6*D* behind the cone tip	Takesue (2001)

LSSCP :	Lateral stress sensing cone penetrometer	u_1 :	Pore pressure at the cone tip
LSCPTU:	Lateral stress piezocone	u_2 :	Pore pressure behind the cone tip
J-LSC:	Japanese lateral stress cone	u_3 :	Pore pressure behind the friction sleeve
J-FLSC	Japanese friction lateral stress cone	u_{LS} :	Pore pressure measured below or above the lateral stress sensor
D:	Diameter of the cone		

Chapter 3 DESCRIPTION OF TEST SITES AND TESTING PROGRAM

3.1 Introduction

Seismic flat dilatometer tests (SDMT), lateral stress seismic piezocone (LSSCPTU) and seismic piezocone (SCPTU) soundings were performed at six different test sites located in the Lower Mainland (LM) of B.C. The locations of the UBC research sites are shown in Figure 3.1. The soil conditions at these test sites cover a fairly wide range of different soil types that include: stiff overconsolidated (OC) silt and silty clay, soft normally (NC) to lightly overconsolidated (LOC) silty clay, NC silt to sandy silt, and loose to dense sand. Also, ConeTec Investigations Ltd. (Canada), TGC Geotecnia (Mexico) and Diego Marchetti (Italy) provided access to additional SDMT and flat dilatometer (DMT) data collected at several sites. This information has been used to complement the SDMT and DMT databases presented in this thesis.

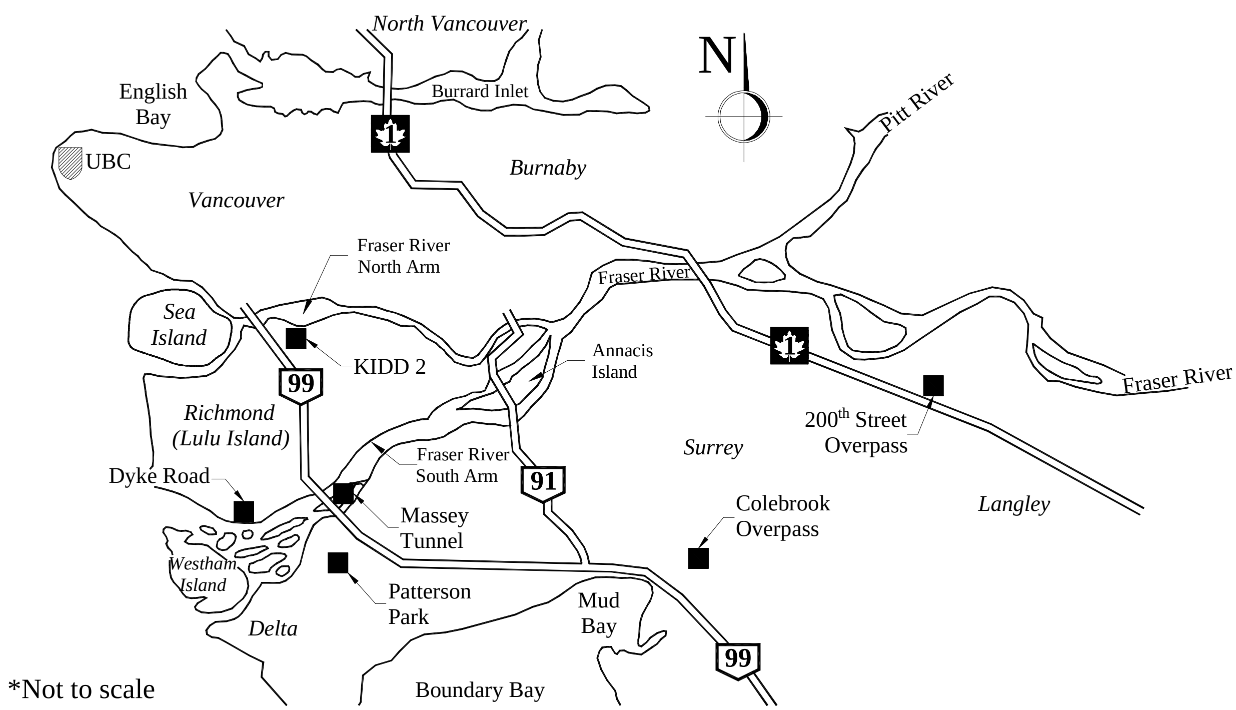

Figure 3.1 Location of test sites.

This chapter presents an overview of the geology of the area, followed by a detailed description of each test site, which provides information on location, soil stratigraphy and basic geotechnical parameters. The in situ testing program performed at each research site is described in terms of type of test and maximum depth reached. A summary of the additional SDMT and DMT data collected at other sites is also presented. The soil profiles presented for each site summarize the results of site characterization carried out over several years. The data reported in this chapter provide the reader with an updated source of information which might be useful as a reference for further research on in situ testing in soils of the LM of B.C.

3.2 Geology

The Fraser River Lowland underlies the southern parts of Greater Vancouver. It extends 150 km east of the Strait of Georgia along the course of the Fraser River. The development of the Fraser River Delta began about 11 000 years ago once the ice had retreated from the area. The base of the Delta consists of Tertiary sedimentary bedrock overlain by Pleistocene deposits of glacial till and glacial outwash. Sediments of the modern Fraser River delta are primarily Holocene. They reach a maximum known thickness of 305 m and overlie Late Pleistocene glaciogenic sediments (Monahan, et al. 1995; Monahan & Levson, 2001).

As described by Monahan & Levson (2001), the Fraser River Delta deposits can be subdivided into bottomset, foreset and topset beds. Bottomset deposits are up to 120 m thick and generally consist of silt and clay. Foreset deposits, overlie the bottomset, and consist of sandy silts that are locally interbedded with sand-dominated units up to 30 m thick. In fact, in the southern part of the delta, sand-dominated units are abundant, whereas they are found locally near the top of the foreset elsewhere. Finally, the topset overlies the foreset and thins westward from over 30 m at the head of the delta to less than 20 m at the western margin of the dyked upper delta plain. The topset is dominated by a lower massive sand facies that is generally 8 to 30 m thick and its origin has been interpreted to represent a complex of distributary channel deposits (Monahan et al, 1993). The massive sand facies is gradationally overlain by an interbedded sand and silt facies and an organic silt facies that together record the upward facies progression from channel to floodplain deposits.

In the Fraser delta, the principal channel environments are distributary and tidal channel. Based upon borehole data, Monahan et al. (1993) conclude that the entire delta plain, with the exception of parts of the western tidal flats and the subaqueous delta plain, has been reworked by distributary channel migration, which has eroded the original tidal flat, subaqueous delta plain and in most places the topset delta front deposits. They conclude that most of the channel migration occurred in a tidal flat environment, as a result of the interaction of tidal and fluvial processes and due to the high proportion of sand in the sediment load.

To the east of the Fraser River Delta lies the upland area where the Langley-Cloverdale basin is located. The sediments are Pleistocene glacial and post-glacial. The earlier glacial deposits consist of dense sands and gravels. The overlying post-glacial sediments have a glaciomarine origin having been deposited during a period when the Fraser River became dammed by ice. The soft clayey silts are known locally as Capilano or Fort Langley sediments. Horizons of interbedded sand are common throughout, the frequency of which die out towards the west (Sully, 1991).

The subsoils in the western region of the Serpentine River lowland are Salish sediments, post-glacial deposits of the Quaternary period that were laid down between 10,000 and 5,000 years ago (Armstrong, 1984). These materials include sediments deposited when the sea level was significantly higher than today. The depositional process of these sediments and the lack of evidence of any unloading (e.g. erosion), suggests that these soils are normally consolidated. However, there is a possibility of light overconsolidation in the upper soil layers as a result of changes in the sea level and/or fluctuations of the groundwater table. Figure 3.2 shows the surficial geology of Quaternary deposits in the Fraser lowland.

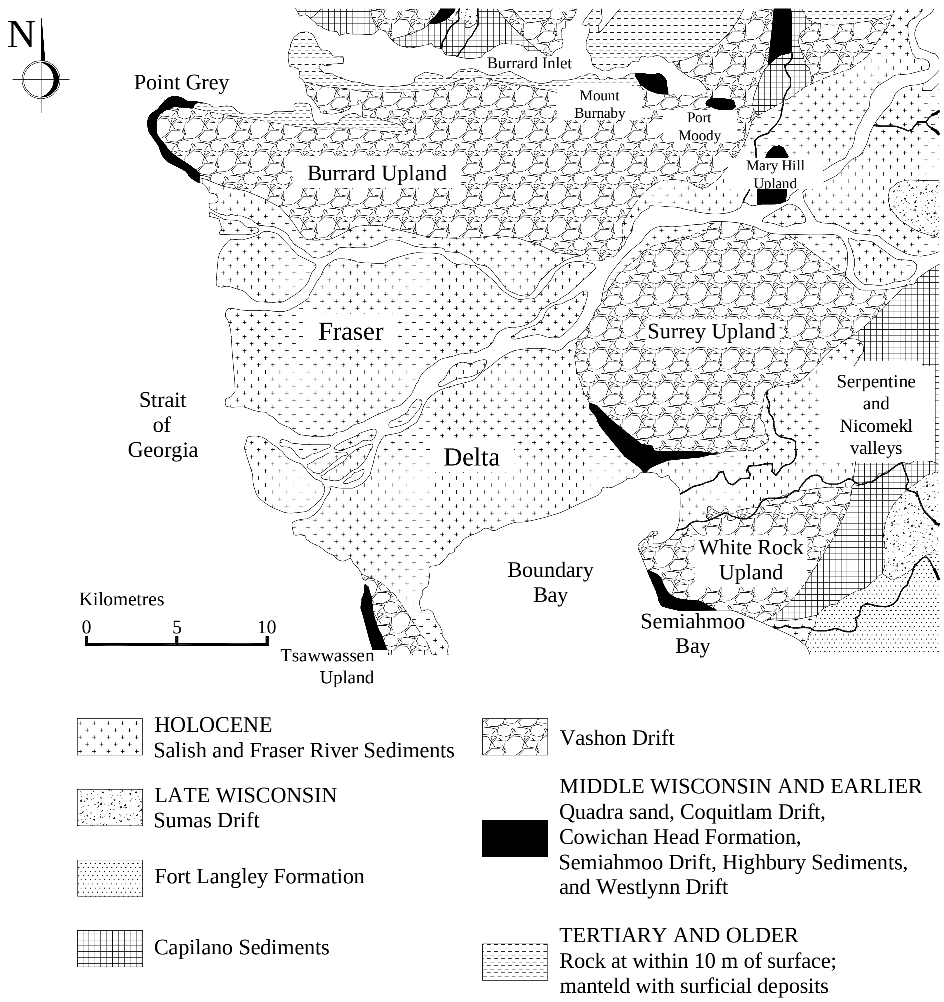

Figure 3.2 Distribution pattern of Quaternary deposits in the Fraser lowland (adapted from Armstrong, 1984).

3.3 Description of test sites

3.3.1 200th Street Overpass, Langley

3.3.1.1 Site location and description

The site is situated within the area of the 200th Street Overpass at Trans-Canada Highway No. 1, in Langley, B.C.. As shown in Figure 3.3 the test area is located within the area delimited by the former westbound exit ramp, and approximately 500 m northwest of the former UBC research site described by Sully (1991).

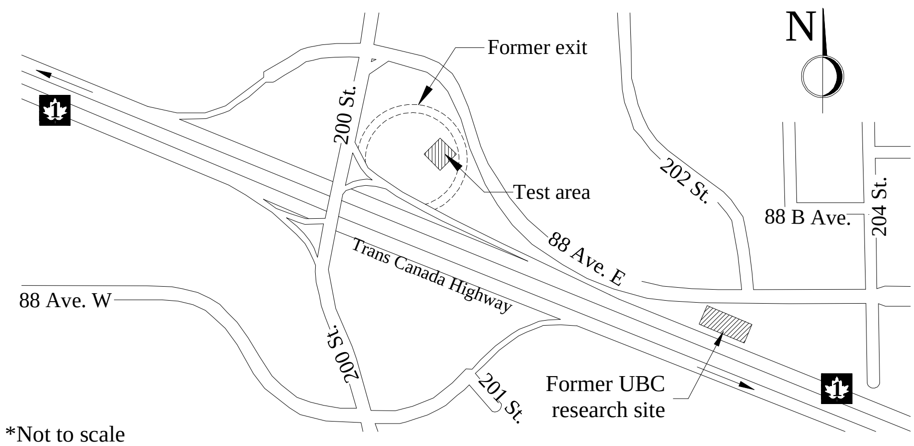

Figure 3.3 Location of 200th Street Overpass test site.

3.3.1.2 Stratigraphy

Figure 3.4 presents the soil profile at the test site as well as basic geotechnical parameters. The general soil stratigraphy consists of a very stiff overconsolidated silt crust transitioning to lightly overconsolidated soft sensitive silty clay with occasional sand lenses underlain by hard Vashon Drift (till). The soil was deposited in a marine environment during the retreat of Vashon ice between 11,000 and 13,000 years ago.

Classification testing by Zergoun et al. (2004) and Sully (1991) indicates the silt to be generally of medium plasticity with some zones of low and high plasticity. Sully (1991) reports natural water (w_N) contents in the range of 31% to 72%. Also, average values of 47% were obtained for the liquid limit (w_L), and 27% for the plasticity index (PI), respectively. Below the desiccated crust, liquidity indices ranged from 1.0 to 1.42. The liquidity index (LI) is an index parameter which relates the water content to the liquid limit (w_L) and plastic limit (w_P) of the soil. Zergoun et al. (2004) report results of field vane shear tests (FVT) that indicate sensitivities of 2.6 to 5.9 with an average of 4.1. They also noted a slight upward ground water gradient close to the till surface. Some surface regrading work has been carried out at this location since the original field work by Sully (1991) which may have altered the stress history slightly.

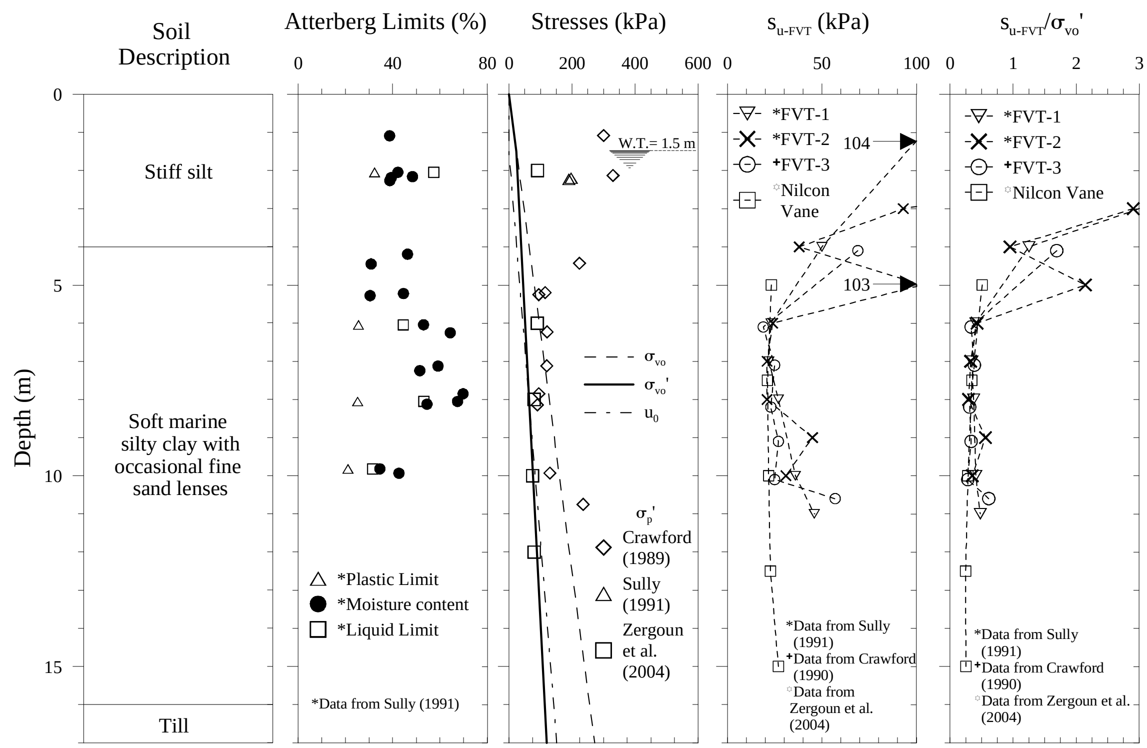

Figure 3.4 Soil profile at 200th Street site

(data from Crawford 1990, Sully 1991, and Zergoun et al., 2004).

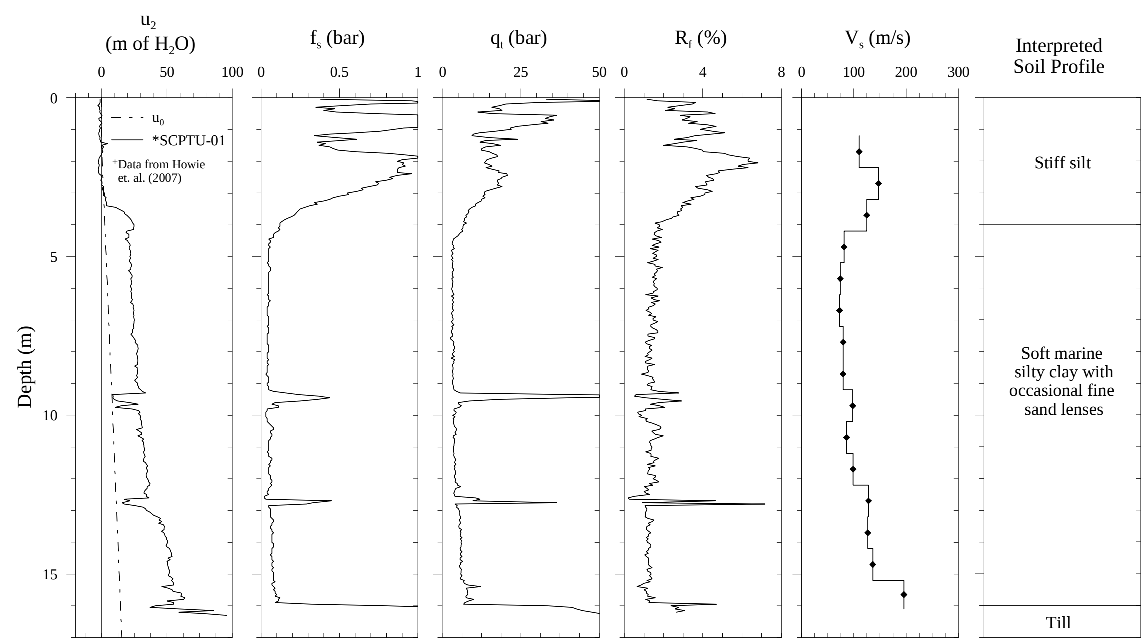

Figure 3.5 SCPTU profile at 200th St.

3.3.2 Colebrook Overpass, Surrey

3.3.2.1 Site location and description

The site is located approximately 30 km southeast of downtown Vancouver, in south Surrey B.C. The test site is situated under the King George Highway 99A overpass over Colebrook Road and the adjacent BC Railway (BCR) right-of-way, and north of its intersection with Highway 99 (Figure 3.6).

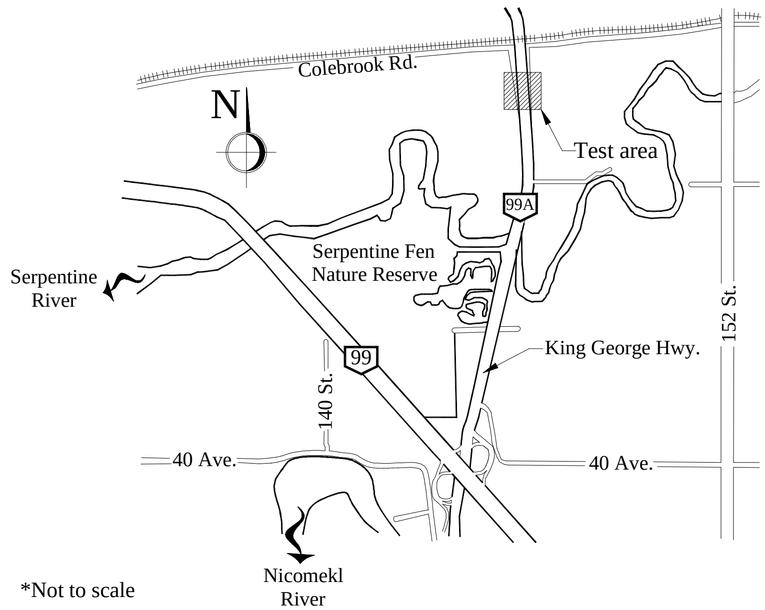

Figure 3.6 Location of Colebrook Overpass test site.

This site is located within the Serpentine River flood plain, and therefore the ground is fairly flat, lying at or slightly below the mean sea level (MSL), and poorly drained. The ground surface elevation at the former test site described by Weech (2002) lies below sea level, varying between -1.1 m and -1.3 m.

3.3.2.2 Stratigraphy

Figure 3.7 presents the soil stratigraphy at the Colebrook overpass site. Also, the profiles of index parameters and basic soil properties reported in previous investigations are included. Typical CPTU profiles at the test area are shown in Figure 3.8. The results from previous site investigations (Crawford & deBoer, 1987; Crawford & Campanella, 1991; Dolan, 2001; Crawford, et al. 1994; and Weech, 2002) indicate that the general soil stratigraphy at the Colebrook overpass consists of a 0.6 m thick layer of fill overlying in some areas a 0.2 m to 0.3 m thick layer of firm to stiff peat that overlies the marine deposits. The peat deposit is underlain by a layer of firm clayey silt interbedded with seams of fine sand to sandy silt which extends to about 2 m in depth. Below this layer, the soil is predominantly soft silty clay with considerable inclusions of organic matter (e.g. grasses and plant stalks) with the thickness of this layer being about 1 m. Dolan (2001) reports a pore water salt concentration of 20 g/l for a sample retrieved in the soft silty clay layer. Terzaghi et al. (1996) report a pore water salt concentration of 25 g/l for a postglacial marine deposit in Norway (Drammen clay). Similarly, Sridharan et al. (2002) report salt concentrations between 0.45 to 30 g/l for the soft marine clay of Ariake Bay in Japan. Therefore, the pore water salt concentration reported by Dolan (2001) suggests that soil at this site was deposited in a salt-water environment.

The surficial soils are underlain by a thick deposit of marine soft clayey silt to silty clay, containing occasional shells and shell fragments underlain by a stiff layer of sand and gravel. The deposit of marine sediments extends to a depth of at least 35 m below the former pile test site, based upon the stratigraphy reported by the MoTH (1969) and the tip depths of the piles on either side of the site. Crawford & Campanella (1991) indicate that the marine silt and clay deposit along the overpass alignment is reasonably uniform, with average values of 45% for the natural water content (w_N), 36% for the liquid limit (w_L), and 11% for the plasticity index (PI). Similarly, Weech (2002) reports for this deposit the following average values of index properties: $w_N \approx 42\% \pm 3$, $w_L \approx 40\% \pm 4$, and PI around 13.5%±4.5.

Weech (2002) points out that field measurements with piezometers located within the upper 10 m of the silt and clay deposit indicate that the water table is typically around 0.7 m below the ground surface, and that there is an upward hydraulic gradient between 5% and 10%. He argues that the upward gradient is likely a result of groundwater recharge from the upland area (just north of the site), which seeps up from the more permeable sand and gravel underlying the marine silt and clay. The position of the groundwater table is subjected to seasonal changes with an observed drop to as low as 1.4 m below ground surface.

The high sensitivity values (S_t) of the fine-grained marine soil deposits at Colebrook ($10<S_t<70$) and 200th St ($2<S_t<9$) may be due to the reduction in salinity by leaching caused by upward gradients. Mitchell & Soga (2005) point out that leaching causes little effect on fabric but the interparticle forces are changed, which results in a decrease in undisturbed shear strength of up to 50 percent, and such a large reduction in remoulded strength that quick clay forms. Therefore, the large increase in interparticle repulsion is responsible for the deflocculation and dispersion of the clay upon mechanical remoulding.

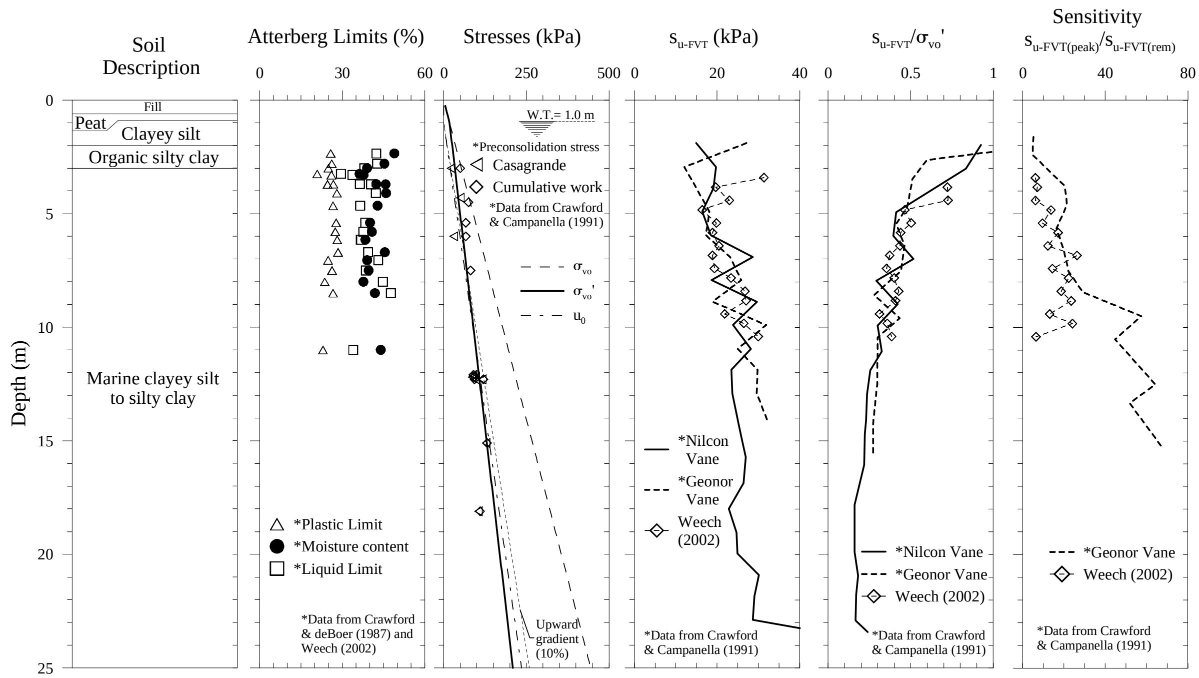

Figure 3.7 Soil profile at Colebrook Overpass site

(data from Crawford & Campanella, 1990; and Weech 2002).

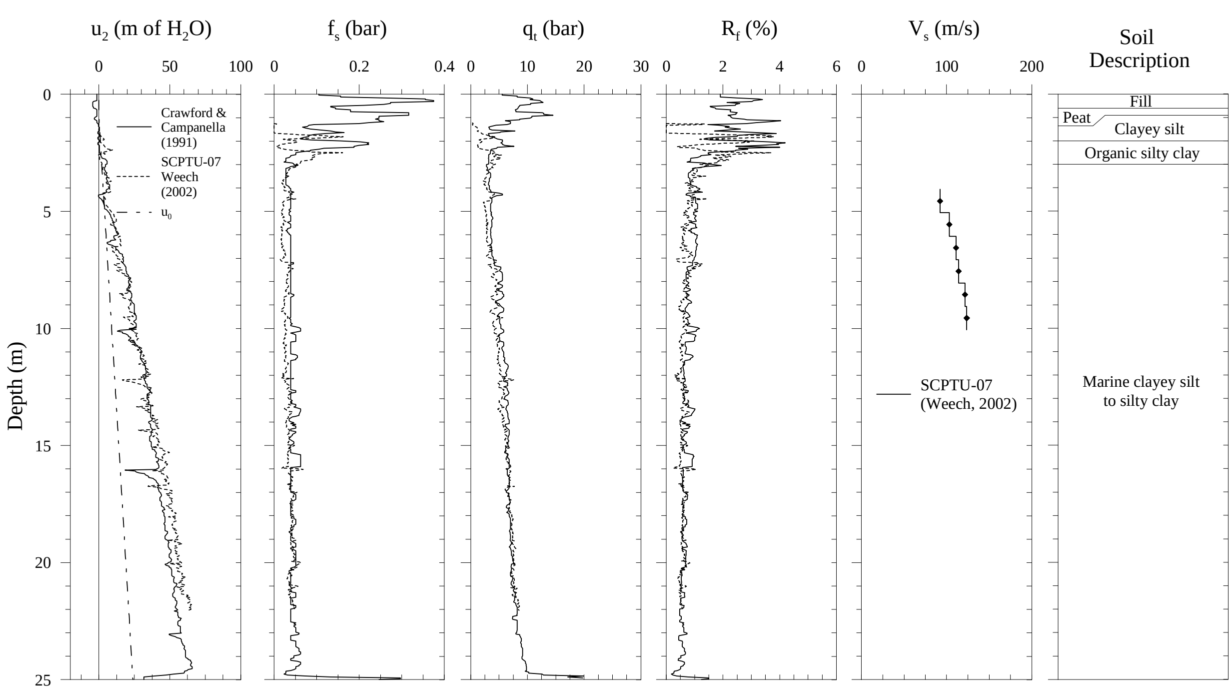

Figure 3.8 CPTU and SCPTU profiles at Colebrook Overpass site

(data from Crawford & Campanella, 1991; and Weech 2002).

Figure 3.9 shows that the location of the site tested by Crawford & Campanella (1991) is slightly different than those of the sites tested by Weech (2002) and the MoTH (1969). Even though the soil stratigraphy at this site is fairly homogeneous, the sensitivity (S_t) profiles shown in Figure 3.8 are quite different, suggesting a different soil fabric or structure at these sites. In addition, the different S_t values reported at this site may be associated with the type of vane used and the test procedures. It is believed that low S_t values reported by Weech (2002) are associated with soil disturbance caused by construction of the foundation for the overpass.

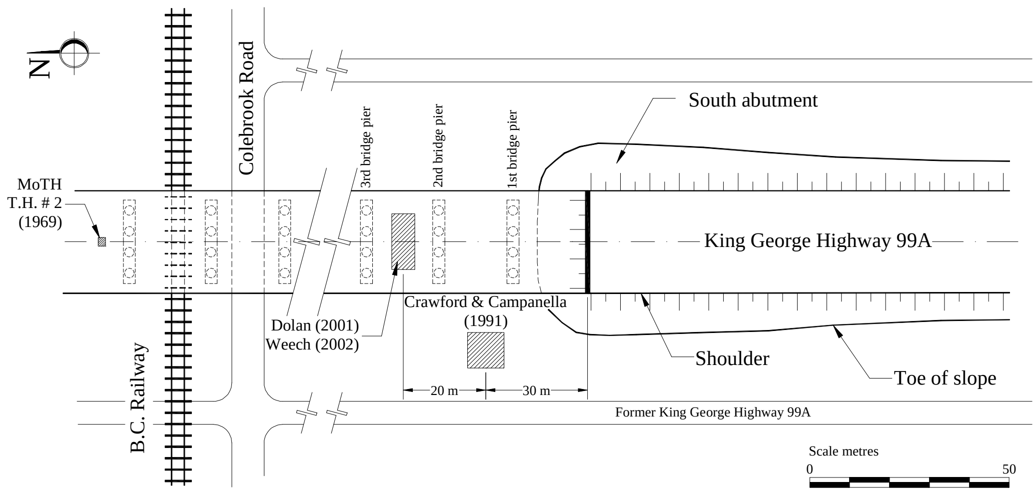

Figure 3.9 Approximate location of previous site investigations performed at the Colebrook Overpass site (adapted from Vyazmensky, 2005).

3.3.3 CANLEX Phase II sites

3.3.3.1 Background

The Canadian Liquefaction Experiment (CANLEX) was an extensive collaborative research project aimed at studying the phenomenon of soil liquefaction. The main objectives of the project were to: develop test sites to study sand characterization, develop and evaluate undisturbed sampling techniques, calibrate and evaluate in situ testing methods, and obtain an improved understanding of soil liquefaction.

The project was divided into four phases and both in situ testing and laboratory testing on undisturbed and reconstituted samples were performed at each site. Phase II of CANLEX was carried out at two sites located in the Fraser River Delta Region, which are the B.C. Hydro Kidd 2 Substation and the south end of the Massey tunnel. Both sites are located in Richmond, B.C. and consist of natural deposits of Fraser River sand. The soil conditions at the target depth ranges set by CANLEX management consist of natural deposits of Fraser River sand that are reasonably clean, uniform, loose and free draining. Wride et al. (2002) describe the in situ testing program performed at the CANLEX Phase II sites and present a summary of the interpretation of the results. A more detailed description of the analysis, calculation and correction procedures of the in situ tests can be found in the CANLEX Phase II reports by the UBC In-Situ Testing Group (1995a, 1995b).

3.3.3.2 KIDD 2 Substation, Richmond

3.3.3.2.1 Site location and description

The site is located at the northern margin of the Fraser River Delta in Richmond, B.C.; in the vicinity of the B.C. Hydro KIDD 2 Substation that is located east of the Oak Street Bridge and close to the intersection of No. 4 Road and River Road. The general outline of the site plan and location of the former CANLEX test area is shown in Figure 3.10.

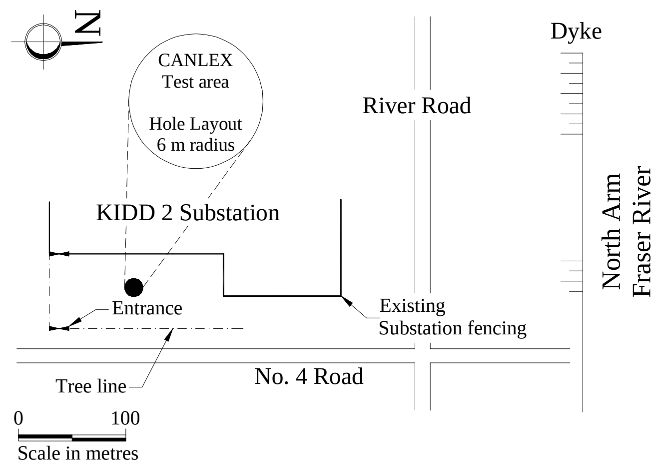

Figure 3.10 KIDD 2 former CANLEX test area (adapted from In-Situ Testing Group, 1995a).

3.3.3.2.2 Stratigraphy

As described by Monahan, et. al. (1995), three stratigraphic units can be recognized at the test site beneath a thin gravel fill (Figure 3.11). The first unit consists of laminated silt and very fine sand with organic laminae. The thickness of this layer is generally between 2 m and 5 m, but it thickens downward to at least 9 m in a linear trend across the substation, where it includes interbeds of medium sand. The second unit, where the CANLEX test and sampling zone was located, is generally between 3.6 m to 12.5 m thick, and consists of medium to coarse sands with granules, pebbles and silt clasts. The last unit consists of normally consolidated light grey clayey silt with scattered shells. This layer thickens southward from 10 m to 30 m across the substation and sharply overlies Pleistocene deposits. The test site is situated approximately 360 m from the North Arm of the Fraser River. At this location, the tidal fluctuations have a significant influence on the river level, and therefore the position of the water table changes throughout the day.

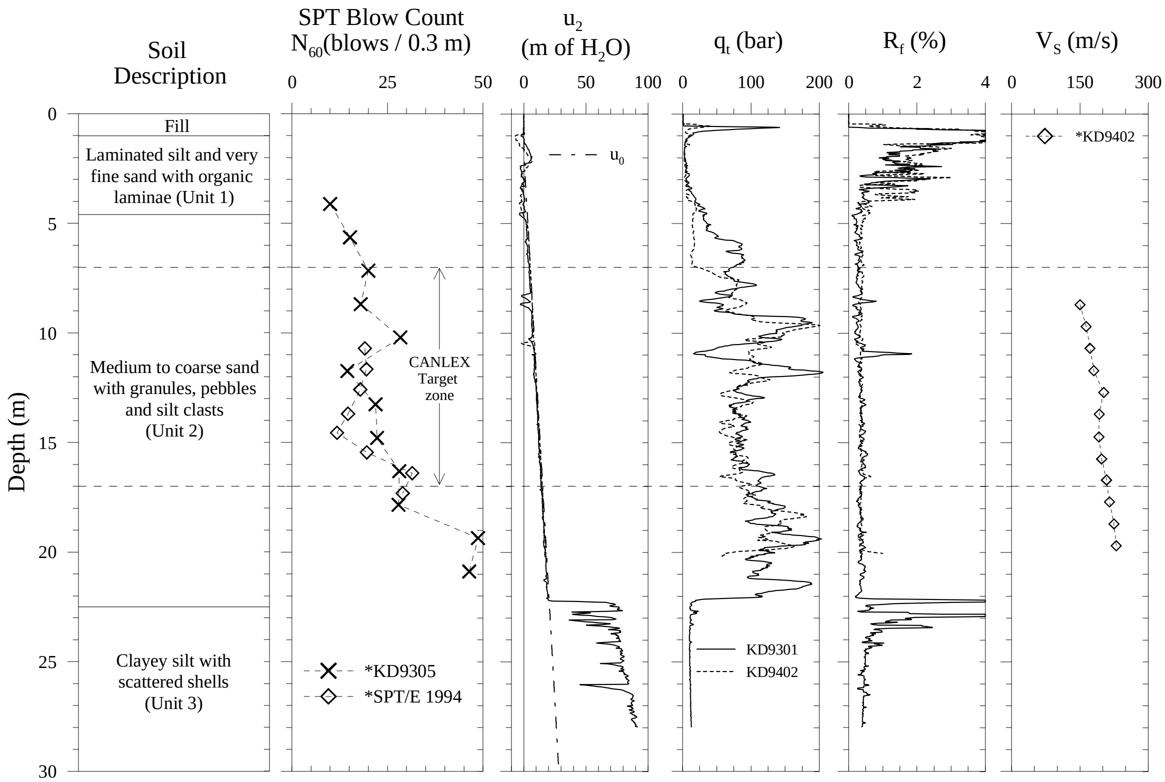

Figure 3.11 Soil profile at KIDD 2 site (data from In-Situ Testing Group 1995a).

3.3.3.3 Massey Tunnel, Richmond

3.3.3.3.1 Site location and description

The highway traffic tunnel is situated on Deas Island on the south side of the North Arm of the Fraser River and south of the city centre of Vancouver. As shown in Figure 3.12 the former CANLEX Phase II site is located near the south end of the Massey Tunnel and close to the southern portal, along the eastern side right-of way on Highway 99.

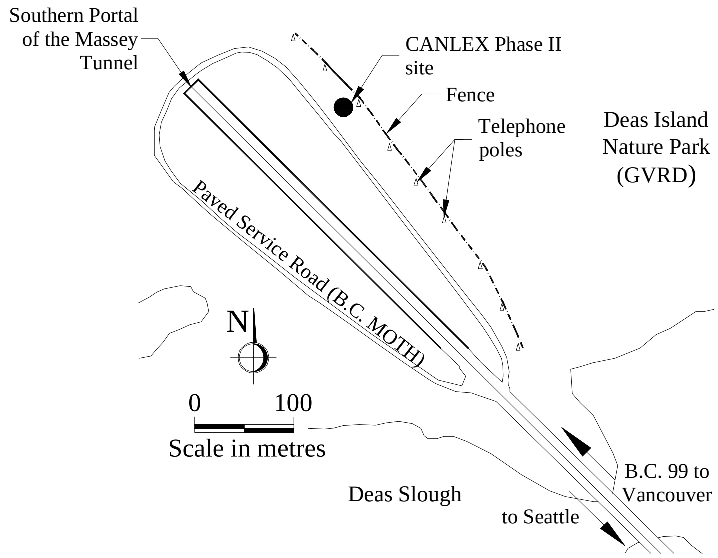

Figure 3.12 Massey Tunnel former CANLEX test area (adapted from In-Situ Testing Group, 1995b).

3.3.3.3.2 Stratigraphy

As shown in Figure 3.13 the test site is covered by a 2.2 m sand fill that overlies deltaic deposits, which can be subdivided into three units as suggested by Monahan et al. (1995). The first unit extends to a depth of about 4.9 m and consists of laminated sandy to clayey silt with scattered organics. This layer is underlain by Unit 2 where the soil is predominantly sand (generally <10% fines) with a thickness of about 26.8 m. The sand between 4.9 m to 17.1 m (Subunit 2a) contains occasional interbeds of medium sand, fine sand to silt with woody organic laminae and silty clay. The CANLEX target zone was located within this layer.

The Subunit 2a is underlain by a deposit of medium sand with some granules and pebbles that extends to a depth of about 21.4 m (Subunit 2b). Then, Subunit 2c (21.4 m to 31.7 m) consists mainly of fine to medium sand with locally abundant silt and concretion clasts and shells. Unit 3 consists primarily of silt interlaminated and interbedded with very fine sand and silty clay. Finally, the test site is located just about 250 m from the South Arm of the Fraser River. Therefore, the ground water conditions are also affected by tidal fluctuations in a similar way as in the KIDD 2 site.

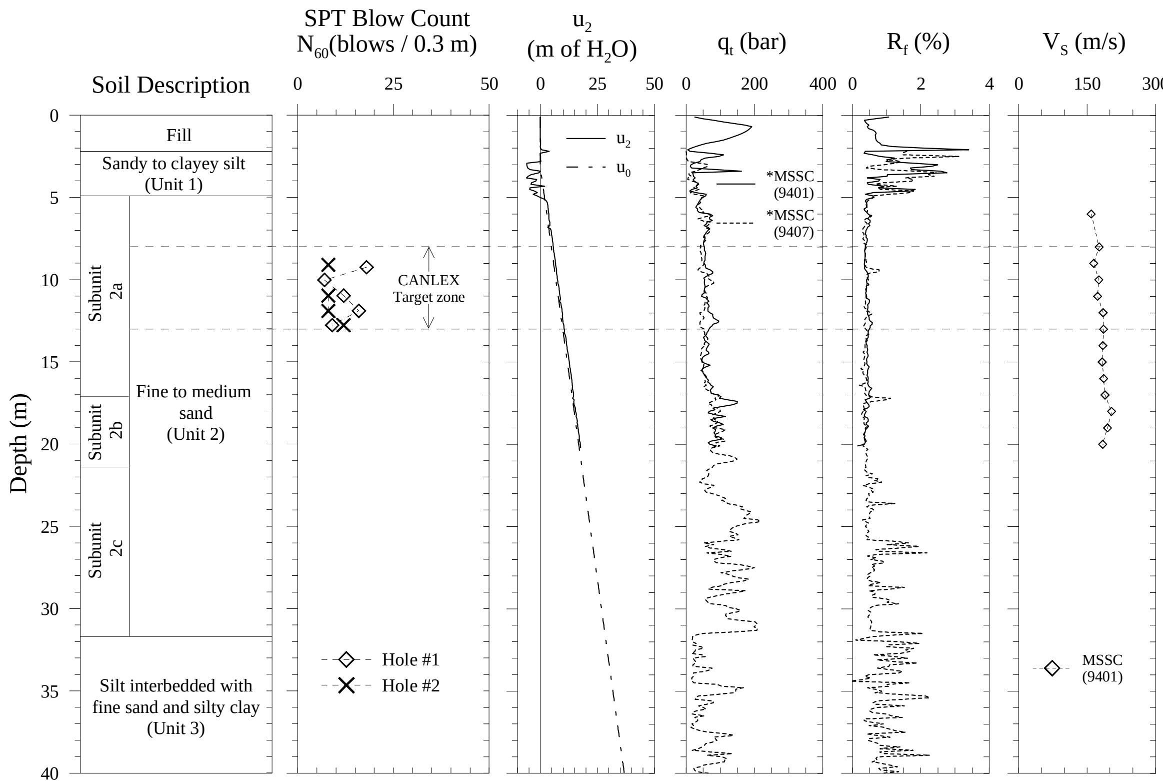

Figure 3.13 Soil profile at Massey Tunnel site (data from In-Situ Testing Group, 1995b).

3.3.4 Patterson Park, Delta

3.3.4.1 Site location and description

Patterson Park is located approximately 22 km south of downtown Vancouver, in Delta B.C., at the intersection of Ladner Trunk Rd. and Highway 17 (Figure 3.14). The park is located on the Fraser River Delta and within the area of a former horse race track. As shown in Figure 3.14 the test site is situated on the southern section of the park near the access road and adjacent to the former track.

Figure 3.14 Location of Patterson Park test site.

3.3.4.2 Stratigraphy

The stratigraphic profile at the test site is presented in Figure 3.15. Daniel (2003) notes that the general soil stratigraphy at this site consists of a thin layer of silt to silty clay overbank deposits overlying sand to silty sand deltaic and distributary channel deposits. The interpretation of in situ measurements and laboratory results reported by Daniel (2003) indicates that the soil column consists of a thin layer of fill in the order of 1 m thick overlying a 1.30 m thick layer of sensitive fines with traces of organics. The sensitive soil layer is underlain by a deposit of interbedded silt and silty fine grained sand which extends to about 7.35 m in depth. Below this layer the soil consists of compact medium grained to fine grained sand with occasional silt laminations to a depth of about 14.50 m. This layer is underlain by interbedded dense fine grained sand and silt that extends to the maximum depth reached of 28.80 m. Results of piezocone (CPTU) dissipations tests indicate that the water table was on average 0.4 m below ground surface at the time of investigation. Figure 3.16 presents the results two CPTU soundings that are located within the area where the current site investigation was performed.

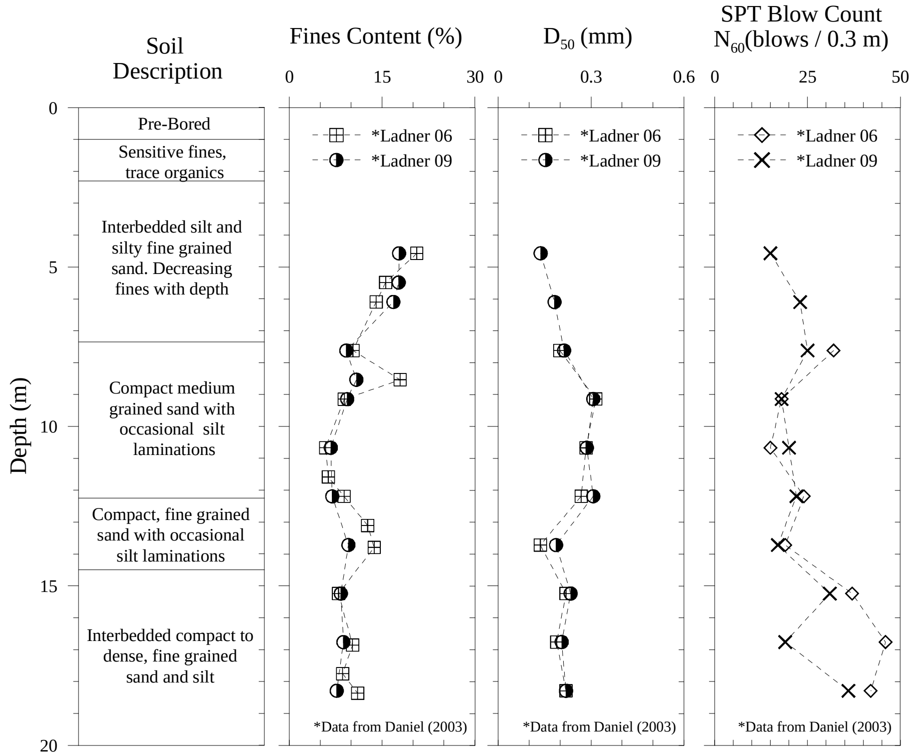

Figure 3.15 Soil profile at Patterson Park site (data from Daniel, 2003).

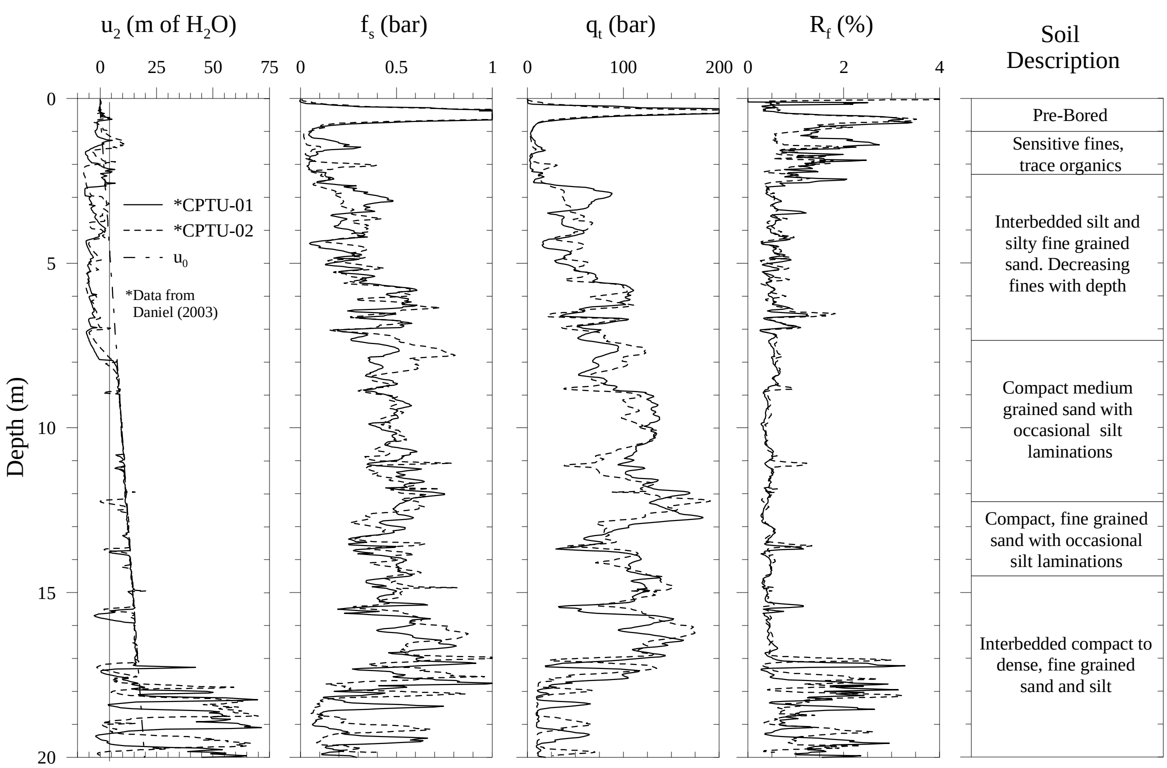

Figure 3.16 CPTU profiles at Patterson Park site (data from Daniel, 2003).

3.3.5 Dyke Road, Richmond

3.3.5.1 Site location and description

The site is located 19 km south of downtown Vancouver and north of the South Arm of the Fraser River, in close proximity to the intersection of No. 3 Road and the east end of Dyke Road in Richmond, B.C. As shown in Figure 3.17 the test site is situated right on the alignment of the south dyke trail.

Figure 3.17 Location of Dyke Road test site.

3.3.5.2 Stratigraphy

Figure 3.18 shows the stratigraphy at the test site with profiles of index parameters and strength parameters. The description of several samples recovered at boreholes drilled by the City of Richmond in at this site indicates that the soil stratigraphy at this site consists of an upper 3.5 m thick layer of coarse grained dyke fill material. The upper layer is underlain by a channel fill deposit of silt, clayey silt and sandy silt with thin sandy silt beds, organic laminae and rare shells, which extends to about 19 m in depth. Below this depth and to about 23 m in depth, the soil is predominantly fine to medium sand with some silt laminae and interbeds. This layer is underlain by the same stratigraphic sequence observed throughout the channel fill deposit, and extends to the maximum depth of 30.6 m reached in previous field work performed at this site.

As described by Sanin & Wijewickreme (2006), data from laboratory tests indicate that the upper part of the channel fill deposit are relatively uniform and of low plasticity. For this layer, they reported average values of 37.2% for the natural water content (w_N), 30.4% for the liquid limit (w_L), and 4.1% for the plasticity index (PI) respectively. Results of sieve analyses on disturbed samples retrieved at this site indicate that the channel fill silt deposit consists of silt with average fines content of 93.2%. Also, results of CPT and SCPTU tests performed by the City of Richmond in 2002 at the test site are shown in Figure 3.19 .

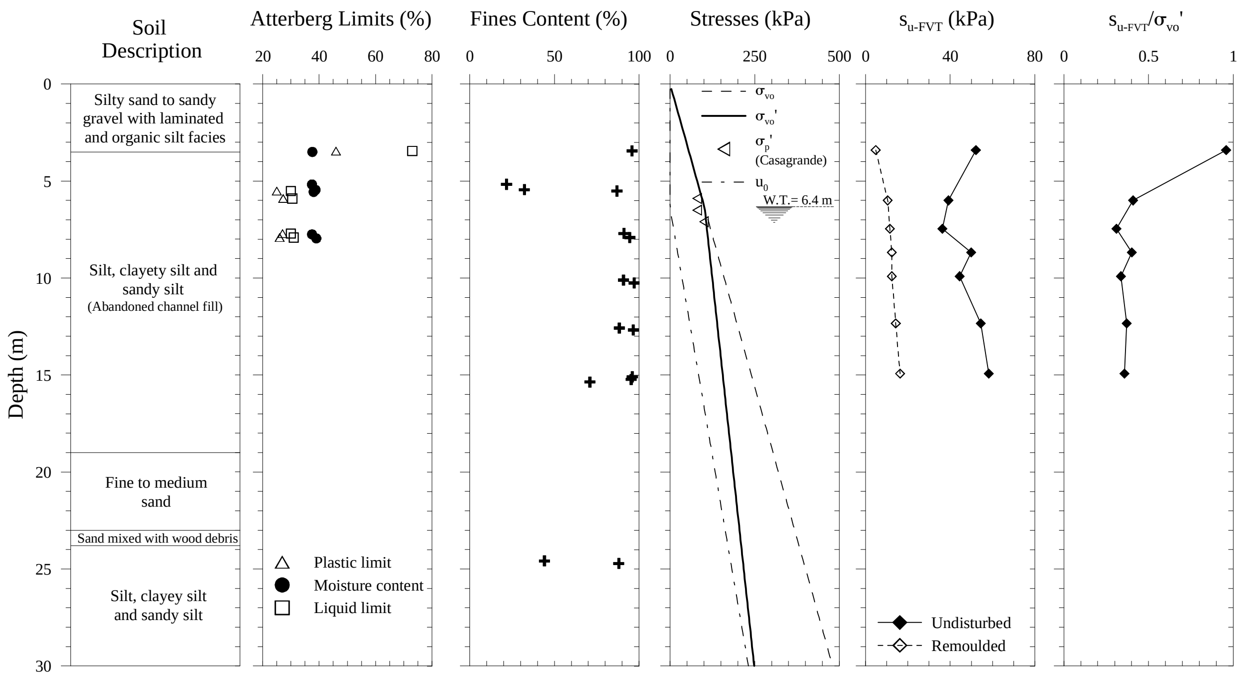

Figure 3.18 Soil profile at Dyke Road site (data from Sanin 2005 and Sanin 2008).

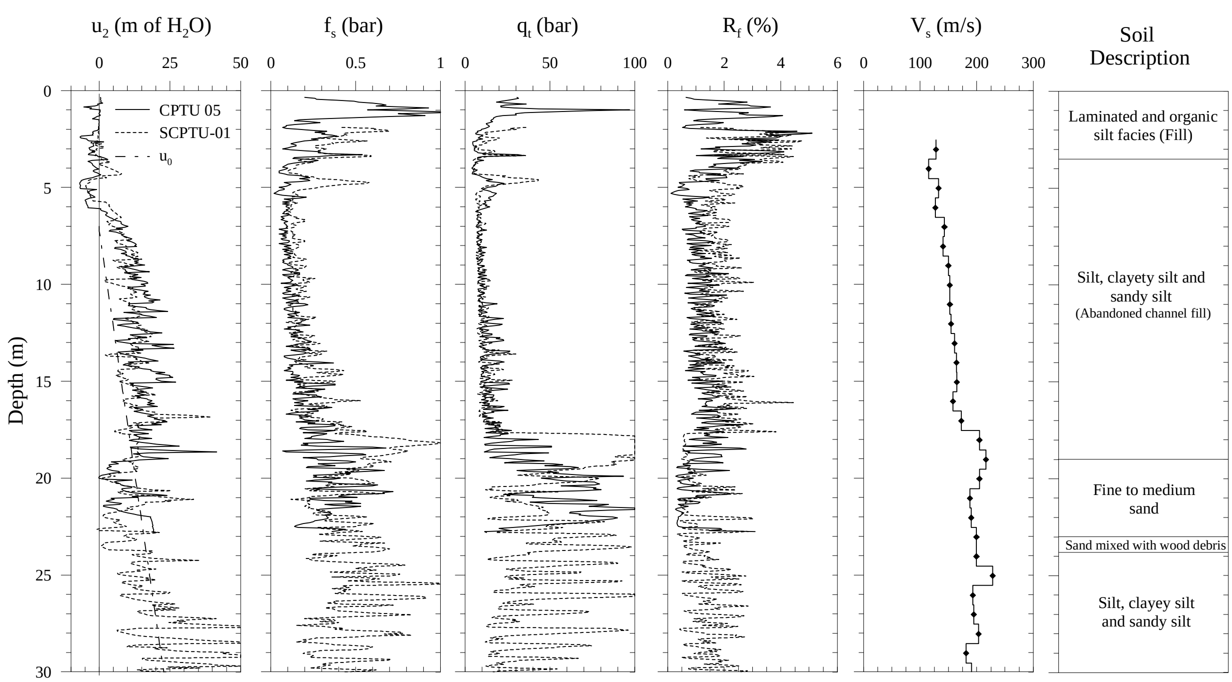

Figure 3.19 CPTU and SCPTU profile at the test site (data from Sanin, 2008).

The test site is located just 22 m from the South Arm of the Fraser River. Therefore, it is not surprising that tidal fluctuations exert a strong influence on the position of the water table, so that its location is not constant and varies throughout the day.

3.4 Field testing program

A comprehensive field testing program was performed by the author at 6 UBC research sites located in the Lower Mainland of B.C. (see Figure 3.1). Table 3.1 provides a summary of the type of in situ tests performed at each research site. At four sites, the characterization work consisted of soundings performed with the seismic flat dilatometer (SDMT) immediately adjacent to a sounding with the UBC lateral stress seismic piezocone (LSSCPTU) described in Chapter 5 of this thesis. The typical separation between tests was on average 2 m. At the remaining sites, the field work consisted primarily of SDMT tests. Field testing was carried out using the in situ testing research vehicle developed by the University of British Columbia (Campanella & Robertson, 1981) and equipment provided by ConeTec Investigations Ltd.

ConeTec Investigations Ltd. (Canada), TGC Geotecnia S.A. de C.V. (Mexico) and Diego Marchetti (Italy) provided access to additional DMT and SDMT data that covers a wide range of in situ measurements in different types of soil. A summary of this information is presented in Table 3.2.

Table 3.1 Summary of in situ tests performed by the author at research sites.

Site	Test Type	Test No.	Max. depth (m)	Dissipation tests
200th St. Overpass	SDMT	03	16.15	✗
	SCPTU	01	16.30	✗
Colebrook Overpass	SDMT	07	15.00	✗
	SDMT	08	10.25	✗
	LS-SCPTU	LSC-06	20.68	✗
	LS-CPTU	LSC-07	20.65	✓
KIDD 2 Substation	SDMT	01	23.91	✗
	SDMT	02	24.00	✗
	LS-CPTU	LSC-01	30.00	✓
	LS-CPTU	LSC-02	30.00	✓
	SCPTU	01-598D	24.90	✗
Massey Tunnel	SDMT	05	20.00	✗
	LS-CPTU	LSC-04	20.00	✓
	LS-SCPTU	LSC-03	20.00	✓
Patterson Park	SDMT	09	20.00	✗
	LS-SCPTU	LSC-05	20.00	✓
Dyke Road	SDMT	04	15.00	✗
	SDMT	06	15.00	✗

SDMT: Seismic flat dilatometer

DMT: Flat dilatometer

SCPTU: Seismic piezocone

LS-CPTU: Lateral stress piezocone

LS-SCPTU: Lateral stress seismic piezocone

Table 3.2 Summary of additional SDMT and DMT data.

Source	Site	Location	Test Type	Max. depth (m)	Soil type
ConeTec Investigations Ltd.	FMC	Calgary, AB	SDMT	12.50	Sandy silt and silty clay till
			SDMT	13.00	
			SDMT	20.00	
	HC	High Prairie, AB	SDMT	25.00	Soft to firm silty clay
	Sea Island	Richmond, B.C.	SDMT	29.90	Silty sand and soft clayey silt
			DMT	11.00	Silty sand
			DMT	20.00	Silty sand and soft clayey silt
	113B	Maple Ridge, B.C.	SDMT	19.40	Silt with occasional sand layers and marine clay
	Lougheed Hwy	Port Coquitlam, B.C.	SDMT	20.50	Soft silt to medium and dense silty sand
	Still Creek Rd.	Burnaby, B.C.	DMT	14.00	Soft silty clay to clay
TGC Geotecnia	Chicle & Azafran	Mexico City	DMT	37.25	High plasticity Mexico city soft clay
			DMT	37.80	
Diego Marchetti	Treporti	Venice, Italy	DMT	47.00	Interbedded sands, silts and silty clays
			DMT	45.40	

SDMT: Seismic flat dilatometer

DMT: Flat dilatometer

Chapter 4 EVALUATION OF SEISMIC FLAT DILATOMETER

4.1 Introduction

The first section of this chapter presents an assessment of the performance in the field of the system developed for the acquisition and interpretation of shear wave velocity measurements with the DMT seismic module. Also, the V_s profiles obtained at several research sites with the seismic flat dilatometer (SDMT) are compared to V_s data from other in situ testing techniques such as the seismic piezocone (SCPTU).

The second section, presents a description of the results of seismic flat dilatometer (SDMT) testing performed in coarse and fine grained soils at six research sites located in the Lower Mainland of British Columbia. The field measurements obtained at research sites from SDMT tests have been summarized for ease of description and comparison. Complete profiles containing in situ measurements and intermediate parameters for all research sites are presented in Appendix A of this thesis.

The last two sections of this chapter describe several relationships identified from SDMT and DMT data collected at research and additional sites listed in Table 3.1 and Table 3.2. Then, based upon these relationships, a new SDMT based soil behaviour type system is proposed and a new empirical correlation for estimation of shear wave velocity (V_s) from DMT data is proposed. Similarly, existing empirical approaches for estimation of the coefficient of earth pressure at rest (K_0) in both sand and clay from DMT parameters are carefully reviewed and new empirical correlations are proposed.

4.2 Assessment of the seismic DMT module

4.2.1 Data acquisition system

The downhole seismic flat dilatometer test (SDMT) provides a simple and cost-effective means for determining the soil stratigraphy, the shear modulus at small strains from shear wave velocity (V_s) measurements, as well as estimating deformation and strength parameters from empirical correlations to DMT parameters. The SDMT test procedure is relatively simple and the software developed by the manufacturer allows real time handling of seismic and standard DMT data. The software (SDMT Elab) has the advantage of presenting on the computer screen the magnitude of the interpreted V_s after the system is triggered and the source waves are generated. Also, the V_s profile can be displayed on the computer screen and it is updated after each test.

The system developed by the manufacturer (Studio Prof. Marchetti) allows triggering of data acquisition in three different ways: (i) automatic, (ii) external and (iii) immediate. Further information on the description of these options can be found in section 2.3.2.4 of this thesis. In the work reported in this thesis, the first two methods were used. Several problems were experienced with the SDMT data acquisition system when performing V_s measurements in the field. For example, when the shear beam was hit for the first time an error was displayed on the computer screen (CHECK SUM ERROR) and data was not recorded. The CHECK SUM error means that the communication between the seismic module and the data acquisition system is not correct, and it may be a result of the following factors:

1. The membrane is not in contact with the blade and the buzzer is off before switching the system to seismic mode.
2. The pneumatic-electric cable is broken or damaged.
3. The ground cable is not in good contact with the rods and/or control box.
4. The cables of the seismic module are not well connected to the blade or the isolation of these connections has been damaged.

In order to overcome the first problem, it is important to ensure that the membrane is in contact with the blade and the sound is on before performing the seismic test. However, if the buzzer is off after the membrane returns to the A position the blade should be pushed a little bit further down until the sound begins again. The electrical continuity between the control unit and the DMT blade is essential for a good transmission of signals from the seismic module to the surface. Therefore, it is necessary to ensure that there is good electrical contact between the ground cable and the rod string, rather than on a rusty part of the pushing ram.

It was also noticed that the automatic trigger was influenced by external vibrations (e.g. CPT truck or nearby traffic) when the seismic test was performed at shallow depths (e.g. less than 2 m). If this is the case, the truck should be turned off for the shallow measurements. Once the probe is deep enough, vibrations will not affect the automatic trigger. However, if the problem continues it may be either due to the alternating current of the power supply of the computer or due to the high frequency of the external source (e.g. compaction plates or rollers). The former problem can be solved by substituting the computer power supply by a direct current power source. The response of the external trigger can also be affected by the alternate current power supply of the computer, and therefore the same solution procedure should be followed.

Marchetti (2008) points out that at a certain depth (generally around 15-20m, according to soil stiffness), the automatic trigger will not recognize the hammer hit any more. In this case, the first thing to do is to increment the sensitivity parameter and retry. The automatic trigger will then work for some more metres until it is incapable of generating a trigger signal, which may lead to immediate triggering. Therefore, at this stage of the test it is necessary to switch to external trigger. By careful observation of these procedures, shear wave velocities can be gathered rapidly during pauses in penetration. The average production rate is on average 7 to 9 m/hour depending on the experience of the operator and soil conditions.

4.2.2 Evaluation of V_s measurements

4.2.2.1 Coarse grained-soils

Figure 4.1 shows the profiles of shear wave velocities measured with downhole seismic tests performed using the SDMT at sites with predominantly coarse-grained soil deposits, i.e. KIDD 2, Massey Tunnel and Patterson Park. For comparison at both CANLEX Phase II sites (KIDD 2 and Massey Tunnel) the results of seismic cone penetration tests reported by In-Situ Testing Group (1995a, 1995b) are also included. Similarly, at the Patterson Park site, the results of SDMT tests are compared to V_s values obtained using the seismic piezocone (SCPTU) described in Chapter 5 of this thesis.

As can be noted from Figure 4.1(a), the V_s profiles measured at the KIDD 2 site show a remarkably good agreement between both SDMT tests. The shear wave velocity (V_s) increases slightly from about 89 m/s at 2 m to 147 m/s at 5 m and then increases to a value of 190 m/s at 9.5 m depth. Below this depth and to about 24 m depth V_s stays approximately constant with average values of 218 m/s to 227 m/s. However, as illustrated in Figure 4.1(a), from 19.5 m to 24 m V_s values vary between about 220 m/s and 277 m/s. The shear wave velocity profiles determined from the SDMT tend to be higher than those reported for the CANLEX target zone. This may be attributed to site variability as indicated by the variability of q_t values shown in Figure 3.11.

Moreover, at the Massey Tunnel site the agreement between the V_s profile determined by the SDMT and that from the V_s CANLEX profile is remarkably good. However, Figure 4.1(b) shows that below about 15 m depth V_s values obtained from the SDMT test are on average slightly larger than those reported by In-Situ Testing Group (1995b). The difference may be attributed to lateral and vertical soil variability between soundings below about 15 m depth.

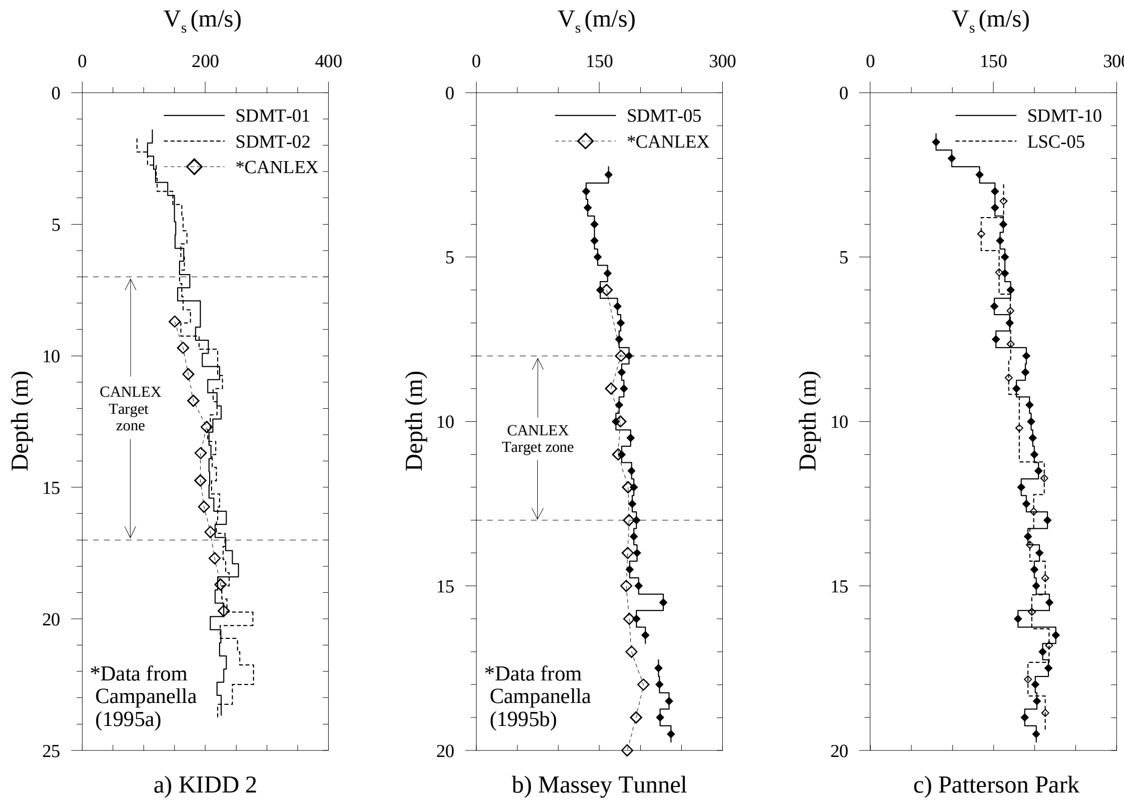

Figure 4.1 Summary of SDMT V_s measurements in coarse-grained soils compared to SCPTU data.

Figure 4.1(c) shows that the V_s profile obtained from SDMT tests is very similar to that from the results of lateral stress seismic piezocone (LSSCPTU) tests. However, the SDMT V_s profile shows more variations over the full depth, suggesting that the results are likely to be more sensitive to stratigraphic details because of the 0.5 m depth interval used for V_s determination as opposed to the 1 m interval in the LSSCPTU test.

4.2.2.2 Fine grained-soils

Figure 4.2 presents a summary of profiles of shear wave velocities (V_s) measured with downhole seismic tests performed using the SDMT at sites with predominantly fine-grained soil deposits, i.e. Colebrook Overpass, Dyke Road and 200th Street Overpass. For comparison, the results of seismic piezocone (SCPTU) and lateral stress seismic piezocone (LSSCPTU) tests are included in the same figure.

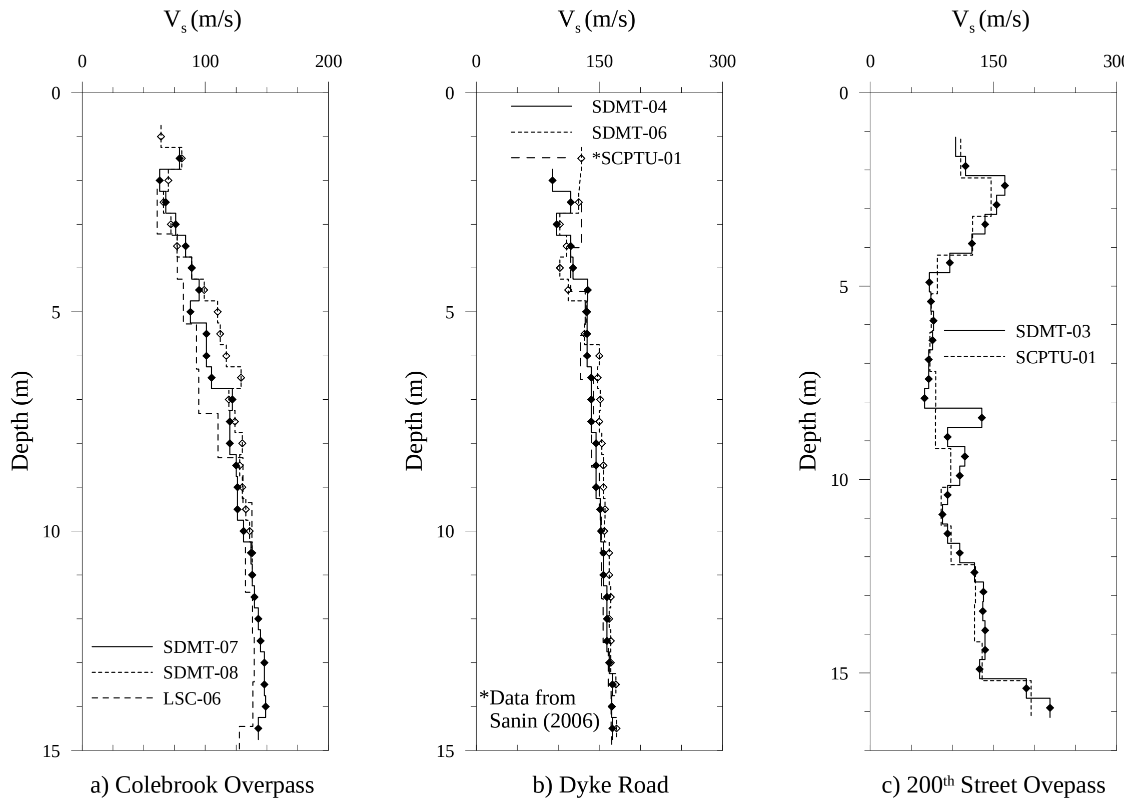

Figure 4.2 Summary of SDMT V_s measurements in fine-grained soils compared to SCPTU data.

At the Colebrook Overpass site, V_s profiles were determined from results of seismic dilatometer (SDMT) and lateral stress seismic piezocone tests (LSSCPTU). Figure 4.2(a) compares the V_s profiles determined with both tests methods. All V_s profiles exhibit similar trends with the exception of a minor variation between about 4.5 m to 8 m depth, where higher V_s values were measured in the second SDMT test (SDMT-08). The difference in V_s values may be attributed to the higher stiffness of the soil at this depth associated with a higher degree of overconsolidation (see Figure 3.7).

Figure 4.2(b) shows that at the Dyke Road site there is a good agreement between the shear wave velocity profiles determined by the seismic flat dilatometer (SDMT) and the seismic piezocone (SCPTU) test performed at this site in previous investigations. The profiles of shear wave (V_s) velocities from both SDMT tests are very similar with the exception of slight variations between about 3.5 m and 4.5 m depth. The variation in V_s may be attributed to lateral soil variability. Despite the fact that the CPTU and SCPTU penetration data presented in section 3.3.5.2 of this thesis indicate a very thin layering at this site, the results of SDMT and SCPTU tests show that V_s increases gradually from 135 m/s at 5 m to about 171 m/s at 14.5 m. These data suggests that the layering effect would be averaged by the V_s measurements.

As can be seen from Figure 4.2(c) the profiles of shear wave velocities determined by the SCPTU and the SDMT at the 200th Street Overpass are very similar with the exception of a variation at 8.4 m. To investigate the reasons for this difference, the wave traces were examined closely. Figure 4.3 shows the recorded waves at depths of 7.9 m to 8.9 m. At 7.9 m and 8.9 m, the initial portions of the shear waves are very similar and would correlate well during cross-correlation. However, at 8.4 m, the early parts of the waves are very different and would not correlate well. Examination of the seismic flat dilatometer profile shown in Figure 4.4 does not indicate anything unusual. However, the SCPTU profile presented Figure 4.5 indicates the presence of a sand lens at about 9.5 m depth. It is likely that the early portions of the waves close to a sand lens are being affected by reflections from this lens.

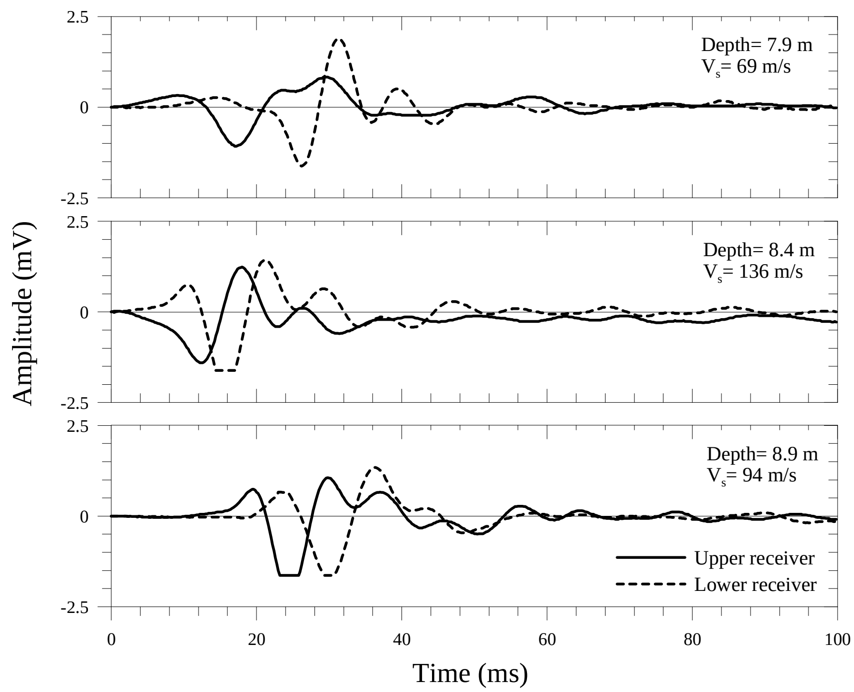

Figure 4.3 Recorded shear wave traces from the SDMT from depths 7.9 to 8.9 metres, 200th Street Overpass.

On the basis of this observation, it is suggested that the early portions of the waves close to the lens at 8.4 m depth are affected by reflections from the sand lens. It is also interesting that at 12.8 m and below about 15.4 m depth, V_s values from SDMT tests are higher than those from SCPTU tests. It is considered likely that reflections from the clayey silt lens and till affected V_s measurements at these depths. Over the full depth, the SDMT values are likely to be more sensitive to stratigraphic details because of the 0.5 m depth interval used for V_s determination as opposed to the 1 m interval commonly used in the SCPTU. This illustrates that it is necessary to review carefully each set of seismic traces in order to detect anomalies in the results that may affect the interpreted shear wave velocity, instead of using the SDMT as a "black box". It also illustrates the advantages of using combinations of in situ tests to delineate soil stratigraphy and soil properties.

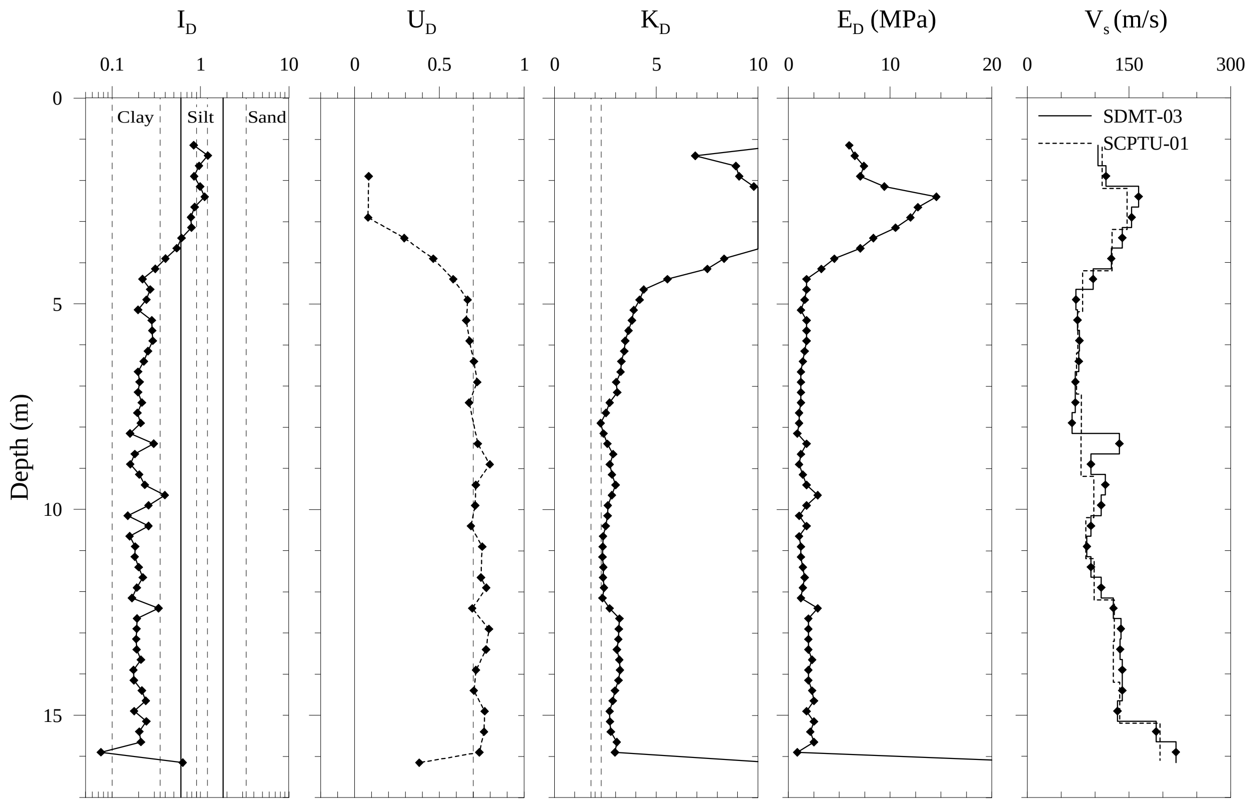

Figure 4.4 SDMT data recorded at 200th Street Overpass.

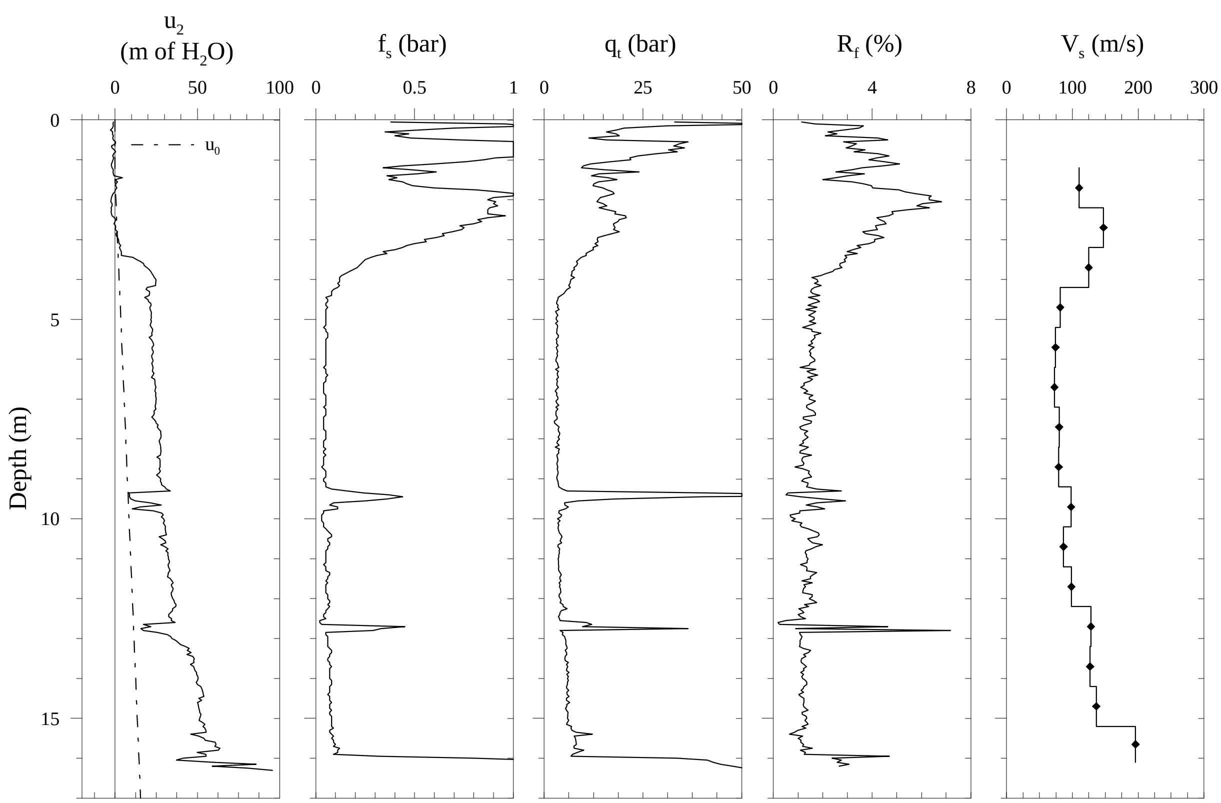

Figure 4.5 SCPTU data recorded at 200th Street Overpass.

4.3 Description of SDMT data

In situ test measurements can be interpreted to define soil behaviour type and site stratigraphy prior to the analysis of field data for estimation of geotechnical parameters. The description and analysis of in situ test results from standard dilatometer (DMT) tests has been extensively researched and has been addressed by various researchers (e.g. Marchetti et al., 2001). However, the benefits of the additional information obtained in the seismic dilatometer (SDMT) test have received limited attention since the introduction of the equipment for commercial applications is fairly recent (Foti, et al., 2006). Indeed, the interpretation of SDMT data has been mainly focused on relationships between small strain shear modulus (G_0), dilatometer modulus (E_D) and constrained dilatometer modulus (M_{DMT}) (e.g. Marchetti, et al, 2007; Marchetti, et. al., 2008a; Marchetti, et al, 2008b).

The configuration of the commercial version of the DMT seismic module allows determination of V_s at 0.5 m intervals. In the work described in this thesis, DMT measurements were taken at 0.25 m. Therefore, it has been possible to calculate the ratio (G_0/E_D) from either averaged E_D values over a 3 readings window, or by using the E_D value obtained in the interval over which the V_s value was obtained, herein termed a "single" point calculation. These depths correspond to the mid-point between the two receivers. E_D values above and below this depth correspond to the locations of the upper and lower receivers installed in the seismic DMT module. The magnitude of E_D represents the response of the soil adjacent to the membrane, whereas V_s reflects the average shear wave velocity of the 0.5 m zone within the upper and lower receiver.

Eslami & Fellenius (1997) discussed the use of averaging of the cone tip resistance (q_c) to determine an average value of q_c representative of the failure zone below and above the pile toe. They argue that filtering the cone data is necessary, because if a mean were produced from the unfiltered data, occasional unrepresentative high and low values would have a disproportionate influence. Two types of averaging techniques can be used: arithmetic and geometric. They point out that the former is only useful where q_c values are uniform, i.e. very uniform soils, and therefore filtering is necessary in most cases. Alternatively, Eslami & Fellenius (1997) suggest that a filtering effect can be achieved directly by calculating the geometric average of q_c values rather than using an arithmetic average. Also, the geometric mean is closer to the dominant value, as opposed to the arithmetic average. On the basis of this argument, this section also discusses the difference between G_0/E_D profiles obtained from geometric average values of E_D, obtained over a 3 readings window, and those based upon "single" point values.

4.3.1 CANLEX Phase II sites

4.3.1.1 KIDD 2

A summary of SDMT profiles for the two soundings carried out at the KIDD 2 site is presented in Figure 4.6. The dilatometer material index (I_D) profiles of both tests indicate that the surficial materials are mainly silty clay to silt, and that from 3 m to 22 m the soil is predominantly silty sand with occasional lenses of sandy silt. Despite the fact that SDMT tests were carried out about 2.5 m apart, the soil classifications differ slightly from one test to the other. Nonetheless, the I_D parameter clearly identifies the transition from sand to clay below about 22 m. Also, both pore pressure index (U_D) profiles show clearly the changes in soil stratigraphy by identifying the transition from permeable ($U_D \approx 0$) to impermeable ($0<U_D<0.7$) layers.

The material index (I_D) soil classification is in fairly good agreement with the soil profile previously described in section 3.3.3.2.2 of this thesis. However, the results of laboratory index tests on samples recovered within the CANLEX target zone, i.e. 7 m to 17 m, indicate an approximate average fines content of <5% (Wride, et al., 2000). The apparent misinterpretation of soil type with I_D, when interpreting DMT data in sandy soils, was recognized by McPherson (1985). He concluded that soil classification based upon I_D tends to predict a finer soil than really exists. On the other hand, the results in Figure 4.6 show that the DMT soil identification can be complemented with the pore pressure index (U_D), which indicates the effect of undrained and drained DMT penetration.

In the sand deposit, K_D varies from 1.3 to 7.4 with an average value of 3.3 to 4.1, whereas in the clay layer below 22 m depth, K_D varies between 1.8 and 2.4. Marchetti (1980) argues that a K_D in clay above about 1.8 to 2.3 indicates the presence of over-consolidation or of a structured soil. Based upon this criterion, the K_D profile suggests the soil is close to normally consolidated below about 22 m depth and unlikely to be structured. In addition, despite the scatter in both I_D and K_D profiles the dilatometer modulus (E_D) profile recorded in both tests is very similar.

The G_0/E_D profile shown in Figure 4.6 gives an average value of about 2.3 in the sandy silt, silty sand and sand, indicated by $I_D>1.2$ and $U_D \approx 0$, i.e a “permeable” layer., In fine grained soils, i.e. $I_D<1.2$ and $U_D>0$, the magnitude of G_0/E_D is considerably higher. Also, it is noted from Figure 4.6 that there is practically no distinction between the “single” point and geometric mean profiles of G_0/E_D in these fairly homogeneous coarse grained soil deposits. However, in the stratified fine grained soils located below about 22 m depth, the scatter in G_0/E_D values is larger than in the coarse grained soils. Also, it is interesting to note that small variations in measured shear wave velocities significantly affect the magnitude of the small strain shear modulus ($G_0=\rho V_s^2$) and therefore the ratio G_0/E_D. The G_0/E_D profiles presented in Figure 4.6 suggest that in stratified fine grained soil deposits, a smoother profile is obtained when the geometric mean is used rather than a "single" point calculation.

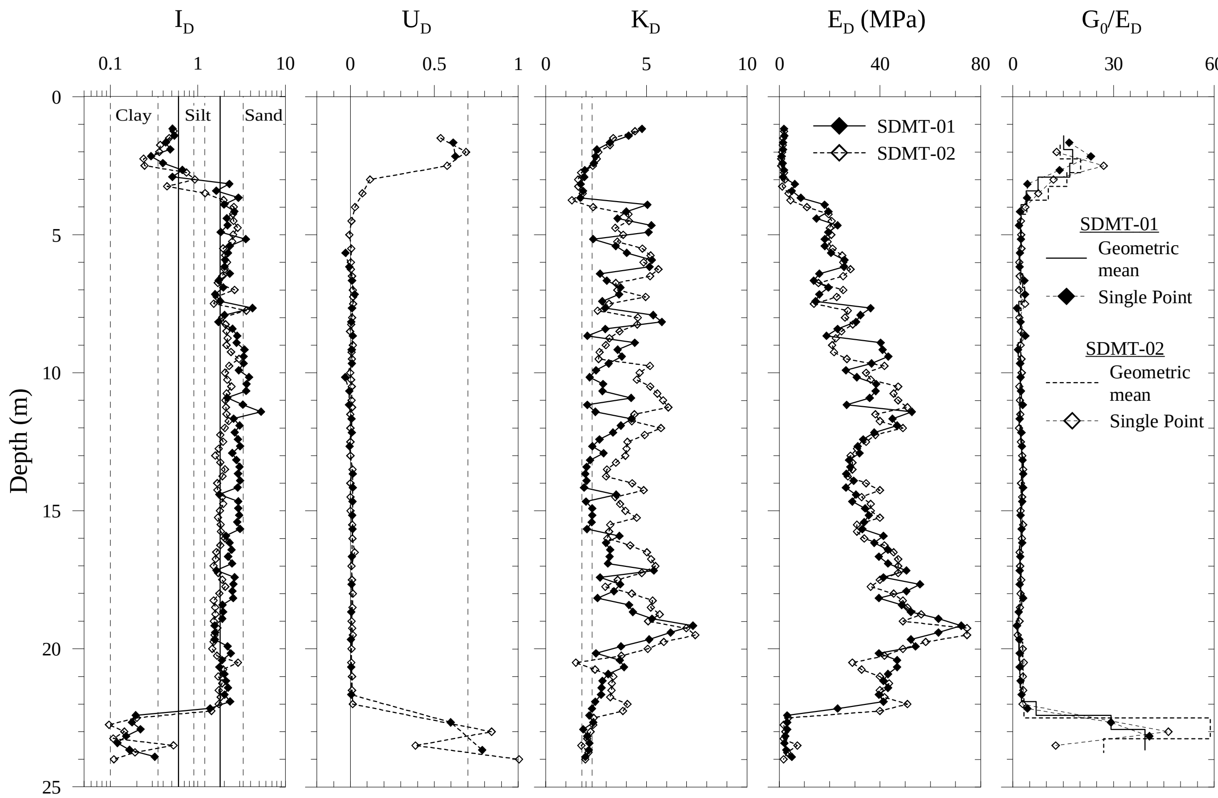

Figure 4.6 SDMT Profiles, KIDD 2.

4.3.1.2 Massey Tunnel

The plots of intermediate DMT parameters and results of seismic dilatometer tests are shown in Figure 4.7. The dilatometer material index (I_D) profile indicates the presence of silty sand with a few interbeds of silty clay and silt above 5 m depth, underlain by predominantly silty sand to the maximum depth of 20 m. Wride et al. (2000) report approximate average fines content in the CANLEX target zone of <5%. Hence, the DMT soil behaviour type profile provides a good indication of soil type at this site. The pore pressure index (U_D) profile clearly shows that the sand deposit is free draining. However, below about 16 m U_D is slightly above zero, which indicates that pore pressure is generated during penetration and has still not fully dissipated when the DMT expansion begins. This suggests an increase in fines content.

The horizontal stress index (K_D) profile provides indication of an upper overconsolidated crust and, below about 1.8 m, K_D varies from 2.1 to 8.5. It is observed that the dilatometer modulus (E_D) profile closely mimics the shape of K_D and appears to increase gradually with depth.

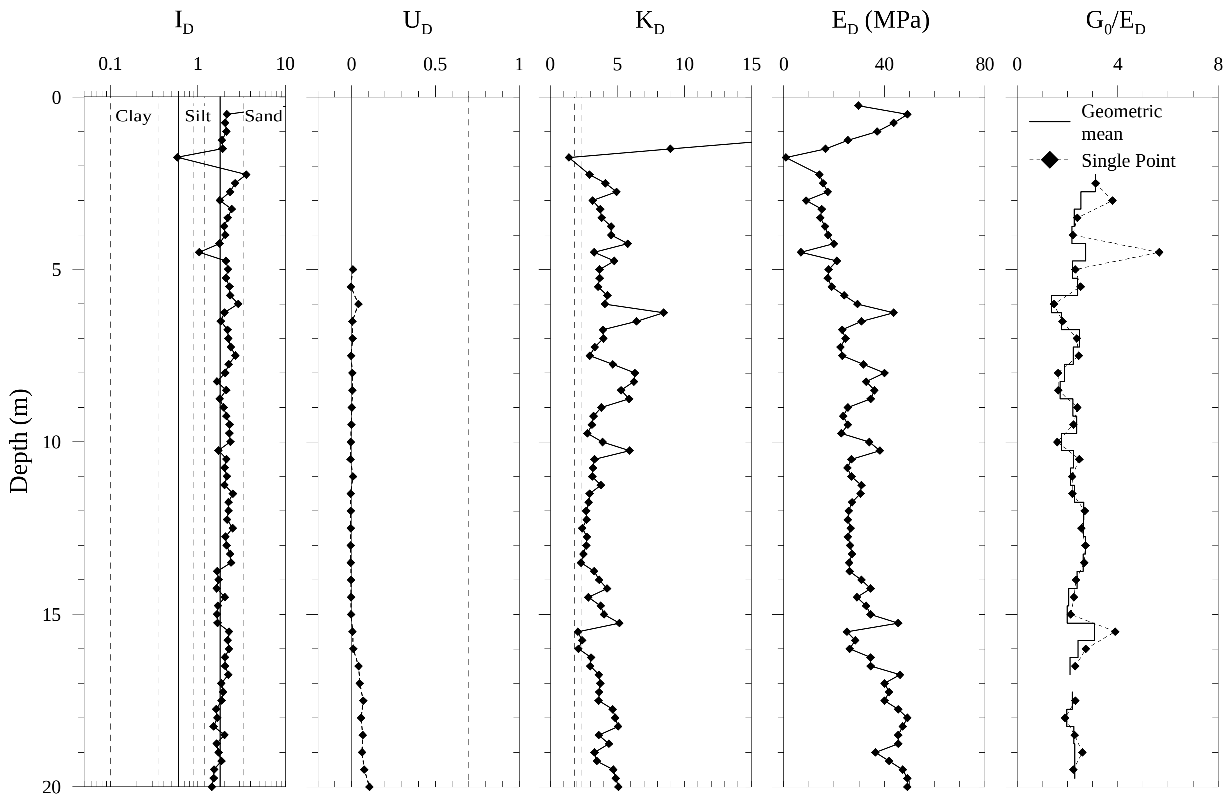

Figure 4.7 SDMT profile, Massey Tunnel.

In addition, the G_0/E_D profile indicates that the "single" point based profile is more sensitive to low E_D values than that based upon geometrically averaged G_0/E_D values. From the latter, it is observed that for the data obtained at this site, the ratio G_0/E_D varies from 1.4 to 3.1 with an average of 2.3 for soils with I_D>1.2 and $U_D \approx 0$. This is the same average value of G_0/E_D obtained at the KIDD 2 site for sandy soils.

4.3.2 Patterson Park

A summary of intermediate DMT parameters and results of seismic dilatometer tests is shown in Figure 4.8. The material index (I_D) profile indicates the presence of a thin layer of silty sand which is underlain by silt to clayey silt to sandy silt to 2.5 m depth. The DMT soil profile is very similar to that reported by Daniel (2003), which has been previously described in section 3.3.4.2. The interpreted high values of both horizontal stress index (K_D) and dilatometer modulus (E_D) within the upper 0.50 m suggest that the material may corresponds to traces of discontinuous pavement. Below about 2.5 m, the I_D profile indicates a deposit of silty sand to sandy silt that extends to about 17.8 m depth. The transition from silty sand to interbedded silty clay and silty sand is detected below about 18 m.

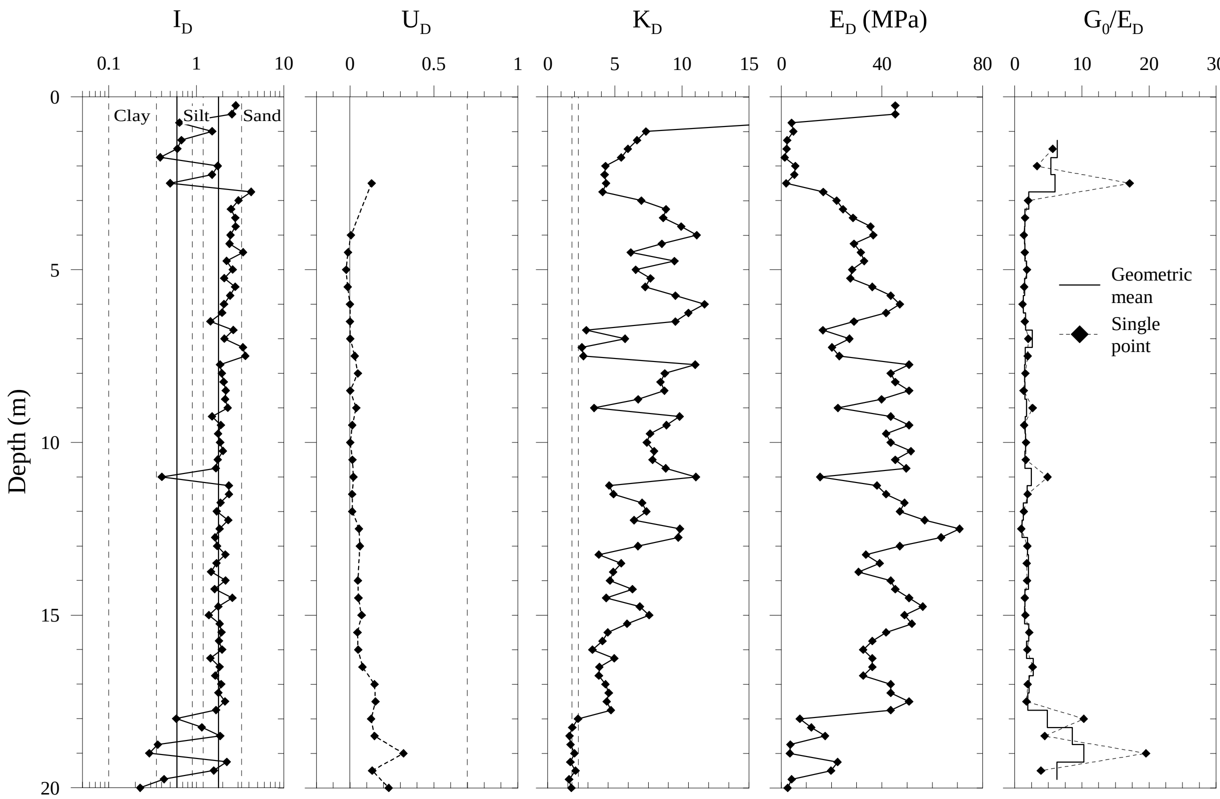

Figure 4.8 SDMT profile, Patterson Park.

Marchetti et al. (2001) suggest that in "permeable" layers $U_D \approx 0$, whereas in "impermeable" layers U_D=0.7, and U_D values between 0 and 0.7 corresponds to "intermediate permeability" layers. On the basis of this criterion, the pore pressure index (U_D) profile suggests that above 4 m depth the soil is non free draining and of intermediate permeability. From 4 m to about 12 m depth, the pore pressure index profile is approximately constant with $U_D \approx 0$, which suggests that the silty sand layer is "permeable". Then, from 12.5 m to 20 m depth the magnitude of the pore pressure index increases slightly from 0.05 at 12.5 m to 0.23 at 20 m with a maximum value of 0.32 at 19 m depth.

It is interesting to note from Figure 4.8 that the I_D profile indicates a silty clay lens at 11 m depth. However, the corresponding U_D parameter at this depth indicates the presence of a free draining soil ($U_D \approx 0$). The piezocone pore pressure profiles reported by Daniel (2003) indicate at this depth pore pressure values below hydrostatic suggesting the presence of dilative soils such as dense sand or stiff fine grained soil (see Figure 3.16).

In addition, from 0.75 m to about 16.5 m, the K_D profile fluctuates considerably in magnitude between about 2.5 and 11.7. The variation in K_D values throughout the soil profile may be an indicator of changes in gradation and density. From 16.5 m to 17.75 m depth, K_D stays approximately constant at about 4.3. From 17.75 m to 20 m depth, it drops off to an average value of 1.8. Based upon the criterion proposed by

Marchetti (1980) and neglecting the zones in the vicinity of the sand lenses, K_D suggests that the interbedded silty clay to clay is normally consolidated below about 18 m.

The G_0/E_D profile obtained at Patterson Park is very similar to that obtained at the KIDD 2 site. At first glance, it is noted that in stratified fine grained soils a smoother G_0/E_D profile is obtained when geometrically averaged values are used rather than "single" point based calculation. Figure 4.8 shows that in soils with I_D>1.2 and $U_D \approx 0$, the calculation method does not affect the magnitude of G_0/E_D. From 2.5 m to about 17.5 m, G_0/E_D varies between 1.1 and 2.8 with an average of 1.8, whereas for the upper and lower stratified fine grained soil deposits average values of 5 and 7.5 are obtained, respectively.

4.3.3 Colebrook Overpass

Figure 4.9 presents a summary of intermediate dilatometer parameters and results of shear wave velocity measurements from SDMT tests. The I_D profile indicates a surface crust of sand to clayey silt overlying clay to 15 m depth. The pore pressure index (U_D) profile from 3.3 m to 11 m is approximately constant with an average value of 0.66 indicating that this layer is "impermeable" according to the criterion proposed by Marchetti et al. (2001). This confirms that the soil behaviour type is clay. The DMT soil classification is in fairly good agreement with the soil profile at this site previously described in section 3.3.2.2 of this thesis (see Figure 3.7).

The horizontal stress index (K_D) provides a good indication of the extent of the desiccated crust. Below about 2.5 m and to 11.75 m depth, K_D is relatively constant and generally above 2.3, suggesting slight overconsolidation or structure. However, from 12 m to 15 m the K_D values vary between 1.8 and 2.3 which indicates that the soil is normally consolidated according to the criterion proposed by Marchetti (1980).

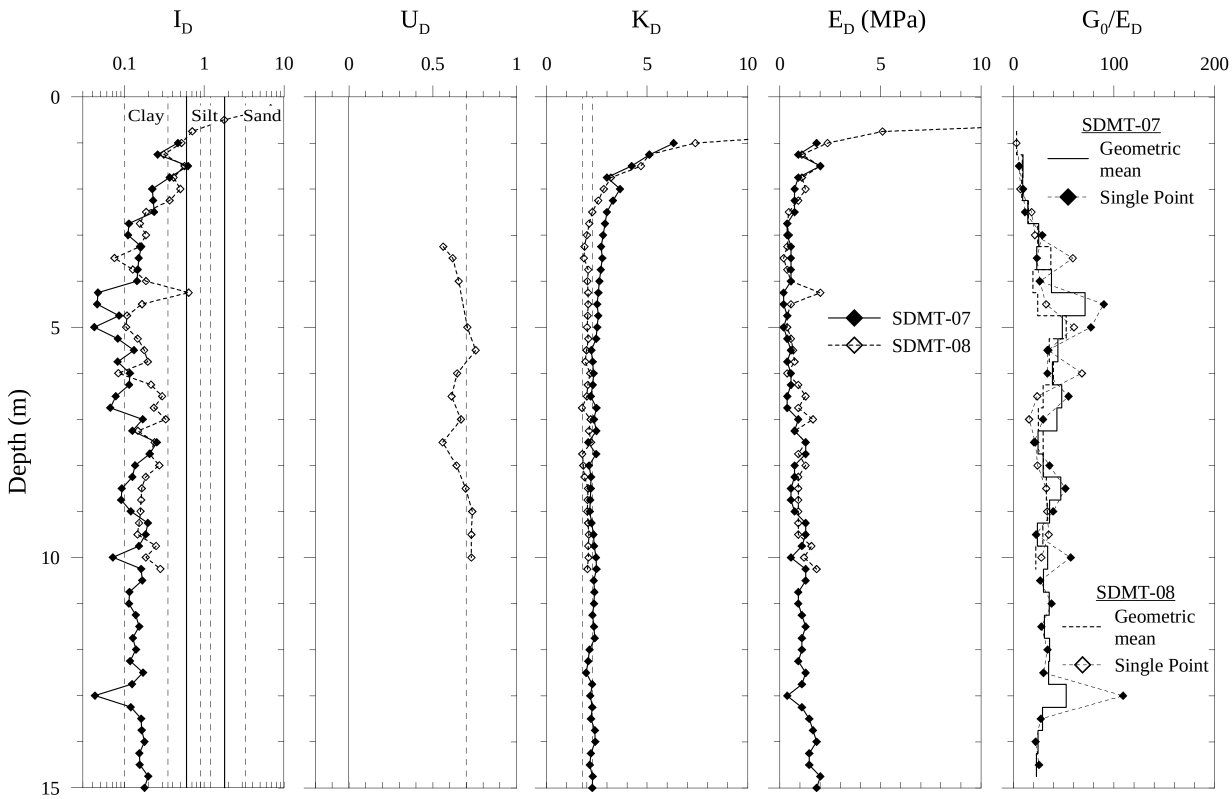

Figure 4.9 SDMT profiles, Colebrook Overpass.

Crawford & Campanella (1991) and Crawford et al. (1994) carried out consolidation tests on relatively undisturbed samples for this site and reported values of preconsolidation pressures (σ_p') that are close to the interpreted in situ vertical effective stress (σ_{vo}'), suggesting that soil is normally consolidated to a depth of about 18 m. Weech (2002) argues that these data may not be representative of the true vertical yield stress of the soil due to sampling disturbance. Instead, he proposed that the overconsolidation ratio (OCR) decreases with depth and is 1.5 or less below about 9 m based upon the interpretation of field vane test (FVT) and piezocone (CPTU) data (Ladd & DeGroot, 2003). An inconvenience of the method used is that its calibration requires a proper matching of corresponding FVT and CPTU data. Also, the selection of an appropriate value for the ratio (s_u/σ_{vo}') for a normally consolidated state requires previous knowledge of plasticity and/or local experience. The brief discussion presented above demonstrates that an appropriate interpretation of the horizontal stress index (K_D) profile provides the engineer with a quick and direct insight into the stress history, i.e. OCR, in soft fine grained soils.

In addition, Figure 4.9 clearly shows that the G_0/E_D profile from geometrically averaged values is smoother than that from "single" point values. The G_0/E_D data shows that both profiles based upon "single" point values are more sensitive to variations in the dilatometer modulus (E_D). Furthermore, G_0/E_D increases rapidly from about 9.6 at 1.5 m to 71 at 7.5 m where it drops off to an average value of 49 and stays approximately constant at 44 to 7 m depth. Then, from 7.5 m to 14.5 the G_0/E_D varies from about 25 to 47. It is interesting to note that high values of G_0/E_D appear to be associated with soft sensitive fine grained soils.

4.3.4 Dyke Road

A summary of seismic flat dilatometer (SDMT) profiles for the Dyke Road site is presented in Figure 4.10. The SDMT soundings were carried out about 2 m apart. The soil type obtained by the material index (I_D) classification indicates the presence of a crust of sand to sandy silt that extends to about 1.5 m depth, underlain by interbedded silty clay, silt and silty sand identified by slight variations in the pore pressure index (U_D) profile. The interpreted stratigraphy based upon DMT measurements is in general agreement with the soil profile previously reported at the test site (see Figure 3.18).

The horizontal stress index (K_D) profile indicates that soil is heavily over-consolidated to about 2 m, where it drops off and stays approximately constant and above 2.3 to 3.5 m depth, with suggests overconsolidation or structure. From 3.8 m to 15 m, K_D values gradually decrease with depth and are generally below 1.8 with an overall average of 1.5. On the contrary, K_D values below or above these limits indicate that either horizontal stresses do not correspond to simple unloading or that the clay is cemented, or both. Sanin (2005) reports values of preconsolidation pressures (σ_p') that are close to the interpreted vertical effective stress (σ_{vo}'), which suggests that soil at the sampled locations is normally consolidated (NC).

The low K_D values obtained at this site suggest that soil may be underconsolidated, i.e. is still consolidating or $\sigma_p' < \sigma_{vo}'$. Underconsolidation can result from conditions such as: (i) deposition at a rate faster than consolidation, (ii) rapid drop in the groundwater table, (iii) insufficient time since the placement of a fill or other loading for consolidation to be completed, and (iv) disturbance that causes a structural breakdown and decrease in effective stress (Mitchell & Soga, 2005). Sanin (2006) points out that soil at the test site originates from a relatively recent channel deposit in the Fraser River Delta. As a result, it is believed that the low K_D values obtained at this site may be caused by soil structure breakdown due to the DMT blade penetration and the young age of the soil deposit.

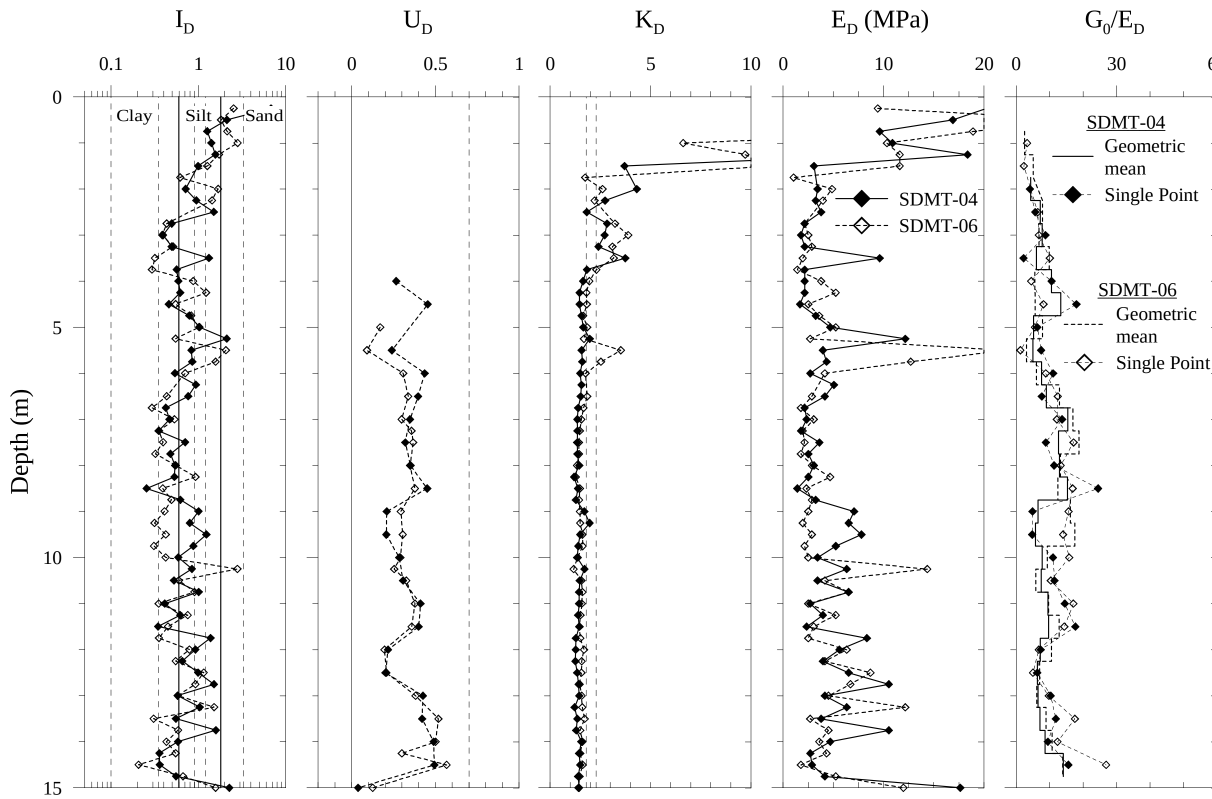

Figure 4.10 SDMT profiles, Dyke Road.

The G_0/E_D profiles presented in Figure 4.10 show similar trends to those obtained at Colebrook Overpass site (see Figure 4.9). Firstly, the profiles obtained from geometrically averaged values are smoother than those from "single" point values. Secondly, despite the fact that both shear wave velocities profiles increase gradually with depth and without sharp increases in magnitude, slight variations in the dilatometer modulus (E_D), clearly affect the magnitude of the ratio G_0/E_D when "single" point values are used. Finally, it is noted from Figure 4.10 that G_0/E_D varies approximately from about 2.6 to 18.8 for silty clay to sandy silt soils, i.e. $0.33<I_D<1.8$, and soils where the pore pressure index (U_D) varies between about 0.1 and 0.6 with the bulk of the data around 0.3, respectively.

4.3.5 200th Street Overpass

Figure 4.11 shows the results of a seismic piezocone penetration test. The interpreted soil profile derived from the non-normalized Soil Behaviour Type (SBT) system of Robertson et al., (1986) indicates the presence of silt, clayey silt and clay (3<SBT<5) above 3.5 m depth, underlain by sensitive fines (SBT=1) extending to a depth of about 15.2 m. Zergoun et al. (2004) describe the results of field vane shear tests that suggest an average sensitivity of 4.1 for the soft fine grained layer. Furthermore, two sandy silt and clayey silt lenses are indicated at 9.4 m and 12.8 m depth respectively.

Also, the SBT profile shows that soil is classified as clayey silt to silt from 15.2 m to 16.3 m, where refusal to penetration was encountered, indicated by high cone tip resistance (q_t). The cone tip and friction ratio (R_f) profiles provide a good indication of the extent of the desiccated crust. Furthermore, the penetration pore pressure (u_2) is constant and around zero from 0 m to 3 m depth, where it picks up and keeps increasing with depth to a value of about 55 m of water at 16 m. Likewise, the q_t profile indicates that from 0 m to 4.5 m the soil is overconsolidated, as indicated by relatively high q_t values, and below 4.5 m the tip resistance increases gradually with depth suggesting that soil is normally to lightly overconsolidated.

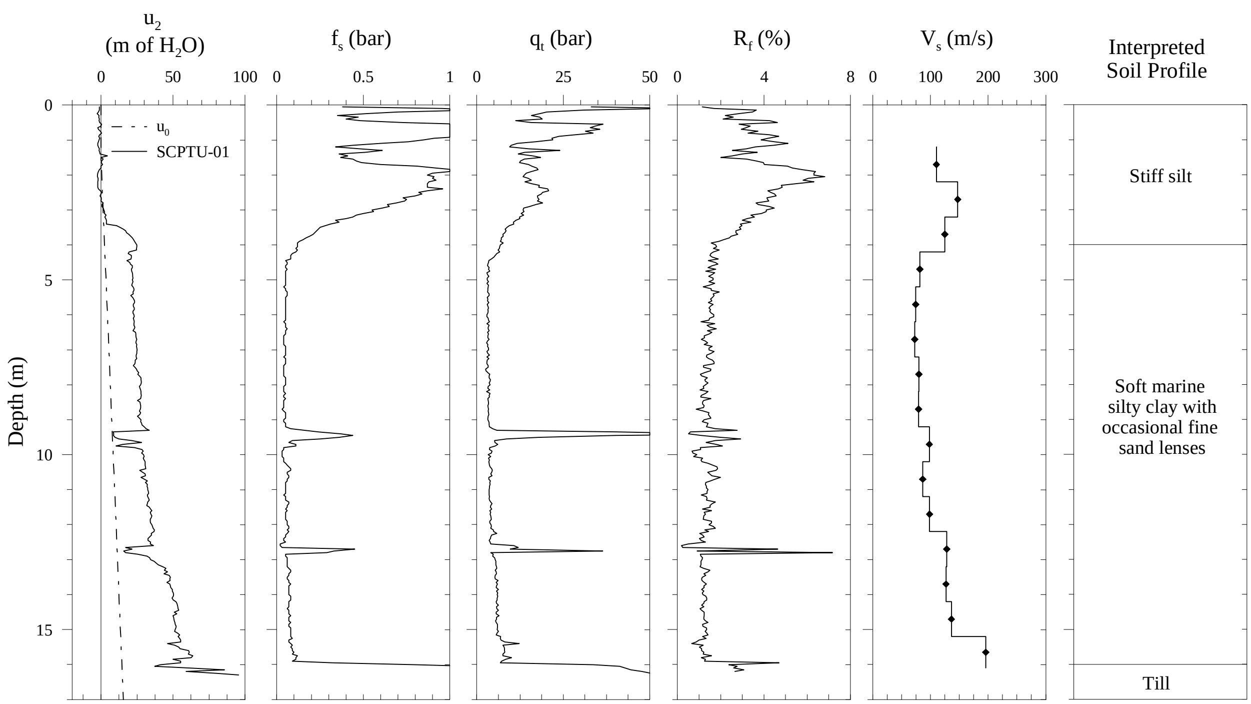

Figure 4.11 SCPTU profile, 200th Street Overpass.

The summary of intermediate dilatometer parameters and results of seismic dilatometer (SDMT) tests is presented in Figure 4.12. The material index profile (I_D) indicates a surface crust of silt overlying clay to 16 m depth. The I_D profile and dilatometer modulus (E_D) show the presence of two silty clay lenses at 9.7 m and 12.4 m, respectively. Also, the pore pressure index (U_D) shows a similar trend to that of the piezocone penetration pore pressure (u_2). In other words, U_D is very close to zero to 2.9 m depth, then it increases to 0.67 at 4.9 m and stays approximately constant at about 0.73 to 15.9 m depth where it drops off to 0.38 at the contact with till. The agreement between the SDMT and SCPTU classification profiles is very good. However, it should be kept in mind that in the SDMT tests readings are taken normally between 0.2 m to 0.3 m intervals in comparison to the 0.05 m intervals commonly used for SCPTU soundings. As a result, the interpreted soil stratigraphy from SDMT measurements is not as detailed as that from piezocone data.

Based upon Marchetti's (1980) criterion, the horizontal stress index (K_D) profile indicates an overconsolidated crust that extends to about 4.4 m depth. Then, K_D decreases from 4.4 at 4.7 m to 2.4 at 12.2 m where it increases and stays approximately constant at 3 to 15.9 m depth, suggesting slight overconsolidation or structure. Data reported by Sully (1991) and Zergoun et al. (2004) confirms the presence of an upper heavily overconsolidated (OC) crust and a lower lightly OC layer of fine grained soil.

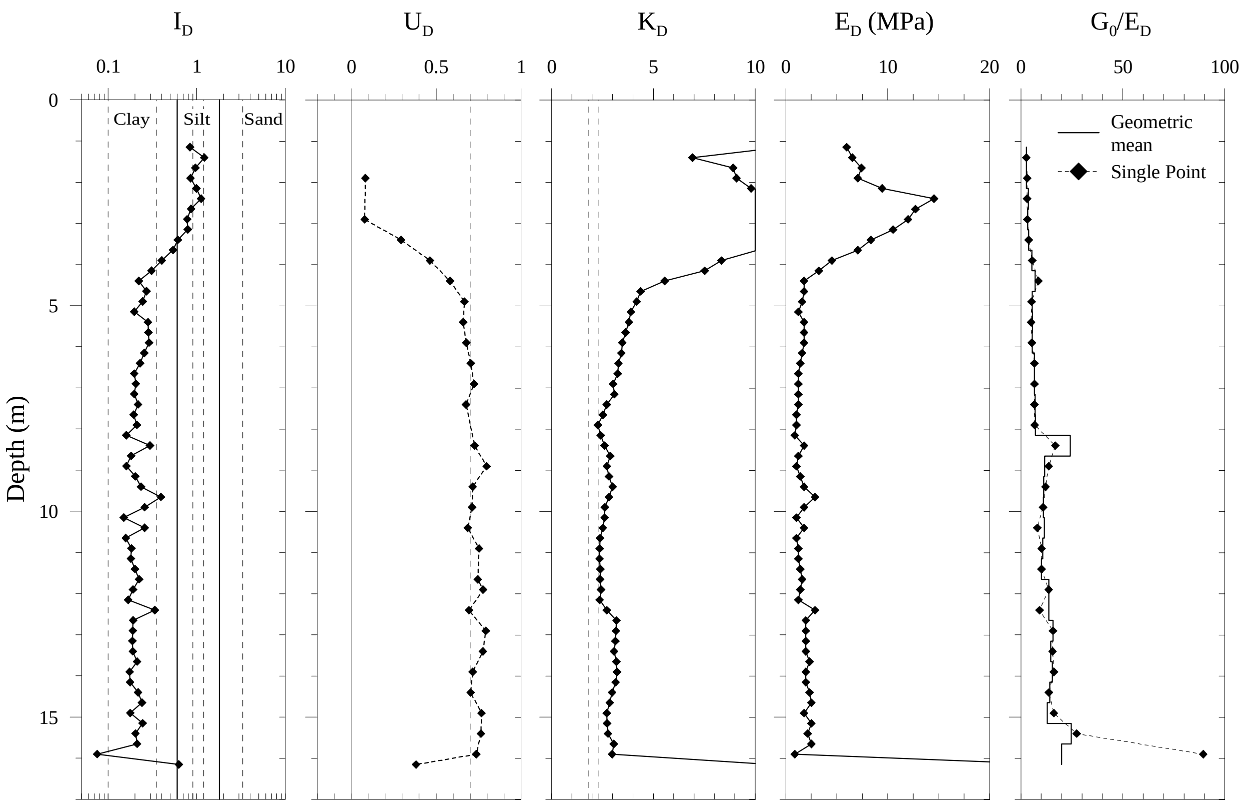

Figure 4.12 SDMT profile, 200th Street Overpass.

The G_0/E_D profiles, i.e. "single" point and geometric mean, presented in Figure 4.12 increase gradually with depth from about 2.7 at 1.4 m to 20 at 15.9 m depth. Furthermore, both profiles are very similar with the exception of variations at 8.4 m and below about 14.4 m depth. As discussed previously, shear waves may have been affected by reflections from dense materials (sandy silt lens and till), and therefore the magnitude of G_0/E_D would also be affected. The geological origin, stress history and plasticity of both soft fine grained soil deposits at 200th Street Overpass and the Colebrook overpass are very similar. However, the data presented in Chapter 3 indicate that the main difference between these two soil deposits is the degree of sensitivity. The SDMT data obtained at both sites indicates that G_0/E_D is significantly higher at Colebrook Overpass than at 200th Street, suggesting a possible relationship between sensitivity and the ratio G_0/E_D.

4.4 Relationships between SDMT parameters

Marchetti et al. (2007) introduced the relationship between the material index (I_D) and the ratio G_0/E_D as a potential indicator of soil type. Similarly, Lutenegger (1988) endeavoured to establish a relationship between I_D and the pore pressure index (U_D) as a potential indicator of soil type and highlighted the usefulness of the DMT C-reading to determine soil stratigraphy. The SDMT data collected at several research sites allows exploration of the combination of standard DMT parameters such as: I_D, E_D and U_D, and the small strain modulus (G_0), obtained from shear wave velocity (V_s) measurements, for an improved soil characterization. This section presents such relationships and describes the development of a new soil behaviour type chart based upon SDMT measurements.

4.4.1 Relationship between I_D and G_0/E_D

The addition of V_s measurements to the standard dilatometer test adds to the options available to assess soil behaviour. There has been a considerable increase in interest in using V_s and the small strain shear modulus G_0, in combination with penetration parameters such as q_t from the SCPTU to identify unusual soil conditions (Schnaid et al. 2004). Previous investigators have investigated the potential use of combinations of G_0 and seismic dilatometer (SDMT) parameters and have attempted to establish correlations between DMT intermediate parameters and V_s or G_0 (Sully & Campanella, 1989; Marchetti et al. 2008a, 2008b). Such studies have suffered the drawback that V_s or G_0 values were measured in adjacent soundings and so were not necessarily representative of the soil tested by the DMT expansion. The new SDMT allows more focussed study of these relationships.

Marchetti et al. (2008a) describe several relationships between the small strain shear modulus (G_0), material index (I_D), dilatometer modulus (E_D), horizontal stress index (K_D), and vertical drained constrained modulus (M_{DMT}). The database used contains information on different soil types collected at several sites located mainly in Italy but also in Spain, Poland, Belgium and USA. The data points consist of relatively "uniform" soil profiles where values of G_0, I_D, E_D, K_D and M_{DMT} differ less than 30% from their arithmetic average. Marchetti, et al (2008a) recognize that G_0/E_D varies between about 1.5 and 3 in sandy soils (I_D>01.8), whereas in silty soils (0.6<I_D<1.8) it varies from 2.5 to 13, and 3 to 25 in clays (I_D<0.6), respectively. They also note that for all soils G_0/E_D decreases as K_D increases.

Figure 4.13 shows the relationship between G_0/E_D and I_D for the research sites and the additional sites listed in Table 3.1 and Table 3.2 . It is noted that G_0/E_D is higher in clays than in sands with a transition that corresponds to silty soils. This reflects the low values of $\Delta p = p_1 - p_0$, and hence E_D, during undrained expansion in soft clays compared to its value in drained expansion in silts and sands. The data show that G_0/E_D varies from 1 to 4 in sands while in silty soils G_0/E_D increases from 4 to about 15 as I_D decreases.

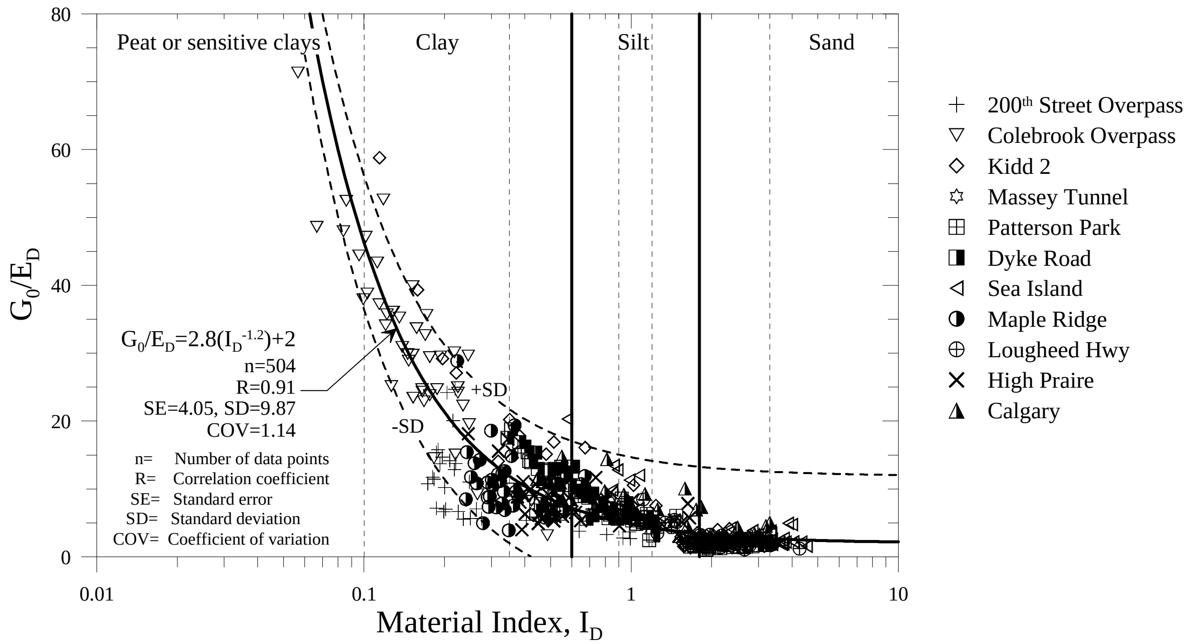

Figure 4.13 Relationship between I_D and G_0/E_D for all research sites and some additional sites.

The scatter of G_0/E_D values in clayey soils (I_D<0.6) is significantly greater than in silts and sands. It is also interesting to note from Figure 4.13 the substantial difference between G_0/E_D values measured at 200th Street Overpass and those measured at Colebrook Overpass. Indeed, the geological origin, stress history and plasticity of the soil at both sites are very similar. However, the data presented in Chapter 3 shows that the main difference between these two soil deposits is the degree of sensitivity determined from results of field vane tests. Therefore, the SDMT data obtained at these sites suggests a relationship between G_0/E_D and the degree of sensitivity.

Figure 4.14 shows the same information as Figure 4.13 but constrained to G_0/E_D values less than 30. For comparison, the range of data reported by Marchetti et al. (2008a) has been plotted in the same figure. It can be noted from Figure 4.14 that the bulk of the data points reported by Marchetti et al. (2008a) in clayey soils are within a range of 1.5 to 20, suggesting that SDMT data was obtained in soils with a lower degree of sensitivity. Also, the data points reported in this thesis fall within the zone of data reported by Marchetti et al. (2008a).

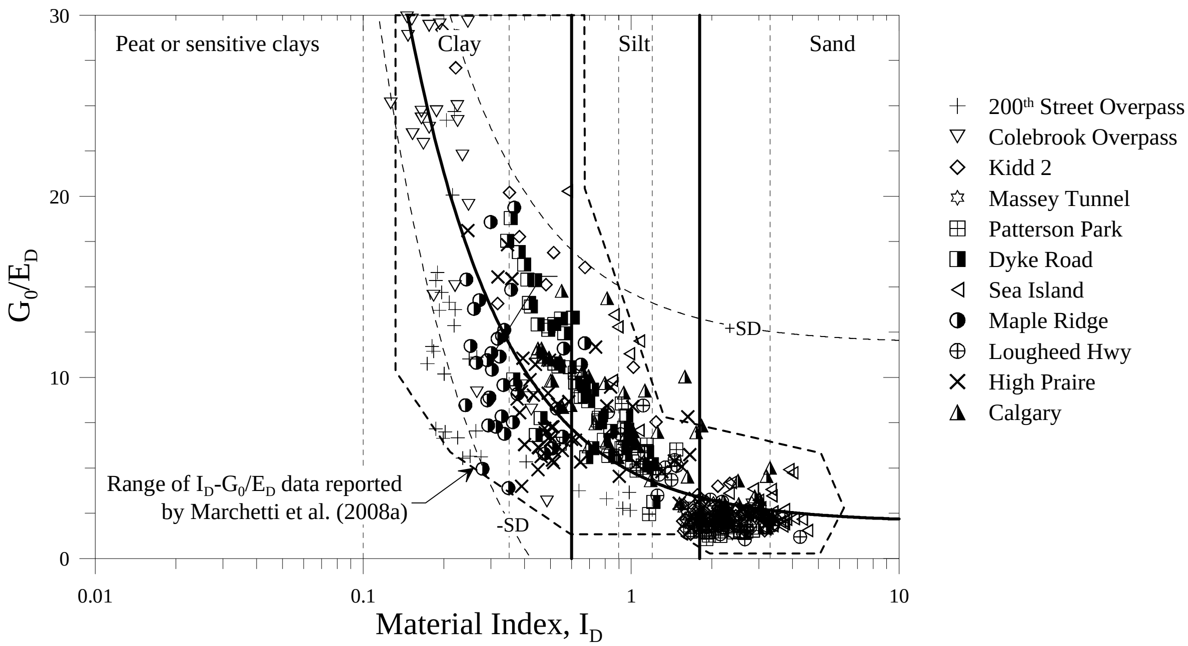

Figure 4.14 Relationship between I_D and G_0/E_D constrained to G_0/E_D <30

4.4.2 Relationship between I_D and U_D

Lutenegger & Kabir (1988) and Lutenegger (1988) point out that variations in the pore pressure index (U_D) reflect drainage conditions. They also argue that if both the material index (I_D) and U_D provide an indication of soil type, a strong relationship between these two parameters is to be expected. Lutenegger (1988) endeavoured to verify this assumption by plotting I_D and U_D data points from several sites with different soil conditions. The data reported by Lutenegger (1988) shows that I_D decreases as U_D increases. This reflects the increase in the excess pore pressure due to penetration as a result of the reduction in permeability as the fines content increases. Similarly, Powell & Uglow (1988b) plotted the ratio between the closing pressure (p_2) and the "lift-off" pressure (p_0) versus the material index from DMT data collected at several clay sites. They identified that the magnitude of the ratio p_2/p_0 is inversely proportional to the magnitude of I_D.

Figure 4.15 shows the relationship between I_D and U_D for the sites considered herein. The data in sandy soils shows less scatter. Also, there is some scatter in the data points corresponding to silty soils ($0.8<I_D<1.8$) but it is significantly less than that for clayey soils ($0.6<I_D$). It is interesting to note that in soft sensitive clays (Colebrook, 200th St., Still Creek and Mexico City), U_D varies from about 0.6 to 1, and it appears to remain fairly constant despite the significant reduction in I_D below 0.1. Also, the bulk of the data shows that a trend exists, with increasing U_D values corresponding to reducing I_D values, with the exception of the data points collected in Mexico City clay.

The extensive ground water extraction by pumping from deep aquifers in Mexico City has significantly modified the hydrostatic pore pressure condition leading to a regional consolidation process, which results in ground surface subsidence. It is believed that the particular pore pressure conditions in this area in combination with the high plasticity and structure of Mexico City clay may affect the relationship between U_D and I_D. The data presented in Figure 4.15 suggest that U_D, measured under hydrostatic conditions, provides additional information that can be used to complement the I_D based soil classification system of Marchetti (1980). Finally, it can be noted from Figure 4.15 that a good agreement exists between the data reported in this thesis and the zone delimited by the data points reported by Lutenegger (1988).

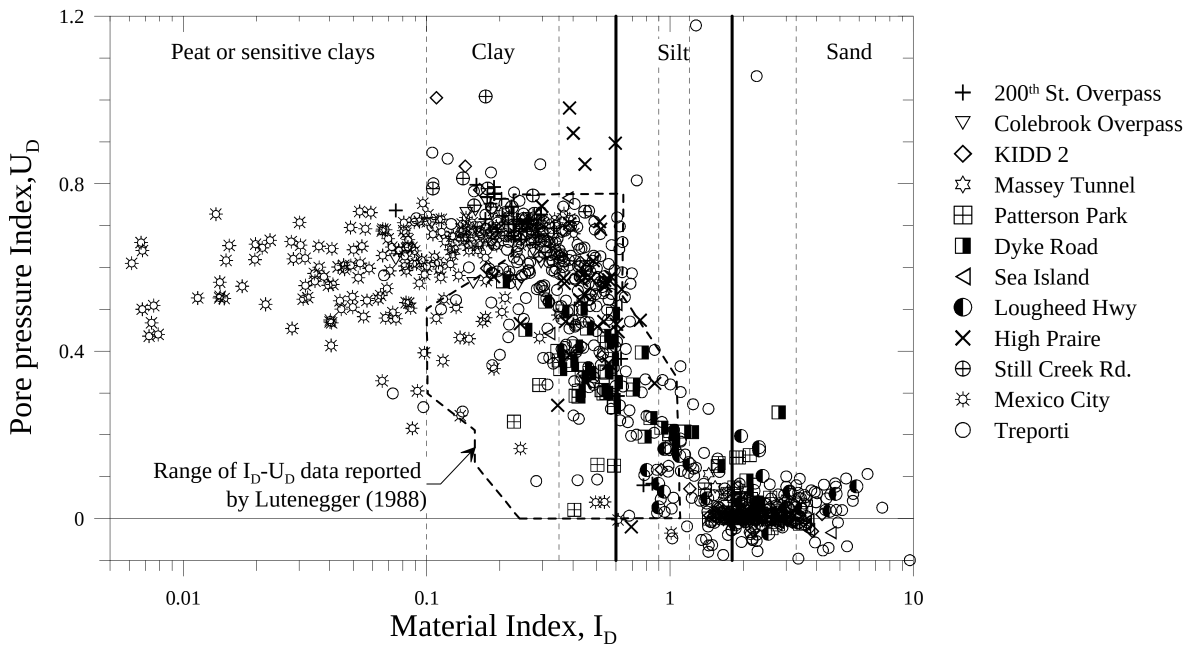

Figure 4.15 Relationship between I_D and U_D for research sites and some additional sites.

4.4.3 Proposed new soil behaviour classification chart based upon SDMT data

As described in section 2.3.3.1 of this thesis, Marchetti (1980) suggested a relatively simple DMT soil classification system to identify the soil type as a function of the material index (I_D). Marchetti & Crapps (1981) proposed a DMT soil classification chart that correlates the material index and dilatometer modulus (E_D), and allows estimation of both soil type and unit weight. Furthermore, Lacasse & Lunne (1988) assessed the soil classification obtained from this chart for several soils tested by the Norwegian Geotechnical Institute (NGI). As a result, they modified the original chart slightly in order to include low I_D values ($0.01<I_D<0.1$) obtained in Norwegian soils. In addition, reference unit weights measured in the laboratory demonstrated that the DMT chart tends to underpredict the unit weight in soft clays. Finally, Marchetti et al. (2001) argue that the original chart of Marchetti & Crapps (1981) provides a good estimate of soil type and a reasonable approximation of the unit weight in “normal” soils. Long (2008) points out that further work on the assessment of the DMT soil type chart has not been carried out.

Despite the fact that the DMT has been used extensively and has been calibrated in several soil types around the world, the writer is not aware of any further work aimed at improving the DMT soil classification system since 1988. Similarly, the potential for combining the material index and the pore pressure index has not yet been explored, and this is an area that well warrants research. Indeed, Marchetti et al. (2001) recognize that the pore pressure index can be used to distinguish soils with partial drainage, such as silts, from free-draining (sands) and non-free draining (clays) soils. Moreover, the addition of a seismic module to the standard DMT allows determination of shear wave velocities and also standard DMT measurements.

The SDMT data reviewed in section 4.4.1 and section 4.4.2 of this thesis demonstrated that relationships exist between the material index (I_D), the stiffness ratio (G_0/E_D), and the pore pressure index (U_D). Also, the trends observed from the data points collected suggest that relationships depend upon the soil type, stress history, sensitivity and drainage conditions. It seem likely that the combination of these parameters, i.e. I_D, U_D and G_0/E_D, may help to increase confidence in the identification of soil type from SDMT measurements. Figure 4.16 shows U_D plotted against G_0/E_D for the UBC research sites and also for some of the additional sites where SDMT data are available.

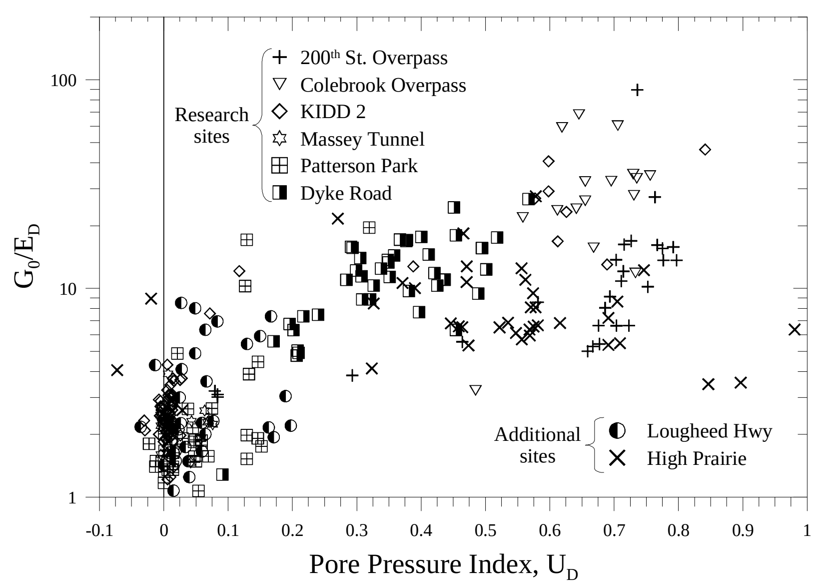

Figure 4.16 Relationship between U_D and G_0/E_D for research and additional sites.

In an attempt to ensure consistency of the data presented in Figure 4.16, G_0/E_D values obtained from a “single” point calculation are plotted against the corresponding U_D value. The rationale behind the use single “point” G_0/E_D values rather than geometrically averaged G_0/E_D is that C-readings, and hence U_D values, were only measured at depths where seismic downhole tests were performed. Therefore, it is not possible to calculate the geometric mean of U_D over a 3 readings window in the same way as with E_D. Even though the data described in section 4.3 has shown fairly significant differences between geometric mean and “single” point profiles, the data reviewed indicates that consistent trends exist in both profiles.

It is noted from Figure 4.16 that data points tend to group according to the SDMT stiffness ratio and “drainage” conditions. For example, data points from sites with predominantly sandy soils (e.g. KIDD 2, Massey Tunnel and Patterson Park) are grouped in a narrow zone. On the contrary, data points obtained at soft sensitive fine grained soils, i.e. Colebrook and 200th St., plot above G_0/E_D of about 5 and U_D of 0.6. It is also observed that silty soils (e.g. Dyke Road) tend to plot within a fairly narrow transitional zone between sandy and clayey soils.

Figure 4.17 shows the same information as in Figure 4.16 but the data points are grouped according to their corresponding K_D value. It can be seen that the bulk of the data points with K_D values higher than 2.3 fall below the dotted line. Following the criterion of Marchetti (1980), this line represents an approximate boundary between normally consolidated (NC) and lightly (LOC) to overconsolidated (OC) fine grained soils, i.e. clays and silts.

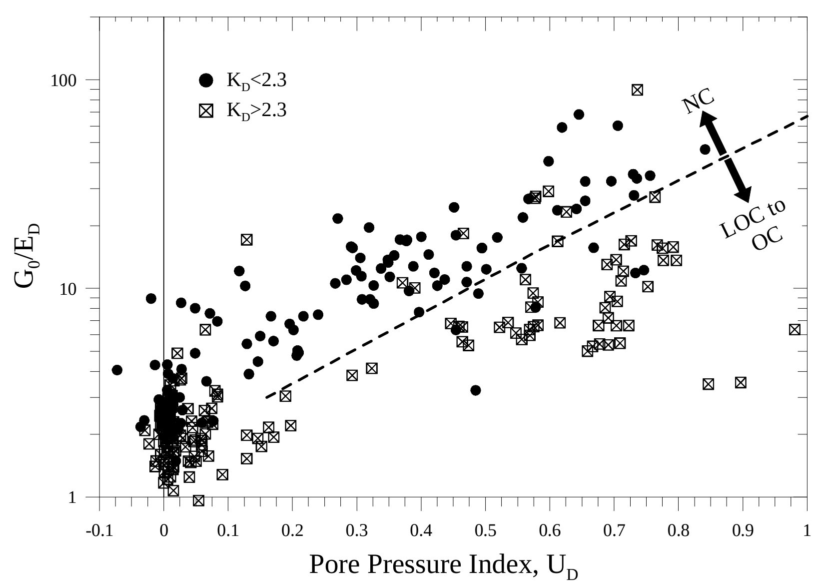

Figure 4.17 Relationship between U_D and G_0/E_D as a function of K_D.

As shown in Figure 4.18, the same database is plotted as a function of the material index (I_D). It can be observed that the data points tend to group according to their I_D and the combination of U_D and G_0/E_D

provides an insight into soil type as well as stress history. Also, it is possible to identify zones of soil type following the I_D based soil type criterion proposed by Marchetti (1980).

The different trends identified in Figure 4.16 and Figure 4.17 provide the basic framework for the development of a soil behaviour soil classification system. Figure 4.19 shows a SDMT soil behaviour type (SBT) chart that represents the first attempt at defining such a system.

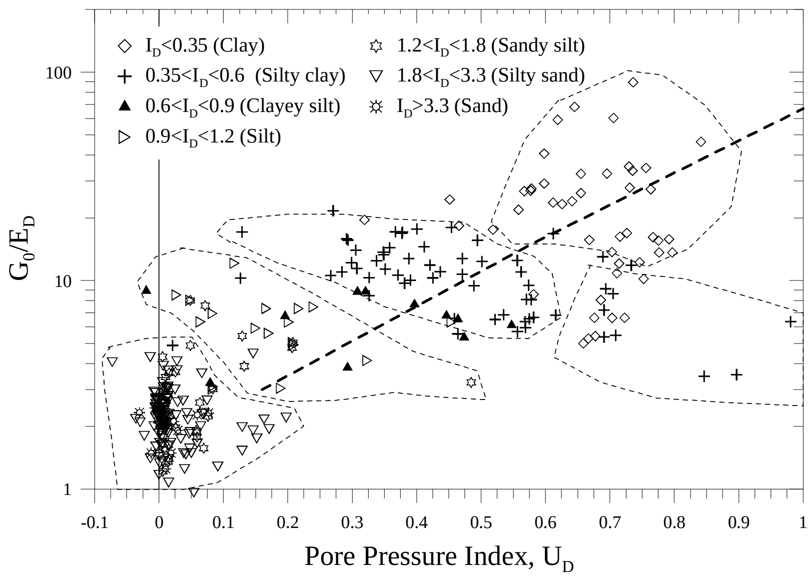

Figure 4.18 Relationship between U_D and G_0/E_D as a function of I_D.

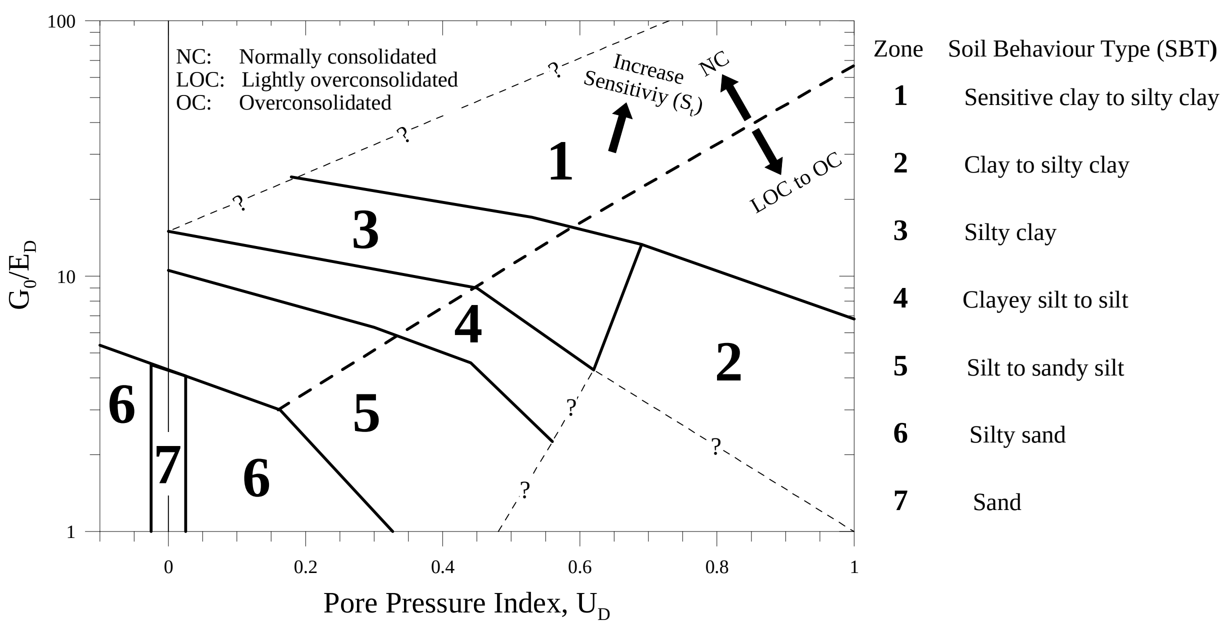

Figure 4.19 Proposed soil behaviour type chart from SDMT data.

The SDMT-SBT chart can be used as a guide for identification of soil behaviour type from SDMT data. In addition, this chart provides a quick assessment of soil behaviour based upon the combination of the stiffness (G_0/E_D) and "drainage" indicator (U_D) for the soil. These parameters are measured in the field, rather than from laboratory index tests on either disturbed or relatively "undisturbed" samples. Moreover, the chart extends the application of the seismic flat dilatometer as a tool to identify sensitive fine grained soils, which seems to be a weakness of the standard DMT soil behaviour type classification. However, the application of the proposed SDMT-SBT chart still remains limited due to the fact that its database only contains SDMT data collected in saturated unaged sands, normally (NC) to lightly overconsolidated (LOC) silts and clays as well as NC to LOC glaciomarine and glaciolacustrine sensitive clay to silty clay. Further research is required to complement the database with SDMT data on different soils such as aged sands and highly overconsolidated silts and clays.

4.5 Development and upgrade of DMT empirical correlations

4.5.1 Correlation between DMT parameters and V_s

The SDMT data presented in Figure 4.13 suggest a relationship between G_0/E_D and I_D for the sites reported herein. On the basis of this relationship and in the absence of SDMT data, it is proposed to estimate the shear wave velocity (V_s) alternatively from standard DMT measurements with the following expression:

$$V_s = \left[\frac{9.81 E_D \left[2 + 2.8 \left(I_D^{-1.2} \right) \right]}{\gamma} \right]^{0.5} \qquad \text{Equation 4.1}$$

in which E_D is the dilatometer modulus in kPa and γ is the total unit weight of the soil in kN/m^3. In the absence of in situ measurements of the shear wave velocity (V_s), Equation 4.1 can be used to obtain an estimate of V_s. The application of this empirical correlation remains limited to soils with characteristics and geological origin similar to those of the database. However, as a first attempt, Figure 4.20 compares estimated shear wave velocity (V_s) profiles to V_s data obtained from seismic piezocone (SCPTU), Cross-hole and Down-hole tests performed at sites located in Canada and Mexico. Likewise, estimates of V_s from Equation 4.1 at McDonald Farm and Mexico City sites are compared to V_s profiles estimated from the empirical correlation of Hegazy & Mayne (1995) between V_s and piezocone data.

$$V_s = \left(10.1 \times \log q_t - 11.4 \right)^{1.67} \left(f_s / q_t \times 100 \right)^{0.3} \qquad \text{Equation 4.2}$$

where q_t is the corrected piezocone tip resistance and f_s is the sleeve friction resistance, both in kPa. Mayne (2007) points out that Equation 4.2 was derived from a database that includes sands, silts, and clays, as well as mixed soils type, and thus attempts to be global and not a soil-dependent relationship.

As can be seen from Figure 4.20, the profiles of shear wave velocities estimated from Equation 4.1 at McDonald Farm and Manzanillo sites are in fairly good agreement with measured V_s values. However, at the Ecatepec site it is clear that Equation 4.1 tends to overestimate measured V_s values. A review of the DMT data and soil conditions at these sites indicates that reasonable estimates of V_s can be obtained in loose to medium sandy soils as well as low to medium plasticity normally consolidated (NC) fine grained soils with K_D values of less than 5. The comparison of measured and estimated V_s profiles for the Ecatepec site suggests that the proposed empirical correlation may not be valid for high plasticity soft fine grained soils such as Mexico City clay.

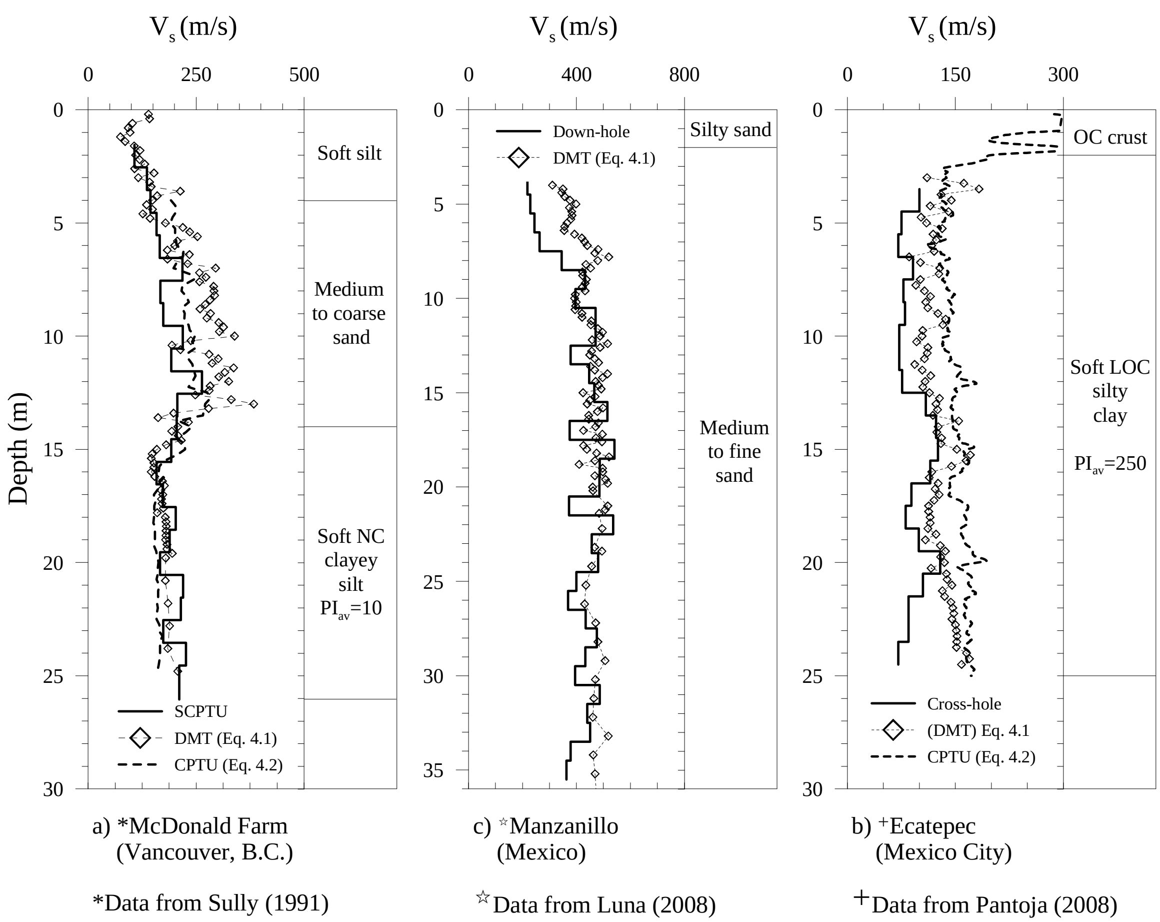

Figure 4.20 Comparison between V_s profiles estimated from DMT data and results from in situ tests.

Additionally, Equation 4.1 gives better estimates of V_s for the Mexico City site than the CPTU based empirical correlation of Hegazy & Mayne (1995). However, the comparison between estimated and measured V_s profiles at the McDonald Farm site indicates that both empirical approaches give fairly good estimates of V_s in sandy soils as well as normally consolidated (NC) clayey silt. Finally, Equation 4.1 provides a conservative approximation of V_s from a relatively economic test such as the DMT. Nonetheless, both local experience and engineering judgement are required to assess estimated values of V_s, and indeed it is highly recommended to obtain V_s values directly from in situ tests rather than through empirical correlations.

4.5.2 Correlations between DMT parameters and K_0

4.5.2.1 Proposed DMT correlation for estimation of K_0 in sand

Baldi, et al. (1986) reviewed results of several DMT calibration chamber (CC) tests performed in Ticino and Hokksund sands, and suggested a correlation between the horizontal stress index (K_D), coefficient of earth pressure from CC tests (K_0), cone tip resistance (q_c) and effective vertical stress (σ_{vo}') using a fitting function of the form:

$$K_0 = D_1 + D_2 K_D + D_3\left(\frac{q_c}{\sigma_{vo}'}\right) \qquad \text{Equation 4.3}$$

The analysis of Baldi et al. (1986) of the available CC-DMT data with Equation 4.3 yielded values of 0.359, 0.071 and -0.00093 for the coefficients D_1, D_2 and D_3, respectively. However, the magnitude of these coefficients was slightly modified by Baldi et al. (1986) in order to obtain better estimates of K_0 values measured in CC tests performed under constant boundary conditions as well as field data obtained at the Po river site (see section 2.3.4.2.1). The best fit to field data points was obtained with an expression of the form:

$$K_0 = 0.376 + 0.095 K_D - 0.00461\left(\frac{q_c}{\sigma_{vo}'}\right) \qquad \text{Equation 4.4}$$

Baldi et al. (1986) argue that Equation 4.4 represents the best available tentative procedure for estimating K_0 from DMT data obtained in natural, predominantly quartz, uncemented sand deposits. Also, they point out that any further improvement to the proposed method will require (i) comparison against results of SBP tests, (ii) assessment of the effect of CC size on DMT measurements and (iii) additional CC tests on sands with different gradation. Marchetti et al. (2001) recommend the use of Equation 4.4 with the following values for the last coefficient (q_c/σ_{v0}'): -0.005 for "seasoned" sand and -0.002 in "freshly" deposited sand. They also point out that the uncertainty in estimates of K_0 values with this empirical approach is significantly increased when the soil tested has experienced cementation and/or ageing, and the inconvenience that the method requires both DMT and CPTU data with a good match between K_D and q_c from adjacent tests. Figure 4.21 compares reference K_0 values derived from the interpretation of results of SBP tests, performed in alluvial sandy soils of the Fraser River delta, and estimates from Equation 4.4 with q_c/σ_{v0}'=-0.005.

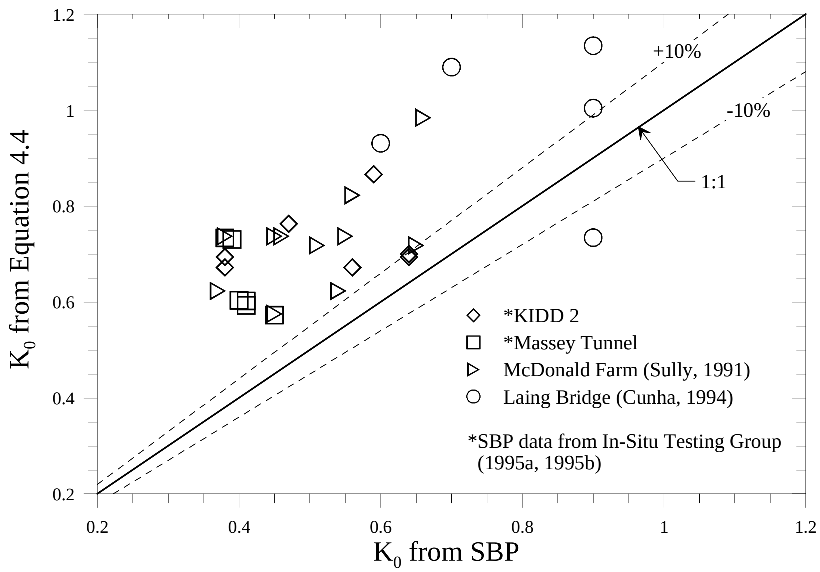

Figure 4.21 Comparison between reference K_0 reference values from SBP tests and estimates with the correlation of Baldi et al. (1986).

The data presented in Figure 4.21 clearly show that the correlation of Baldi et al. (1986) significantly overestimates K_0 reference values from results of SBP tests. Therefore, it seems worth exploring the potential for improvements in estimates of K_0 from DMT data by slightly modifying Equation 4.4. The data collected for this thesis, from adjacent seismic flat dilatometer (SDMT) and lateral stress seismic piezocone (LSSCPTU) tests at both CANLEX Phase II sites (KIDD 2 and Massey Tunnel), provides an excellent opportunity for re-evaluating the correlation of Baldi, et al. (1986). This correlation is modified by calculating for each pair of field data the value of D_3 from field measurements using the following equation:

$$D_3 = \frac{\sigma_{vo}'\left(0.376 + 0.095K_D - K_0\right)}{q_c} \qquad \text{Equation 4.5}$$

In Equation 4.5, K_0 is the estimated coefficient of earth pressure at rest obtained from analysis of SBP results using curve fitting to the Carter et al., (1986) model (In-Situ Testing Group 1995a, 1995b). Also, the magnitudes of q_c and σ_{vo}' correspond to averages value calculated over a 25 cm window for each depth at which K_D is reported. Table 4.1 and Table 4.2 present a summary of reference $K_{0(SBP)}$ and average

$K_{D(avg)}$, σ_{vo}' and q_c values as well as the magnitude of D_3 obtained from Equation 4.5. The several pairs of values of q_t/σ_{vo}' and D_3 obtained from the data collected at both CANLEX Phase II sites allow direct calculation of an average value for the product of the last two terms in Equation 4.3, i.e. $D_3(q_t/\sigma_{vo}')$. Then, in an attempt to improve the correlation of Baldi et al. (1986), the last term in Equation 4.4 is substituted by $D_3(q_t/\sigma_{vo}')_{avg}$, which yields the following expression:

$$K_0 = 0.132 + 0.095K_D \qquad \text{Equation 4.6}$$

This expression has been derived from data collected from in situ tests performed in relatively “young” (200 to 4000 years) uncemented normally consolidated Holocene sands, composed primarily of quartz minerals with mica and feldspar. The sand at both test sites, and within the CANLEX target zone, is subrounded and uniformly graded with a mean grain size (D_{50}) of 0.20 mm and fines content less than 5% (Wride, et al., 2000).

Figure 4.22 compares K_0 reference values to estimates of K_0 with the empirical approach proposed in this section (Equation 4.6). Despite the scatter in the data, estimates of K_0 from Equation 4.6 are closer to reference K_0 values, suggesting that the minor improvements in the correlation of Baldi et al. (1986) might lead to better estimates of K_0 in alluvial sandy soils from DMT measurements.

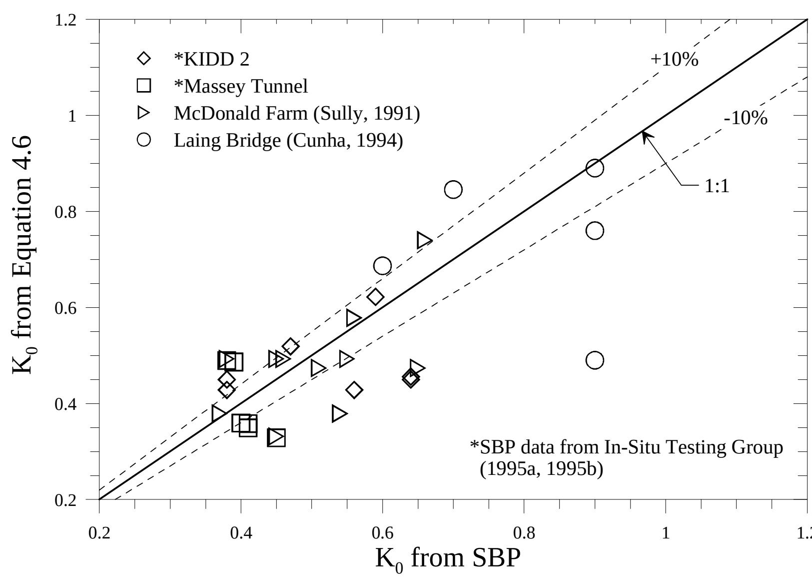

Figure 4.22 Comparison between reference K_0 reference values from SBP tests and estimates with Equation 4.6.

Table 4.1 Summary of parameters determined from adjacent SDMT and LSSCPTU tests, KIDD 2.

Depth (m)	$K_{0(SBP)}$	$K_{D(avg)}$	$\left(\frac{q_c}{\sigma_{vo}'}\right)_{avg}$	D_3	$D_3\left(\frac{q_c}{\sigma_{vo}'}\right)$
6.25	0.58	5.4	89.7	0.0035	0.3139
7.25	0.53	4.3	42.2	0.0060	0.2554
8.25	0.69	5.2	77.1	0.0023	0.1759
9.25	0.38	3.1	95.8	0.0031	0.2974
10.25	0.38	3.3	97.0	0.0032	0.3138
11.15	0.47	4.1	55.9	0.0069	0.3869
8.30	0.59	5.2	83.1	0.0034	0.2827
9.30	0.56	3.1	91.2	0.0012	0.1122
10.30	0.64	3.3	95.7	0.0006	0.0541
13.00	0.64	3.4	31.8	0.0019	0.0601

Table 4.2 Summary of parameters determined from adjacent SDMT and LSSCPTU tests, Massey Tunnel.

Depth (m)	$K_{0(SBP)}$	$K_{D(avg)}$	$\left(\frac{q_t}{\sigma_{vo}'}\right)_{avg}$	D_3	$D_3\left(\frac{q_t}{\sigma_{vo}'}\right)$
10.25	0.43	5.9	46.7	0.0109	0.5083
12.00	0.38	2.7	39.8	0.0064	0.2545
13.50	0.38	2.3	31.9	0.0067	0.2133
14.75	0.38	3.8	27.4	0.0132	0.3615
15.75	0.41	2.4	36.0	0.0054	0.1940
17.00	0.39	3.7	70.7	0.0048	0.3412
12.50	0.40	2.4	32.5	0.0063	0.2037
13.50	0.41	2.3	31.9	0.0057	0.1833
15.50	0.45	2.1	29.1	0.0043	0.1250

In an attempt to assess the applicability of Equation 4.6 in different types of soils, Figure 4.23 presents a database that contains K_D and K_0 values obtained from the interpretation of results of DMT and SBP tests carried out at several sites (solid symbols), as well as measured in Calibration Chamber (CC) tests performed in different well documented sands (open symbols). For comparison, the correlation of Baldi et al. (1986) and the empirical approach proposed herein are plotted on the same figure.

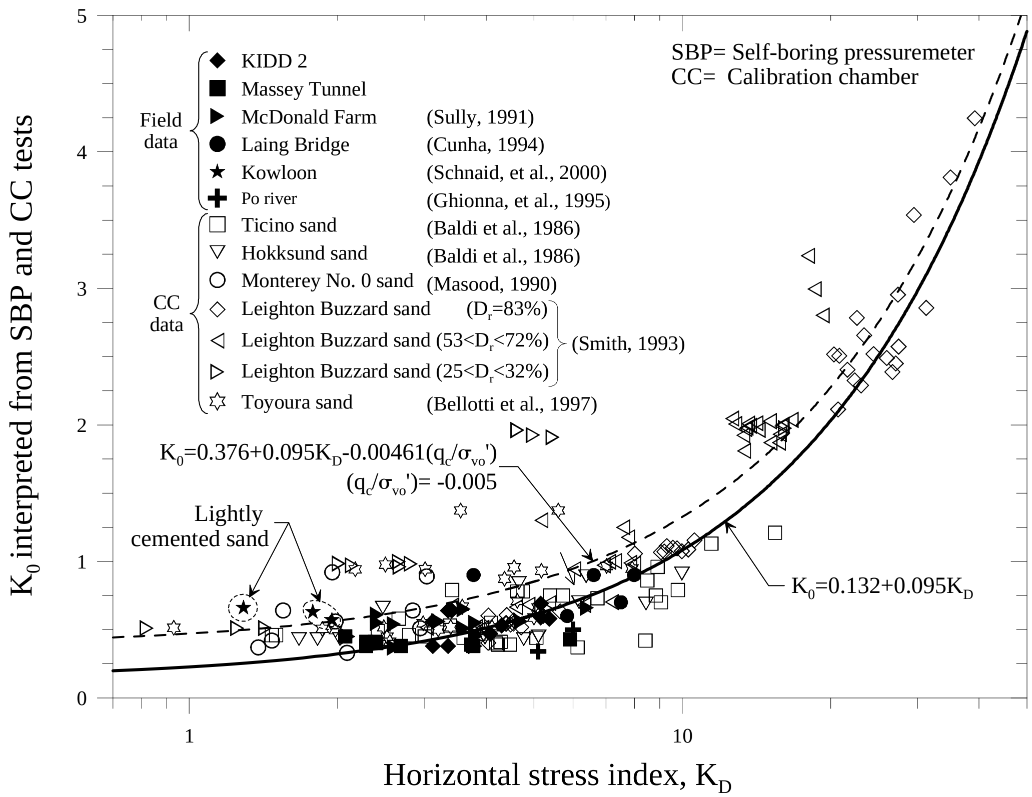

Figure 4.23 Relationship between K_D and K_0 interpreted from SBP and CC tests.

As can be noted from Figure 4.23, the bulk of the field and CC data plot below about $K_D \approx 10$. Also, the correlation of Baldi et al. (1986) tends to overestimate the CC and field data points, whereas with Equation 4.6 it is possible to estimate K_0 measured in the field and CC at low stress ratios (K_0<1), with a standard deviation of 0.15. It is also interesting to note that at K_D>10 both correlations give quite similar estimates of K_0 values for dense Leighton Buzzard sand tested at high stress ratios, i.e. K_0>2. Marchetti et al. (2001) point out that a unique correlation between K_0 and DMT parameters can not be established since the coefficient of earth pressure at rest in sandy soils depends upon the effective friction angle (ϕ') and relative density (D_r). Nonetheless, the data shown in Figure 4.23 suggests that in natural predominantly quartz, and uncemented sand deposits, fairly good estimates of K_0 can be obtained from the empirical correlation proposed in this thesis. Also, the correlation of Baldi et al. (1986) seems to give good estimates of K_0 in lightly cemented sand (Kowloon site) despite the difference in depositional history. However, more field data is required to assess estimates of K_0 with this approach in similar sandy soils. Furthermore, the empirical approach given by Equation 4.6 adds to the options available to estimate K_0 from DMT parameters. It also illustrates that the assessment of old correlations in combination with the addition of more data points significantly improves the reliability of derivation of geotechnical parameters from empirical correlations to DMT data.

4.5.2.2 Proposed DMT correlation for estimation of K_0 in clay

As described in section 2.3.4.1.1 of this thesis, Mayne & Kulhawy (1990) proposed a direct correlation between flat dilatometer (DMT) data and the coefficient of earth pressure (K_0) obtained from interpretation of results of self boring pressuremeter (SBP) tests (Equation 4.7). The database of Mayne & Kulhawy (1990) contains information on twelve clay sites tested by SBP and DMT with different stress states that vary from normally consolidated (NC) to highly overconsolidated (OC). In addition, the plasticity indices of those clays ranged from 10 to 57, and sensitivities varied from 3.5 to 60.

$$K_0 = 0.27K_D \qquad \text{Equation 4.7}$$

Mayne & Kulhawy (1990) argue that from a practical standpoint, only a first-order estimate of the in situ K_0 may be required for geotechnical analysis. Therefore, Equation 4.7 represents a practical empirical approach to obtain fairly good estimates of K_0 in a wide variety of clayey soils with different characteristics and stress conditions. However, the writer is not aware of any recent improvement of this database or development of new empirical correlations between K_0 and DMT data. Indeed, Long (2008) concludes that a possible weakness of the DMT is that derivation of geotechnical parameters involves the use of empirical correlations developed some time ago.

In order to overcome this drawback, the database used to develop Equation 4.7 has been updated with published information on K_0 values derived from the interpretation of adjacent SBP and DMT tests, performed in fine grained soils at several sites from different parts of the world. The new database contains DMT measurements and reference K_0 values obtained from the interpretation of results of total stress cells (TSC): Strong Pit (Sully, 1991) and Genesee (Chan & Morgenstern, 1986) sites, and results of self boring load cells (SBLC): Lr. 232 St. (Sully, 1991) and Massena (Huang & Haefele, 1990) sites. Table 4.3 and Table 4.4 present a summary of these sites including information on the average plasticity index (PI_{av}), soil type, stress history (OCR) and source of data.

Mayne & Kulhawy (1990) and Lunne et. al., (1990) published simultaneously empirical correlations between DMT data and K_0 reference values obtained from the interpretation of both SBP and TSC. The first 19 sites listed correspond to those reported in 1990 by both pioneering research groups, whereas the remaining sites have been compiled for this thesis from fourteen separate well documented clay and silt sites that have been described in several publications.

As was done by Mayne & Kulhawy (1990), the data were collected at depths where just SBP, SBLC, TSC and DMT tests were performed. Figure 4.24 compares the updated K_D-K_0 database to several DMT correlations previously described in section 2.3.4 of this thesis. Furthermore, the variability of the data presented may be attributed to errors in measurement of in situ parameters, interpretation of K_0 values from results of in situ tests, and soil variability. It is interesting to note that the bulk of the data obtained in normally (NC) to overconsolidated (OC) clays with K_D<5 falls within a fairly narrow band delimited by the correlations of Lunne, et al. (1990) proposed for "young clays". Also, there is some scatter in data points with K_D<5 but it is significantly less than that of data points with 5<K_D<10. It can also be noted that the correlation of Mayne & Kulhawy (1990) provides a better relationship between K_0 and K_D despite the wide range of soil types and stress histories. Additionally, at low K_D values, i.e. K_D<3, estimates of K_0 with this approach are very similar to those from the correlations of Marchetti (1980) and Lunne et al. (1990).

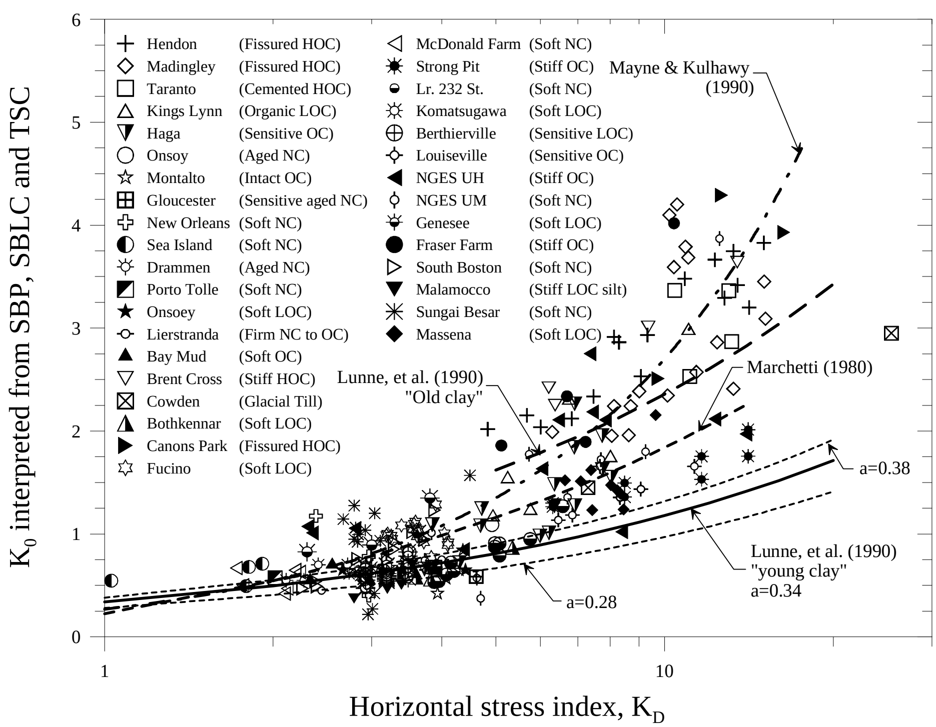

Figure 4.24 Comparison between K_0, obtained from interpreted SBP, SBLC and TSC data, and several K_D based empirical DMT correlations.

The data set presented in Figure 4.24 was analyzed with regression analysis in order to obtain the best fit line. The correlation coefficient (R), also known as the product-moment coefficient of correlation or

Pearson's correlation, and the standard error (SE) are used to assess the quality of the fit. In statistics, the correlation coefficient measures the strength of the linear relationships between two *X* and *Y* and ranges from -1 (for perfect negative correlation) to 1(for perfect positive correlation). Thus, for any given sample size n, the closer the coefficient of correlation is to ± 1, the stronger the linear relationship between *X* and *Y*. On the contrary, as R approaches 0, the linear relationship between *X* and *Y* becomes weaker (Berenson, et al. 1988). In other words, a higher value of $|R|$ means a greater reduction in the conditional variance associated with the linear regression equation, and hence a more accurate prediction of *Y* based upon the regression of *Y* on *X* (Ang & Tang, 2007). On the other hand, the standard error is used to measure the amount of variability or scatter around the regression line. It represents the standard deviation of the observed values around the predicted values, rather than around the mean as in the usual standard deviation (Berenson, et al. 1988).

Firstly, the regression analysis of 235 data points using the linear function given by Equation 4.7 indicates a correlation coefficient and standard error of 0.84 and 0.58, respectively. Based upon regression analysis of the original database consisting of 69 data points, Mayne & Kulhawy (1990) reported 0.82 for the square of the correlation coefficient (R^2) and 0.48 for the standard deviation (SD). For comparison, the regression analysis of the database presented in Figure 4.24 yields R^2=0.7 and SD=0.99. Thus, it is evident that the larger the data base the larger the scatter and therefore R^2 reduces and the standard deviation increases. However, from a practical standpoint and considering the wide range of different soil types and the scatter in the data, the correlation of Mayne & Kulhawy (1990) represents a simplified method that provides reasonable estimates of K_0 in fine grained soils.

Alternatively, the data shown in Figure 4.24 suggests that beyond K_D=10, the scatter in K_0 reference values increases significantly. It is interesting to note that data points obtained in highly overconsolidated fissured soils tend to fall outside the proposed limit, suggesting that fissuring significantly affects lateral stress measurements in these types of soils. Then, regression analysis performed for the data with K_D<10 (n=198) give the best fit line of the form:

$$K_0 = 0.24K_D + 0.1 \qquad \text{Equation 4.8}$$

As can be noted from Figure 4.25, the standard error (SE) of this fit line is significantly less than that of Equation 4.7. Also, the correlation coefficient (R) of the latter is slightly higher than that of Equation 4.8, which at first sight suggests that the correlation of Mayne & Kulhawy (1990) still provides good estimates of K_0. However, due to the fact that the database has been significantly improved by increasing the number of data points by 74%, it will be worth verifying with other statistical indicators, if the use of Equation 4.8 rather than Equation 4.8 for K_D<10, may lead to a better estimates of K_0.

The coefficient of variation (COV) provides a statistical measure of the dispersion of data points in a data series around the mean. It represents the ratio of the standard deviation to the mean, and it is a useful statistic for comparing the degree of variation from one data series to another. For comparison, the correlations between K_D and K_0 given by Equation 4.7 and Equation 4.8 indicate a COV of 0.46 and 0.42, respectively for data points with K_D<10. Therefore, the COV and SE of the latter are somewhat less than those of the correlation of Mayne & Kulhawy (1990).

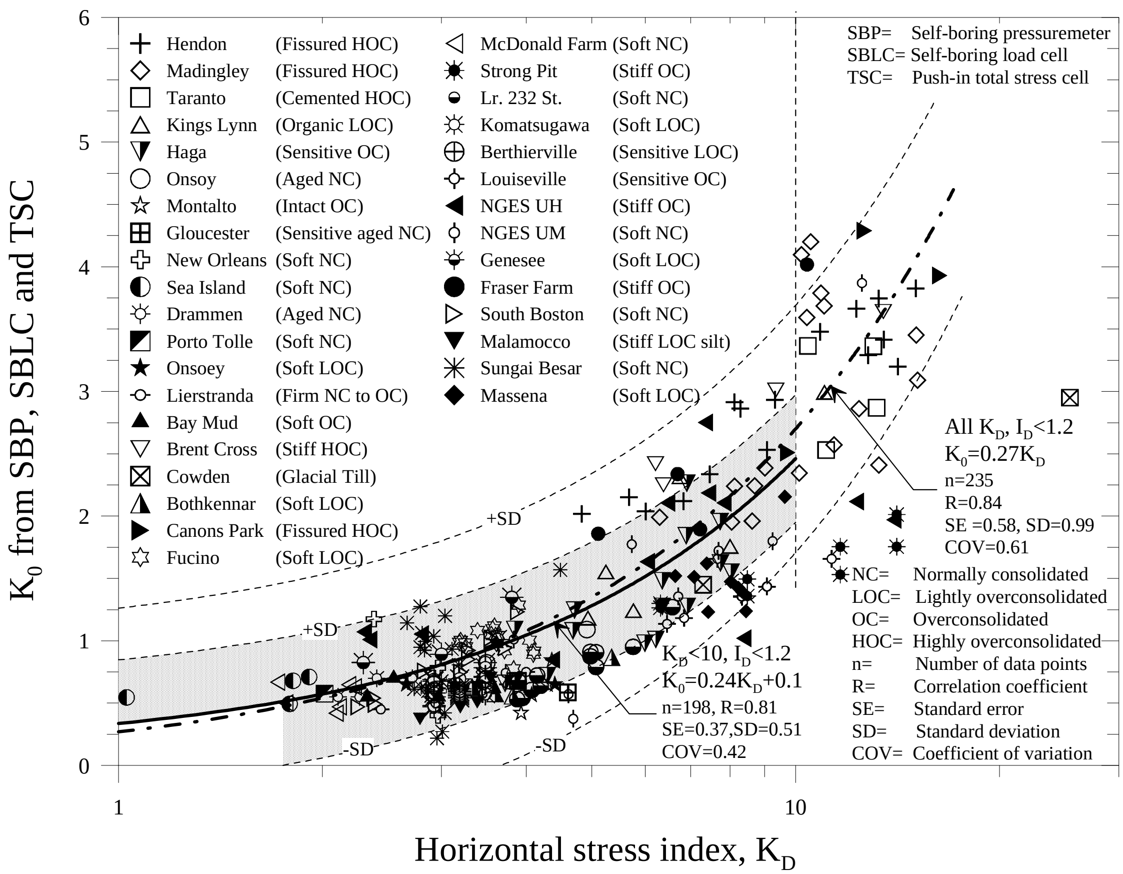

Figure 4.25 Proposed relationships between K_0, from interpreted SBP, SBLC and TSC data, and K_D from flat dilatometer (DMT) tests.

It has been demonstrated that the correlation of Mayne & Kulhawy (1990) gives reasonable estimates of K_0 despite the fact it was developed some time ago. However, the database has not been upgraded. The alternative empirical approach derived in this section, from a large database, seems to give relatively better estimates of K_0 for soils with K_D<10; but as can be noted in Figure 4.25 the difference between both fitted relationships is practically negligible, and therefore it seem reasonable that either Equation 4.7

or Equation 4.8 can be used to estimate K_0 in a wide variety of fine-grained soils. In highly overconsolidated clays, with K_D>10, K_0 can be conservatively estimated from the correlation of Mayne & Kulhawy (1990). However, it should be born in mind that both local experience and engineering judgement are required to assess estimates of K_0 from any of these empirical approaches. Finally, the detailed assessment of the reliability of an “old” empirical correlation and the improvement of the database used for its development, represent a positive contribution to the upgrade of derivation of geotechnical parameters from DMT data.

4.6 Summary

4.6.1 Overview

The seismic flat dilatometer (SDMT) is a combination of the standard flat dilatometer (DMT) equipment with a seismic module for downhole measurement of the shear wave velocity (V_s). The SDMT provides a simple and cost-effective means for determining the soil stratigraphy, the shear modulus at small strains (G_0) from shear wave velocity (V_s) measurements, as well as estimating deformation and strength parameters from empirical correlations to DMT parameters.

The performance of the data acquisition system and seismic module of the SDMT has been assessed through a comprehensive field testing program undertaken at several research sites located in the Lower Mainland of BC. Field measurements have been critically reviewed in an attempt to explore the potential of an improved site characterization through a combination of several SDMT parameters.

4.6.2 Assessment of the SDMT module

The SDMT test procedure is relatively simple and the software developed by the manufacturer (Studio Prof. Marchetti) allows real time handling of seismic and standard DMT data. The software (SDMT Elab) has the advantage of presenting on the computer screen the magnitude of the interpreted V_s after the system is triggered and the source waves are generated. Also, the V_s profile can be displayed on the computer screen and it is updated after each test.

Several problems were experienced with the SDMT data acquisition system when performing V_s measurements in the field. It was found that the main reason for these problems was a lack of communication between the seismic module and the data acquisition system. In order to overcome this problem it is important to ensure that the membrane is in contact with the blade and the sound is on before performing a seismic test.

Good agreement was observed between the V_s profiles obtained at several research sites with the seismic flat dilatometer (SDMT) and those from seismic piezocone tests (SCPTU). Furthermore, the shear wave velocities measured with the seismic flat dilatometer (SDMT) are likely to be more sensitive to stratigraphic details because of the 0.5 m depth interval used for V_s determination as opposed to the 1 m interval typically used in the seismic piezocone test. Consequently, it is necessary to carefully review each set of seismic traces in order to detect anomalies in the results that may affect the interpreted shear wave velocity, rather than using the SDMT as a "black box".

4.6.3 Relationships between SDMT parameters

The analyses of SDMT measurements at research sites have illustrated the potential for an improved soil characterization through the combination of standard DMT parameters such as: (i) material index (I_D), (ii) dilatometer modulus (E_D) and (iii) pore pressure index (U_D), and the small strain shear modulus (G_0). The usefulness of the DMT-C closing pressure for soil identification has been shown and therefore it is strongly recommended to include its measurement in the routine procedure.

The relationships identified between DMT parameters and G_0 provide a rational framework for the development of a new soil type behaviour system based upon SDMT measurements. The proposed soil classification system based upon SDMT measurements represents a contribution to the current state of the flat dilatometer, and adds to the options available to identify soil behaviour from in situ measurements.

4.6.4 Improved DMT correlations for estimating V_s and K_0

Based upon a comprehensive review of SDMT collected at research and additional sites an empirical correlation has been proposed for evaluating the shear wave velocity (V_s) in coarse and fine grained soils from standard flat dilatometer (DMT) measurements. Empirical correlations have also been proposed to estimate the coefficient of earth pressure at rest (K_0) in fine and coarse grained soils from DMT measurements. The approaches proposed have been derived from updated databases based upon a comprehensive review of published information in the last 10 years. The proposed empirical DMT-K_0 correlations add to the options available for the interpretation of DMT data. Also, from a practical standpoint K_0 values derived from these correlations may be used as a first-order estimate for geotechnical analysis.

Table 4.3 Summary of sites tested by both SBP and DMT

No.	Symbol	Site	PI_{av} (%)	Soil type	Reference
1	☼	Drammen	22	Aged NC	Lacasse, et al, 1981; Lunne, et al. 1990
2	⊞	Gloucester	28	Sensitive aged NC	Konrad & Law, 1987
3	⧩	Haga	18	Sensitive OC	Aas, et al., 1986; Lunne, et al., 1990
4	+	Hendon	42	Fissured HOC	Windle & Wroth, 1977a
5	△	Kings Lynn	57	Organic LOC	Wroth & Hughes, 1973
6	◇	Madingley	46	Fissured HOC	Windle & Wroth, 1977b; Lunne, et al., 1990
7	○	Onsoy	28	Aged NC	Lacasse, et al., 1981
8	◩	Porto Tolle	30	Soft NC	Ghionna, et al, 1981, 1985
9	◐	Sea Island	10	Soft NC	Konrad, et al, 1985
10	□	Taranto	27	Cemented HOC	Ghionna, et al., 1981, 1985
11	☆	Montalto	34	Intact OC	Ghionna, et al., 1981
12	✙	New Orleans	51	Soft NC	Canou & Tumay, 1986
13	★	Onsoey	27	Soft LOC	Lunne, et al. 1990
14	-○-	Lierstranda	20	Firm NC to OC	Lunne, et al. 1990
15	▲	Bay Mud	49	Soft OC	Lunne, et al. 1990
16	▽	Brent Cross	51	Stiff HOC	Lunne, et al. 1990
17	⊠	Cowden	19	Glacial Till	Lunne, et al. 1990

Table 4.4 Summary of sites tested by both SBP and DMT (Cont.)

No.	Symbol	Site	PI_{av} (%)	Soil type	Reference
18		Bothkennar	39	Soft LOC	Lunne, et al. 1990
19		Canons Park	43	Fissured HOC	Lunne, et al. 1990
20		Fucino	60	Soft LOC	Burghignoli, et al., 1991
21		McDonald Farm	10	Soft NC	Sully, 1991
22		Strong Pit	15	Stiff OC	Sully, 1991
23		Lr. 232 St.	24	Soft OC to NC	Sully, 1991
24		Komatsugawa	20	Soft LOC	Iwasaki, et al, 1991
25		Berthierville	22	Sensitive LOC	Hamouche, et al., 1995
26		Lousieville	45	Sensitive OC	Hamouche, et al., 1995
27		NGES UH	29	Stiff OC	O’Neill & Yoon, 1995; O’Neill, 2000
28		NGES UM	20	Soft NC	Benoît & Lutenegger, 1993
29		Genesee	54	Soft LOC	Chan & Morgenstern, 1986
30		Fraser Farm	22	Stiff OC	Mahbudul, 1993
31		South Boston	28	Soft NC	Ladd, et al., 1998
32		Malamocco	14	Stiff LOC silt	Ricceri, et al., 2002
33		Sungai Besar	70	Soft NC	Wong, et al, 1993
34		Massena	41	Soft LOC	Huang & Haefele, 1990

Chapter 5 EVALUATION OF LATERAL STRESS SEISMIC PIEZOCONE

5.1 Introduction

Section 2.4 of this thesis summarized the history of development of additional modules to measure lateral stresses mounted behind cones. It also outlined some of the challenges encountered when attempting to measure and interpret the lateral stresses and pore pressures on these instruments. This chapter focuses on the particular experience gained at UBC with such instrumentation.

5.2 Equipment description

5.2.1 Development of the lateral stress module Model II (LSM-II)

Early attempts at UBC to develop a lateral stress module (LSM) were based upon use of a cone friction sleeve instrumented to also allow measurement of hoop stresses. Campanella et al. (1990) showed that the lateral stress measured with the instrumented friction sleeve of the UBC lateral stress piezocone Model I (LSCPTU-I) was sensitive to both axial loads on the friction sleeve and on temperature. Even though these effects can be calibrated out by making appropriate corrections to the measured data, modifications to the lateral stress measuring section are required in order to improve data quality and sensitivity. Sully (1991) suggested that further development work on the lateral stress module should be focused on the following aspects:

- Reduce the cross talk effects by re-designing the friction sleeve so that the stress sensitive under-reamed section is on the section of the sleeve that is in tension rather than on the main body which is in compression.
- Design a thinner instrumented section so that the balance between wall thickness, sensitivity and durability is improved.
- Improve the sensitivity of the friction load cell and the lateral stress pore pressure (u_{LS}) transducer if reliable estimations of coefficient of earth pressure at rest (K_0) are to be achieved.
- Provide accurate high resolution data for both σ_{LS} and u_{LS} sensors.
- Modify the existing LSCPTU-I so that the stress sensing sleeve could be located at varying distances behind the cone tip.

In an attempt to increase the resolution of the measurements of the lateral stress section, a new instrumented friction sleeve with a wall thickness of 0.75 mm was designed and built at UBC. However, the reduction in thickness resulted in lateral stress measurements that were more sensitive to changes in temperature and “cross-talk” effects. The use of instrumented friction sleeves for measuring lateral stresses involves several challenges in both the instrumentation and the robustness of the element in contact with the soil. As a result, further development work at UBC between 1997 and 2001 resulted in a new lateral stress module Model II (LSM-II) equipped with a passive sensing element. The new instrument measures the lateral stress in a similar manner to that described by Bayne & Tjelta (1987) and Takesue & Isano (2001).

5.2.2 Equipment details

5.2.2.1 Instrumentation

The UBC lateral stress Model II (LSM-II) consists of an external curved pressure receiving plate or load transfer “button”, with a fine setscrew on its centre and a Honeywell Model 13 compression subminiature load cell installed inside the body of the instrumented section. The load transfer “button” is mounted flush on one side of the instrumented section with an O-ring mounted on it to provide a radial seal that prevents the ingress of both soil and water into the body. Figure 5.1 shows a schematic diagram of the lateral stress Model II developed and built at UBC.

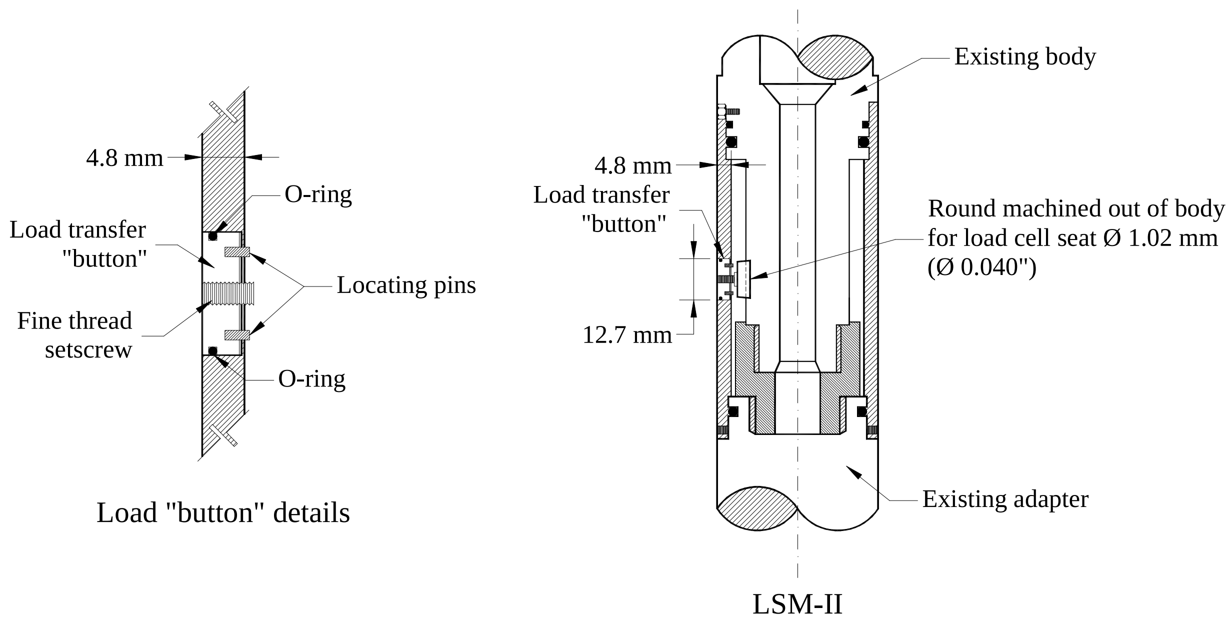

Figure 5.1 UBC Lateral stress module Model II (LSM-II) (after Jackson, 2007).

The instrumented section was originally designed to be mounted on a standard 15 cm^2 UBC seismic piezocone unit. However this unit was not easy to assemble or disassemble and had some instrumentation problems. Therefore, the new lateral stress module is now mounted behind a standard 10 cm^2 UBC seismic piezocone. A special low angle adaptor located 43.5 cm above the cone tip provides a gradual transition in diameter from a 35.7 mm to 43.5 mm. The lateral stress sensor is located 69.5 cm behind the cone shoulder (19.5*D*) and the pore pressure developed during penetration is measured by a pore pressure transducer located 58.5 mm above the lateral stress sensor or 21.1*D* behind the cone shoulder, where *D* is the diameter of the cone.

The eight-channel lateral stress seismic piezocone (LSSCPTU) has a tip area of 10 cm^2, a friction sleeve area of 150 cm^2 and allows simultaneous measurement of the following parameters: tip resistance (q_c), pore pressure behind the tip (u_2), sleeve friction (f_s), pore pressure behind the friction sleeve (u_3), inclination, lateral stress 19.5 diameters behind the tip (σ_{LS}), and pore pressure at about 21.1 diameters behind the tip (u_{LS}) (see Figure 5.2). These channels operate over a 10 V range, and the sensitivity of the lateral stress sensor is 0.005 V or 1 kPa. Downhole shear wave velocity tests can also be performed using a seismic module mounted just behind the cone that contains an accelerometer as a receiver of the seismic waves. The piezocone unit also contains a temperature sensor. However, when the lateral stress module is attached this sensor is not activated. The effect of temperature on both σ_{LS} and u_{LS} sensors is discussed in section 5.3 of this chapter.

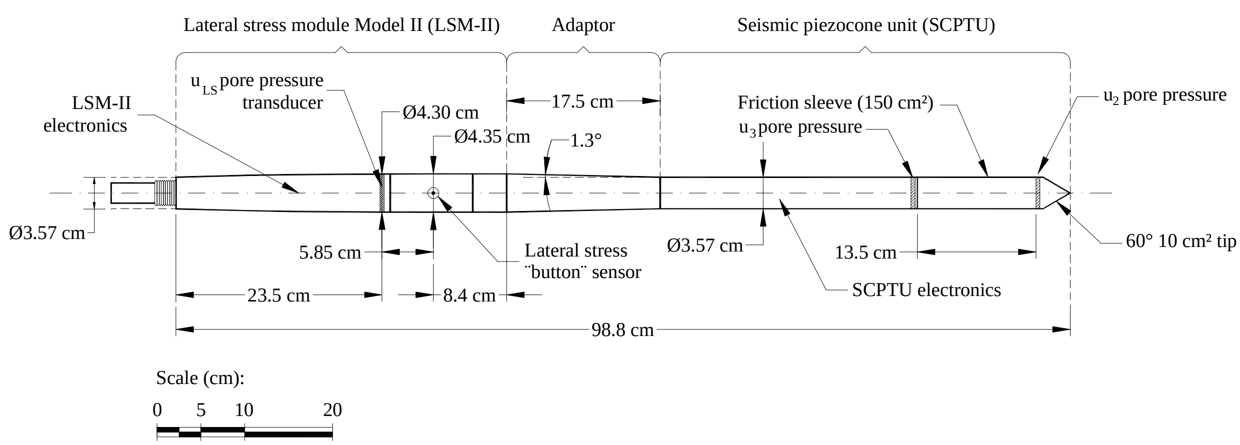

Figure 5.2 UBC lateral stress seismic piezocone cone (LSSCPTU).

5.3 Laboratory evaluation of LSM-II measurements

5.3.1 Introduction

The calibrations of load cells and pore pressure transducers of the piezocone unit were performed according to standard procedures adopted at UBC (e.g. Campanella & Howie, 2005). The lateral stress module Model II (LSM-II) was calibrated for the following conditions: (i) hydrostatically applied confining pressure, (ii) temperature sensitivity, (iii) calibration for axial load effect, and (iv) time-dependent stability of both σ_{LS} and u_{LS} sensors.

5.3.2 Hydrostatic calibration

The calibration was performed with a calibration chamber fitted over the lateral stress module (LSM-II). An air line was connected to the cylinder and O-rings were mounted internally on each end of the calibration device to provide an air-tight seal between the LSM-II and the chamber. Pressure increments of 138 kPa ($\approx$20 psi) were used, up to a maximum of 690 kPa ($\approx$100 psi). The room temperature was monitored throughout the calibration process and measurements indicate a constant temperature of about 22°C. The hydrostatic pressure was applied in loading and unloading sequences. Figure 5.3 shows the results of the calibration of both lateral stress and pore pressure sensors.

The calibration factor for the lateral stress sensor (σ_{LS}) is 0.0055 V/kPa or 181.8 kPa/V, whereas for the pore pressure (u_{LS}) is 0.0044 V/kPa or 227.3 kPa/V respectively. The hysteresis effect on the load-unload response of the u_{LS} sensor is fairly small with an average value of about 0.51% of the full scale (FS). The maximum hysteresis effect on the lateral stress sensor is about 1 % of FS and requires careful consideration when assessing the field measurements.

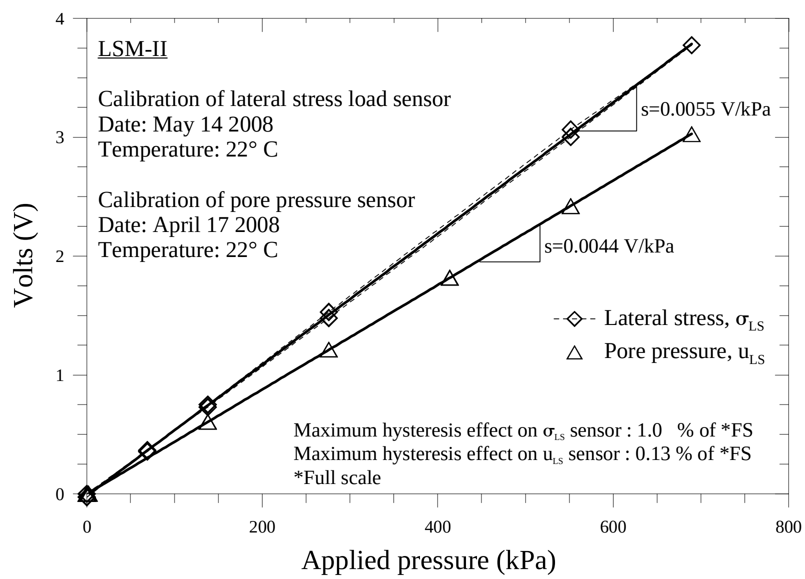

Figure 5.3 Pressure calibration of lateral stress module (σ_{LS} and u_{LS}).

5.3.3 Calibration for temperature effects

The subminiature load cell of the lateral stress sensor is temperature compensated for a range of 15.6°C to 71.1°C (60°F to 160°F). However, in addition to the temperature compensation of the load cell it is important to check the effect of temperature variations on the baseline of the lateral stress sensor. Prior to calibration, the cavities of pore pressure transducers for the piezocone (u_2 and u_3 sensors) and lateral stress module (u_{LS}) were saturated according to standard procedures adopted at UBC (Campanealla & Howie, 2005). The whole piezocone was immersed in a bath of water in order to evaluate the temperature sensitivity of the lateral stress module. Readings on all channels were taken over a 15 minute period at a temperature of 21° C, and these measurements were used as reference values for assessment of temperature effects. After stable readings were recorded on each channel the temperature was rapidly reduced to 0° C by adding ice. This temperature was kept constant for approximately 25 min. After that, the temperature was increased in steps by adding hot water and readings on all channels were taken over a 20 min period.

Throughout the calibration process special care was taken to maintain the water level constant and readings on all channels were taken every 20 seconds. The results of this calibration are presented in Figure 5.4 and Figure 5.5. They indicate the non linearity of both σ_{LS} and u_{LS} sensors. Also, the magnitude of the baseline shift in the lateral stress is larger than that of the pore pressure. However, the effect of temperature on both channels is fairly small, so it was judged that a correction for temperature effects is not necessary. It is recommended to carefully review the shifts in the baselines of these channels at the end of each sounding in order to assess the temperature effects on field measurements. The calibration clearly shows that the lateral stress module Model II (LSM-II) is less sensitive to temperature effects than the lateral stress module described by Campanella et al. (1990) and Sully (1991). Campanella et al. (1990) reported that the temperature coefficient B_t for the lateral stress channel was +0.0036 V/°C on cooling for a temperature range from 10 °C and 19 °C. The value of B_t for the new design would be about +0.0028 V/°C or +0.51 kPa/°C on cooling for a temperature range from 5 °C to 21 °C.

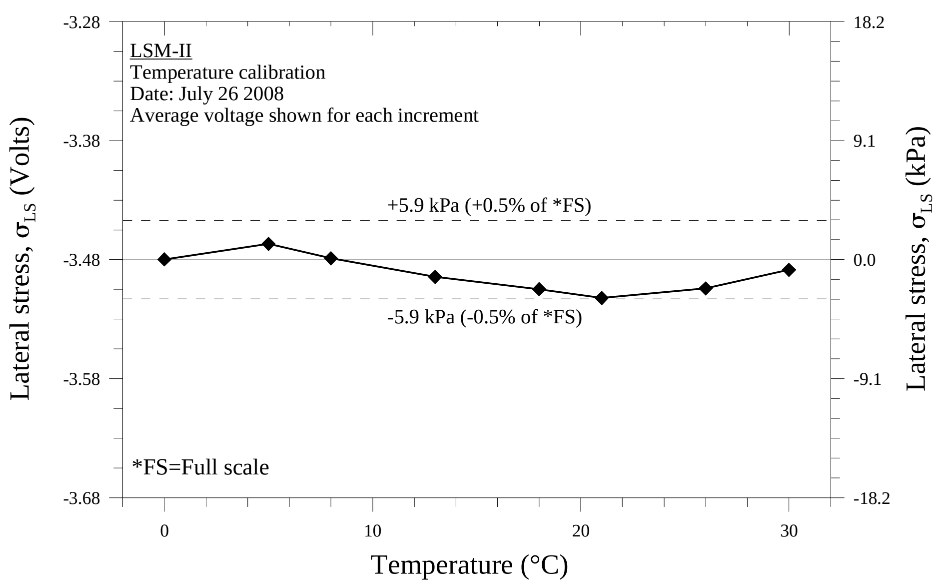

Figure 5.4 Temperature sensitivity of lateral stress (σ_{LS}) baseline.

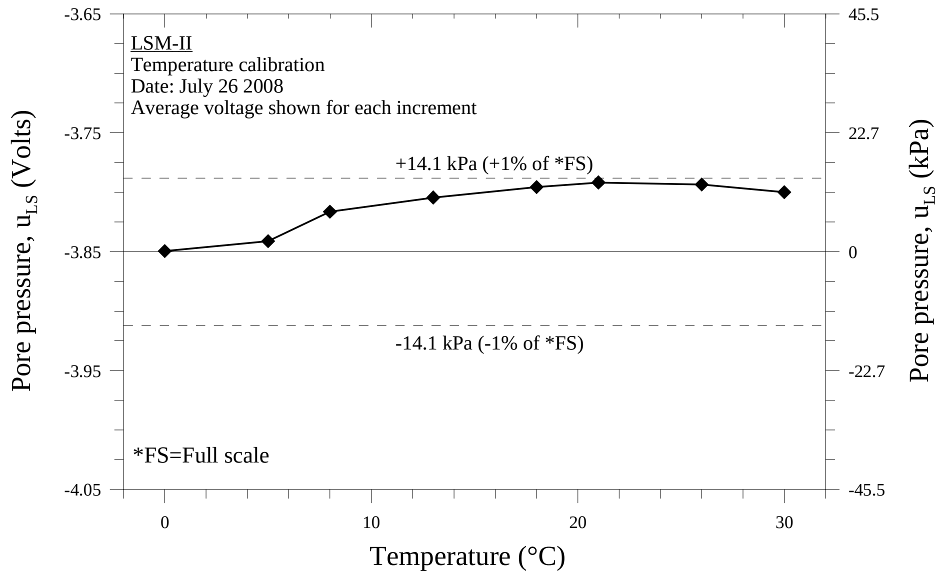

Figure 5.5 Temperature sensitivity of pore pressure (u_{LS}) baseline.

5.3.4 Calibration for axial load effect

This calibration was performed in order to assess the variation in zero reading of the lateral stress sensor due to axial loading of the cone. Due to space limitations of the hydraulic loading frame at UBC the LSM-II was removed from the seismic piezocone unit. Then, the LSM-II was set up in the calibration frame and axial load was applied. A total of four load-unload cycles were performed under zero confining pressure and at constant temperature. Load increments of 1.11 kN ($\approx$250 lb) were used, up to a maximum of 11.6 kN($\approx$2600 lb), and for each increment the load was maintained constant for 1 minute. The maximum load applied of 11.6 kN is equivalent to a cone tip resistance (q_c) of 115.6 bar. Figure 5.6 presents the results of the calibration for axial load effect. The results in Figure 5.6 indicate that the current design of the lateral stress sensor still remains fairly sensitive to axial loading. For example, the variation in the zero reading for an axial load of 11.6 kN is 0.33 Volts or 57 kPa, which corresponds to 5.2% of the full scale. Linear regression analysis of the data gave a calibration factor of 0.028 V/kN or 5.1 kPa/kN for loading and unloading. On the basis of these results, the lateral stress data can be related to the cone tip resistance (q_c), and therefore corrected to account for cross talk according to the equation

$$\sigma_{LS} = \sigma_{LS(m)} - 0.00508 q_c \qquad \text{Equation 5.1}$$

in which σ_{LS} is the corrected lateral stress for cross talk effects, $\sigma_{LS(m)}$ is the measured lateral stress, and q_c is the cone tip resistance. All stresses are in bars.

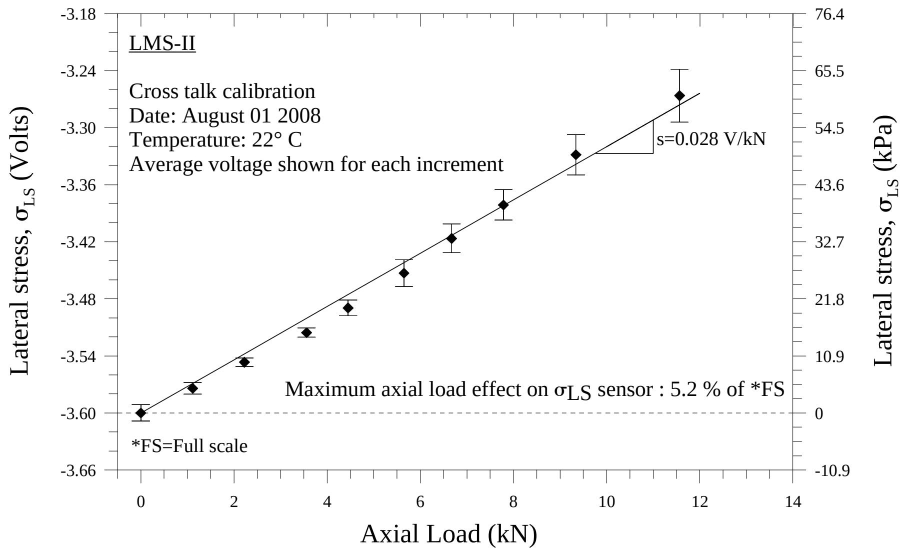

Figure 5.6 Evaluation of cross talk on lateral stress channel due to axial load.

5.3.5 Evaluation of baseline stability

After baselines were taken the piezocone was left at a room temperature of 23° C ±1° and under conditions of zero axial and hydrostatic loads. The baseline drift over time on all channels was monitored over a 6.8 hour period, during which time readings on all channels were taken every minute. Figure 5.7and Figure 5.8 show the time-dependent drift of the lateral stress and pore pressure sensors respectively. The baseline in both channels is fairly stable and with small variations. For instance, the deviation from the zero point in the lateral stress sensor is ±0.46 kPa or ±0.04% of full scale, whereas in the pore pressure it is ±0.45 kPa or ±0.07% of full scale respectively. It is observed in Figure 5.7 and Figure 5.8 that the baselines of both channels are relatively stable.

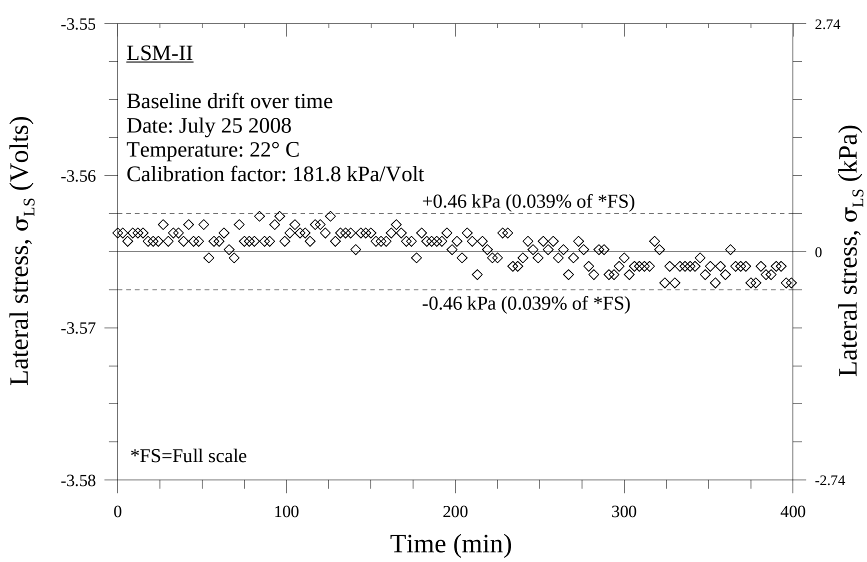

Figure 5.7 Evaluation of baseline shift on σ_{LS} channel over time.

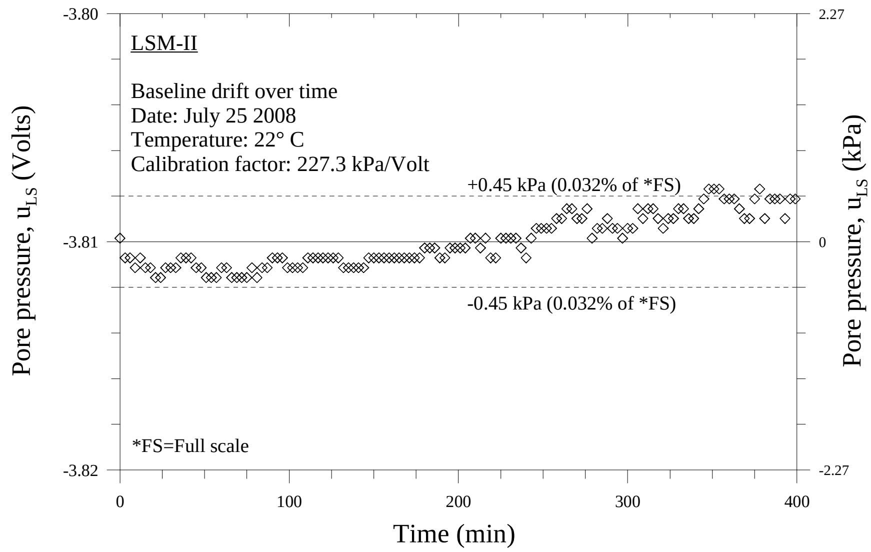

Figure 5.8 Evaluation of baseline shift on u_{LS} channel over time.

5.3.6 Discussion of calibration results

Results of laboratory calibrations have shown that the measured lateral stress is fairly sensitive to axial loads on the cone and on temperature. The effect of temperature variations on lateral stress data is less than that of the cross talk effect due to axial load. For a temperature range of 5 °C to 21 °C, the maximum baseline drift recorded was 9.5 kPa, whereas a baseline shift of 57 kPa was observed for an axial load range from 0 to 11.6 kN. In terms of the full scale of the lateral stress sensor, the baseline shift due to temperature variations is 0.82%, while for axial load it is 5.2%.

The cross talk effect on the lateral stress sensor due to axial loading of the cone is quite significant. The lateral stress module was designed to be separated from the body of the penetrometer by providing clearance at the top and bottom, with the sleeve held in place by several O-rings (see Figure 5.1) as it was originally also to be a friction sleeve. The “floating” configuration allows the LSM-II to be isolated from the cone body and therefore from any axial load. However, the interaction between the set screw and the load cell will be affected by relative movement between the components. This behaviour requires further study to assess repeatability and to consider design changes to mitigate the effects.

Results of calibrations have demonstrated that in the current design, lateral stress measurements are sensitive to axial loads acting on the cone and variations in temperature. Both effects can be calibrated out by making appropriate corrections to the measured data. Equation 5.1 allows correction of measured lateral stress for the effect of axial loads. However, it is not possible to correct the data for temperature effects since the LSM-II does not have a temperature sensor. Nonetheless, the results of laboratory calibrations indicate that the effect of temperature variation on measured lateral stress (σ_{LS}) and pore pressure (u_{LS}) data is small. The temperature sensor of the piezocone unit could be used to monitor temperature variations. However, when the lateral stress module (LSM-II) is attached this sensor is not activated.

Lunne et al. (1997) stated that problems remain with the instrumentation of the lateral stress cone. They observed that it was difficult to maintain a robust cone while obtaining the required sensitivity of the readings. The results of laboratory calibrations indicate a good performance of the LSM Model II with the load transfer "button" configuration providing a balance between the robustness of the cone and the sensitivity of the lateral stress sensor. However, the results of laboratory calibration indicate that lateral stress measurements still remain fairly sensitive to axial loads and, to a lesser degree, on temperature. Also, the load-unload response of the sensor is affected by the friction between the radial O-ring and the body of the module (see Figure 5.1). As a result, minor improvements in the design are required in order to reduce the effect of these factors and increase the sensitivity.

Table 5.1 Summary of LSM-II calibration results

Sensor	Stress range (kPa)	Calibration factor (kPa/V)	Hysteresis (% of FS)	Temperature sensitivity (% of FS/°C)	Cross talk due to axial loading (% of FS)	Baseline drift at 22°C (% of FS)
σ_{LS}	1170	181.8	1.0	0.044 (5 to 21°C)	5.2 (0 to 11.6 kN)	0.039 (0 to 6.8 h)
u_{LS}	1406	227.3	0.13	0.045 (5 to 21°C)	N/A	0.032 (0 to 6.8 h)

5.4 Field evaluation of LSSCPTU measurements

The assessment of the field performance of the lateral stress seismic piezocone (LSSCPTU) was undertaken at one former CANLEX Phase II site. The KIDD 2 site was selected due to the fact that the soil profile consists primarily of a relatively clean sand deposit underlain by normally consolidated silty clay as described in section 3.3.3.2. This allowed piezocone (CPTU) and lateral stress data to be collected under drained and undrained conditions in the same sounding. Additionally, information on lateral stress conditions was available at this site from the interpretation of results of self-boring pressuremeter (SBP) tests (In-Situ Testing Group, 1995a).

The objective of the field testing program carried out at the KIDD 2 site were: (i) assess the sensitivity of lateral stress (σ_{LS}) and pore pressure (u_{LS}) sensors to changes in stratigraphy during penetration, (ii) monitor the response of σ_{LS} and u_{LS} in dissipation mode and (iii) assess the repeatability of LSM-II data by comparing the results of two adjacent soundings (LSC-01 and LSC-02). It is important to point out that shear wave velocity measurements were not performed with the LSM-II at this site since testing was aimed at assessing the performance of the lateral stress module rather than collecting a full set of data.

5.4.1 Testing procedures

Prior to performing each sounding with the lateral stress seismic piezocone (LSSCPTU), all pore pressure measuring systems, i.e. u_2, u_3 and u_{LS}, are de-aired and saturated with glycerine according to standard procedures adopted at UBC (Campanella & Howie, 2005). The cable is connected to the LSSCPTU and the data acquisition system is started. Baseline voltage readings on all channels are taken with the cone suspended above the ground and zero load on all channels. The warm up time before baselines were taken varied between 5 to 10 min. Then, the cone is lowered through the guide/wiper sleeve until the apex of the cone is at ground level or the reference starting depth in case of a predrilled hole. The verticality of the cone rods is checked manually in two directions with a level. Also, if downhole shear wave velocity tests are to be performed, the accelerometer inside the cone is aligned parallel to the axis of the shear beam, and the distance between the cone and the shear beam is measured. For the UBC research truck the distance between the rod string and the centre of the shear beam is 1 metre.

The lateral stress seismic piezocone is pushed into the ground at a standard rate of 2 cm/sec and tip resistance, q_c, sleeve friction, f_s, pore pressures, u_2, u_3 and u_{LS}, and lateral stress, σ_{LS}, are recorded at intervals of 2.5 cm. At the end of the sounding, the LSSCPTU is retrieved to the surface and baselines on all channels are taken again. The comparison of pre and post-penetration baselines allows evaluation and correction for any drift which may have taken place during the duration of the sounding. During the sounding, the penetration is stopped at selected depth intervals (usually every metre when rods are being added) and the rod string is unloaded. In SCPTU soundings, seismic waves are generated at the surface using a consistent energy by dropping a sledge hammer in a standard manner to strike the end of a steel beam, which is anchored using the stabilizers of the cone truck. This procedure results in a vertical profile of vertically propagating shear wave velocities.

At selected depths, penetration is halted in order to perform dissipation tests. The decay of pore pressure is monitored on u_2, u_3 and u_{LS} channels at the same time. Likewise, the relaxation of total lateral stress, σ_{LS}, is recorded. Campanella & Howie (2005) recommend removing the load on the rod string prior to execution of pore pressure dissipation measurement for all piezometer element locations. A detailed and updated description of the seismic piezocone penetration test (SCPTU) as well as its use, application and interpretation can be found in Campanella & Howie (2005).

5.4.2 Repeatability of LSSCPTU field measurements

Figure 5.9a compares the pore pressures (u_{LS}) and total lateral stresses (σ_{LS}) recorded with LSM-II in both tests (LSC-01, LSC-02). It also shows the response of the u_{LS} and σ_{LS} sensors before and after pauses in penetration, where dissipation tests were performed. A remarkably good agreement between the two pore pressure profiles is evident throughout the soil profile with minor variations below about 22 m depth. It is also interesting to note that in both u_{LS} and σ_{LS} profiles, the distance required to regain the original penetration values is practically the same after penetration was resumed upon completion of the dissipation test performed at about 24.25 m depth.

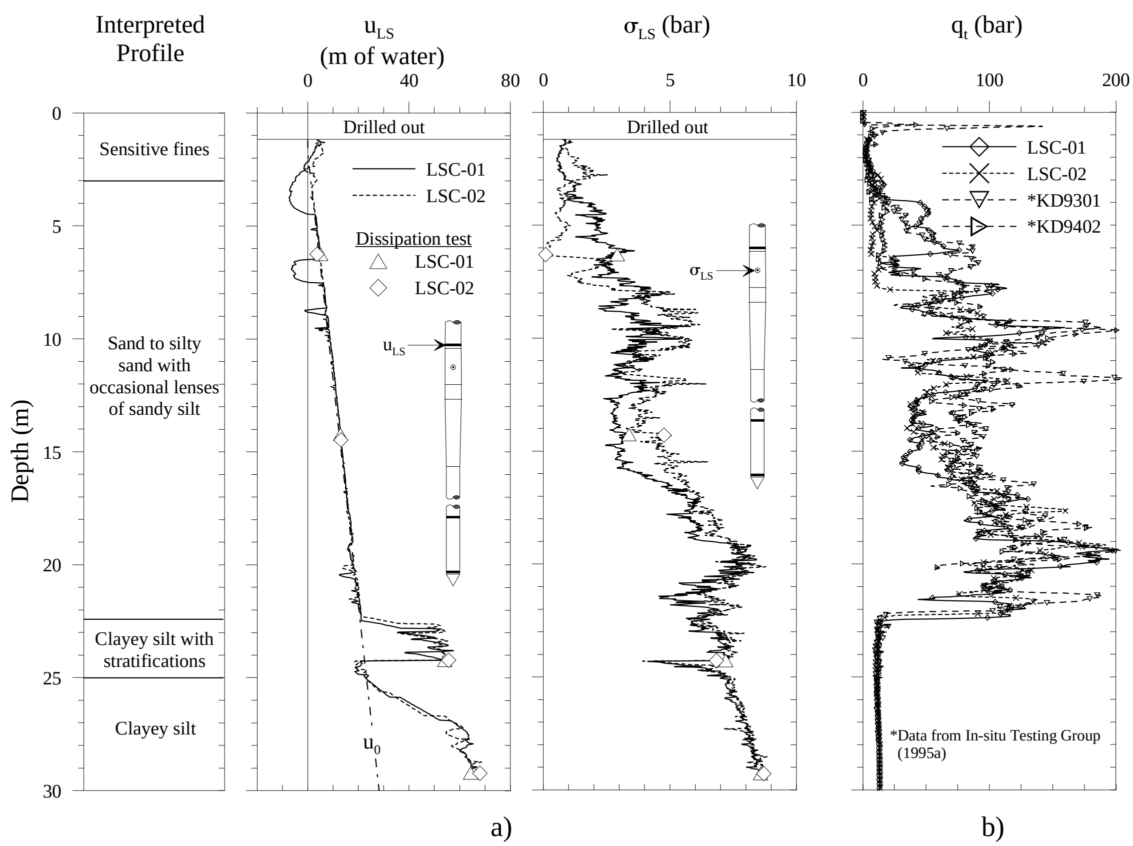

Figure 5.9 Comparison of LSM-II and CPTU data collected in both tests, KIDD 2 site.

The pore pressure profiles recorded in both tests exhibit similar trends before and after dissipation, suggesting a good degree of repeatability of the u_{LS} data recorded. On the contrary, the lateral stress profile shows significant variations above 20 m depth but below this depth, both σ_{LS} profiles exhibit similar trends and even the same response upon completion of dissipation tests. It is considered that the difference between σ_{LS} profiles is caused predominantly by the soil variability and not by problems with the instrumentation of the LSM-II. The soil variability is illustrated in Figure 5.9b which shows a comparison of several q_t profiles performed in the same area. In summary, the data collected at the KIDD 2 site demonstrates excellent performance of the LSM-II in terms of repeatability of data recorded.

5.4.3 Assessment of LSM-II baselines shift

The results of laboratory calibration showed that total lateral stress measurements are fairly sensitive to axial loads and, to a lesser degree, temperature. Likewise, the pore pressure sensor mounted on the lateral stress module Model II (LSM-II) is fairly sensitive to temperature changes but within an acceptable range. As previously described, initial baseline voltage readings on all channels of the LSSCPTU are taken with the instrument suspended above the ground and zero loads on all channels. Once the target depth is reached, the LSSCPTU is retrieved to the surface and voltage readings on all channels are taken again under similar conditions. The comparison of pre and post-penetration baselines allows evaluation of and correction for any drift which may have taken place during the duration of the sounding, and also allows a preliminary assessment of the performance of the instrumentation of the LMS-II in the field. Table 5.2 presents a summary of baseline shifts observed in the lateral stress and pore pressure sensors at the end of each test.

Table 5.2 Summary of baseline shifts of lateral stress and pore pressure sensors of the LSM-II.

Site (*Date*) (*Ambient temperature*)	Test No.	Baseline shift					
		Lateral stress sensor (σ_{LS})			Pore pressure sensor (u_{LS})		
		(V)	(kPa)	% of FS	(V)	(kPa)	% of FS
KIDD 2 *(14/06/2008)* *(16.7°C)*	LSC-01	0.087	15.9	1.36	0.020	4.6	0.33
	LSC-02	0.004	0.7	0.06	0.022	4.9	0.35
Massey Tunnel *(18/06/2008)* *(16.6°C)*	LSC-03	0.067	12.2	1.04	0.013	3.0	0.21
	LSC-04	0.090	16.4	1.40	0.017	3.8	0.27
Patterson Park *(20/06/2008)* *(19.3°C)*	LSC-05	0.040	7.2	0.62	0.054	12.2	0.87
Colebrook Overpass *(09/07/2008)* *(22.4°C)*	LSC-06	0.104	18.9	1.62	0.017	3.8	0.27
	LSC-07	0.044	8.0	0.68	0.017	3.8	0.27

The ASTM standard method for performing electronic friction cone and piezocone tests indicates that the magnitude of the baseline shift should not exceed 1% of full scale output (FS) for the cone tip resistance and 2% of FS for the friction sleeve (ASTM D 5778). If the magnitude of the baseline shift exceeds these limits the cone should be cleaned allowed to equalize to the ambient temperature, and a new baseline is recorded. If this value is in good agreement with the initial baseline, and the difference is within the specified limits, a load range calibration check is not required. However, if the baseline shift is still not within the specified criteria the linearity should be checked with a load range calibration. For further information on the load range calibration the reader is referred to the standard test method ASTM D 5778.

A detailed review of raw data recorded in both tests performed at the KIDD 2 site indicates a baseline shift of 0.014% to 0.001% of the full scale output (FS) in the total lateral stress channel (σ_{LS}), whereas for the pore pressure channel (u_{LS}) the shift was 0.328% and 0.348% of FS, respectively. It can be noted that the maximum baseline shift in the σ_{LS} sensor occurred in the first test performed at the Colebrook Overpass site. The magnitude of the maximum shift is 18.9 kPa or 1.62% of the full scale (FS) of the sensor. The maximum ambient temperature the day when LSSCPTU testing was performed at this site was about 22°C. Results of laboratory calibrations indicate a temperature sensitivity of 0.044 % of FS/°C. Then, if the temperature of the ground was assumed to be around 11°C, the reduction in temperature, when the probe came in contact with the ground, would result in a baseline shift of about 0.48% of FS. The temperature sensitivity and hysteresis of the sensor result in a total theoretical baseline shift of 1.48% of FS, which is very close to the recorded value and confirms the results of laboratory calibrations of the lateral stress sensor.

The maximum baseline shift in the u_{LS} sensor occurred in the test performed at the Patterson Park site. A maximum baseline shift of 12.2 kPa or 0.87% of FS was recorded. Temperature records indicate a maximum ambient temperature of 19.3°C the day when the LSSCPTU was pushed at this site. If an analysis similar to that of the temperature sensitivity of the lateral stress sensor is performed and the similar assumptions are made, the theoretical baseline shift in the u_{LS} sensor will be about 0.37% of FS. Then, the addition of the hysteresis of the sensor yields a total theoretical baseline shift of 0.50% of FS, which is less than the measured value. It is suggested that the difference between measured and calculated baseline shifts in the u_{LS} sensor at this site was caused predominantly by temperature variations when penetrating through dense sand layers. Lunne et al. (1997) suggest that the use of a temperature sensor mounted in the cone body may explain anomalies detected when penetrating through mixed soil deposits, which is the case of the soil profile at the Patterson Park site. It may also help to understand the temperature regime before, during and after pauses in penetration. They also point out that temperature effects are not restricted to the cone; changes in temperature of the data acquisition system can also result in zero shifts in the recorded data. Further research is required to investigate these effects on the data recorded with the LSM-II.

Campanella & Howie (2005) suggest that the zero load error or baseline shift of the cone tip resistance should, in general, not exceed 0.5% to 1% of the full scale output (FS), and in soft soils the error should be considerably less than 0.5%. Similarly, as previously discussed, the ASTM standard method (ASTM D 5778) indicates that the change in initial and final baseline values should not exceed 1% of FS for the tip and 2% of FS for the sleeve. If these recommendations are used to assess the accuracy of the pore pressure data recorded with the LSM-II, the maximum baseline shift in the u_{LS} sensor is acceptable. However, the bulk of zero load errors observed in the lateral stress sensor are considerably above the limit suggested by Campanella & Howie (2005) and the ASTM standard method, and hence minor improvements in the design are required to reduce the hysteresis effect.

5.4.4 Assessment of penetration measurements

Figure 5.10 and Figure 5.11 present profiles of field measurements recorded with the lateral stress seismic piezocone (LSSCPTU) at the KIDD 2 site. The locations of pauses in penetration to allow monitoring of changes in pore pressure and lateral stress with time are also indicated. Firstly, considering the proximity of the test holes (approximately 3 m), the q_t profiles are very similar with the exception of a variation between 0 m to 7.5 m depth. The difference in q_t values within this zone can be attributed to variations in thickness of the upper layer. Similar variations were identified from the results of piezocone tests performed at the same site as part of CANLEX (see Figure 3.11). It is observed in both profiles that from 4.5 m to about 22.5 m the penetration pore pressures throughout the sand deposit are close to hydrostatic, which indicates that penetration was performed under drained conditions.

Whenever excess pore pressures are generated in finer grained soils, u_{LS} is consistently less than u_3 which is less than u_2. This is particularly noticeable in the fine grained deposits beginning at a depth of about 22.5 m. The q_t values drop rapidly to around 10 bar and large excess pore pressures are recorded in all channels, which indicate the transition from drained to undrained penetration and from coarse grained to fine grained soil. The variations in magnitude of pore pressure values from 22.5 m to 25 m are indicators of interbedding of sand and silt, as indicated by variation in the friction ratio (R_f) profile. Also, below about 25 m depth, both R_f and pore pressures profiles indicate that soil is fairly homogeneous and without interbeds.

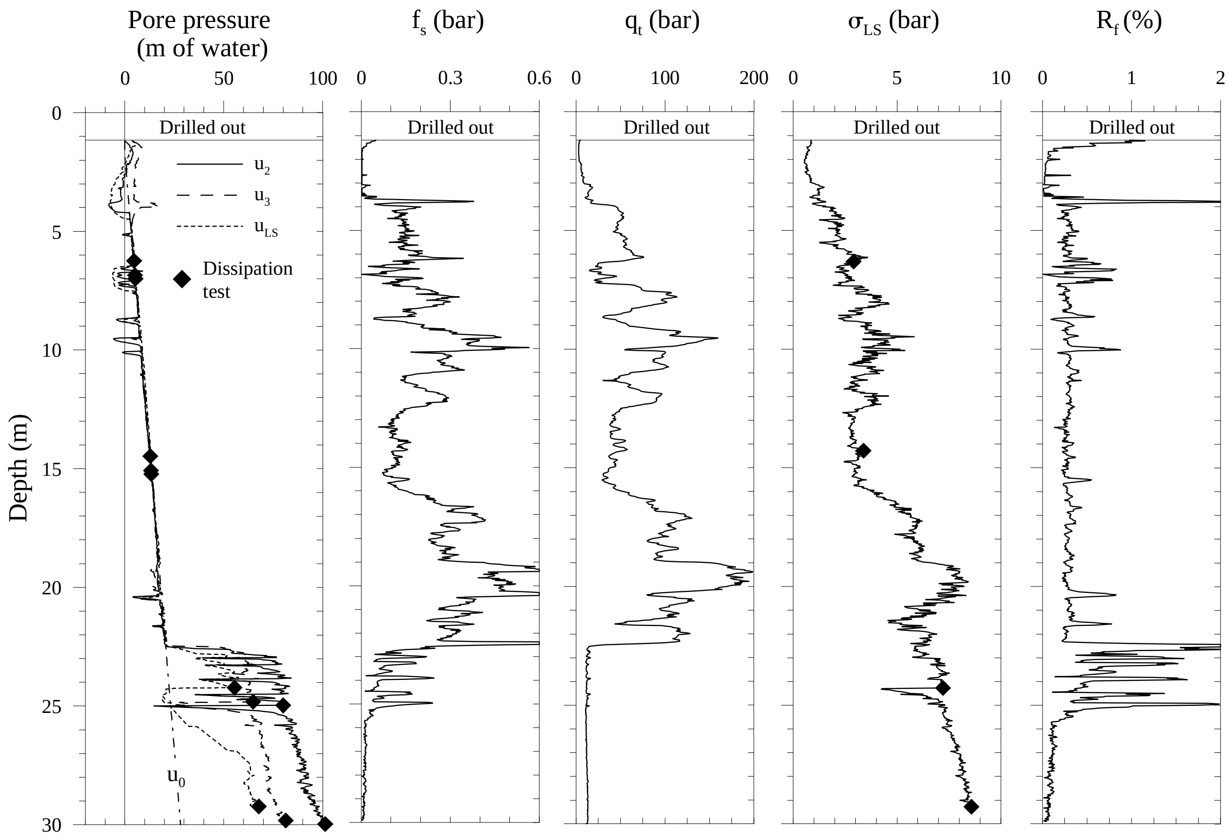

Figure 5.10 Results of lateral stress piezocone test at KIDD 2 (Test No. LSC-01).

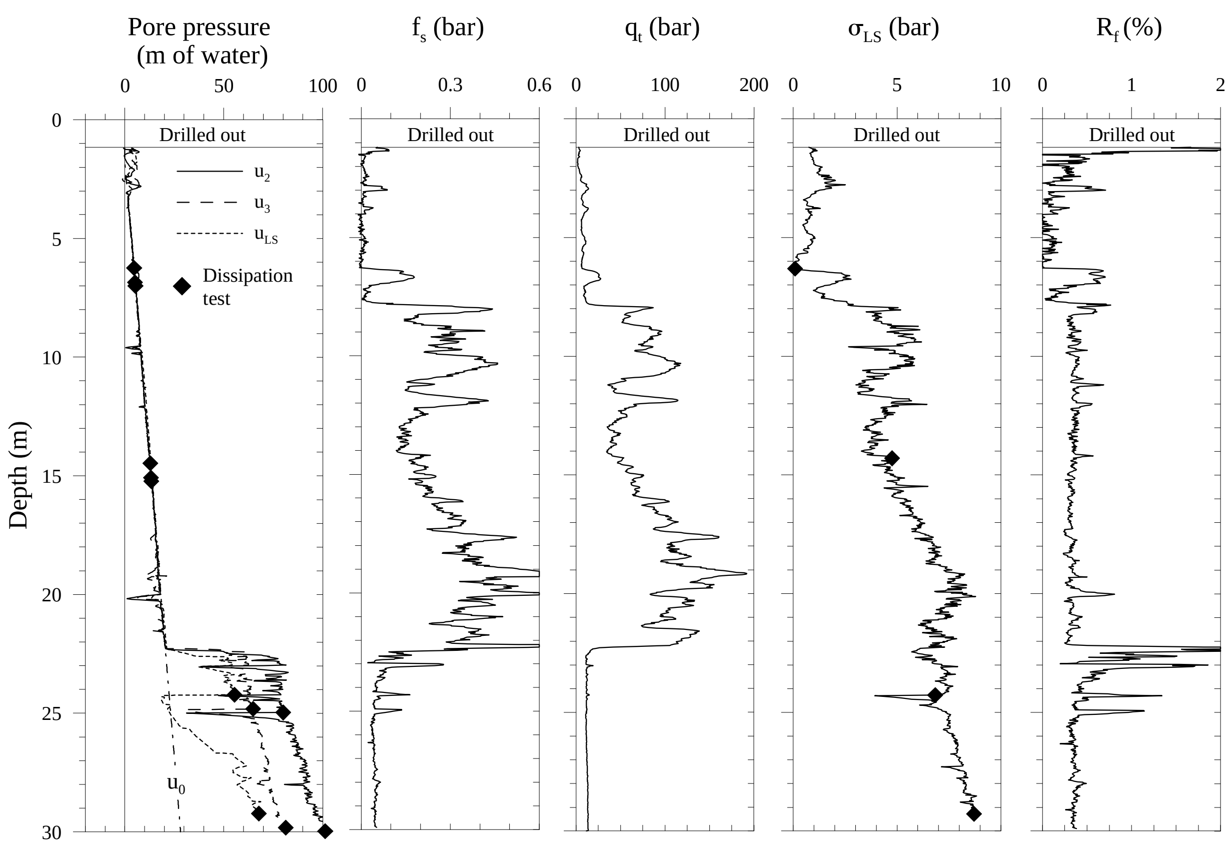

Figure 5.11 Results of lateral stress piezocone test at KIDD 2 (Test No. LSC-02).

In Figure 5.10 and Figure 5.11, the variations in pore pressures measured behind the tip (u_2) and behind the friction sleeve (u_3) indicate the presence of large gradients within the zone immediately above the cone tip. The tip resistance, q_t, is clearly more sensitive to the transition from drained to undrained penetration which occurs at about 22.5 m depth than σ_{LS}. Whereas q_t drops considerably, σ_{LS} continues to increase with depth with a slope very similar to that of the pore pressure profiles. In sands the ratio $\sigma_{LS}/q_t<0.1$, whereas in undrained penetration $\sigma_{LS}/q_t \approx 0.6$. This is not surprising since pore pressure makes up a significant portion of the measured total lateral stress in undrained penetration, suggesting a good response of the lateral stress sensor to changes in stress and pore pressure due to enlargement of the hole as the cone advances.

5.4.4.1 Preliminary assessment of geometry effects on measured data

During penetration, soil in contact with the cone experiences high stresses beneath the tip followed by rapid unloading as it passes the shoulder of the cone. As discussed in section 2.4.2 of this thesis, the friction on the cone rods becomes relatively constant beyond a distance of about 10 to 11 cone diameters (*D*) behind the cone tip. In the case of the UBC LSSCPTU, the gradual increase in diameter will likely cause an increase in lateral stress as the soil is displaced outwards again. This is a different condition than existed at the location of the lateral stress piezocone Model I (LSCPTU-I) tested by Sully (1991).

The tapered section of the lateral stress seismic piezocone (LSSCPTU) is similar to that of the instrumented sharp cone developed by Ladanyi & Longtin (2005). The sharp cone test (SCT) consists of pushing a low-angle truncated cone into a smaller diameter predrilled pilot hole. A system of pressure transducers installed at several levels of the surface of the cone record the resistance of the soil against the enlargement of the pilot hole due to the cone penetration. Ladanyi & Longtin (2005) point out that taper angles of 1° to 2° are found convenient for testing saturated clays, because they can cover the most important portion of the stress strain curve. The taper angle for the adaptor of the LSSCPTU is about 1.3°. A schematic diagram of the instrumented sharp cone is shown in Figure 5.12.

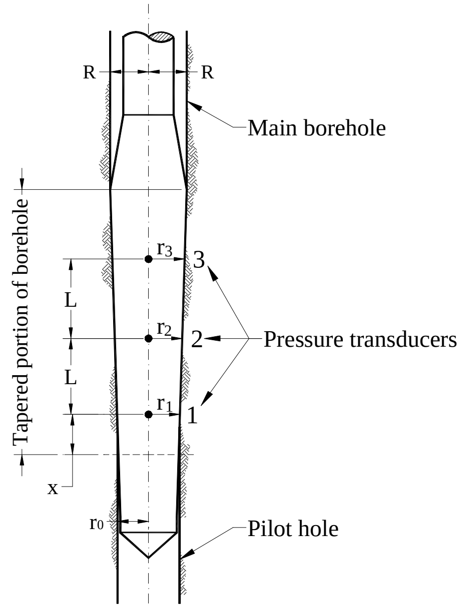

Figure 5.12 Schematic diaphragm of the instrumented sharp cone
(adapted from Ladanyi & Longtin, 2005).

Furthermore, the field measurements recorded with the sharp cone are translated into a relationship between radial pressure and volumetric cavity strain (ΔV/V), similar to the expansion curve of a pressuremeter test. In other words, the sharp cone test is aimed at producing in the soil the expansion of a quasi-cylindrical cavity similar to that of a pressuremeter test. Typical pressure-expansion curves deduced from the results of sharp cone tests are illustrated in Figure 5.13.

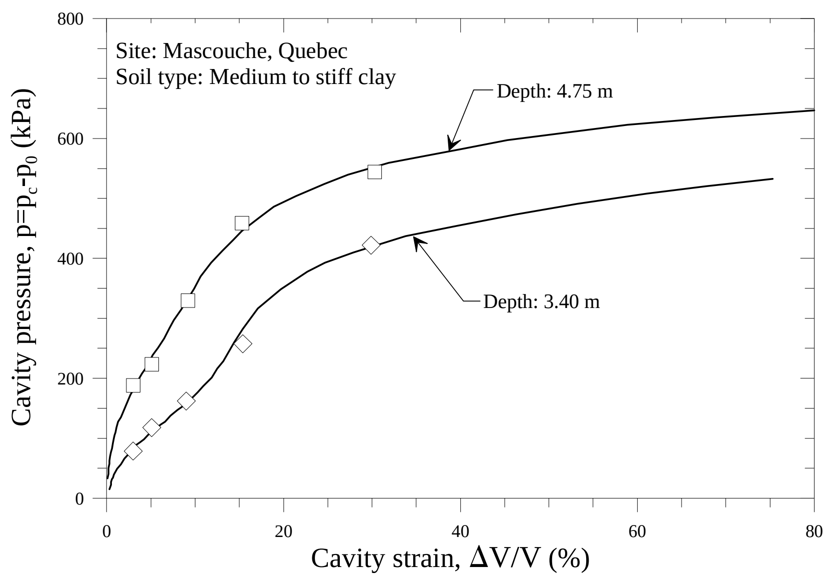

Figure 5.13 Example of pressure-expansion curves deduced from results of sharp cone tests
(adapted from Ladanyi & Longtin, 2005).

The pressuremeter is a cylindrical instrument which can be expanded against the soil. The expanding section typically consists of a rubber membrane which can be inflated by gas or fluid pressure. The deformation of the cavity is measured by displacement transducers mounted inside the membrane or by recording the volume of fluid required to achieve expansion. The pressuremeter unit may be installed in a prebored hole, may be drilled or jetted in or may be pushed in. The pushed in pressuremeter is a full-displacement pressuremeter (FDPM) or cone pressuremeter (CPM). In the CPM, the soil experiences unloading as it passes the shoulder of the cone and then is reloaded during the subsequent pressuremeter test which is carried out during a pause in penetration. The Cauchy strain (ε) at the wall of an expanding quasi-cylindrical cavity during a pressuremeter test is given by:

$$\varepsilon = \frac{(r - r_0)}{r_0} \qquad \text{Equation 5.2}$$

where r_0 the initial radius of the cavity and r the current radius, which is often referred to as the cavity strain. In addition, the change in volume of the cavity, or volumetric cavity strain, $(\Delta V/V)$ due to quasi-cylindrical cavity expansion is

$$\frac{\Delta V}{V} = \frac{(r^2 - r_0^{\ 2})}{r^2} \qquad \text{Equation 5.3}$$

In Equation 5.2 and Equation 5.3, r_0 can be approximated by the cone radius of the lateral stress seismic piezocone (LSSCPTU) (r_0=17.85 mm) and r is the radius at the location where the lateral stress is measured (r=21.75 mm). Therefore, the enlargement of the hole as the LSSCPTU descends results in a maximum cavity strain of about 22% and a cavity volumetric strain of about 33%, respectively. Figure 5.14 and Figure 5.15 show the results of CPM tests in overconsolidated clay (Houlsby & Withers, 1988) and UBC CPM tests in organic normally consolidated clayey silt (Hers 1989), respectively. In Figure 5.14, the expansion curve has reached a limit pressure by the time the cavity has been expanded to 23% cavity strain. In Figure 5.15, the test does not reach 23% strain but is levelling off at the maximum expansion of 20%.

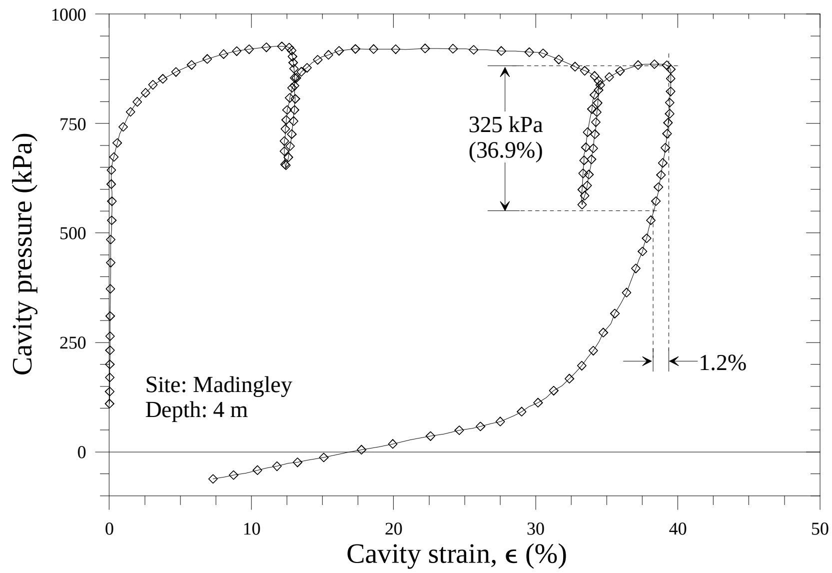

Figure 5.14 Cone-pressuremeter expansion-contraction curve in NC clay (data from Houlsby & Withers, 1988)

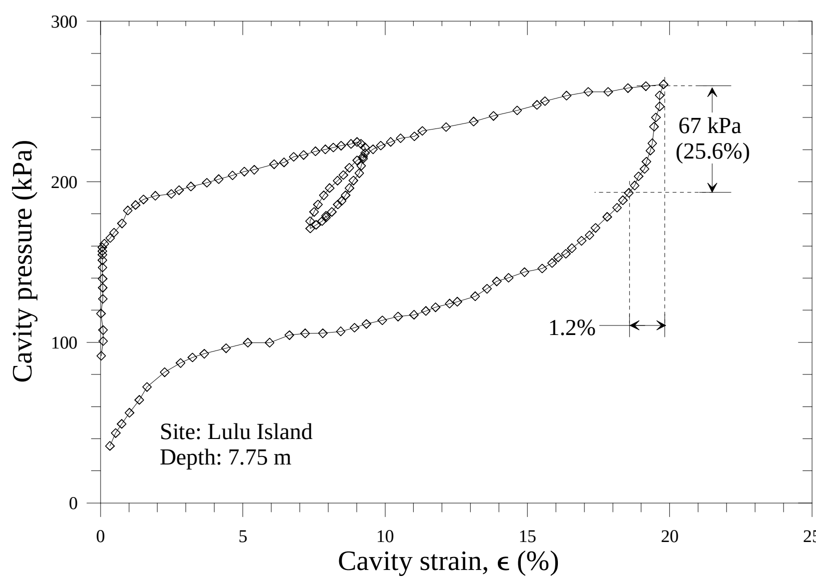

Figure 5.15 Cone-pressuremeter expansion-contraction curve in NC clayey silt (data from Hers 1989).

Figure 5.16 shows the results of a series of cone pressuremeter (CPM) tests carried out in sand (Withers et al., 1989; Ghionna et al. 1995). In the figure, the cavity expansion occurs at a fairly constant pressure beyond a cavity strain of about 15 to 20%.

The expanding sections of the Fugro and UBC CPMs have length to diameter (*L/D*) ratios of 5 and 10 respectively and the relationship between the maximum pressure measured in PM tests and the theoretical model of cavity expansion is affected by the *L/D* ratio of the expanding section, the maximum strain attained and the stiffness of the soil. Nevertheless, it appears that the lateral stress measured with the

LSM-II should be of a similar magnitude to a limit pressure measured in a CPM test. Also, the fact that the enlarged section of the LSSCPTU also works as a friction reducer should not be undervalued.

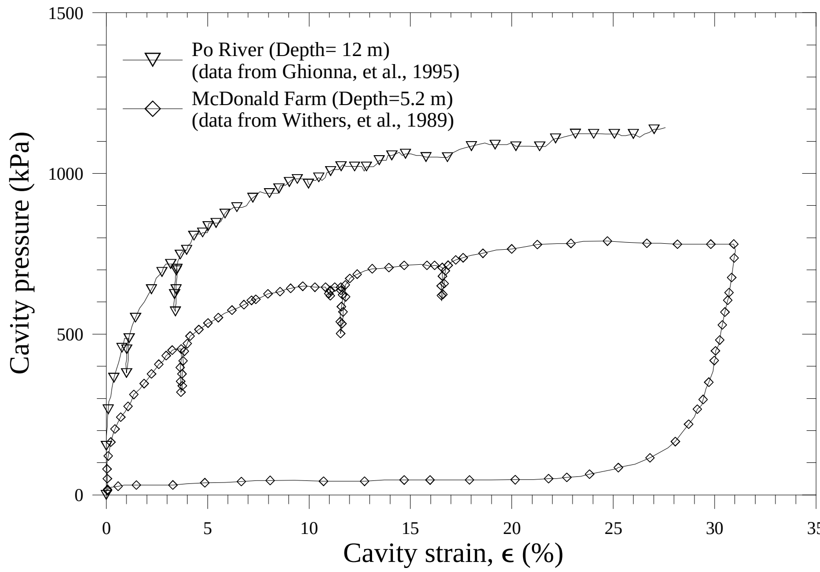

Figure 5.16 Example of CPM tests in natural sand deposits.

As shown in Figure 5.2 the diameter of the lateral stress seismic piezocone (LSSCPTU) remains fairly constant along the lateral stress section, i.e. 43.5 mm, and above the upper pore pressure sensor (u_{LS}) the diameter of the probe gradually reduces to the initial cone diameter of 35.7 mm. However, the diameter of the probe where u_{LS} is measured is slightly smaller than that of the section where the lateral stress (σ_{LS}) is recorded. The reduction of 0.5 mm in radius corresponds to a cavity contraction of about 1.2%.

The effect of cavity contraction on the measured pore pressure (u_{LS}) does not exist if there is no excess pore-water pressure when penetration is under drained conditions, since u_{LS} is equal to the in situ pore water pressure (u_0), i.e. $u_{LS} \approx u_0$. However, when penetration is under undrained conditions, i.e. $u_{LS}>u_0$, the cavity contraction results in a decrease of both total lateral stress and the excess pore-water pressure. An estimate of the likely stress changes can be obtained by consideration of the results of cone pressuremeter (CPM) tests presented in Figure 5.14 and Figure 5.15. During unloading from maximum expansion, a contraction of 1.2% results in changes of total stress of 36.9% and 25.6% in normally consolidated clay and normally consolidated organic clayey silt, respectively. These data suggest that a significant reduction in total stress and hence of pore pressure will occur due to the unloading induced by the change in probe diameter between the measurement locations of σ_{LS} and u_{LS}. The magnitude of the stress changes will vary with soil stiffness. As a result, the quantity $\sigma_{LS}' = \sigma_{LS} - u_{LS}$ is likely to be an overestimate of the true effective lateral stress adjacent to the LSM-II during penetration.

5.4.5 Assessment of dissipation measurements

Dissipation tests were carried out at various depths for periods of up to just over one hour. The decay of pore pressures in all channels (u_2, u_3 and u_{LS}) and the relaxation of total lateral stress (σ_{LS}) were monitored with time and readings on all channels were taken every 20 seconds. In order to assess the performance of the lateral stress module Model II (LSM-II) in dissipation mode, tests were performed at similar depths in both soundings.

5.4.5.1 Dissipation data recorded in drained conditions

Figure 5.17 presents and example of total stress relaxation records obtained with the LSM-II at similar depths in clean sand at the KIDD 2 site. The results of pore pressure measurements during the strain holding tests indicate that the water table was located on average 1.8 m below ground level at the time where these tests were performed. The position of water table derived from the pore pressure data recorded with the LSM-II, i.e. u_{LS}, is in good agreement with that interpreted from u_2 and u_3 measurements, suggesting a good saturation and response of the pore pressure sensor mounted on the lateral stress module.

However, the total lateral stress relaxation curves exhibit similar trends but the magnitude of the σ_{LS} data recorded in the first test (LSC-01) is considerably smaller than that of the second test (LSC-02). It is proposed that the difference is caused predominantly by vertical and lateral soil variability identified by variations in the piezocone tip resistance profile as illustrated in Figure 5.9b. The strain holding tests performed in sand with the LSM-II are analogous to results of strain holding test performed with a cone pressuremeter (CPM) in clean sand. Howie (1991) and Nutt & Houlsby (1995) report that strain holding phases in CPM tests result in an immediate and gradual decrease of pressure due to stress relaxation. However, it is interesting to note from Figure 5.17 that the σ_{LS} dissipation curves do not indicate the occurrence of stress relaxation. Instead of decreasing the measured total lateral stress slightly increases with time with an average increase of 20.1 kPa or 1.7% of full scale of the sensor.

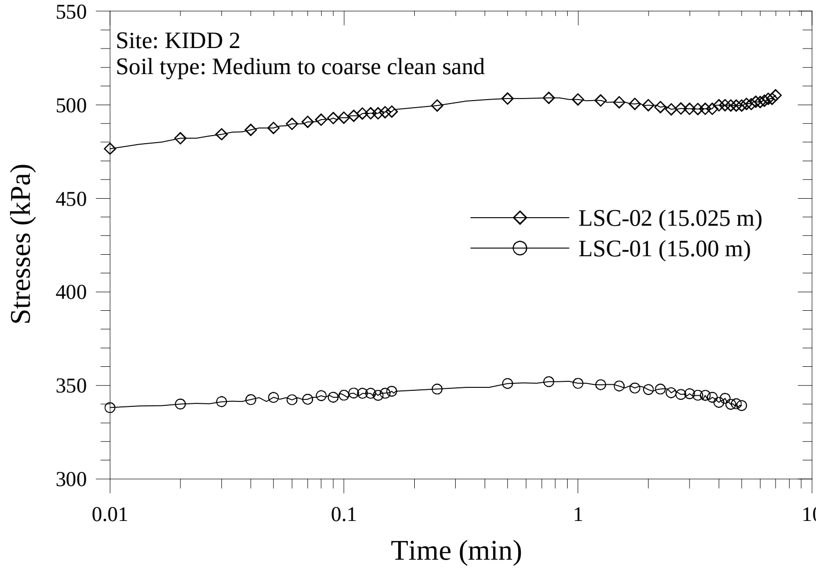

Figure 5.17 Total stress relaxation data recorded with the LSSCPTU in clean sand, KIDD 2.

Results of laboratory calibration for temperature effects indicate in increase in the voltage of the lateral stress sensor for temperatures higher than 21°C (see Figure 5.4). The temperature coefficient (B_t) for the lateral stress would be about +0.0026 V/°C or +0.47 kPa/°C on warming for a temperature range from 21 °C to 30 °C. As mentioned before, in sands the temperature is likely to increase due to friction between the cone and sand particles. If a temperature increase of 10°C degrees is assumed, the increase in lateral stress would be 4.7 kPa. Then if the hysteresis of the sensor is added the total stress would be 16.4 kPa, which is fairly close to the observed value of 20.1 kPa. Therefore, it is believed that the initial increase and eventual decrease in measured total lateral stress is caused by temperature changes in combination with the non-linearity and hysteresis of the sensor.

Figure 5.18 shows the variation with time of the normalized lateral stress ratio ($\sigma_{LS}/\sigma_{LS(i)}$) derived from the results of dissipation tests, or strain holding tests, performed in sand with the LSSCPTU at the Patterson Park site. The normalized dissipation curves show an initial increase in measured lateral stress. After reaching peak values, $\sigma_{LS}/\sigma_{LS(i)}$ decreases at an approximately constant rate, indicating the occurrence of stress relaxation. Nutt & Houlsby (1995) describe the results of several CPM tests performed in Dogs Bay Carbonate sand in a large calibration chamber (CC). The results of these tests indicate stress relaxation gradients (s_r) that vary between about 0.02 to 0.07. Furthermore, the data presented in Figure 5.18 indicates stress relaxation gradients of 0.048 to 0.035 for dissipation tests performed 5 m and 15 m depth, respectively. Based upon a comparison between laboratory and field data and neglecting the effect of stress redistribution along the rod string due to unloading on the initial measurements, the field measurements recorded with the LSM-II are consistent with data reported in sandy soils, which translates into a fairly good performance of the instrument.

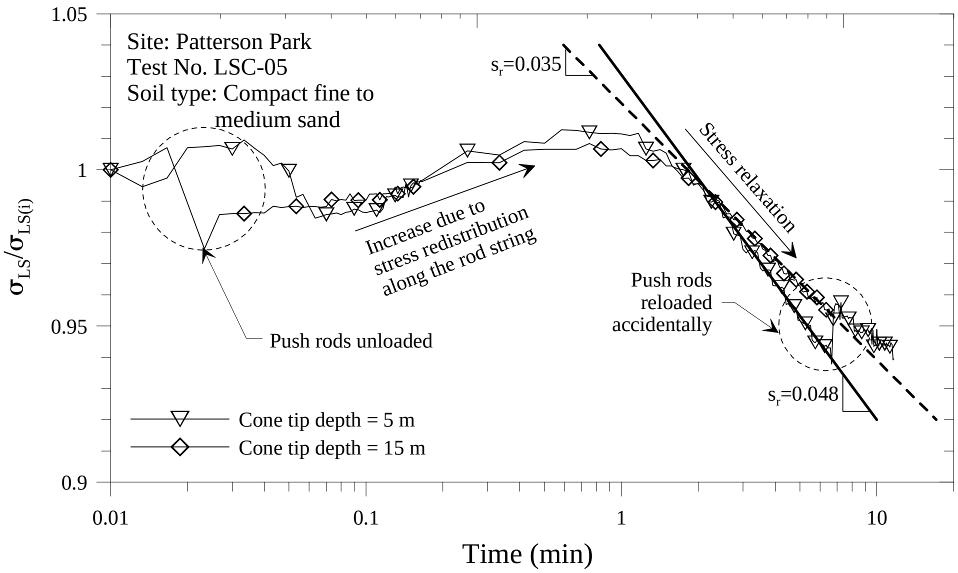

Figure 5.18 Results from strain holding tests performed with the LSSCPTU at Patterson Park.

5.4.5.2 Dissipation data recorded in undrained conditions

An example of dissipation data recorded in soft clayey silt at the KIDD 2 site is presented in Figure 5.19. The results of pore pressure dissipation tests indicate that 80% and 89% of dissipation was reach in the first and second tests, respectively. Also, the u_{LS} dissipation records are similar to each other and exhibit similar trends. For example, the difference between initial and peak values is only about 16 kPa and the time required to reach peak in both test is in the order of 0.8 min. It is interesting to note that neither pore pressure curve decreases immediately upon halting penetration; rather, both curves show a slight initial increase before decreasing toward in situ values. Sully et al. (1999) point out that this response is typical of filter locations located behind the tip (u_2 or u_3) for penetration in overconsolidated soils. Nevertheless, geological evidence suggests that fine grained sediments of the Lower Mainland of BC have not been ice-loaded and therefore are generally normally consolidated (Sully, 1991). In this section, the dissipation records are only described in qualitative terms and in order to assess the performance of the instrumentation. However, a more detailed analysis and discussion of dissipation data collected with the LSSCPTU in fine grained soils at different sites is presented in subsequent sections of this chapter.

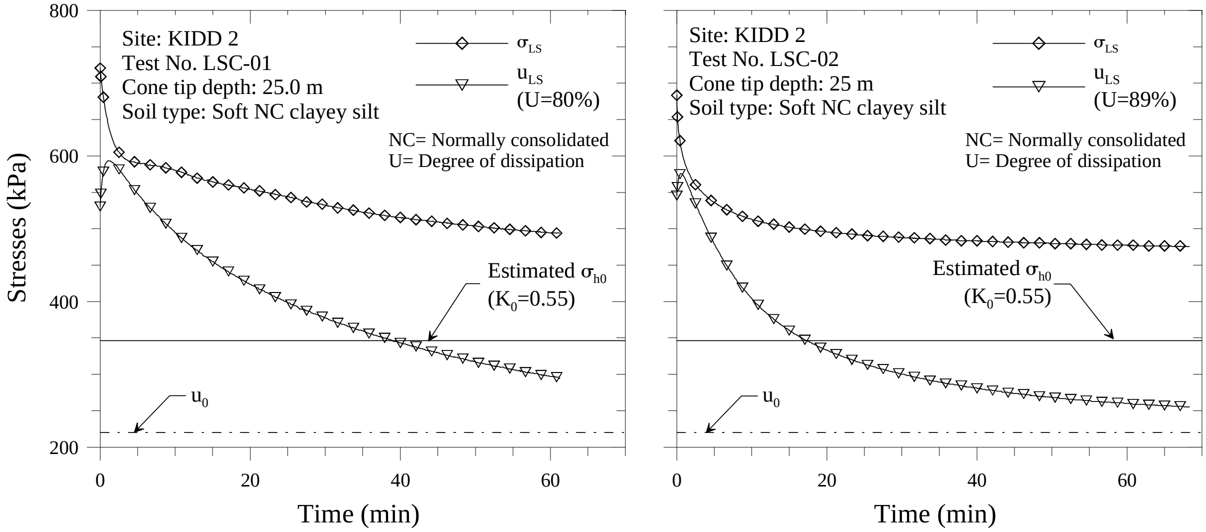

Figure 5.19 Dissipation data recorded with the LSM-II in clayey silt, KIDD 2.

As can be noted from Figure 5.19, reloading of the soil due to the enlarged section of the LSM-II caused a significant increase in the total lateral stress (σ_{LS}) and the pore pressure makes up a significant portion of measured σ_{LS} values in undrained penetration. The horizontal lateral stress acting on the shaft of the penetrometer 0.01 min after penetration was halted ranges between 683 kPa to 721 kPa, which translates into a difference of 38 kPa. Similarly, a slight difference of 18 kPa is observed between σ_{LS} values recorded at the end of each test. Furthermore, the dissipation curves plot nearly parallel to each other in the period from 0.01 min to 3.4 min. However, the results of the first test (LSC-01) show a significant reduction in gradient between 3.4 min to 8.3 min with almost constant σ_{LS} values. After this period, the original stress relaxation gradient is nearly recovered. The reason for this is not clear, but it may have been caused by friction developed between the O-ring mounted around the load transfer "button" and the body of the cone, or by soil particles that penetrated into this interface.

5.4.6 Assessment of lateral stress distribution along the shaft of the LSSCPTU

As mentioned before, the total lateral stress measured with the LSSCPTU (σ_{LS}) should be similar to the maximum pressure measured in a cone pressuremeter (CPM) test due to the increase in diameter at the location where σ_{LS} is recorded. Hughes & Robertson (1984) qualitatively describe the lateral stress reduction around an advancing cone in sand. They point out that at the shoulder of the cone tip, a large normal stress reduction occurs as the soil passes the cone shoulder, and hence the lateral stress acting on the cone sleeve is not very high and is close to the in situ lateral stress. Herein, a similar approach is used to estimate the lateral stresses that exist on the boundary of the LSSCPTU as it is pushed into sand.

The effective lateral stress (σ_h') acting on the friction sleeve of the LSSCPTU can be conservatively estimated from the interface friction angle (δ) and measured sleeve friction stress (f_s), i.e. $\sigma_h' = f_s/\tan\delta$. At very large relative shear displacements the friction angle between sand and steel can be assumed to be approximately 90% of the constant volume friction angle (ϕ_{cv}') of the interfacing sand (Rinne, 1989). The constant volume friction angle for the sand deposit at this site is about 31° (In-Situ Testing Group 1995a). Figure 5.20 presents the estimated distribution of effective lateral stress as a ratio of the effective vertical (σ_h'/σ_{v0}') stress plotted against the relative distance to the cone tip (z/*D*).

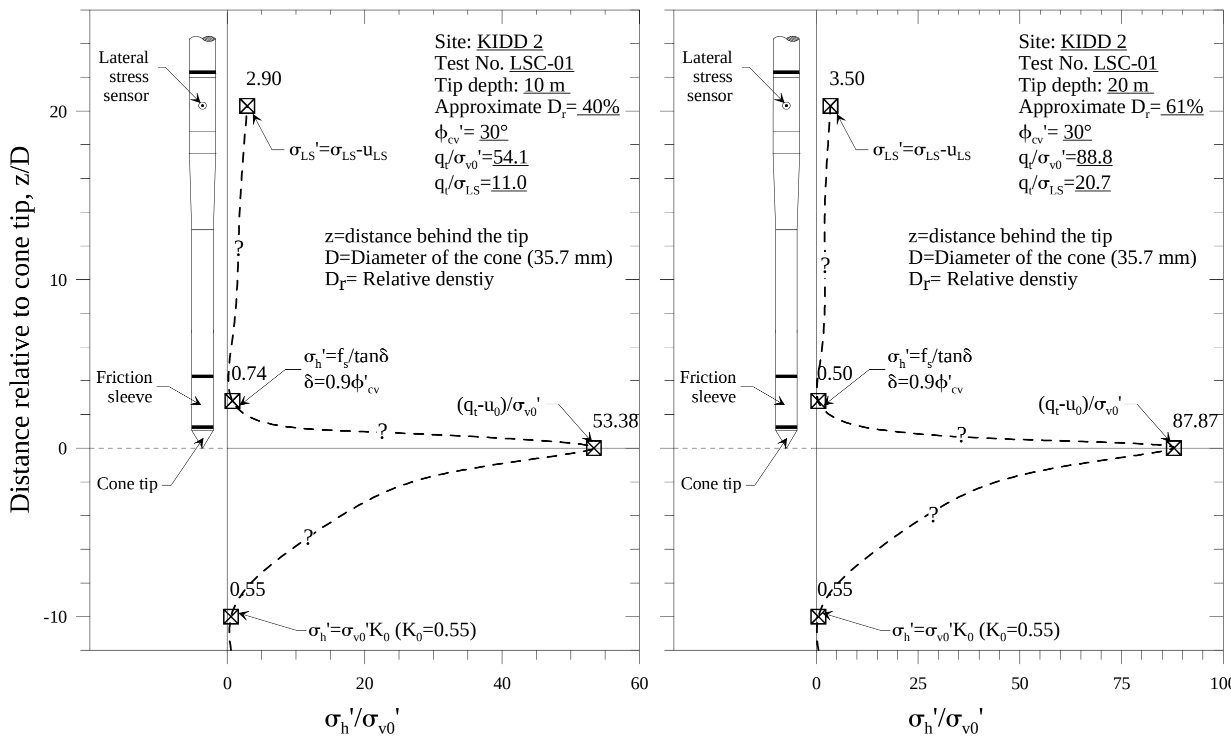

Figure 5.20 Qualitative evaluation of lateral stress distribution along the shaft of the LSSCPTU, KIDD 2.

The data presented in Figure 5.20 indicates that in drained penetration, and when there is no excess pore-water pressure, the effective lateral stress acting on the shaft of the LSSCPTU does not remain constant behind the tip due to the gradual increase in probe diameter. When the cone tip passes an element in the sand, very high stresses are developed as the sand is pushed out of the path of the cone. Figure 5.20 also shows that $(q_t-u_0)/\sigma_{v0}$' values are between 54 and 88. As the sand passes the shoulder of the cone, the sand particles are less constrained and the lateral stresses drop. The lateral stresses estimated from f_s measurements confirm that the average lateral effectives stress on the friction sleeve has dropped to close to the in situ lateral effective stress. Then, as penetration continues, the diameter of the probe starts to increase at approximately 13.1*D* above the cone tip and the sand element is gradually reloaded until a maximum cavity expansion of 22% is reached at which point the lateral effective stress has increased to about 3 to 4 times the in situ vertical effective stress.

In addition, Figure 5.20 shows that the ratio of piezocone tip resistance to measured total lateral stress, i.e. q_t/σ_{LS}, is 11 and 21 for estimated relative densities of 40% and 61%, respectively, suggesting that the effective lateral stress measured at 20.3*D* behind the tip is dependent on the relative density of the sand. Schnaid (1990) describes the results of several cone pressuremeter calibration chamber (CC) tests performed on loose to dense dry Leighton Buzzard sand ($16\%<D_r<89\%$). A detailed review of the results of CC tests of the 10 cm^2 cone pressuremeter indicates that the ratio of cone tip resistance to cavity limit pressure (q_c/p_L) varies between about 5 and 13. The difference between field and laboratory data may be attributed to differences in sand properties or the fact that of CC tests were performed on unaged sand specimens, which is a condition rarely found in natural sand deposits. Further research is required to investigate these effects.

5.5 LSSCPTU dissipation tests

The analysis and interpretation of dissipation of excess pore pressures due to cone penetration has been mainly focused on estimation of in situ flow and consolidation characteristics, and have been addressed by various researchers (e.g. Tortensson, 1977; Randolph & Wroth, 1979; Baligh & Levadoux, 1980; Gillespie & Campanella, 1981; Baligh & Levadoux, 1986; Teh 1987; Campanella & Robertson, 1988; Burns & Mayne, 1998; Sully, et al., 1999; Mayne, 2001; Imre et al., 2008). However, the interpretation of the variation with time of both pore pressure and total lateral stress measured by lateral stress modules is fairly limited and is constrained by the particular geometry of the probe used and to specific soil conditions (e.g. Takesue & Isano, 2001). This section presents a description of the results of both pore pressures and lateral stress dissipation data recorded with the lateral stress seismic piezocone (LSSCPTU) in soft fine grained soil deposits at the KIDD 2 and Colebrook Overpass sites. This section also includes a brief discussion of data recorded when penetration of the LSSCPTU was resumed after each dissipation test and during pauses or rod “breaks” in the penetration process.

5.5.1 Analysis and discussion of dissipation data

Dissipation tests were carried out with the lateral stress seismic piezocone (LSSCPTU) at several research sites located in the Lower Mainland of British Columbia. The interpretation of data recorded in fine grained soils provides an insight into the changes of both pore pressure and total lateral stress around the probe. As previously discussed in section 5.4.4.1of this thesis, the pore pressure measured above the lateral stress sensor (u_{LS}) is likely to be less than the pore pressure at a maximum cavity expansion due to the fact that the diameter of the probe at the location where u_{LS} is measured is slightly smaller that that of the section where the total lateral stress (σ_{LS}) is recorded. The reduction in radius corresponds to a cavity contraction of about 1.2%. As a result, the magnitude of the interpreted effective lateral stress on the shaft of the LSM-II (σ_{LS}'= σ_{LS}-u_{LS}), does not represent the true change in effective lateral stress due to cavity expansion during penetration or when dissipation tests are performed.

Figure 5.21 and Figure 5.22 present the changes with time of pore water pressure (u_{LS}) as well as total (σ_{LS}) and estimated effective (σ_{LS}'=σ_{LS}-u_{LS}) lateral stresses recorded in marine soft normally consolidated (NC) clayey silt (KIDD 2 site) and lightly overconsolidated (LOC) soft sensitive marine silty clay (Colebrook Overpass site). As can be seen from these figures, there are similar patterns between all dissipation curves. Firstly, the total lateral stress (σ_{LS}) remains fairly constant for the first few seconds and then decreases significantly during consolidation. Secondly, after penetration is halted the pore pressure measured above the lateral stress sensor (u_{LS}) rises to reach a maximum value in a period of between about 60 s to 215 s, and then reduces monotonically towards hydrostatic values.

The curves of effective lateral stresses (σ_{LS}') shown in Figure 5.21 and Figure 5.22 show that after an initial drop, σ_{LS}' increases gradually and after partially completed consolidation, i.e. U<100%, σ_{LS}' values are much greater than estimates of initial stress. Additionally, the pore pressure dissipation and total lateral stress relaxation curves recorded in fine grained soils with the lateral stress module Model II (LSM-II) are very similar in shape, and exhibit similar trends to those reported by Baligh et al. (1985), Lehane & Jardine (1994), Takesue & Isano (2000) and Ladanyi & Longtin (2005).

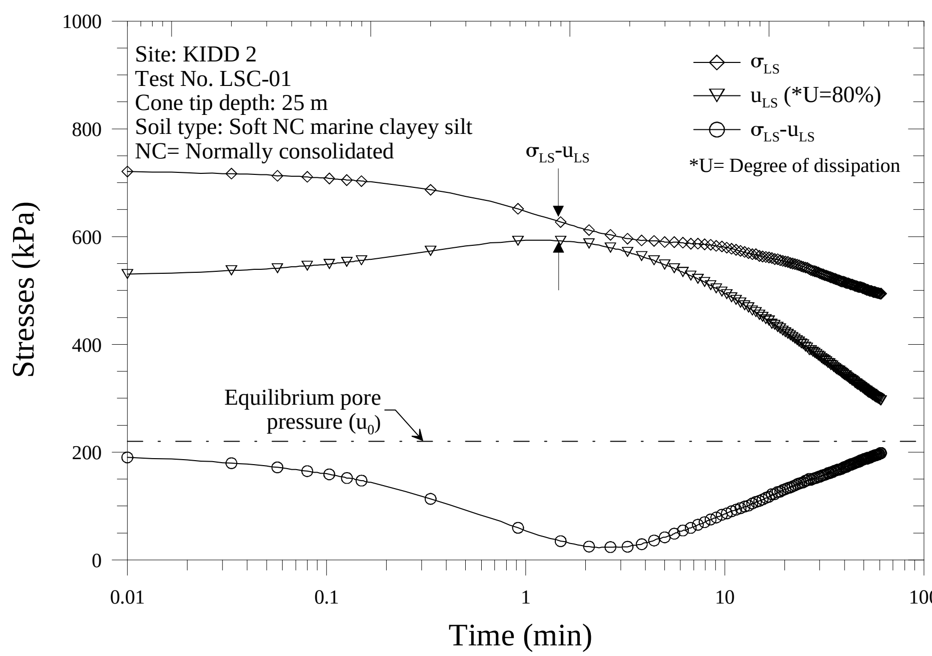

Figure 5.21 Variations of pore pressure and lateral stress during dissipation, KIDD 2

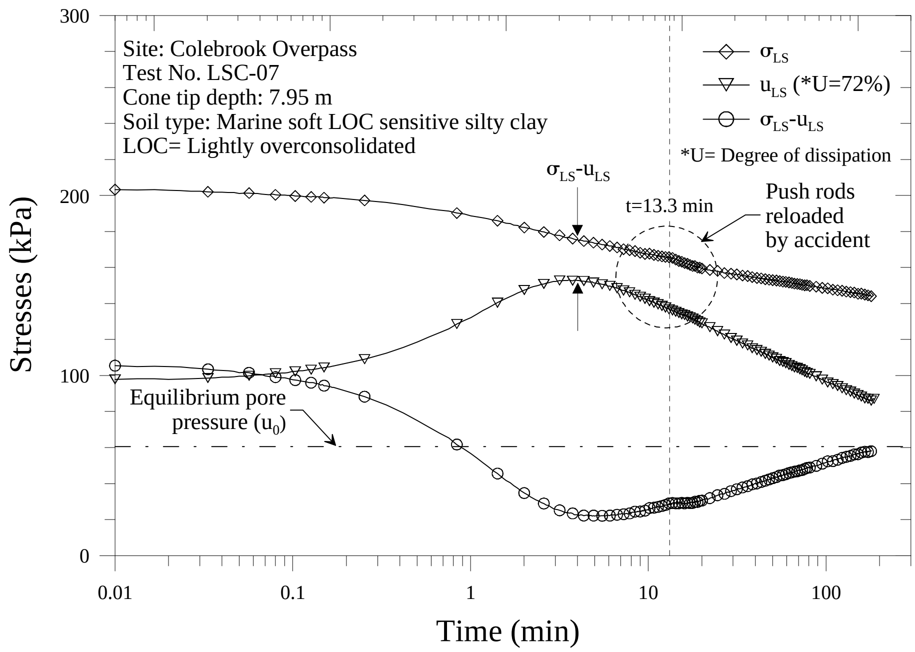

Figure 5.22 Variations of pore pressure and lateral stress during dissipation, Colebrook Overpass

These researchers performed dissipation tests for periods of up to 4 days with instrumented full displacement probes capable of monitoring simultaneously the dissipation of excess pore pressure and total lateral stress relaxation with time. The results of these tests indicate that after consolidation the final effective lateral stress (σ_{LS-f}') increases to values far greater than estimates of the initial effective lateral stress. They also indicate that the lateral effective stress drops during the initial stages of dissipation before increasing again towards a final value.

For example, Figure 5.23 presents a set of pore pressure (u_{LS}) and total lateral stress (σ_{LS}) dissipation data obtained with the Japanese lateral stress cone (J-LSC) described by Takesue & Isano (2000). It can be noted from Figure 5.23 that the pore pressure increases rapidly and reaches a maximum value in approximately 0.25 min before dissipating towards equilibrium. The magnitude of σ_{LS} reduces during consolidation to a final value that is considerably larger than that estimated from the results of SBP tests. Furthermore, the initial value of effective lateral stress, i.e. σ_{LS}'=σ_{LS}-u_{LS}, immediately after penetration is halted, is very close to the in situ horizontal effective lateral stress estimated from the interpretation of results of SBP tests but then falls to a minimum before increasing to a final value considerably above the estimate of in situ lateral effective stress.

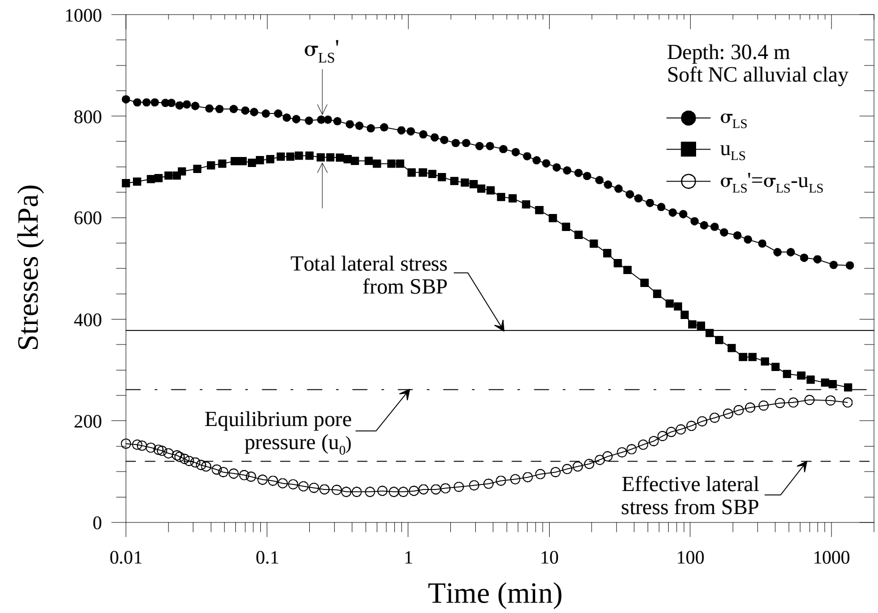

Figure 5.23 Variation of total lateral stress and pore pressure with time measured with the J-LSC in soft lightly overconsolidated alluvial clay (data from Takesue & Isano, 2000).

Similarly, Ladanyi & Longtin (2005) report results of a dissipation test, or strain holding test as named by them, performed in high plasticity stiff clay with the instrumented sharp cone (ISC) previously described in section 5.4.4.1 of this thesis. The dissipation data recorded with the ISC indicates that total lateral stress relaxation was over after about 10 hours, whereas dissipation of excess pore pressure continued for up to 20 hours, and the effective lateral stress did not reach equilibrium during the period of monitoring.

Even though the geometry of the LSSCPTU is different from that of the J-LSC, the dissipation curves recorded with the former exhibit similar trends to those reported by Takesue & Isano (2001), suggesting that the instrumentation of the lateral stress module is performing well. However, it must be borne in mind that the magnitude of $\sigma_{LS}'=\sigma_{LS}-u_{LS}$ derived from LSSCPTU measurements is not representative of the true change in effective lateral around the total lateral stress sensor.

Figure 5.24 and Figure 5.25 present the excess pore pressure measured at all locations, i.e, Δu_2, Δu_3 and Δu_{LS}, normalized by the corresponding estimated effective vertical stress ($\Delta u/\sigma_{vo}'$) at Colebrook Overpass and KIDD 2 sites, respectively. The ratio $\Delta u/\sigma_{vo}'$ has been chosen in order to compare data recorded with the LSSCPTU to the results of dissipation tests performed at Colebrook Overpass by Weech (2002). The results of dissipation tests indicate that at the u_{LS} location, 80% dissipation of excess pore pressure was achieved at the KIDD 2 site, whereas at the Colebrook Overpass site 72% of dissipation was reached. As mentioned before, the execution of these tests was aimed at evaluating the performance of the LSSCPTU rather than achieving equilibrium readings in all channels.

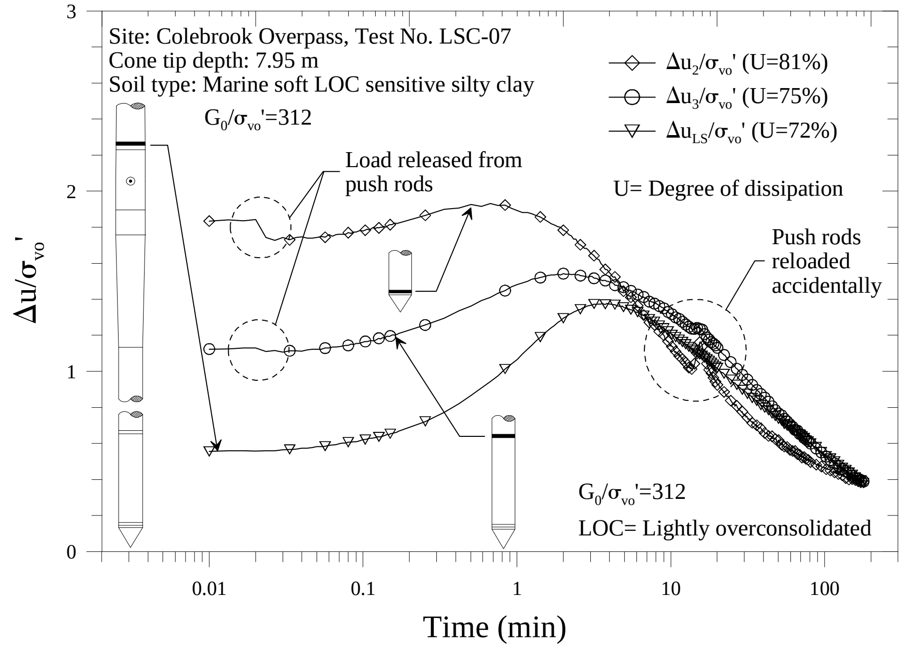

Figure 5.24 Variation of normalized pore pressures with time, Colebrook Overpass.

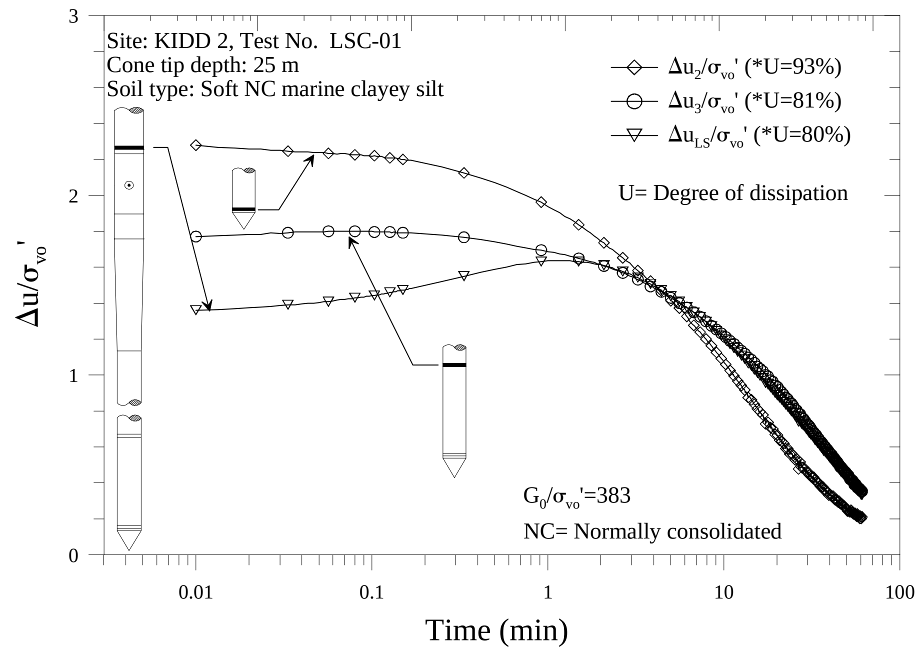

Figure 5.25 Variation of normalized pore pressures with time, KIDD 2.

The normalized pore-water pressure dissipation data recorded at u_2, u_3 and u_{LS} locations at the Colebrook Overpass site show a delay in the response to pore pressure changes followed by a rise in pore-water pressure values to a peak before dissipation commences. According to the classification by Sully et al. (1999) of the idealized pore pressure dissipation response around a piezocone, the u_{LS}, u_2 and u_3 curves in Figure 5.24 are classified as type III response, typical of filters located behind the cone tip (e.g. u_2 and u_3) for cone penetration in overconsolidated soils (Sully et al., 1999). In Figure 5.25, the u_2 and u_3 curves decrease monotonically, typical of a normally consolidated soil, whereas the u_{LS} response is more typical of overconsolidated soils. Therefore, the dissipation of excess pore-water pressure measured at the u_{LS} location is inconsistent with those recorded at u_2 and u_3 locations, respectively.

The results of dissipation tests at the Colebrook Overpass site described by Weech (2002) are presented in Figure 5.26. They show a consistent increase from the penetration values to a peak value during the early stages of the test at both u_2 and u_3 locations. In Figure 5.24 and Figure 5.26, both showing Colebrook data, the initial values of $\Delta u/\sigma_{v0}'$ at the u_2 are very similar. The values at the u_3 location show some scatter but are again of a similar magnitude. However, it is interesting to note that $\Delta_{u(peak)}/\sigma_{v0}'$ at u_2 is 2.3 to 2.4 for the piezocone but is only 1.9 for the LSSCPTU. At u_3, $\Delta_{u(peak)}/\sigma_{v0}'$ is 1.8 to 2.0 for the piezocone and only 1.6 for the LSSCPTU. This suggests that the different geometry of the LSM may be affecting the initial pore pressure distribution and hence the dissipation regime around the u_2 and u_3 locations. The fact that the times required to reach peak pore pressure ($\Delta_{u(peak)}/\sigma_{v0}'$) at the u_2 location were about 0.7 minutes for the LSSCPTU and 0.5 to 0.75 minutes for the piezocone but 2 minutes at u_3 for the LSSCPTU compared to only 0.92 to 1.5 minutes for the piezocone may be another indication of geometry effects.

Whittle et al. (2001) analyzed the excess pore pressure distribution and resulting dissipation around a tapered probe in Boston Blue Clay and compared modelled dissipation curves to field data. Their analysis confirms that the initial excess pore pressure regime and observed dissipation behaviour are complex and very dependent upon probe geometry. Numerical modelling of the LSSCPTU would improve our ability to interpret the data shown in Figure 5.24 and Figure 5.25.

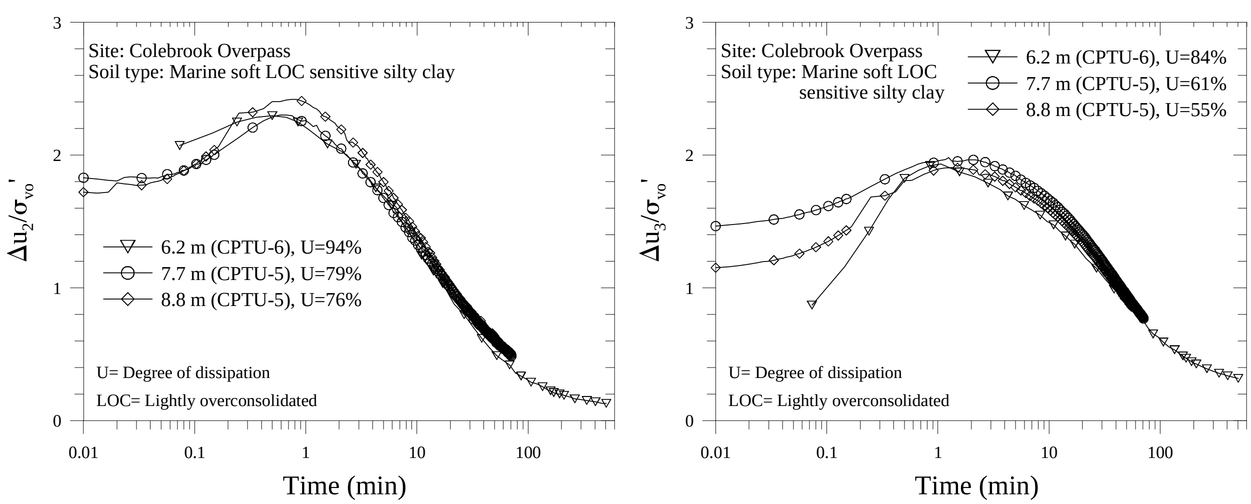

Figure 5.26 Variation of normalized pore pressures with time at u_2 an u_3 filter locations, Colebrook Overpass (data from Weech 2002).

5.5.2 Effect of dissipation and pauses in penetration on measured data.

The pore pressures and total lateral stress profiles recorded at the KIDD 2 site indicate that a significant amount of movement was required in order to recover the original penetration values (see Figure 5.10 and Figure 5.11). Campanella & Robertson (1988) argue that the amount of movement required to regain the original penetration values appears to vary with soil type and can range from about 2 cm to 50 cm, and that no clear explanation has been proposed to clarify these large differences. Alternatively, they suggest to either remove or clearly identify the pauses in the penetration when presenting piezocone data.

The data gathered with the UBC LSSCPTU permits an examination of the pore pressure response when restarting pushing after a dissipation phase. Figure 5.27 and Figure 5.26 present data from KIDD 2 and Colebrook, respectively. They are profiles of measured pore pressures at the u_2, u_3 and u_{LS} locations as well as of σ_{LS} showing the response of the sensors before, during and after substantial pauses in penetration. The location of the dissipation and of short pauses required to allow addition of additional rods are indicated on the figures. The location of the cone tip during the long pauses in penetration is also shown. The response of each sensor depends on its location relative to the cone tip and on the soil type. For example, the post dissipation responses at the u_2, and u_3 locations are very different at KIDD 2 than at Colebrook. In both cases, the penetration pore pressures return to what would have been measured during steady penetration (i.e. with no dissipation) by about 0.45 m to 0.6 m or 12-17 cone diameters beyond the cone tip location during the dissipation. The same is true of σ_{LS}. The u_{LS} measurement does not recover as quickly.

Insight can be gained by examining the post dissipation response in detail. As can be seen from Figure 5.27 and Figure 5.26, u_2 begins to increase immediately the cone starts moving again whereas both u_3 and u_{LS} appear to decrease before beginning to increase again and recover steady penetration values. The post dissipation response in the zone close to the cone tip is likely due to the soil in this region being denser and stiffer than it would have been during steady penetration. It thus has less tendency to generate pore pressure than in its virgin state. The soil in this zone has a different stress history than the rest of the stratum and so a different pore pressure response in this reconsolidated zone is to be expected as the pore pressure response at u_2 and u_3 is known to be affected by stress history. The observed response of u_{LS} requires a different explanation.

As noted earlier, the u_{LS} pore pressure element is located on a sloping surface behind the lateral stress sensor as the LSM tapers back down to the standard cone rod diameter. Consequently, when penetration resumes, the wall of the cavity is unloaded and the soil may not even be in contact with soil during the initial phases of penetration. This explains the reduction in u_{LS} in both cases when penetration resumes after the long dissipation and also the increases in u_{LS} observed during rod breaks thereafter. It is clear that the pore pressure element needs to be relocated in a redesigned instrument so that true measurements of the effective lateral stress on the LSM-II can be made during penetration.

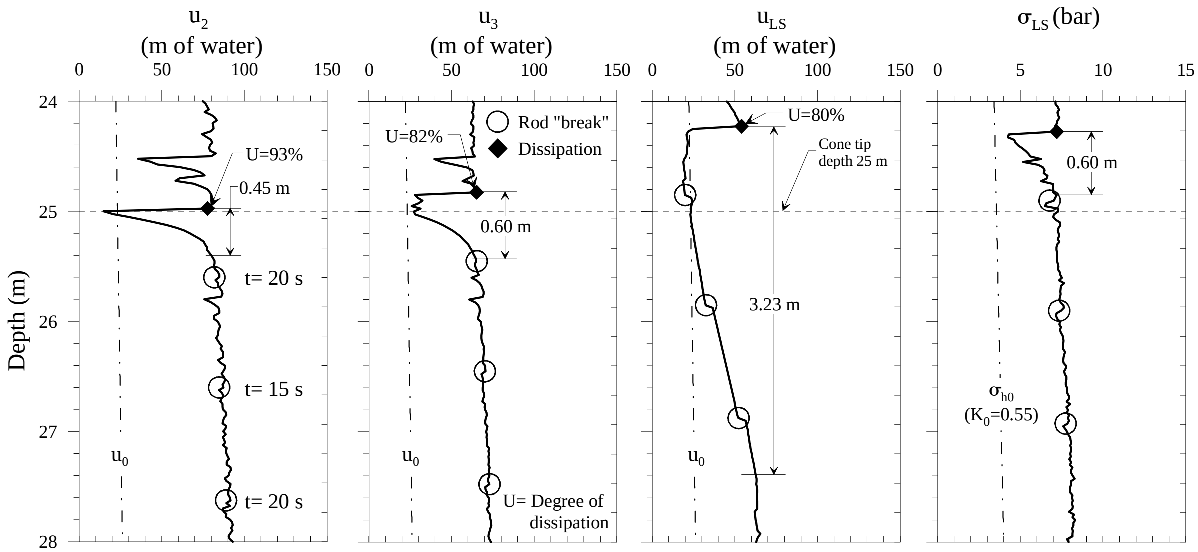

Figure 5.27 Effect of dissipation and rod “breaks” on penetration measurements (LSC-01), KIDD 2.

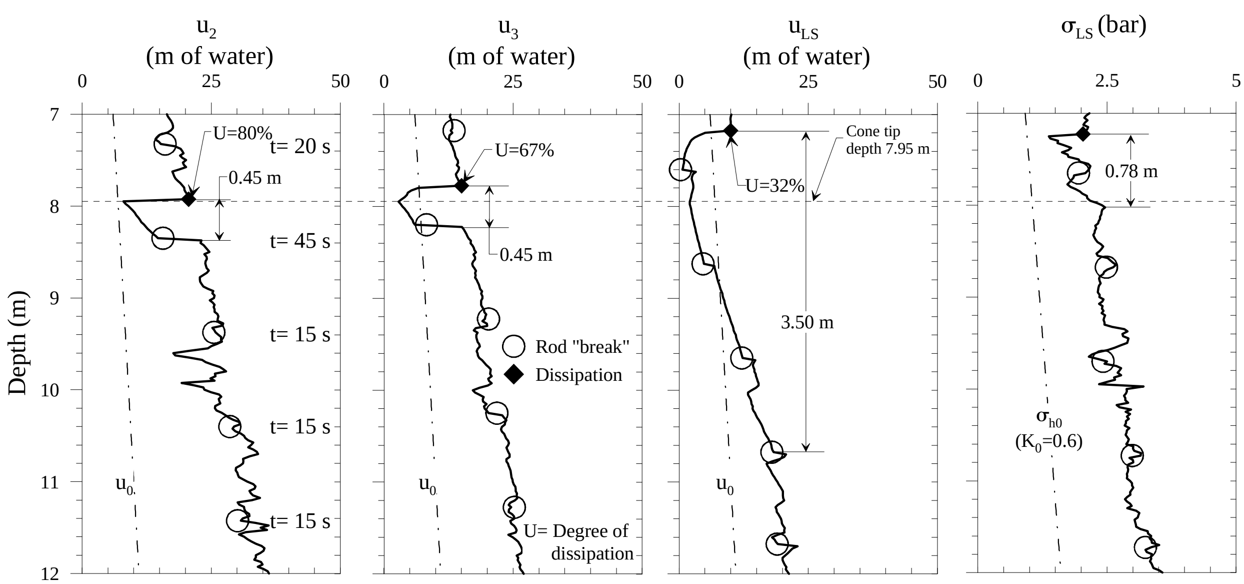

Figure 5.28 Effect of dissipation and rod “breaks” on penetration measurements (LSC-07), Colebrook Overpass.

5.6 Summary

5.6.1 Overview

The use of instrumented friction sleeves for measuring lateral stresses involves several challenges in both the instrumentation and the robustness of the external element in contact with the soil. In an attempt to overcome the major drawbacks of this type of design, a new lateral stress module (LMS-II), equipped with a passive sensing element rather than an instrumented friction sleeve, was designed and built at UBC. The LSM-II is mounted on a standard 10 cm^2 UBC seismic piezocone (SCPTU). The lateral sensor is located 69.5 cm behind the cone shoulder (19.5*D*) and the pore pressure developed during penetration is measured by a pore pressure transducer located 58.5 mm above the lateral stress sensor or 21.1*D* behind the cone shoulder, where *D* is the diameter of the cone.

The use of additional sensors such as a lateral stress module complements the information typically recorded from a seismic piezocone tests, i.e., q_c, u_2, f_s and V_s. Herein, the combination of the SCPTU with LSM-II is termed as the lateral stress seismic piezocone (LSSCPTU). The eight-channel LSSCPTU allows simultaneous measurement of the following parameters: tip resistance (q_c), pore pressure behind the tip (u_2), sleeve friction (f_s), pore pressure behind the friction sleeve (u_3), inclination, lateral stress 19.5 diameters behind the tip (σ_{LS}), and pore pressure at about 21.1 diameters behind the tip (u_{LS}). Also, downhole shear wave velocity (V_s) tests can be performed with a seismic module mounted just behind the cone that contains an accelerometer.

The diameter of the LSM-II is larger than that of the SCPTU, so that the addition of a special low angle adaptor provides a gradual transition in diameter from 35.7 mm to 43.5 mm. Furthermore, the diameter of the cone remains fairly constant along the lateral stress section, and above the upper pore pressure sensor (u_{LS}) the diameter of the probe gradually reduces to the initial cone diameter of 35.7 mm. However, it was found that the diameter of the probe where u_{LS} is measured is slightly smaller than that of the section where the lateral stress is recorded. The reduction of 0.5 mm in radius corresponds to a cavity contraction of about 1.2%. The effect of cavity contraction on the measured pore pressure (u_{LS}) does not exist if there is no excess pore-water pressure when penetration is under drained conditions, i.e. $u_{LS}=u_0$. However, when penetration is under undrained conditions, i.e. $u_{LS}>u_0$, the cavity contraction results in a decrease of both total lateral stress and the excess pore-water pressure. Consequently, it is likely that the pore pressure measured at the LSM-II is less than the pore pressure at a maximum cavity expansion in undrained penetration.

5.6.2 Laboratory and field assessment of LSSCPTU data

The performance of the instrumentation and design of the LSM-II was assessed through a comprehensive laboratory and field testing program. Firstly, laboratory calibrations were performed for the following conditions: (i) hydrostatically applied confining pressure, (ii) temperature sensitivity, (iii) calibration for axial load effect, and (iv) time-dependent stability of both lateral stress (σ_{LS}) and pore pressure (u_{LS}) sensors. Secondly, field data recorded in two adjacent soundings performed at the KIDD 2 site was reviewed in order to: (i) assess the sensitivity of lateral stress (σ_{LS}) and pore pressure (u_{LS}) sensors to stratifications during penetration, (ii) monitor the response of both σ_{LS} and u_{LS} sensors in dissipation mode and (iii) assess the repeatability of recorded LSM-II data by comparing results of the two adjacent soundings.

Results of laboratory calibrations have shown that both lateral stress and pore pressure sensors are fairly sensitive to temperature variations but within acceptable ranges. Also, it was found that axial loading on the cone caused an output voltage on the lateral stress channel. The cross-talk effect due to axial load is higher than that caused by temperature variations. Both effects could be calibrated out by making appropriate corrections to the measured data. Unfortunately, it is not possible to correct the data for temperature effects since the LSM-II does not have a temperature sensor and the thermistor mounted on the seismic piezocone unit is not activated when the LSM-II is attached. Moreover, in an attempt to account for axial load effects an equation was proposed to correct the measured lateral stresses.

The result of LSSCPTU testing performed at the KIDD 2 site indicate that the lateral stress profile shows variations in soil stratigraphy just as the q_t profile does. Additionally, it has been demonstrated that in clean sands the effective lateral stress acting on the shaft of the LSSCPTU does not remain constant behind the tip and rather increases due to reloading of the soil caused by the tapered geometry of the probe. On the contrary, in fine grained soil when penetration is undrained the pore pressure makes up a significant portion of the measured total lateral stress.

The magnitude of penetration pore pressures recorded at the three sensor locations, i.e. u_2, u_3 and u_{LS}, gets progressively smaller as the cone advances, suggesting a reduction in hydraulic gradients once away from the cone shoulder. A comparison of field measurements recorded with the LSSCPTU in adjacent soundings at the KIDD 2 site indicates a good degree of repeatability between data sets, suggesting a good performance of the instrumentation of the LSM-II regardless the inherent soil variability observed at this site.

The review of dissipation data recorded in fine grained soils suggests a remarkably good performance of the pore pressure sensor of the LMS-II. On the contrary, the total lateral stress relaxation data recorded in coarse grained soils indicate that early portions of dissipation curves seem to be affected by stress redistribution along the rod string due to unloading. Consequently, when presenting LSSCPTU dissipation data careful attention to detail is required to identify anomalies in the curves and distinguish whether they were caused by equipment characteristics or by the actual soil behaviour. Failure to recognize these effects will likely yield inconsistent conclusions about the dissipation data recorded with the LSSCPTU.

5.6.3 Interpretation of LSSCPTU data collected at research sites

5.6.3.1 Dissipation measurements

Dissipation tests were performed in fine grained soils at the KIDD 2 and Colebrook Overpass sites for periods of a bit more than one hour to 3.1 hour. The decay of pore pressures in all channels (u_2, u_3 and u_{LS}) and the relaxation of total lateral stress (σ_{LS}) were monitored with time. The pore pressure dissipation and total lateral stress relaxation curves recorded with the lateral stress module Model II (LSM-II) are very similar to those measured with several instrumented full displacements probes (Baligh et al., 1985; Lehane & Jardine, 1994; Takesue & Isano, 2000; and Ladanyi & Longtin, 2005).

A crude comparison of data recorded at each site indicates that the u_{LS} and σ_{LS} dissipation curves exhibit similar trends. Furthermore, the dissipation records show that the total lateral stress (σ_{LS}) remains fairly constant for the first few seconds and then decreases significantly during consolidation. On the contrary, after penetration is halted the pore pressure measured above the lateral stress sensor (u_{LS}) rises to reach maximum values in a period between about 60 s to 215 s, and then reduces monotonically towards hydrostatic values. According to the classification of idealized pore pressure dissipation response of Sully et al. (1999), the u_{LS} dissipation curves recorded with the LSM-II are classified as type III response.

The dissipation data recorded at u_2, u_3 and u_{LS} locations at the Colebrook Overpass site show a delay in the response to pore pressure changes followed by a rise in pore-water pressure values, which is a typical response of data recorded in overconsolidated soils. Results of laboratory tests indicate a slight degree of overconsolidation in the upper 10 m of the soil at this site. Also, the data measured at the u_{LS} location at the KIDD 2 site exhibit a similar trend. However, the dissipation curves at the u_2 and u_3 dissipate monotonically immediately after penetration was halted, suggesting that soils is normally consolidated. Geological evidence suggests that fine grained sediments of the Lower Mainland of BC have not been ice-loaded and therefore are generally normally consolidated (Sully, 1991). A preliminary explanation to the observed behaviour is proposed. It is suggested that the “dilative” pore-water pressure dissipation response observed at the u_{LS} location is likely to be caused by drainage from the zone slightly deeper below the sloping surface (high pressure) to the zone where the diameter of the probe is slightly reduced (low pressure) and the pore pressure sensor is located.

The pore pressures (u_2, u_3 and u_{LS}) and total lateral stress (σ_{LS}) profiles recorded at the KIDD 2 and Colebrook Overpass sites show that at the end of dissipation tests, when penetration is resumed, a significant amount of movement is required in order to recover the original penetration values. The post-dissipation responses observed at both sites are very similar despite the fact that the duration of the test performed at the Colebrook Overpass was longer than that at KIDD 2. The amount of movement required is on average 45 cm for u_2, 53 cm for u_3, 337 for u_{LS} and 69 for σ_{LS}, respectively.

When the cone starts moving again u_2 immediately begins to increase whereas both u_3 and u_{LS} appear to decrease before beginning to increase again and recover penetration values. It is believed that the magnitude of u_2 and u_3, before the original pore pressure values are recovered, may be caused by the dilative response of the reconsolidated soil located between the u_3 sensor and within the influence zone below cone tip. On the contrary, the significant amount of penetration required to recover original u_{LS} values may be partially associated with the apparent dilative response of the soil between the lateral stress module and the influence zone below the cone tip. Also, the u_{LS} pore pressure element is located on a sloping surface behind the lateral stress sensor and when penetration is resumed the soil approaching is unloaded, which results in a decrease of both total lateral stress and excess pore pressure.

Chapter 6 SUMMARY AND CONCLUSIONS

6.1 Overview

The performances of the seismic flat dilatometer (SDMT) and lateral stress seismic piezocone (LSSCPTU) have been assessed through a comprehensive testing program carried out at several research sites. Field measurements were recorded in a fairly wide range of different soil types such as alluvial coarse grained soils and glaciomarine fine grained deposits. In each case, the instruments were being assessed for the first time in Lower Mainland soils. The former has been introduced commercially only relatively recently whereas the latter is still in the research phase. For each probe, the instrumentation was subjected to detailed assessment before the data were interpreted to assess soil behaviour.

The results of field tests performed by the author with the SDMT and LSSCPTU confirm the strong link between the imposed strains due to probe geometry and the stress and pore-water pressure increments in the surrounding soil. Also, it has been demonstrated that stresses around full displacement probes such as the SDMT and LSSCPTU, are very dependent upon small changes in geometry, and therefore standardization of equipment and transducer location is essential for consistent measurement of parameters and for derivation and use of empirical correlations. Cavity expansion approaches can provide a basis for interpreting in situ penetration test data but its application requires the use of empirical coefficients. In addition, the use of more powerful tools such as numerical modelling would improve the interpretation of data recorded with full displacement probes.

6.2 Seismic flat dilatometer (SDMT)

The data presented represents the first critical examination in Lower Mainland soils of the newly-introduced SDMT, in which shear wave velocity is measured in the same sounding as the conventional DMT parameters. The only difference from the standard flat DMT is that a seismic module comprising two geophones mounted 0.5 m apart is added above the flat blade to allow V_s to be measured using a true interval technique. Proprietary software supplied with the instrument calculates V_s in real time. The usual DMT procedure was altered to take readings at 0.25 m intervals of depth instead of the more conventional 0.20 m. This was found to be operationally efficient and also simplified data assessment and interpretation.

Several problems were experienced with the SDMT data acquisition system when performing V_s measurements in the field. It was found that the electrical continuity between the control unit and the DMT blade is essential for a good transmission of signals from the seismic module to the surface. In order to overcome this problem it is important to ensure that the membrane is in contact with the blade and the sound is on before performing a seismic test. Also, it is important to ensure that there is good electrical contact between the ground cable and the rod string, rather than on a rusty part of the pushing ram.

Several comparisons between the shear wave velocities (V_s) determined by the SDMT and seismic piezocone (SCPTU) indicate that SDMT values are likely to be more sensitive to stratigraphic details because of the 0.5 m depth interval used for V_s determination as opposed to the 1 m interval used in the SCPTU tests. The results of SDMT tests performed at research sites and flat dilatometer (DMT) and SDMT measurements at different sites located in western Canada, Mexico and Italy have been used to develop the databases presented in this thesis. The analyses of SDMT measurements at research sites have shown the potential for an improved soil characterization through the combination of standard DMT parameters such as: (i) material index (I_D), (ii) dilatometer modulus (E_D) and (iii) pore pressure index (U_D), and the small strain shear modulus (G_0). The usefulness of the DMT-C closing pressure for soil identification has been shown and therefore it is strongly recommended that it be included in the routine procedure.

The review of field measurements from SDMT tests suggests that it is possible to enhance site characterization in terms of soil stratigraphy by combining standard SDMT data with the pore pressure index (U_D). The relationships identified between DMT parameters and G_0 provide the theoretical framework for the development of a new soil type behaviour system based upon SDMT measurements (see Figure 4.19). The proposed chart should be only used as a guide to estimate soil behaviour type from SDMT data. Further improvement work and local experience may be required to adjust this chart to soils with different geological origin and therefore provide a better local correlation.

Based upon a comprehensive review of SDMT collected at research and additional sites an empirical correlation has been proposed for evaluating the shear wave velocity (V_s) in coarse and fine grained soils from standard flat dilatometer (DMT) measurements (Equation 4.1). Moreover, the data reviewed indicates that V_s can be conservatively estimated from the proposed DMT-V_s correlation in sands, silts and low to medium plasticity clays, whereas V_s appears to be significantly overestimated in sensitive high plasticity soft soils such as Mexico City clay. Additionally, the comparison of estimates of V_s with the proposed DMT correlation to those from fairly recent CPTU based expression, demonstrates the advantage of the proposed approach. However, until this correlation becomes established for a wider range of soils, local experience and engineering judgement are required to assess estimates of V_s with this correlation.

While the flat dilatometer has been widely used to estimate several geotechnical parameters, there is a significantly higher degree of confidence in this instrument as a tool for estimation of coefficient of earth pressure at rest (K_0). However, reliable estimates of K_0 from DMT data entirely depend upon the choice of appropriate correlations, which were developed some time ago. In this thesis, empirical correlations have been proposed to estimate the coefficient of earth pressure at rest (K_0) in fine and coarse grained soils from DMT measurements (Equation 4.6 and Equation 4.7).

The approaches proposed have been derived from updated databases based upon a comprehensive review of published information in the last 10 years. The proposed empirical DMT-K_0 correlations represent an upgrade in interpretation of DMT data and add to the options available to estimate geotechnical parameters from DMT measurements. Also, from a practical standpoint K_0 values derived from the proposed approaches may be used as a first-order estimate for geotechnical analysis.

6.3 Lateral stress seismic piezocone (LSSCPTU)

The use of additional sensors such as a lateral stress module (LSM) complements the information typically recorded from a seismic piezocone test (SCPTU). Herein, the combination of the SCPTU with a new LSM Model II (LSM-II), developed and built at UBC, is termed as the lateral stress seismic piezocone (LSSCPTU). The LSSCPTU allows simultaneous measurement of the following parameters: tip resistance (q_c), pore pressure behind the tip (u_2), sleeve friction (f_s), pore pressure behind the friction sleeve (u_3), inclination, lateral stress 19.5 diameters behind the tip (σ_{LS}), and pore pressure at about 21.1 diameters behind the tip (u_{LS}). Also, downhole shear wave velocity (V_s) tests can be performed with a seismic module mounted just behind the cone that contains an accelerometer.

The analysis of LSSCPTU field data collected in saturated fine grained soils, has illustrated that cavity contraction, caused by the slight reduction in probe diameter above the lateral stress sensor, significantly affects the magnitude of measured pore-water pressure recorded at this location. A preliminary explanation to the observed behaviour is proposed. The initial increase in pore pressure observed at the u_{LS} location is likely to be a result of drainage from the zone slightly deeper below the sloping surface (high pressure) to the zone where the diameter of the probe is slightly reduced (low pressure) and that drainage from the tip as suggested by Sully et al. (1999) does not affect the dissipation response recorded at this location.

The main drawbacks of the current design of the LSM-II are the cross talk effect and the reduction in diameter at the location where pore pressure is measured above the lateral stress sensor. The cross talk effect on the lateral stress sensor due to axial loading of the cone is quite significant, and therefore minor improvements in the current design are required to reduce its magnitude. Consequently, it is recommended to machine the upper section of the LSSCPTU in order to maintain a constant diameter throughout the lateral stress module, and therefore eliminate any uncertainty associated with minor variations in probe geometry. Also, the pore pressure element needs to be relocated in the redesigned instrument so that true measurements of the effective lateral stress on the LSM-II can be made during penetration and dissipation.

The lateral stress seismic piezocone (LSSCPTU) represents a promising tool for an improved site characterization. However, the results of laboratory calibrations and field measurements have shown that the hysteresis and non-linearity of the sensor may slightly affect measured lateral stresses. Consequently, further improvement work on the LSSCPTU should be focused on exploring means to reduce this effect to less than 1% of the full scale output. Additionally, extreme attention to detail is required to review the results of LSSCPTU tests in order to identify which anomalies among recorded data are due to soil behaviour and not to equipment characteristics or testing procedures.

6.4 Suggestions for further research

6.4.1 Seismic flat dilatometer

The soil classification system based upon SDMT measurements proposed in this thesis represents a contribution to the current state of the flat dilatometer, and adds to the options available to identify soil behaviour from in situ measurements. However, it is highly recommended to collect more SDMT data in different soil types in order to assess the reliability of this approach, and therefore promote its application. Also, the combination of the small strain shear modulus (G_0) with DMT parameters may provide means to identify unusual soil conditions (e.g. cementation and/or ageing). Additional SDMT tests should be carried out to increase the database developed.

The DMT based empirical correlations proposed in this thesis increase our confidence in the derivation of geotechnical parameters from DMT data. Correlations have been available since the introduction of the DMT as a site investigation tool to estimate several geotechnical parameters. The work described herein represents a first step to update some of those correlations. It is recommended to perform further research to improve the interpretation of DMT data.

6.4.2 Lateral stress seismic piezocone

Wroth (1975) and Schmertmann (1985) pointed out that the in situ lateral stress represents a key condition that should be considered in both site investigation and any geotechnical analysis. It is recognized that reliable estimates of in situ lateral stress can be obtained from the interpretation of results of self-boring pressuremeter (SBP) tests and push-in total stress cells (TSC). Alternatively, the in situ lateral stress can be estimated from empirical correlations to piezocone (CPTU) or flat dilatometer (DMT) data. Attempts have been also made to estimate the in situ lateral stress through the interpretation of lateral stress cone data by empirical correlations and cavity expansion methods (Tseng, 1989; Sully 1991; Takesue & Isano 2001). Indeed, the results reported by Sully (1991) and Takesue & Isano (2001) are encouraging, and therefore it is recommended to perform further interpretation of the data recorded with the LSSCPTU for estimation of in situ stress conditions.

The use of numerical modelling would improve the interpretation of data recorded with the LSSCPTU in terms of the distribution of strains, stresses and pore-water pressures generated during penetration. as well as consolidation and stress relaxation during pauses in the penetration. Whittle et al. (2001) describe the results of numerical analysis of the pore pressure dissipation around a tapered probe using a non-linear coupled consolidation analysis, with effective stress parameters characterized by the MIT-E3 model. Similarly, Vyazmensky (2005) analyzed the pore-water pressure dissipation data reported by Weech (2002) using the critical state Nor-Sand constitutive model coupled with the Biot formulation. The results of his analyses demonstrated that a fully coupled NorSandBiot modelling framework provides good estimates of pore pressure dissipation in fine-grained soils. It is hoped that the use of numerical approaches, may improve our understanding of soil behaviour around a full displacement tapered probe.

The ultimate axial compression load capacity of a single pile can be estimated by either indirect methods based upon fundamental soil parameters or directly from results of in situ tests such as piezocone and flat dilatometer. When the majority of the pile resistance is made up shaft friction the state of lateral and shear stresses at the interface between the pile and soil primarily control the shaft resistance. On this basis, it seems worthwhile to explore the applicability of LSSCPTU data for the development of a direct design method for piles installed in fine and coarse grained soils.

REFERENCES

Aas. G., Lacasse, S., Lunne, T., and Hoeg, D. 1986. Use of in situ tests for foundation design on clay. *In* Proceedings of the Conference of Use of In Situ Tests in Geotechnical Engineering, Blacksburg, VA, USA, pp. 1-30.

Ang A.H.S., and Tang, W.H. 2007. Probability Concepts in Engineering - Emphasis on Applications in Civil & Environmental Engineering. John Wiley & Sons, New Jersey.

Armstrong, J.E. 1984. Environmental and engineering applications of the surficial geology of the Fraser River Lowland, British Columbia. Canada Geological Surver, paper 83-23.

ASTM D6635-01. 2002. Standard Test Method for Performing the Flat Plate Dilatometer. Book of Standards Vol. 04.09.

ASTM D5778-07. 2007. Standard Test Method for Electronic Friction Cone and Piezocone Penetration Testing of Soils. Book of Standards Vol. 04.08.

Baldi, G., Bellotti, R., Ghionna, V., Jamiolkowski, M., Marchetti, S. & Pasqualini, E. 1986. Flat dilatometer tests in calibration chambers. *In* Proceedings of In Situ '86, ASCE Special Conference on Use of In Situ Tests in Geotechnical Engineering, Virginia Tech, Blacksburg, VA, June, ASCE Geotechnical Special Publication No. 6, pp. 431-446.

Baligh, M.M. 1975. Theory of deep site static cone penetration resistance. MIT Publication No. R-75-56.

Baligh, M.M., and Levadoux, J.N. 1980. Pore pressure dissipation after cone penetration, Massachusetts Institute of Technology, Department of Civil Engineering, Construction Facilities Division, Cambridge, Massachusetts 02139.

Baligh, M.M., Martin, T.R., Azzouz, A.S., and Morrison, J.M. 1985. The Piezo-Lateral stress cell. *In* Proceedings of the 11th ICSMGE, San Francisco, pp. 841-844.

Baligh, M.M., and Levadoux, J.N. 1986. Consolidation after undrained piezocone penetration. II: Interpretation. Journal of Geotechnical Engineering, ASCE, 112(7): 727-745.

Bang, E.S., Sung, N.H., Park, S.G., Kim, J.H., Kim , Y.S., Seo, D.N., Kim D.S., and Lee, S.H. 2008. Development and application of a resistivity seismic flat dilatometer testing system for efficient soft soil site characterization. *In* Proceedings of the 3rd International Conference on Site Characterization, Taipei, Taiwan, pp. 1247-1253.

Bayne, J.M., and Tjelta, T.I. 1987. Advanced cone penetrometer development for in-situ testing at Gulfaks C. *In* Proceedings of the 19th Offshore Technology Conference, Richardson, Texas, USA, 531-540.

Been, K., Lingnau, B.E., Crooks, J.H.A. and Leach, B.G. 1987. Cone penetration test calibration for Erksak (Beaufort Sea) sand. Canadian Geotechnical Journal, 24: 173-177.

Bellotti, R., Benoît, J., Fretti, C., and Jamiolkowski, M. 1997. Stiffness of Toyoura sand from dilatometer tests. Journal of Geotechnical and Geoenvironmental Engineering, 123(9): 836–846.

Benoît, J., and Lutenegger, A.J. 1993. Determining lateral stress in soft clays. *In* Proceedings of the Wroth Memorial Symposium, Oxford, UK, pp. 135-155.

Berenson, M.L., Levine, D.M., and Rindskopf, D. 1988. Applied statistics – A first course. Prentice Hall, New Jersey.

Bolton, M.D. 1986. The strength and dilatancy of sands. Géotechnique, 36(1): 65-78.

Brooker, E.W., and Ireland, H.O. 1965. Earth pressures al rest related to stress history. Canadian Geotechnical Journal, 2: 1-15.

Burghignoli, A., Cavalera, L., and Chieppa, V. 1991. Geotechnical characterization of Fucino clay. *In* Proceedings of the 10th European Conference on Soil Mechanics and Foundation Engineering, Florence, Italy, Vol. 1. 27-40.

Burns. S.E., and Mayne, P.W. 1998. Monotonic and dilatory pore-pressure decay during piezocone tests in clay. Canadian Geotechnical Journal, 35: 1063-1073.

Bustamante, M., and Gianeselli, L. 1982. Pile Bearing Capacity Prediction by Means of Static Penetrometer CPT. *In* Proceedings of the 2nd European Symposium on Penetration Testing, Amsterdam, 493-500.

Campanella, R.G., and Robertson, P.K. 1981. Applied cone research. *In* Proceedings of Symposium on Cone Penetration Testing and Experience, Geotechnical Engineering Division, ASCE. October 1981, pp. 343-362.

Campanella, R.G., and Robertson, P.K. 1984. A seismic cone penetrometer to measure engineering properties of soil. *In* Proceedings of the 54th Annual International Meeting and Exposition of the Society of Exploration Geophysics. Atlanta, Georgia, pp.138–41.

Campanella, R.G., Robertson, P.K, Gillespie, D.G., and Greig, J. 1985. Recent developments in in-situ testing of soils. *In* Proceedings of the 11th ICSMGE, San Francisco, Vol. 2, pp. 849-854.

Campanella, R.G., and Robertson P.K. 1988. Current status of the piezocone tests. *In* Proceedings of the First International Symposium on Penetration Testing, Orlando, Florida, Vol. 1, pp. 93-116.

Campanella, R.G., and Robertson, P.K. 1989. Use an interpretation of a research DMT. Soil Mechanics Series No. 127. Department of Civil Engineering, University of British Columbia, Vancouver, BC, Canada.

Campanella, R.G, Sully, J.P., Greig J.W., and Jolly, G. 1990. Research and development of a lateral stress piezocone. Transportation Research Record, 1278: 215-224.

Campanella, R.G., and Robertson, P.K. 1991. Use and interpretation of a research dilatometer. Canadian Geotechnical Journal, 28: 113-126.

Campanella, R.G., and Howie, J.A. 2005. Guidelines for the use, interpretation and application of seismic piezocone test data - A manual on interpretation of seismic piezocone test data for geotechnical design. Geotechnical Research Group, Department of Civil Engineering, The University of British Columbia, Vancouver.

Canou, J., and Tumay, M. 1986. Field evaluation of French SBPMT in soft deltaic Louisiana clay. *In* Proceedings of The pressuremeter and its marine application. ASTM, Special Technical Publication 950, pp. 97-118.

Carter, J.P, Booker, J.R., and Yeung, S.K. 1986. Cavity expansion in cohesive frictional soils. Géotechnique, 36(3): 349-358.

Chan, A.C., Y., and Morgenstern, N.R. 1986. Measurement of Lateral Stresses in a Lacustrine Clay Deposit. *In* Proceedings of the 39th Canadian Geotechnical Conference, Ottawa, Ontario, pp. 285–290.

Chang, M.F. 1991. Interpretation of overconsolidation ratio from in situ tests in recent clay deposits en Singapore and Malaysia. Canadian Geotechnical Journal, 28: 210-225.

Crawford, C.B., and deBoer, L.J. 1987. Field observations of soft clay consolidation in the Fraser Lowland. Canadian Geotechnical Journal, 24: 308-317.

Crawford, C.B. 1990. Comparison of measured settlements with predictions based on laboratory and in situ tests. Presentation at UBC, Geotechnical Seminar Series, March.

Crawford, C.B., and Campanella, R.G. 1991. Comparison of field consolidation with laboratory and in situ tests. Canadian Geotechnical Journal, 28: 103-112.

Crawford, C.B., Jitno, H., and Byrne, P.M. 1994. The influence of lateral spreading on settlements beneath a fill. Canadian Geotechnical Journal, 31: 145-150.

Cunha, R. P. 1994. Interpretation of self boring pressuremeter tests in sand. Ph. D. Thesis, Department of Civil Engineering, University of British Columbia, Vancouver, BC, Canada.

Daniel, C.R. 2003. Preliminary report on CPTU, SCPTU and SPT data collected at Patterson Park. In-situ Testing Group, University of British Columbia, Vancouver, BC, Canada.

Dolan, K. 2001. An in-depth geological and geotechnical site characterization study, Colebrook road overpass, Highway 99A, Surrey, B.C. B.A.Sc. Thesis, Department of Civil Engineering, University of British Columbia, Vancouver, BC, Canada.

Durgunoglu, H.T., and Mitchell, J.K. 1975. Static penetration resistance of soils: I analysis, II. Evaluation of the theory and implications for practice. *In* Proceedings of the ASCE Conference on In situ Measurement of Soil Properties, Raleigh, NC, USA, Vol. 1, pp. 151-171.

Eslami, A., and Fellenius, B.H. 1997. Pile capacity by direct CPT and CPTu method applied to 102 case histories. Canadian Geotechnical Journal 34(6): 886-904.

Eurocode 7 (1997). Geotechnical design - Part 3: Design assisted by field testing, Section 9: Flat dilatometer test (DMT). Final Draft, ENV 1997-3, Apr., 66-73. CEN -European Committee for Standardization.

Finno, R.J. 1993. Analytical interpretation of dilatometer penetration through saturated cohesive soils. Géotechnique, 43(2): 241-254.

Foti, S., Lancellotta, R., Marchetti,D., Monaco, P. and Totani, P. 2006. Interpretation of SDMT tests in a transversely isotropic medium. *In* Proceedings of the 2nd International Conference on the Flat Dilatometer, Washington, D.C., pp. 275-280.

Gibson, R.E., and Anderson, W.F. 1961. In-situ measurement of soil properties with pressuremeter. Civil Engineering and Public Works Review, 56(958): 615-618.

Ghionna, V., Jamiolkowski, M., Lancellotta, R., Tordella, M., and Ladd, CC. 1981. Performance of SBPMT in cohesive deposits. Report RD-81/173. FHWA, U.S. Department of Transportation.

Ghionna, V. 1984. Influence of chamber size and boundary conditions on the measured cone resistance. Sem. Cone Penetration Testing in the Laboratory, University of Southampton.

Ghionna, V.N., Jamiolkowski, M., Lacasse, S., Ladd, C.C., Lancellotta, R., and Lunne, T. 1985. Evaluation of self-boring pressuremeter, Norwegian Geotechnical Institute, Oslo, Report 159, pp. 1-9.

Ghionna, V.N., Jamiolkowski, M., Pedroni, S., and Piccoli, S. 1995. Cone pressuremeter tests in Po river sand. *In* Proceedings of the 4th International Symposium on Pressuremeter: The Pressuremeter and its New Avenues, Sherbrooke, Québec, Canada, 471-480.

Gillespie, D.G. 1981. The Piezometer Cone Penetration Test. M.A.Sc. Thesis, Department of Civil Engineering, University of British Columbia, Vancouver, BC, Canada.

Gillespie, D.G., and Campanella, R.G. 1981. Consolidation characteristics from pore pressure dissipation after piezometer cone penetration, Soil Mechanics Series No. 47, Department of Civil Engineering, University of British Columbia, Vancouver, BC, Canada.

Gillespie, D.G. 1990. Evaluating shear wave velocity and pore pressure data from the seismic cone penetration test. Ph.D. Thesis, Department of Civil Engineering, University of British Columbia, Vancouver, BC, Canada.

Gravesen, S. 1960. Elastic semi-infinite medium bounded by rigid wall with circular hole. Dansk Selkab Bygningsstatik, Bygningsstatiske Meddelelsser, Copenhagen, Denmark, 30(3): 93-111.

Hamouche, K.K., Leroueil, S., Roy, M., and Lutenegger. 1995. In situ evaluation of K_0 in eastern Canada clays. Canadian Geotechnical Journal, 32: 677-688.

Hepton, P. 1988. Shear wave velocity measurements during penetration testing. *In* Proceedings of Penetration Testing in the UK, Birmingham, UK: 275-278.

Hers. I. 1989. The analysis and interpretation of the cone pressuremeter in cohesive soils. M.A.Sc. Thesis, Department of Civil Engineering, University of British Columbia, Vancouver, BC, Canada.

Hegazy, Y.A., and Mayne, P.W. 1995. Statistical correlations between V_s and CPTU data for different soil types. *In* Proceedings of the Symposium on Cone Penetration Testing, Vol. 2, Sweden, pp. 173-178.

Houlsby, G.T., and Whiters, N.J. 1988. Analysis of the cone pressuremeter test in clay. Géotechnique, 38(4): 575-587.

Howie, J.A., 1991. The interpretation of full-displacement pressuremeter tests in sand. Ph. D. Thesis, Department of Civil Engineering, University of British Columbia, Vancouver, BC, Canada.

Huang, A.B. 1989. Strain path analyses for arbitrary three-dimensional penetrometers. International Journal for Numerical and Analytical Methods in Geomechanics, vol. 13, issue 5, pp. 551-564

Huang, A. B., and Haefele, K.C. 1990. Lateral Earth Pressure Measurements in a Marine Clay. Transportation Research Record, 1278: 156-163.

Hughes, J.M.O., and Robertson, P.K. 1984. Full displacement pressuremeter testing in sand. Soil Mechanics Series No. 78. Department of Civil Engineering, University of British Columbia, Vancouver, BC, Canada.

Huntsman, S. R., 1985. Determination of in-situ lateral pressure of cohesionless soils by static cone penetrometer. Ph.D. Thesis, University of California at Berkeley, USA.

Huntsman, S.R., Mitchell, J.K., Klejbuk, L.W. Jr., and Shinde, S.B. 1986. Lateral stress measurement during cone penetration. *In* Proceedings of the Conference of Use of In Situ Tests in Geotechnical Engineering, Blacksburg, VA, USA, 617-634.

Imre, E., Trang, P.Q., Telekes, G., Rózsa, P., and Fityus S. 2008. Evaluation of short non-monotonous dissipation test data. *In* Proceedings of the 3rd International Conference on Site Characterization, Taipei, Taiwan, pp. 1035-1041.

In-Situ Testing Group (Department of Civil Engineering, University of British Columbia). 1995a. General site characterization at KIDD 2 site. Report, CANLEX, Phase II, Activity 3A.

In-Situ Testing Group (Department of Civil Engineering, University of British Columbia). 1995b. General site characterization at Massey Tunnel. Report, CANLEX Phase II, Activity 3A.

Iwasaki, K, Tsuchiya, H., Sakai, Y., and Yamamoto, Y. 1991. Applicability of the Marchetti dilatometer test to soft ground in Japan. *In* Proceedings of Geo-Coast 91, Yokohama, Japan, Vol. 1. pp. 29-32.

Jackson, S. 2007. Personal communication

Jamiolkowsky, M. 1982. Personal communication to James K. Mitchell.

Jamiolkowski, M., and Robertson, P.K. 1988. Closing address. Future trends for penetration testing. Penetration Testing in the UK, Birmingham, UK: 321-342.

Jamiolkowski, M., Ghionna, V.N., Lancellotta, R., and Pasqualini, E. 1988. New correlations of penetration tests for design practice. *In* Proceedings of the First International Symposium on Penetration Testing, Orlando, Florida, Vol. 1, pp. 263-296.

Jefferies, M.G., Jonsson L., and Been, K. 1987. Experience with measurement of horizontal geostatic stress in sand during cone penetration test profiling. Géotechnique, 37(4): 483-498.

Keaveny, J.M. and Mitchell, K. 1986. Strength of fine-grained soils using the piezocone. *In* Proceedings of Use of In-Situ Tests in Geotechnical Engineering, ASCE, New York, pp. 668-685.

Kim, T., Kim, N.K., Tumay, M. T., and Lee. W. 2007. Spatial distribution of excess pore-water pressure due to piezocone penetration in overconsolidated clay. Journal of Geotechnical and Geoenvironmental Engineering, ASCE, 133(6): 674-683.

Konrad, J., Bozozuk, M., and Law, K. 1985. Study of in situ test methods in deltaic silt. *In* Proceedings of the 11th ICSMFE, San Francisco, Vol. 2, pp. 879-886.

Konrad, J. M., and Law, K.T., 1987. Undrained shear strength from piezocone tests. Canadian Geotechnical Journal, 24: 392-405.

Kulhawy, F.H. and Mayne, P.W. 1990. Manual on Estimating Soil Properties for Foundation Design, Report No.EL-6800, Electric Power Research Institute, Palo Alto, CA, August 1990, 306 p.

Lacasse, S., Jamiolkowski, M., Lançellotta, R., and Lunne, T. 1981. In situ characteristics of two Norwegian clays. *In* Proceedings of the 10th ICSMFE, Stockholm, Rotterdam, The Netherlands. Vol. 2, pp. 507–511.

Lacasse, S., and Lunne T. 1988. Calibration of dilatometer correlations. *In* Proceedings of the First International Symposium on Penetration Testing, Orlando, Florida, Vol. 1, pp. 539-548.

Ladanyi, B., and Longtin, H. 2005. Short- and long-term sharp cone tests in clay. Canadian Geotechnical Journal, 42: 136-146.

Ladd, C.C., Young, G.A., Kraemer, S.R., and Burke, D.M. 1998. Engineering Properties of Boston Blue Clay from Special Testing Program. *In* Proceedings of sessions of Geo-Congress 98, ASCE, Boston, MA, USA, pp. 1-24.

Ladd, C.C., and DeGroot, D.J. 2003. Recommended practice for soft ground site characterization. *In* Proceedings of 12th Panamerican Conference on Soil Mechanics and Geotechnical Engineering and 39th U.S. Rock Mechanics Symposium, Arthur Casagrande Lecture. Cambridge, Massachusetts, Vol.1, pp. 3-57.

Lehane, B.M., and Jardine, R.JL. 1994. Displacement-pile behaviour in a soft marine clay. Canadian Geotechnical Journal, 31: 181-191.

Long, M. 2008. Design parameters from in situ tests in soft ground – recent developments. *In* Proceedings of the 3rd International Conference on Site Characterization, Keynote lecture, Taipei, Taiwan, pp. 89-116.

Luna, O. G. 2008. Personal Communication

Lunne, T., Powell, J.J.M., Hauge, E.A., Mokkelbost, K.H. and Uglow, I.M. 1990. Correlation of dilatometer readings with lateral stress in clays. Transportation Research Record, 1278: 183-193.

Lunne, T., Robertson, P.K., and Powell, J.J.M. 1997. Cone penetration testing in geotechnical practice. Blackie Academic & Professional.

Lutenegger, A.J. 1988. Current status of the Marchetti dilatometer test. *In* Proceedings of the First International Symposium on Penetration Testing, Orlando, Florida, Vol. 1, pp. 137-155.

Lutenegger, A.J. & Kabir, M.G. 1988. Dilatometer C-reading to help determine stratigraphy. *In* Proceedings of the First International Symposium on Penetration Testing, Orlando, Florida, Vol. 1, pp. 549-554.

Lutenegger, A.J. 1990. Determination of In situ Lateral Stresses in a Dense Glacial Till. Transportation Research Record, 1278: 194-203.

Lutenegger, A.J., and Miller, G.A. 1993. Evaluation of dilatometer method to determine axial capacity of driven model pipe piles in clay. *In* Proceedings of Design and performance of deep foundations: piles and piers in soil and soft rock, Dallas, Texas, USA, pp. 41-163.

Lutenegger, A.J. 2006. Consolidation lateral stress ratios in clay from flat Dilatometer tests. *In* Proceedings of the 2nd International Flat Dilatometer Conference, Washington D.C., USA, pp. 327-333.

Mahbudul, A. K. 1993. Strength-deformation behaviour of a weathered clay crust. Ph.D. Thesis, University of Ottawa, Canada.

Marchetti, S. 1975. A new in situ test for the measurement of horizontal soil deformability. *In* Proceedings of the ASCE Conference on In situ Measurement of Soil Properties, Raleigh, NC, USA, Vol. 2, pp. 255-259.

Marchetti, S. 1979. Contribution to discussion, Session 7. *In* Proceedings of the 7th European Conference on Soil Mechanics and Foundation Engineering, Brighton, Vol. 4, pp.237-242 and 243-244.

Marchetti, S. (1980). In situ tests by flat dilatometer. Journal of the Geotechnical Engineering Division, ASCE, 106(3): 299–321.

Marchetti, S. and Crapps, D.K. 1981. Flat Dilatometer Manual. Internal Report of G.P.E. Inc.

Marchetti, S. 1985. On the field determination of K_0 in sand. *In* Proceedings of the 11th ICSMGE, San Francisco, pp. 2667-2672.

Marchetti, S., Totani, G., Campanella, R.G., Robertson, P.K., and Taddei B. 1986. The DMT-σ_{hc} method for piles driven in clay. *In* Proceedings of the Conference of Use of In Situ Tests in Geotechnical Engineering, Blacksburg, VA, USA, pp. 765-779.

Marchetti, S., and Totani, G. 1989. C_h evaluations from DMTA dissipation curves. *In* Proceedings of the 12th ICSMGE, Rio de Janeiro, pp. 841-844.

Marchetti, S. 1997. The Flat Dilatometer: Design Applications. *In* Proceedings of the 3rd International Geotechnical Engineering Conference, Keynote lecture, Cairo University, Jan., pp. 421-448.

Marchetti, D., Monaco, P., Totani, G. and Calabrese, M. 2001. The flat dilatometer test (DMT) in soil investigations. A report by the ISSMGE Committee TC16. *In* Proceedings of the International Conference on in situ measurement of soil properties, In Situ 2001, Bali, Indonesia, May 2001, 41 pp.

Marchetti, s. 2006. Origin of the Flat Dilatometer. *In* Proceedings of the 2nd International Flat Dilatometer Conference, Washington D.C., USA, pp. 2-3.

Marchetti, D., Marchetti, S., Monaco, P., and Totani, G. 2007. Risultati di prove in sito mediante dilatometro sismico (SDMT). Memoria per XXIII Convegno Nazionale di Geotecnica "Previsione e controllo del comportamento delle opere" Padova-Abano Terme (document in italian).

Marchetti, S., Monaco, P., Totani, G., and Marchetti, D. 2008a. In Situ tests by Seismic Dilatometer (SDMT). ASCE Geotechnical Special Publication honoring Dr. John H. Schmertmann. From Research to Practice in Geotechnical Engineering. GSP No. 170, Geo-Institute Meeting in New Orleans March 9 to 12, 2008.

Marchetti, S., Marchetti, D., Monaco, P., and Totani, G. 2008b. Experience with seismic dilatometer (SDMT) in various soil types. *In* Proceedings of the 3rd International Conference on Site Characterization, Taipei, Taiwan, 1139-1345.

Marchetti, D. 2008. Personal Communication.

Martin, G.K., and Mayne, P.W. 1997. Seismic Flat Dilatometer tests in Connecticut valley varved clay. Geotechnical Testing Journal, 20(3): 357-361.

Martin, G.K. and Mayne, P.W. 1998. Seismic flat dilatometer in Piedmont residual soils. *In* Proceedings of the 1st International Conference on Site Characterization - ISC'98, Atlanta, 2, pp. 837-843.

Mayne, P.W., and Kulhawy, F.H. 1990. Direct and indirect determinations of in situ K_0 in clays. Transportation Research Record, 1278: 141-149.

Mayne, P.W. and Chen, B.S-Y. 1994. Preliminary calibration of PCPT-OCR model for clays. *In* Proceedings of the 13th International Conference on Soil Mechanics and Foundation Engineering, New Delhi, India, Vol. 1, pp. 283-286.

Mayne, P.W., and Martin, G.K. 1998. Commentary on Marchetti Flat Dilatometer Correlations in Soils. Geotechnical Testing Journal, 21(3): 222-239.

Mayne, P.W., Schneider, J.A., and Martin, G.K. 1999. Small and large-strain soil properties from seismic flat plate dilatometer tests. *In* Proceedings of Pre-failure Deformation Characteristics of Geomaterials, Torino, Italy, 419-425.

Mayne, P.W. 2001. Stress-strain-strength-flow parameters from enhanced in-situ tests. *In* Proceedings of the International Conference on In-Situ Measurement of Soil Properties and Case Histories, Bali, Indonesia, pp. 27-48.

Mayne, P.W. 2005. Integrated Ground Behavior: In-Situ and Lab Tests. Deformation Characteristics of Geomaterials, Vol. 2 (Proceedings IS Lyon), Taylor & Francis, London: 155-177.

Mayne, P.W. 2007. Synthesis on Cone Penetration Testing: State-of-Practice. NCHRP Project 20-05; Task 37-14, Transportation Research Board, National Academies Press, Washington, D.C.

Masood, T. 1990. Determination of lateral earth pressure in soils by in-situ measurement. Ph.D. Thesis, University of California at Berkeley, USA.

McPherson, I.D. 1985. An evaluation of the flat dilatometer as an in situ testing device. M.A.Sc. Thesis, Department of Civil Engineering, University of British Columbia, Vancouver, BC, Canada.

Miller, G.A, and Tan, N.K. At-rest lateral stress from pressuremeter tests in an unsaturated soil calibration chamber. *In* Proceedings of the 3rd International Conference on Site Characterization, Taipei, Taiwan, pp. 621-626.

Mitchell, J.K., and Soga, K. 2005. Fundamentals of Soil Behavior. 3rd ed., John Wiley & Sons, New Jersey.

Mollé, J. 2005. The accuracy of the interpretation of CPTbased soil classification methods for soft soils. MScThesis Section for Engineering Geology, Department of Applied Earth Sciences, Delft University of Technology. Memoirs of the Centre of Engineering Geology in the Netherlands, No. 242. Report AES/IG/05-25, December.

Monaco, P., and Marchetti, S. 2007. Evaluating liquefaction potential by Seismic Dilatometer (SDMT) accounting for aging/stress history. *In* Proceedings of the 4th International Conference on Earthquake Geotechnical Engineering, Thessaloniki, Greece, Vol. 1, pp. 247-252.

Monahan, P.A., Luternauer, J.L., and Barrie, J.V. (1993). A delta plain sheet sand in the Fraser River Delta, British Columbia, Canada. Quaternary International, 20: 27-38.

Monahan, P.A., Luternauer, J.L., and Barrie, J.V. (1995). The geology of the CANLEX Phase II sites in Delta and Richmond British Columbia. *In* Proceedings of the 48th Canadian Geotechnical Conference, Vancouver, B.C., pp. 59–68.

Monahan, P.A., and Levson, V.M. (2001). Development of a shear-wave velocity model of the near-surface deposits of southwestern British Columbia, Canada. *In* Proceedings of the 4th International Conference of Recent Advances in Geotechnical Earthquake Engineering and Soil Dynamics, San Diego, USA.

Nutt, N.R.F., and Houlsby, G.T. 1995. Time dependent behaviour of sand from pressuremeter tests. *In* Proceedings of the 4th International Symposium on Pressuremeter: The Pressuremeter and its New Avenues, Sherbrooke, Québec, Canada, 95-100.

O'Neill, M.W., and Yoon, G. 1995. Engineering Properties of Overconsolidated Pleistocene Soils of Texas Gulf Coast. Transportation Research Record, 1479: 81-88.

O'Neill, M.W. 2000. National Geotechnical Experimentation Site - University of Houston. National Geotechnical Experimentation Sites, Geotechnical Special Publication No. 93, Benoît, J., and Lutenegger, A.J., ASCE, USA, pp. 72-101.

Pantoja, A. S. 2008. Personal Communication.

Parkin, A. and Lunne, T. 1982. Boundary effects in the laboratory calibration of a cone penetrometer in sand. *In* Proceedings of the 2nd European Symposium on Penetration Testing, Amsterdam, Vol. 2, pp. 761-768.

Powell, J.J.M., and Uglow, I.M. 1986. Dilatometer Testing in Stiff Overconsolidated Clays. *In* Proceedings of the 39th Canadian Geotechnical Conference, Ottawa, Ontario, pp. 317–326.

Powell, J.J.M., and Uglow, I.M. 1988a. The interpretation of the Marchetti dilatometer tests in UK clays. Penetration Testing in the UK, Birmingham, UK: 269-273.

Powell, J.J.M., and Uglow, I.M. 1988b. Marchetti dilatometer testing in UK soils. *In* Proceedings of the First International Symposium on Penetration Testing, Orlando, Florida, Vol. 1, pp. 555-562.

Powell, J.J.M., Lunne, T., and Frank, R. 2001. Semi empirical design procedures for axial pile capacity in clays. *In* Proceedings of the 15th ICSMGE, Istanbul, Turkey, 991-994.

Powell, J.J.M. 2008. Can we reliably determine in situ horizontal stress from the Cone Pressuremeter in clay soils?. *In* Proceedings of the 3rd International Conference on Site Characterization, Taipei, Taiwan, pp. 1129-1134.

Randolph, M.F., and Wroth, C.P. 1979. An analytical solution for the consolidation around a driven pile. International Journal for Numerical and Analytical Methods in Geomechanics, (3): 217-229.

Ricceri G. Simonini P., and Cola, S. 2002. Applicability of piezocone and dilatometer to characterize the soils of the Venice Lagoon. Geotechnical and Geological Engineering, 20: 89-121.

Robertson, P.K. 1982. In-situ testing of soil with emphasis on its application to liquefaction assessment. Ph. D. Thesis, Department of Civil Engineering, University of British Columbia, Vancouver, BC, Canada.

Robertson, P.K., and Campanella, R.G. 1983. Interpretation of cone penetration tests - Part I (sand). Canadian Geotechnical Journal, 20(4): 718-733.

Robertson, P.K., Campanella, R.G., Gillespie, D., and Greig. J. 1986. Use of piezometer cone data. *In* Proceedings of the Conference of Use of In Situ Tests in Geotechnical Engineering, Blacksburg, VA, USA, pp. 1263-1280.

Robertson, P.K., Campanella, R.G., Gillespie, D., and By T. 1987. Excess pore pressures and the DMT. Soil Mechanics Series No. 112. Department of Civil Engineering, University of British Columbia, Vancouver, BC, Canada.

Robertson, P.K. 1990. Soil classification using the cone penetration test. Canadian Geotechnical Journal, 27(1): 151–158.

Robertson, P.K., Sasitharan, S., Cunning, J.C., and Segs, D.C. 1995. Shear wave velocity to evaluate flow liquefaction. Journal of Geotechnical Engineering, ASCE, 121(3): 262–273.

Robertson, P.K., Wride (Fear), C.E., List, B.R., Atukorala, U., Biggar, K.W., Byrne, P.M., Campanella, R.G., Cathro, D.C., Chan, D.H., Czajewski, K., Finn, W.D.L., Gu, W.H., Hammamji, Y., Hofmann, J.A., Howie, J.A., Hughes, J., Imrie, A.S., Konrad, J. M., Küpper, A., Law, T., Lord, E.R.F., Monahan, P.A., Morgenstern, N.R., Phillips, R., Piché, R., Plewes, D., Scott, D., Sobkowicz, J., Stewart, R.A., Watts, B.D., Woeller, D.J., Youd, T.L., and Zavodni, Z. 2000. The Canadian Liquefaction Experiment: an overview. Canadian Geotechnical Journal, 37: 499–504.

Salgado R. R. 1993. Analysis of penetration resistance in sands. Ph.D. Thesis, University of California at Berkeley, USA.

Sanin, M. 2005. Cyclic shear loading response of Fraser River Delta silt. M.A.Sc. Thesis, Department of Civil Engineering, University of British Columbia, Vancouver, BC, Canada.

Sanin, M. and Wijewickreme, D. 2006. Cyclic shear response of channel-fill Fraser River Delta silt. Soil Dynamics and Earthquake Engineering, 26: 854-869.

Sanin, M. 2008. Personal Communication.

Schmertman, J.H. 1978. Guidelines for cone penetration test performance and design. Federal Highway Administration Report No. FHWA-TS-78-209, Washington, D.C.

Schmertmann, J.H. 1982. A method for determining the friction angle in sands from the Marchetti dilatometer test (DMT). *In* Proceedings of the 2nd European Symposium on Penetration Testing, ESOPT-II, Amsterdam, Vol. 2, pp 853-861.

Schmertmann, J.H. 1983. Revised procedure for calculating K_0 and OCR from DMT's with $I_D > 1.2$ and which incorporates the penetration measurement to permit calculating the plane strain friction angle. DMT Digest No. 1. GPE Inc., Gainesville, FL.

Schmertmann, J.H. 1985. Measure and use of the in situ lateral stress. *In* The Practice of Foundation Engineering – a Volume honoring Jorj O. Osterberg, Department of Civil Engineering, Northwestern University, pp. 189-213.

Schmertmann, J.H. 1988. Guidelines for Using the CPT, CPTU and Marchetti DMT for Geotechnical Design". Report No. FHWA-PA-87-022+84-24 to Pennsylvania Department of Transportation, Office of Research and Special Studies, Harrisburg, PA, 5 vols., Gainesville, FL.

Schnaid, F. 1990. A study of the cone-pressuremeter test in sand. Ph. D. Thesis, University of Oxford, U.K.

Schnadi, F., Ortigao, J.A.R., Mántaras, F.M., Cunha, R.P., and MacGregor, I., Analysis of self-boring pressuremeter (SBPM) and Marchetti dilatomter (DMT) tests in granite saprolites. Canadian Geotechnical Journal, 37: 796-810.

Schnaid, F., Lehane, B. M., and Fahey, M. 2004. In situ test characterization of unusual soils. Keynote Lecture. *In* Proceedings of the 2nd International Conference on Geotechnical and Geophysical Site Characterization, Porto, Vol. 1, pp. 49–74.

Schneider, J.A., Randolph, M.F., Mayne, P.W., and Ramsey, N. 2008. Influence of partial consolidation during penetration on normalized soil classification by piezocone. *In* Proceedings of the 3rd International Conference on Site Characterization, Taipei, Taiwan, pp. 1159-1165.

Smith, M.G. 1993. A laboratory study of the Marchetti Dilatometer. Ph. D. Thesis, University of Oxford, U.K.

Sridharan, A., El-Shafei, A., and Miura, N. 2002. Mechanisms controlling the undrained strength behavior of remolded Ariake Marine Clays. Marine Resources and Geotechnology (20):21-50.

Stephenson, B., and Lomnitz, C. 2005. Shear-wave velocity profile at the Texcoco strong-motion array site, Valley of Mexico. Geofísica Internacional, Vol. 44, Num. 1, pp. 3-10.

Sully, J.P. and Campanella, R.G. 1989. Correlation of maximum shear modulus with DMT test results in Sand. *In* Proceedings of the 12th ICSMGE, Rio de Janeiro, Brazil, Vol. 1, pp. 339-345.

Sully, J.P. and Campanella, R.G. 1990. Measurement of lateral stress in cohesive soils by full-displacement in situ test methods. Transportation Research Record, 1278: 164-171.

Sully, J.P., and Campanella, R.G. 1991. Effect of lateral stress on CPT penetration pore pressures. Journal of Geotechnical Engineering, ASCE, 117(7): 1082–1088.

Sully, J.P. 1991. Measurement of in-situ lateral stress during full-displacement penetration tests. Ph. D. Thesis, Department of Civil Engineering, University of British Columbia, Vancouver, BC, Canada.

Sully, J.P., Robertson, P.K., Campanella, R.G., and Woeller, D.J. 1999. An approach to evaluation of field CPTU dissipation data in overconsolidated fine-grained soils. Canadian Geotechnical Journal, 36: 369-381.

Takei, K., and Isano, T. 1999. Development of a lateral stress cone. *In* Proceedings of the 34th Japan National Conference on Geotechnical Engineering, 275-276, (document in Japanese).

Takesue, K., and Isano T. 2000. Development and application of a lateral stress cone. Annual report Kajima Technical Research Institute, Kajima Corporation, Vol. 48, 61-66. (document in Japanese).

Takesue, K., and Isano T. 2001. Development and application of a lateral stress cone. *In* Proceedings of the International Conference on In-situ Measurement of Soils Properties and Case Histories, Bali, India, 623-629.

Takesue, K. 2001. In-situ friction test using a friction and lateral stress measurement cone. *In* Proceedings of Annual Meeting of the Architectural Institute of Japan. pp. 627-628. (document in Japanese).

Teh, C.I., and Houlsby, G.T. 1991. An analytical study of the cone penetration test in clay. Géotechnique, 41(1): 17-34.

Terzaghi, K., Peck, R.B., and Mesri, G. 1996. Soil Mechanics in Engineering Practice, 3rd edition, John Wiley & Sons, Inc.

Tseng, Dar-Jen. 1989. Prediction of cone penetration resistance and its application to liquefaction assessment. Ph.D. Thesis, University of California at Berkeley, USA.

Torstensson, B.A. 1984. A new system for ground water monitoring. Ground Water Monitoring Review, 4: 131-138.

Tringale, P.T. 1983. Soil identification in-situ using an acoustic cone penetrometer. Ph.D. Thesis, University of California at Berkeley, USA.

Tsang. C. 1987. Research dilatometer testing in sands and in clayey deposits. M.A.Sc. Thesis, Department of Civil Engineering, University of British Columbia, Vancouver, BC, Canada.

Vesic, A.S. 1972. Expansion of cavities in infinite soil mass. Journal of the Soils Mechanics and Foundations Division, ASCE, 98 (SM3):603–24.

Villet, W.C.B. 1981. Acoustic emissions during the static penetration of soils. Ph.D. Thesis, University of California at Berkeley, USA.

Vyazmensky A. M. 2005. Numerical modelling of time dependent pore pressure response induced by helical pile installation. M.A.Sc. Thesis, Department of Civil Engineering, University of British Columbia, Vancouver, BC, Canada.

Weech, C. (2002). Installation and load testing of helical piles in a sensitive fine-grained soil. M.A.Sc. Thesis, Department of Civil Engineering, University of British Columbia, Vancouver, BC, Canada.

Whittle, A.J., Sutabutr, T., Germaine, J. T., and Varney, A. 2001. Prediction and interpretation of pore pressure dissipation for a tapered piezoprobe. Géotechnique, 51(7): 601-617.

Windle, D., and Wroth, C.P. 1977a. The use of SBPMT to determine the undrained properties of clays. Ground Engineering, 10(6): 37-46.

Windle, D., and Wroth, C.P. 1977b. In situ measurements of stiff clays. *In* Proceedings of the 9th ICSMFE, Tokyo, Vol. 1, pp. 347-352.

Withers, N.J., Howie, J. Hughes, J.MO., and Robertson, P.K. 1989. Performance and analysis of cone pressuremeter tests in sands. Géotechnique, 39(3): 433-454.

Wong, J.T.F., Wong, M.F., and Kassim, M. 1993. Comparison between Dilatometer and Other In-situ and Laboratory Tests in Malaysian Alluvial Clay. *In* Proceedings of the 11th Southeast Asian Geotechnical Conference, Singapore, pp. 275-279.

Wride (Fear), C.E., Robertson, P.K., Biggar, K.W., Campanella, R.G., Hofmann, B.A., Hughes, J.M.O., Küpper, A., and Woeller, D.J. 2000. Interpretation of in situ test results from the CANLEX sites. Canadian Geotechnical Journal, 37: 505–529.

Wroth, C.P. 1975. In situ measurement of initial stresses and deformation characteristics. *In* Proceedings of the ASCE Conference on In situ Measurement of Soil Properties, Raleigh, NC, USA, Vol. 2, pp. 181-230.

Wroth, C.P., and Hughes, J.M.O. 1973. An instrument for the in-situ measurement of the properties of soft clays. *In* Proceedings of the 8th ICSMFE, Moscow, pp. 487-494.

Yu, H.S., Schnaid, F., and Collins, I.F. 1996. Analysis of Cone Pressuremeter Tests in Sands. Journal of Geotechnical Engineering, ASCE, 122(8): 623–632.

Yu, H.S. 2004. In situ soil testing: from mechanics to interpretation. *In* Proceedings of the 2nd International Conference on Site Characterization, James K. Mitchell Lecture, Porto, Portugal, 3-38.

Zergoun, M., O'Brien, J.A. and Broomhead, D. 2004. Transcanada Highway – 200th Street Langley Interchange British Columbia Canada – Part 1: Test Fill Observations. *In* Proceedings of the 57th Canadian Geotechnical Conference

APPENDIX A Seismic flat dilatometer (SDMT) profiles

UBC

Sounding: SDMT-01	γ_{av} = 18.50 kN/m^3	W.T.= 1.80 m	Date: 30/10/2007
Location: Kidd 2 Substation	Max. depth: 23.91 m	Rig: UBC-CPT Truck	Crew: IRC/MAS/GM

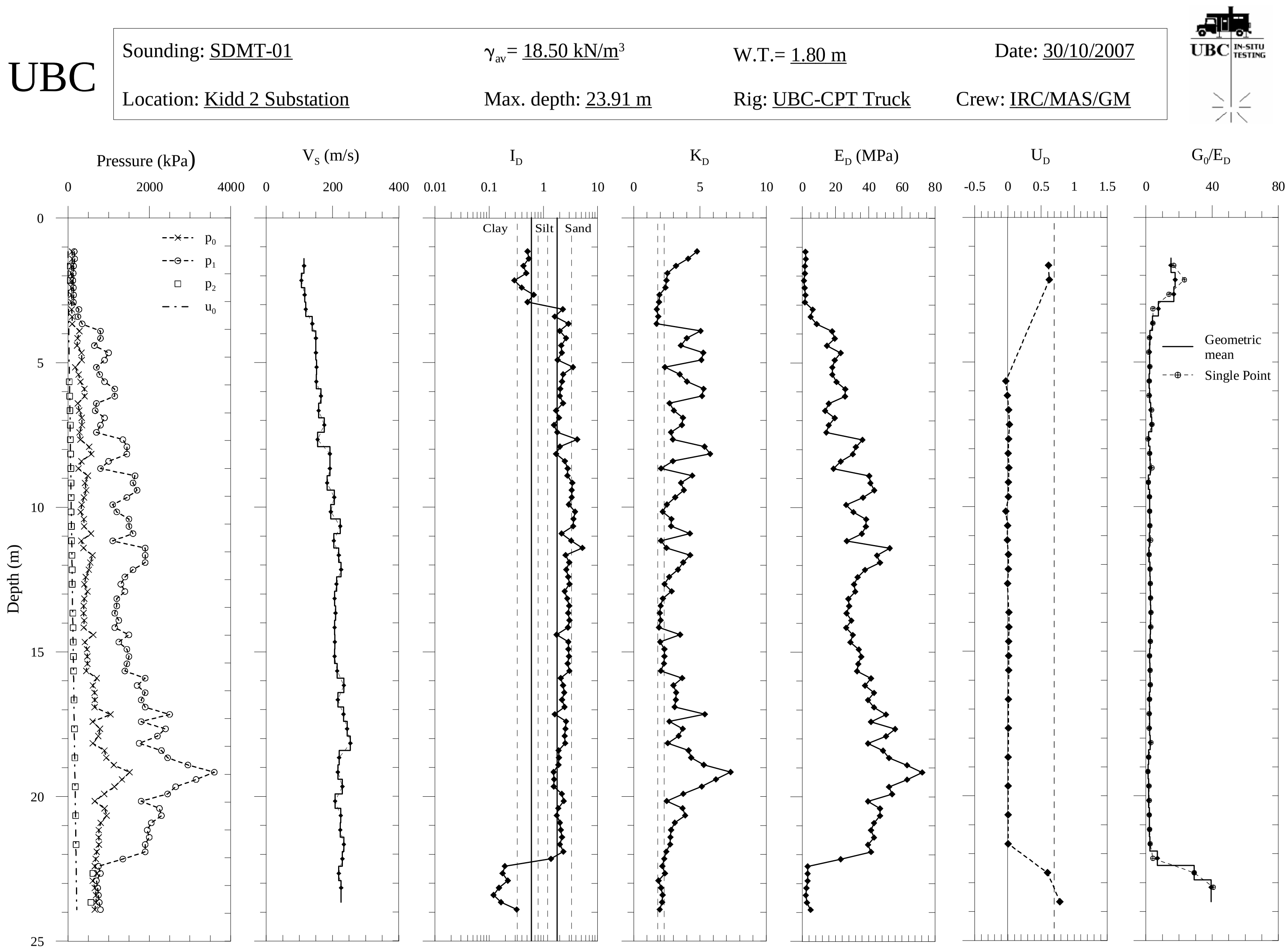

Max. depth: 23.91 m

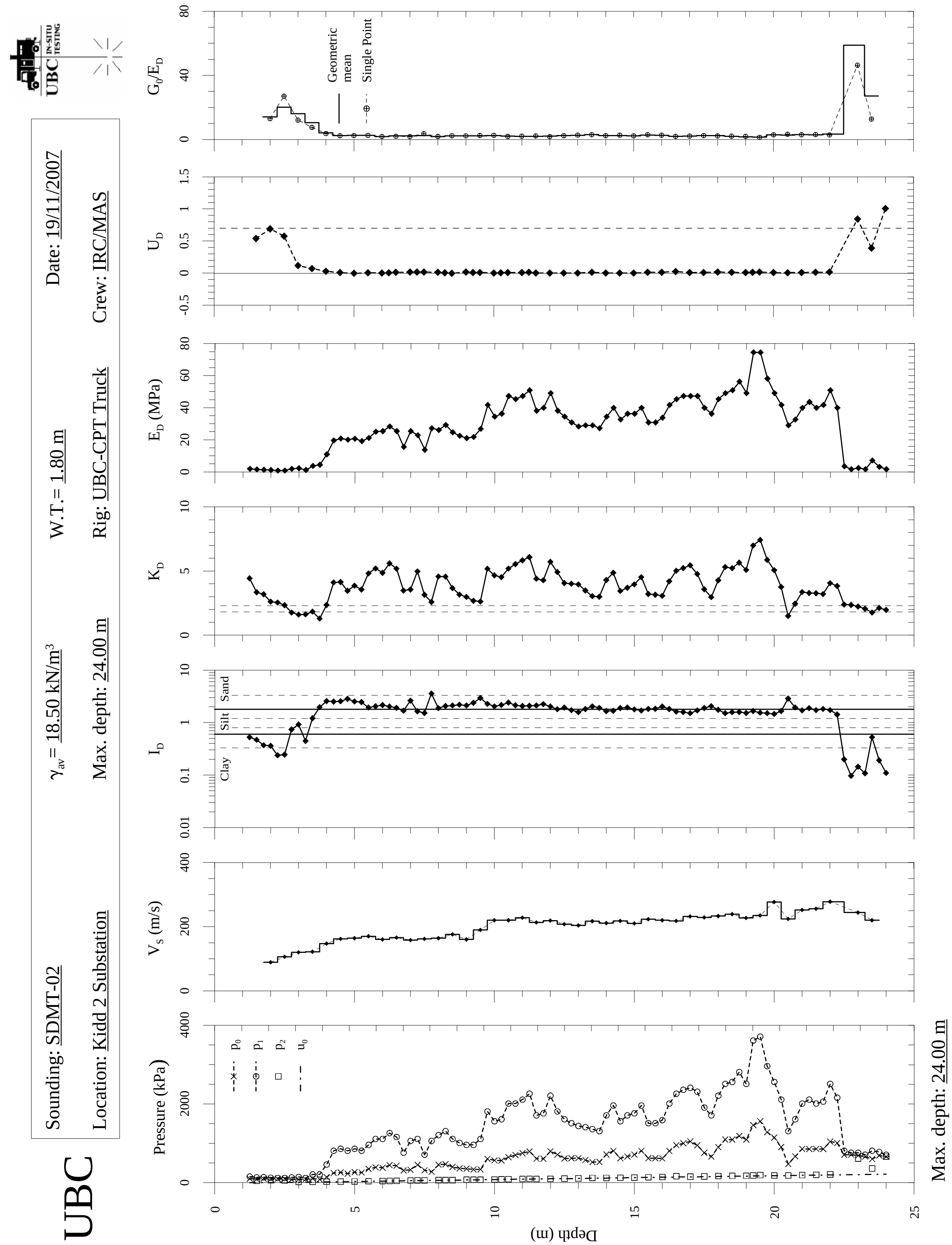

UBC
UBC IN-SITU TESTING
Sounding: SDMT-02
Location: Kidd 2 Substation
γ_{av} = 18.50 kN/m^3
Max. depth: 24.00 m
W.T.= 1.80 m
Rig: UBC-CPT Truck
Date: 19/11/2007
Crew: IRC/MAS
Pressure (kPa)
p_0
p_1
p_2
u_0
V_S (m/s)
I_D
Clay
Silt
Sand
K_D
E_D (MPa)
U_D
G_0/E_D
Geometric mean
Single Point
Depth (m)
Max. depth: 24.00 m

UBC

Sounding: SDMT-03 | γ_{av}= 18.00 kN/m^3 | W.T.= 2.50 m | Date: 31/05/2007

Location: 200th Street Overpass | Max. depth: 16.15 m | Rig: ConeTec 4x4 | Crew: IRC/JH/ME/IW

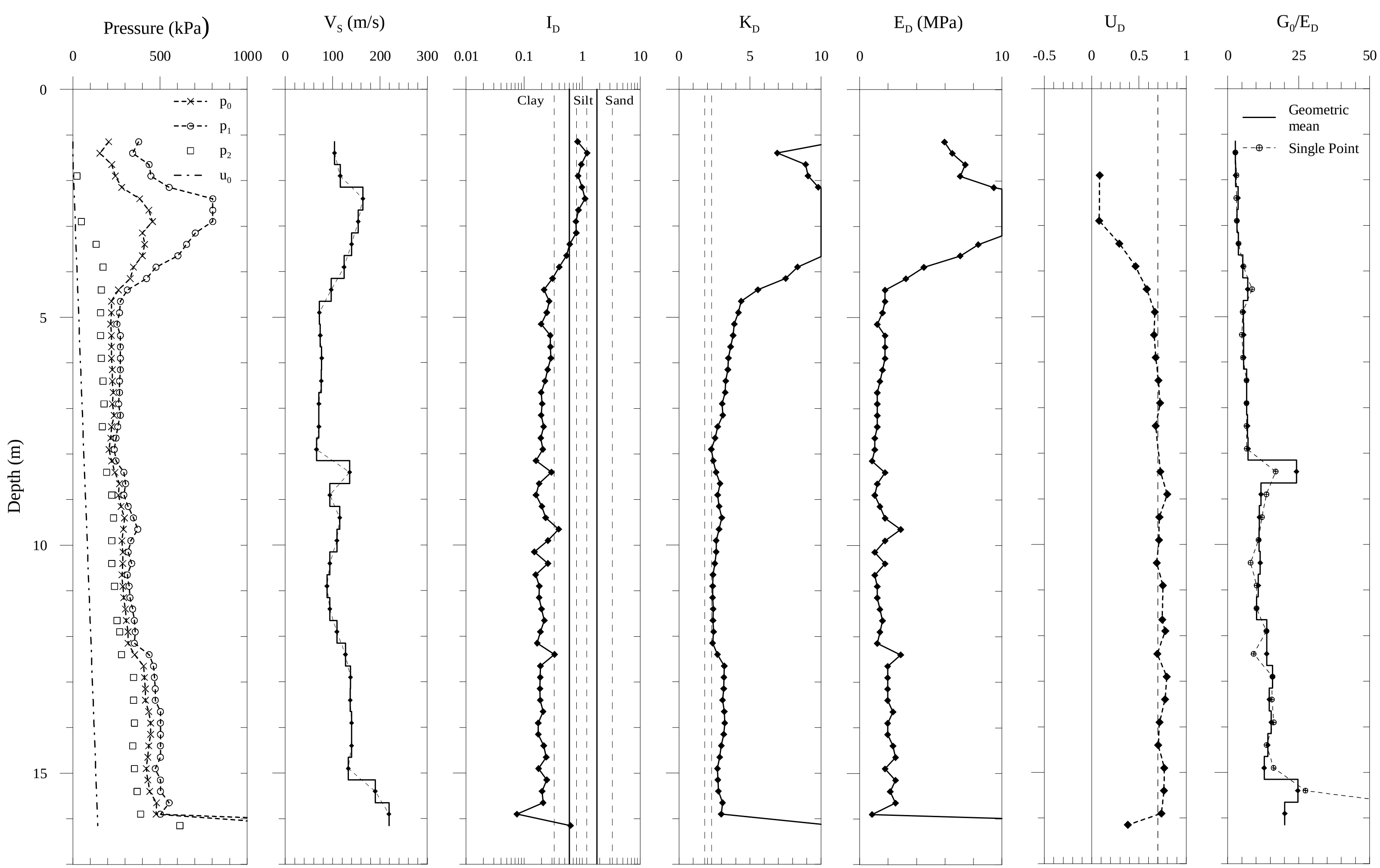

Max. depth: 16.15 m

UBC

Sounding: SDMT-04	γ_{av}= 16.00 kN/m³	W.T.= 5.50 m	Date: 13/02/2008
Location: Dyke Road, Richmond, B.C.	Max. depth: 15.00 m	Rig: UBC CPT Truck	Crew: IRC/MAS/MS

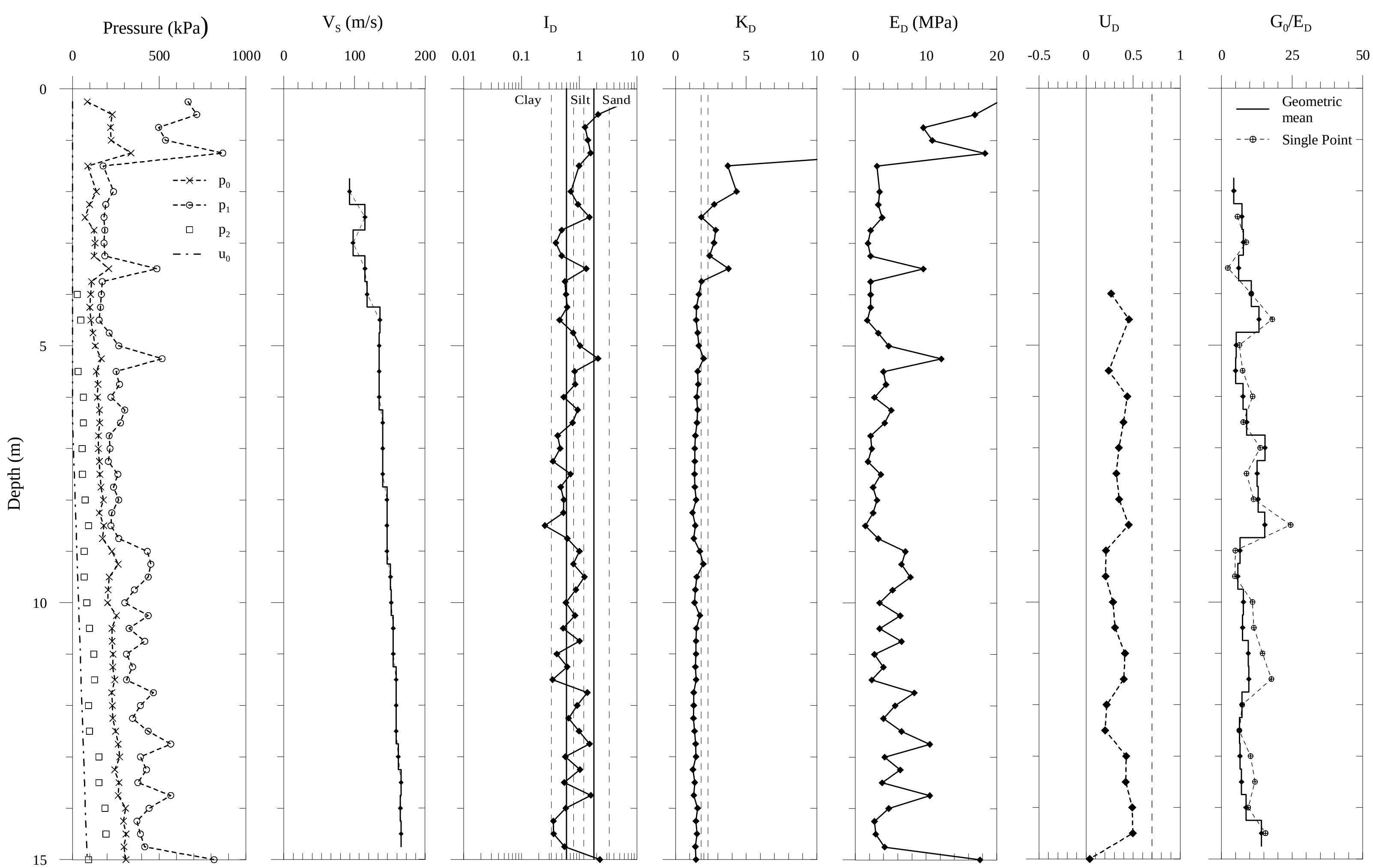

Max. depth: 15.00 m

UBC

Sounding: SDMT-05 | γ_{av} = 18.50 kN/m^3 | W.T.= 2.00 m | Date: 14/03/2008

Location: Massey Tunnel (Southern portal) | Max. depth: 20.00 m | Rig: UBC CPT Truck | Crew: IRC

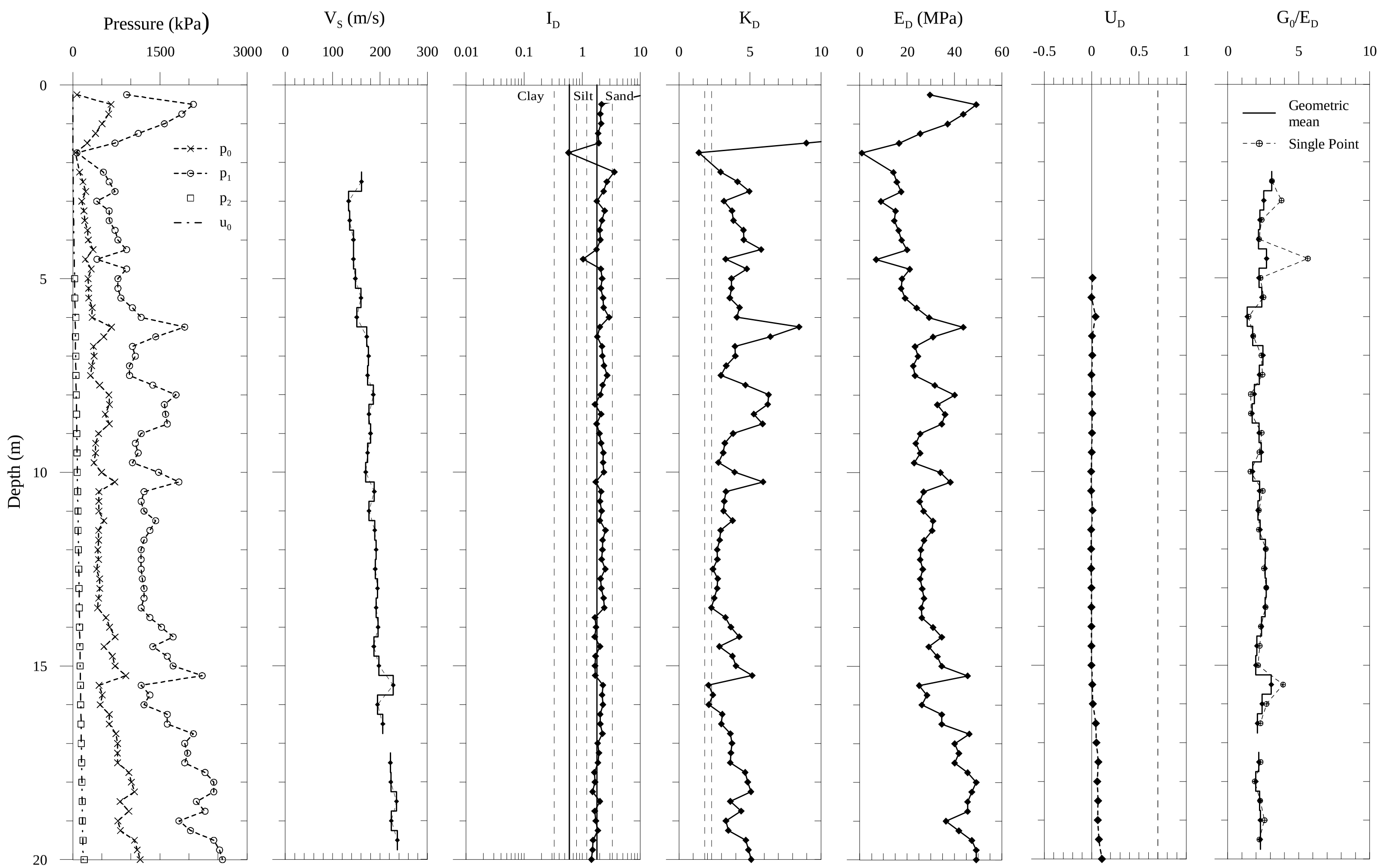

Max. depth: 20.00 m

UBC

Sounding: SDMT-06 | γ_{av} = 16.00 kN/m^3 | W.T.= 7.00 m | Date: 16/04/2008

Location: Dyke Road, Richmond, B.C. | Max. depth: 15.00 m | Rig: UBC CPT Truck | Crew: IRC/MAS

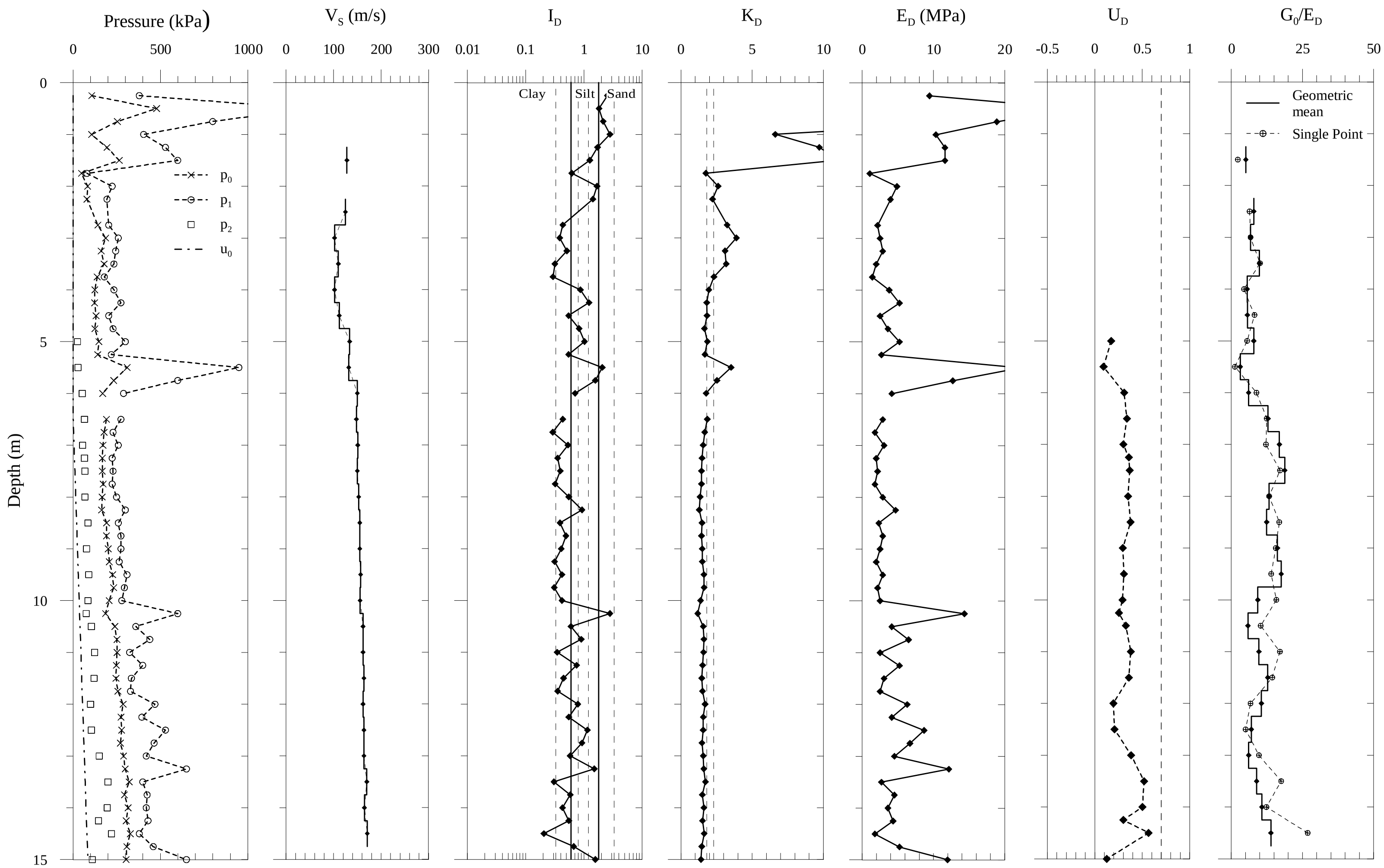

Max. depth: 15.00 m

UBC

Sounding: SDMT-07	γ_{av}= 17.80 kN/m^3	W.T.= 1.80 m	Date: 09/05/2007
Location: Colebrook overpass	Max. depth: 15.00 m	Rig: ConeTec 4x4	Crew: ME/IW

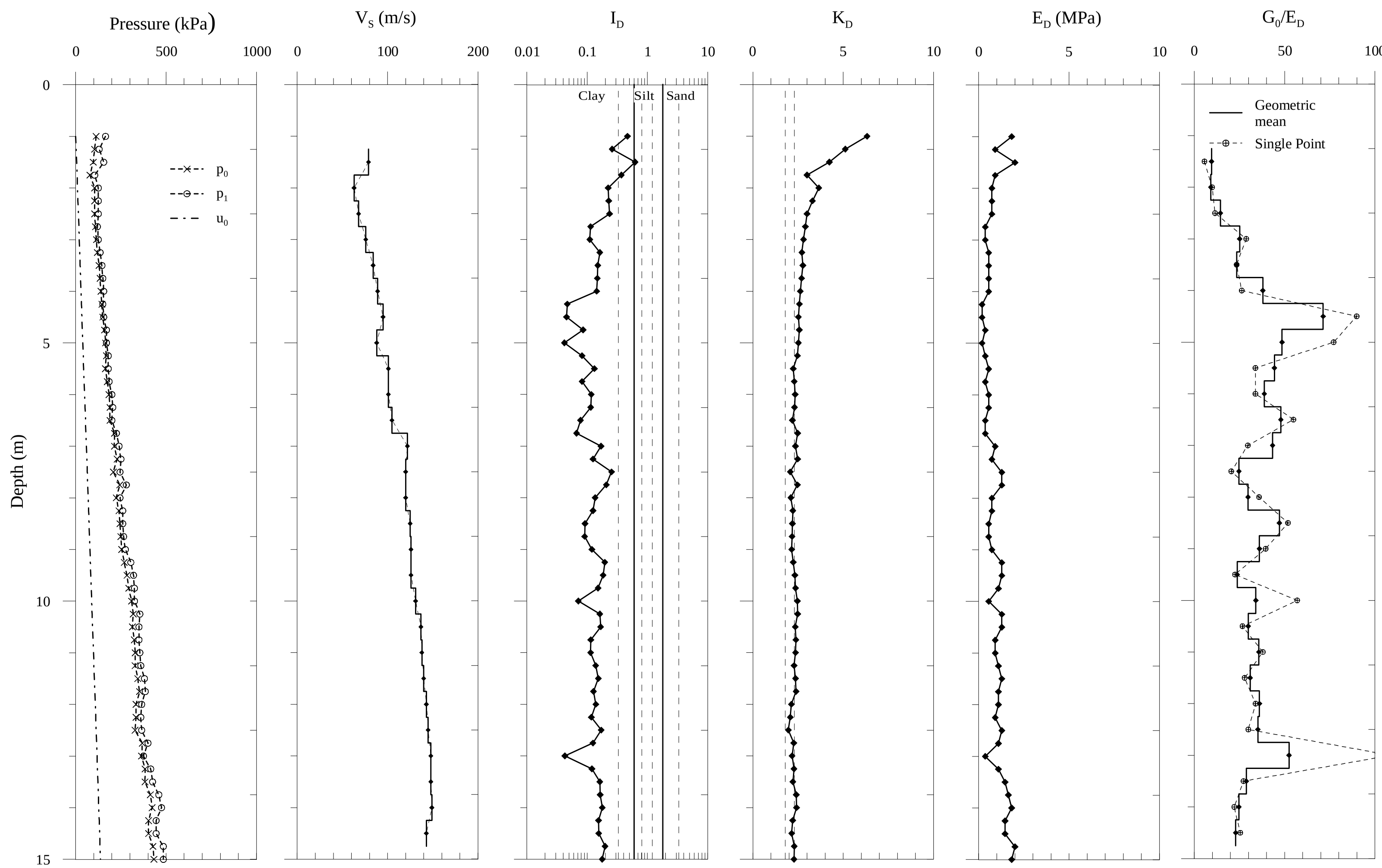

Max. depth: 15.00 m

UBC

Sounding: SDMT-08 | γ_{av}= 17.80 kN/m^3 | W.T.= 1.80 m | Date: 09/05/2008

Location: Colebrook overpass | Max. depth: 11.25 m | Rig: ConeTec M5 | Crew: IRC/JP

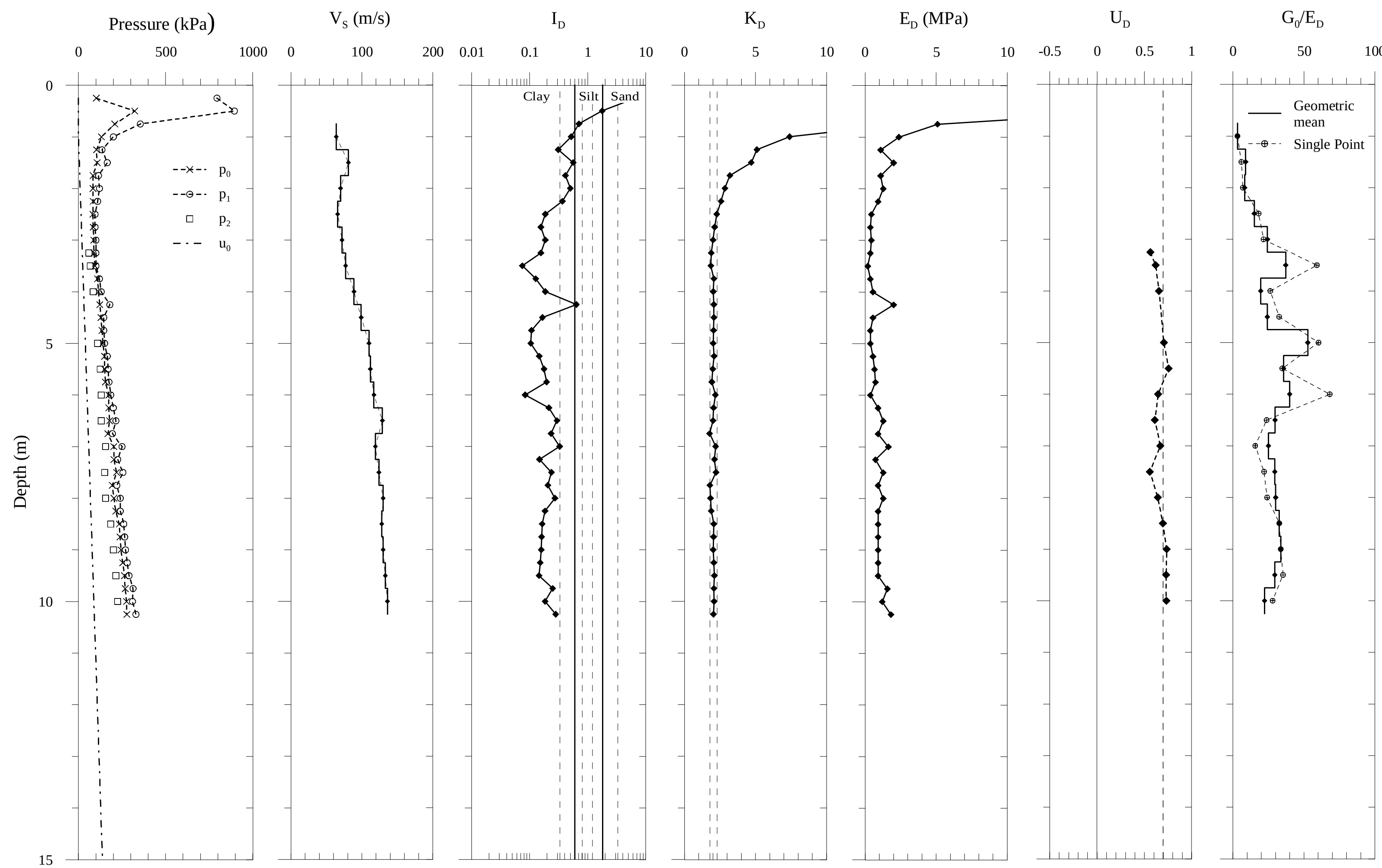

Max. depth: 10.25 m

UBC

Sounding: SDMT-09 | γ_{av} = 18.50 kN/m^3 | W.T.= 0.40 m | Date: 20/06/2008

Location: Patterson Park | Max. depth: 20.00 m | Rig: UBC-CPT truck | Crew: IRC/MAS

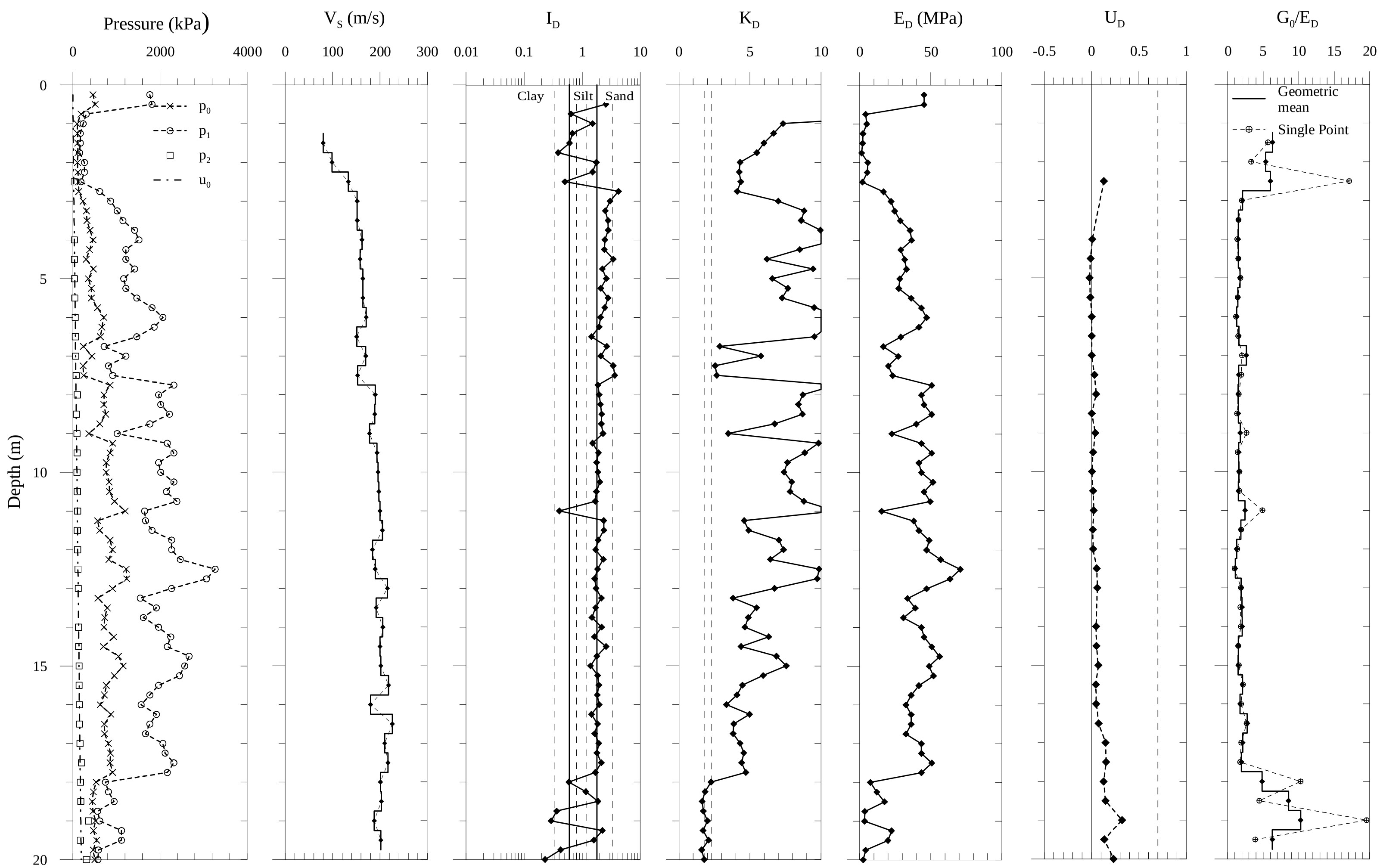

Max. depth: 20.00 m

APPENDIX B Lateral stress seismic piezocone (LSSCPTU) profiles

UBC

Sounding: LSC-01 | γ_{av} = 18.50 kN/m^3 | W.T.= 1.80 m | Date: 13/06/2008

Location: Kidd 2 Substation | Max. depth: 30.00 m | Rig: UBC-CPT truck | Crew: IRC/MAS/BL

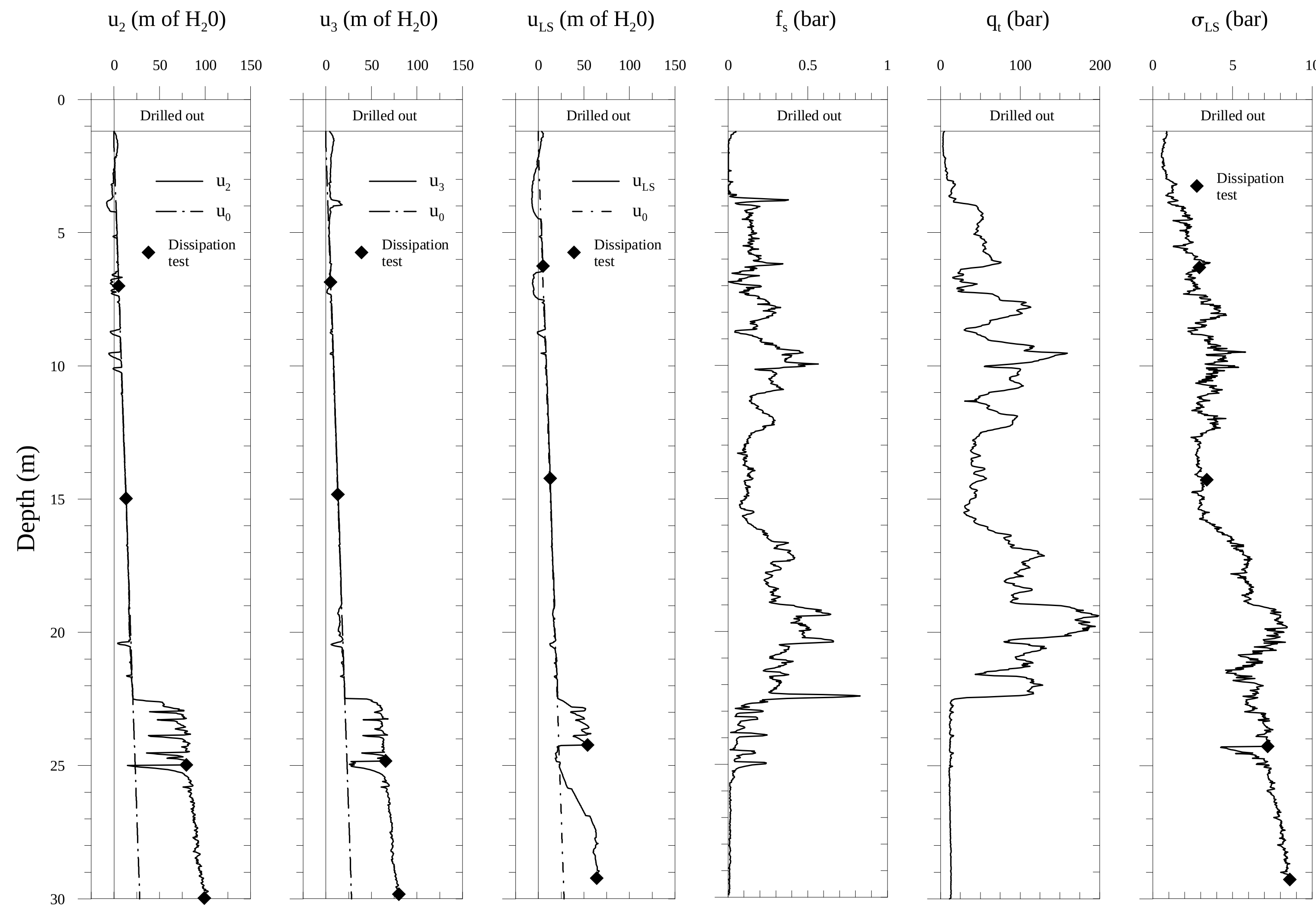

UBC

Sounding: LSC-01	γ_{av}= 18.50 kN/m^3	W.T.= 1.80 m	Date: 13/06/2008
Location: Kidd 2 Substation	Max. depth: 30.00 m	Rig: UBC-CPT truck	Crew: IRC/MAS/BL

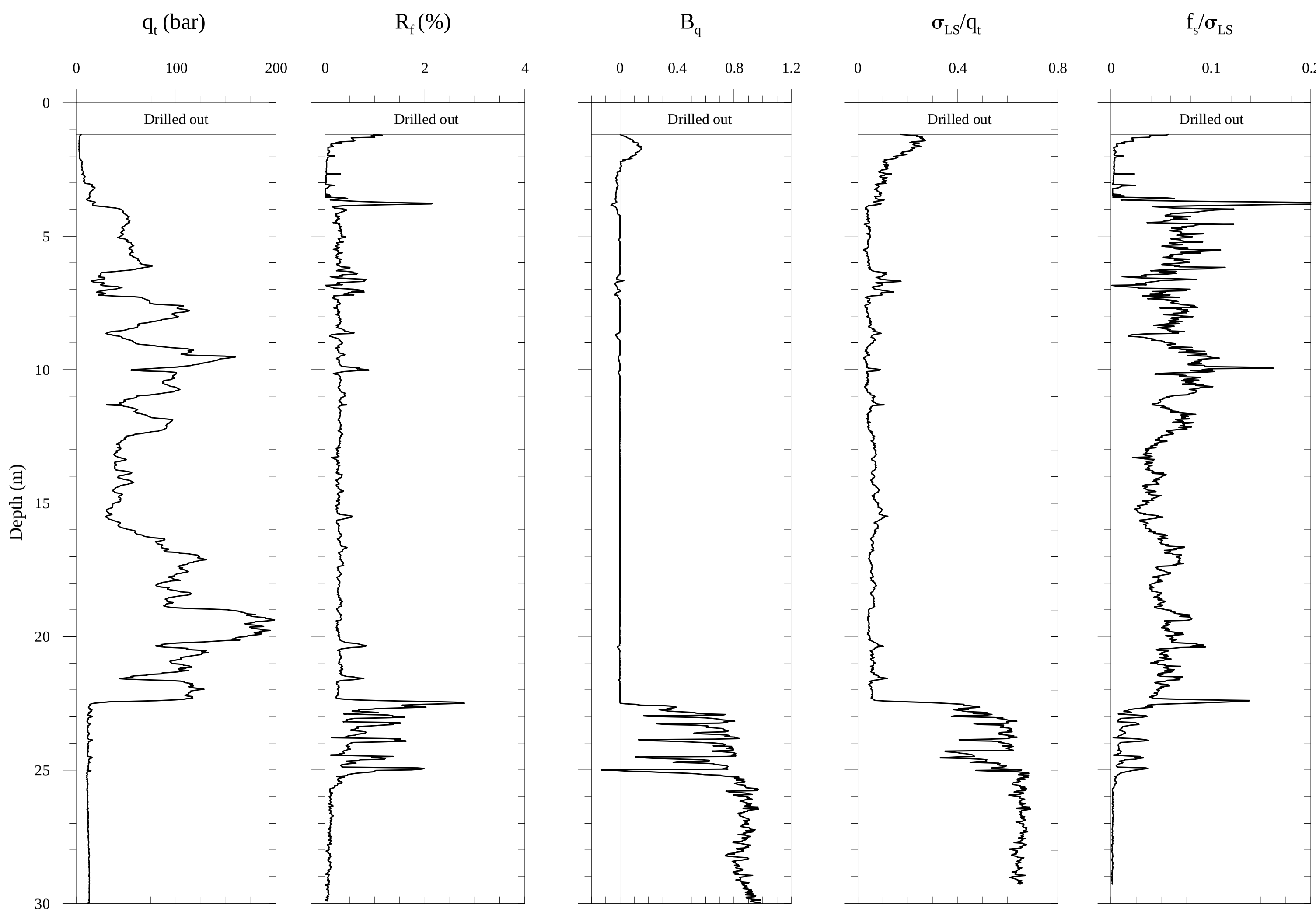

UBC

Sounding: LSC-02	γ_{av}= 18.50 kN/m^3	W.T.= 1.80 m	Date: 13/06/2008
Location: Kidd 2 Substation	Max. depth: 30.00 m	Rig: UBC-CPT truck	Crew: IRC/MAS/BL

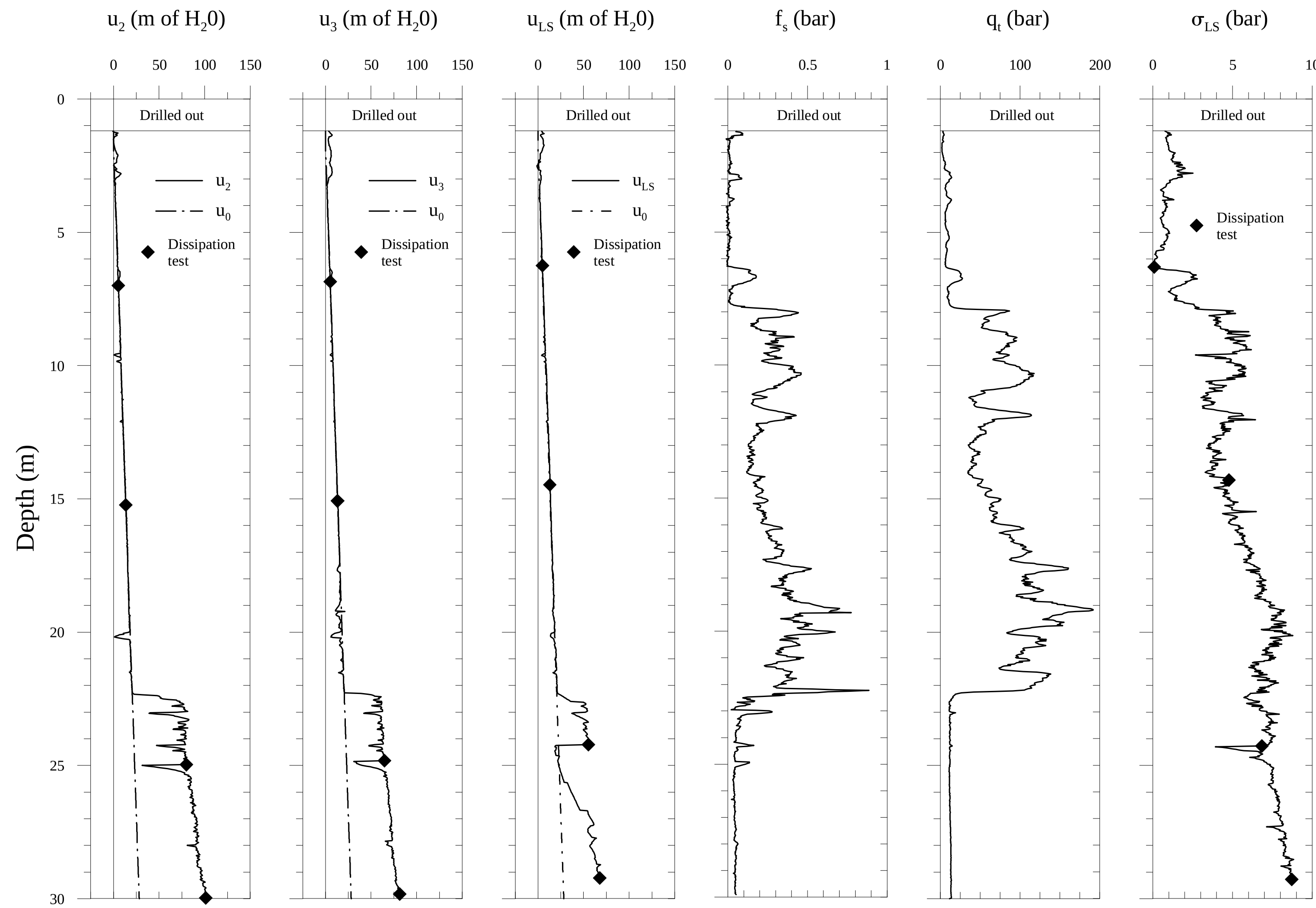

UBC

Sounding: LSC-02	γ_{av}= 18.50 kN/m^3	W.T.= 1.80 m	Date: 13/06/2008
Location: Kidd 2 Substation	Max. depth: 30.00 m	Rig: UBC-CPT truck	Crew: IRC/MAS/BL

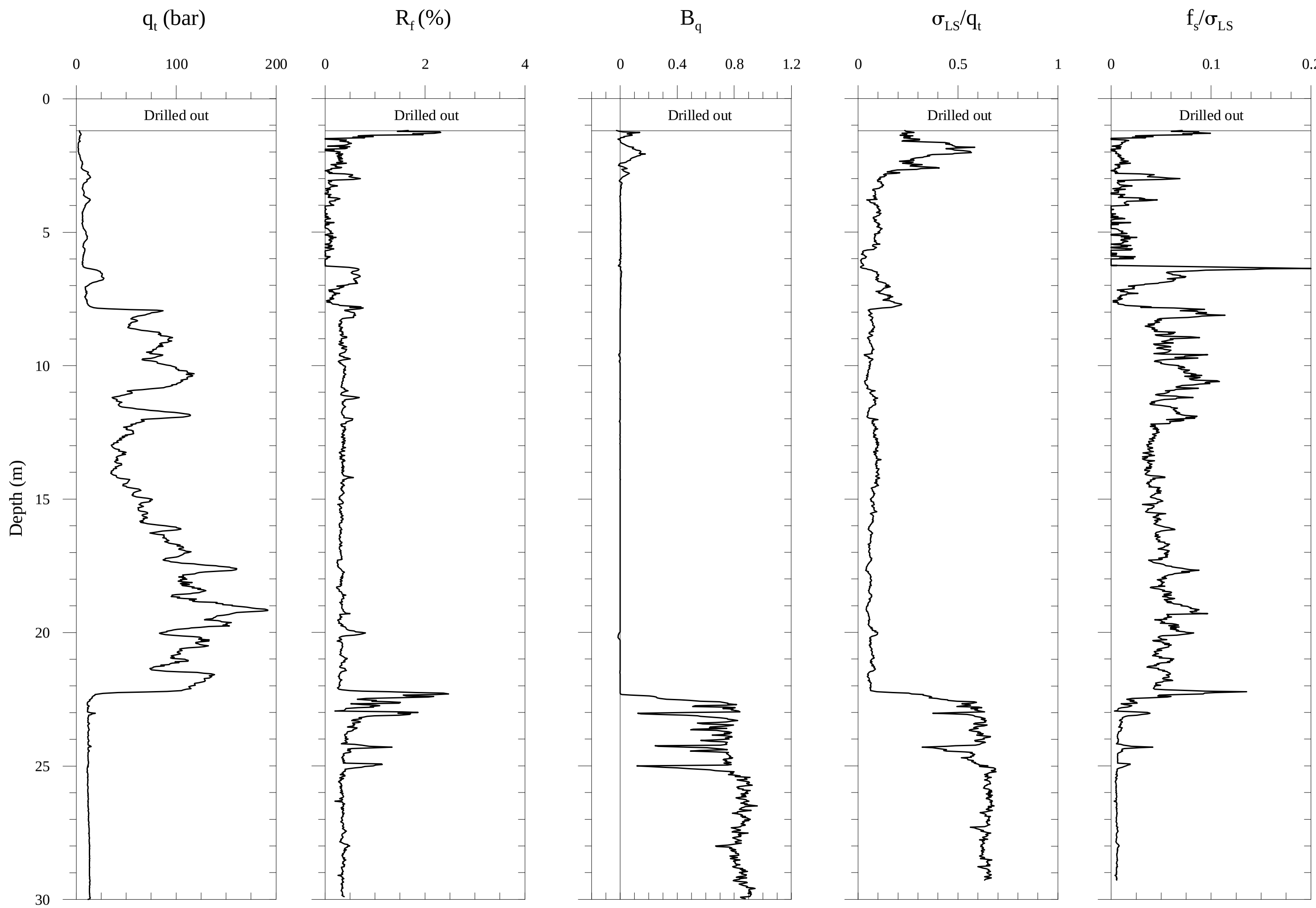

UBC

Sounding: LSC-03 | γ_{av}= 18.50 kN/m^3 | W.T.= 3.20 m | Date: 18/06/2008

Location: Massey Tunnel | Max. depth: 20.00 m | Rig: UBC-CPT truck | Crew: IRC/MAS

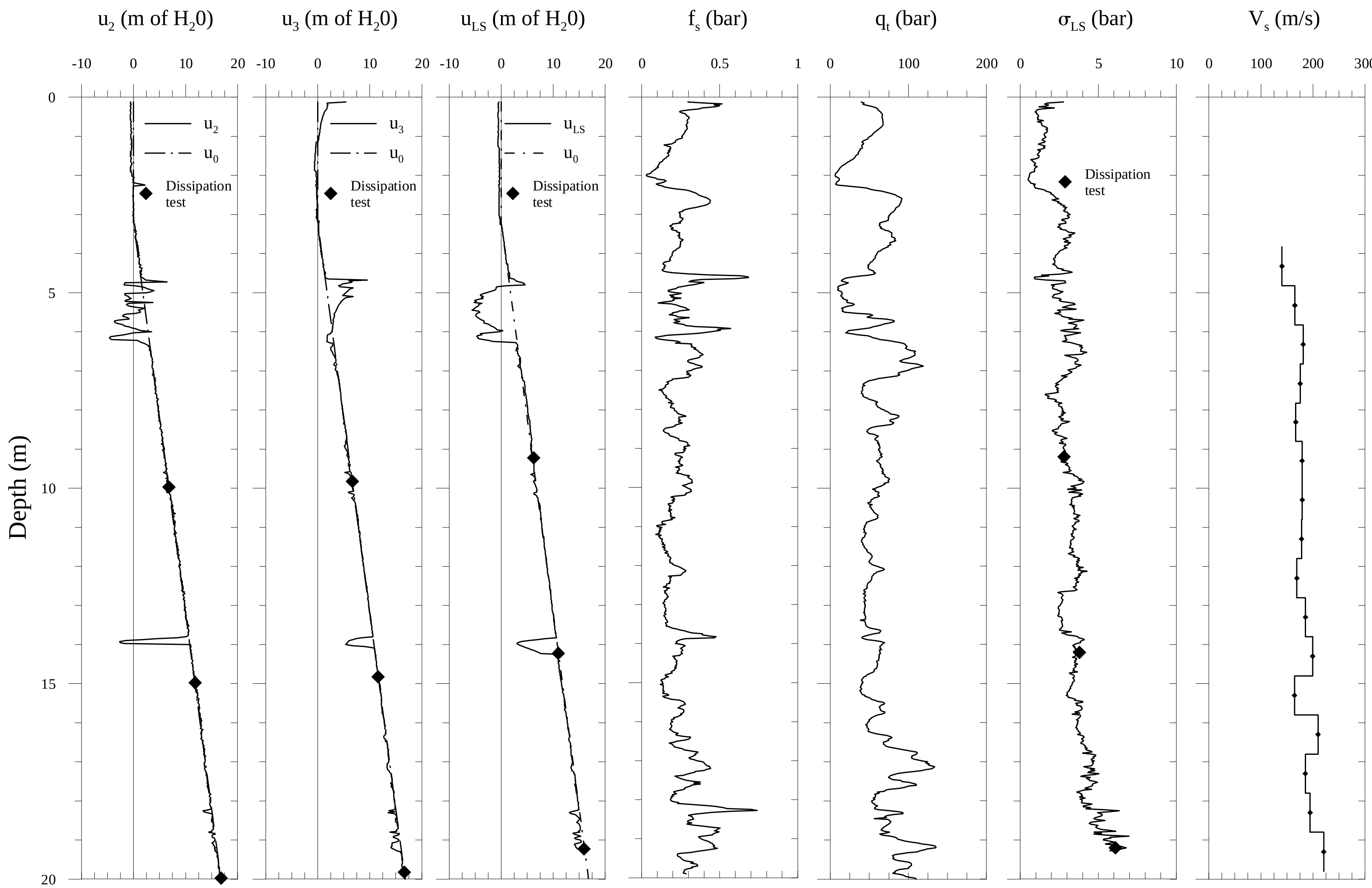

UBC

Sounding: LSC-03 | γ_{av} = 18.50 kN/m^3 | W.T.= 3.20 m | Date: 18/06/2008

Location: Massey Tunnel | Max. depth: 20.00 m | Rig: UBC-CPT truck | Crew: IRC/MAS

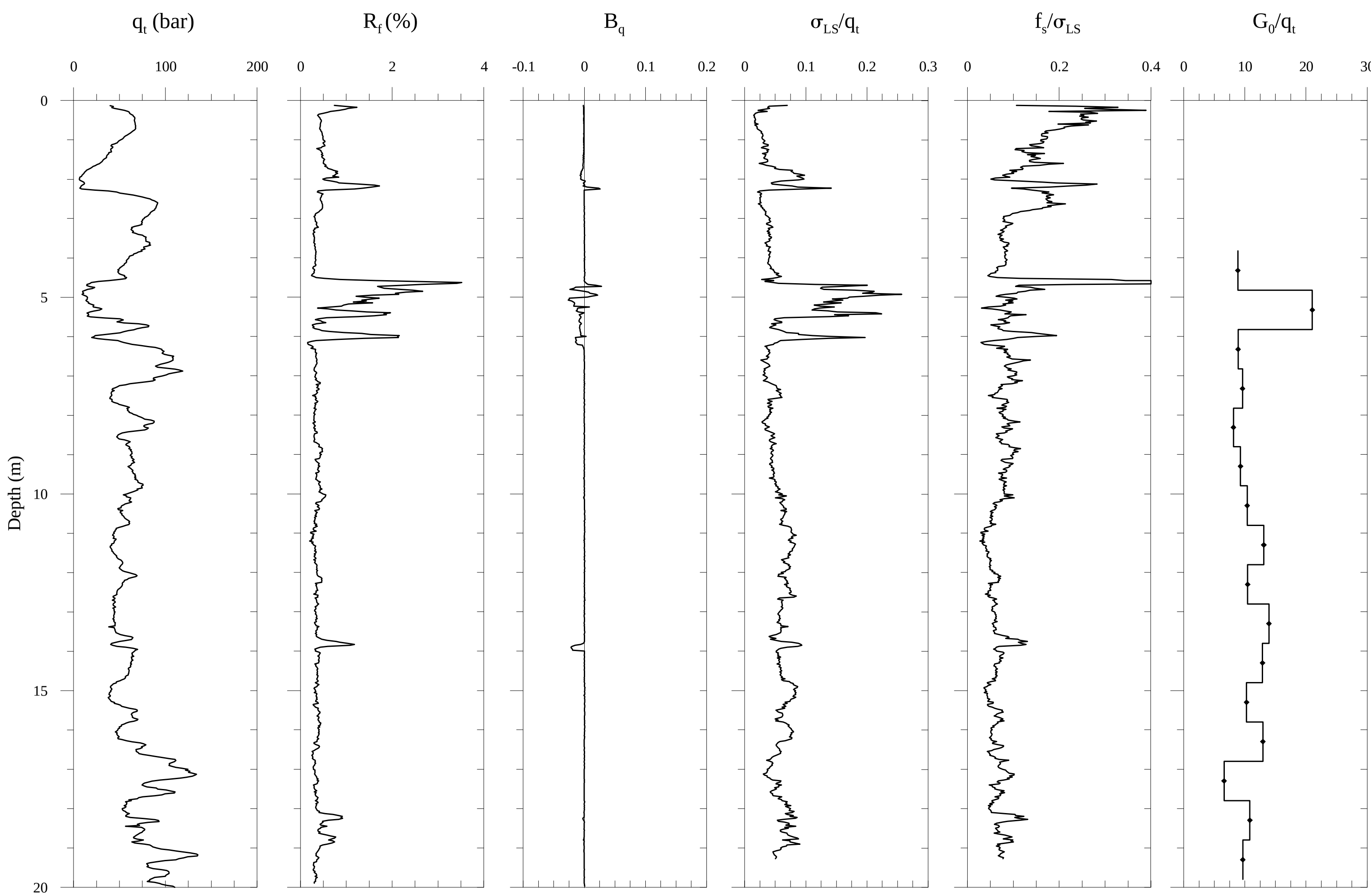

UBC

Sounding: LSC-04 | γ_{av}= 18.50 kN/m^3 | W.T.= 3.20 m | Date: 18/06/2008

Location: Massey Tunnel | Max. depth: 20.00 m | Rig: UBC-CPT truck | Crew: IRC/MAS

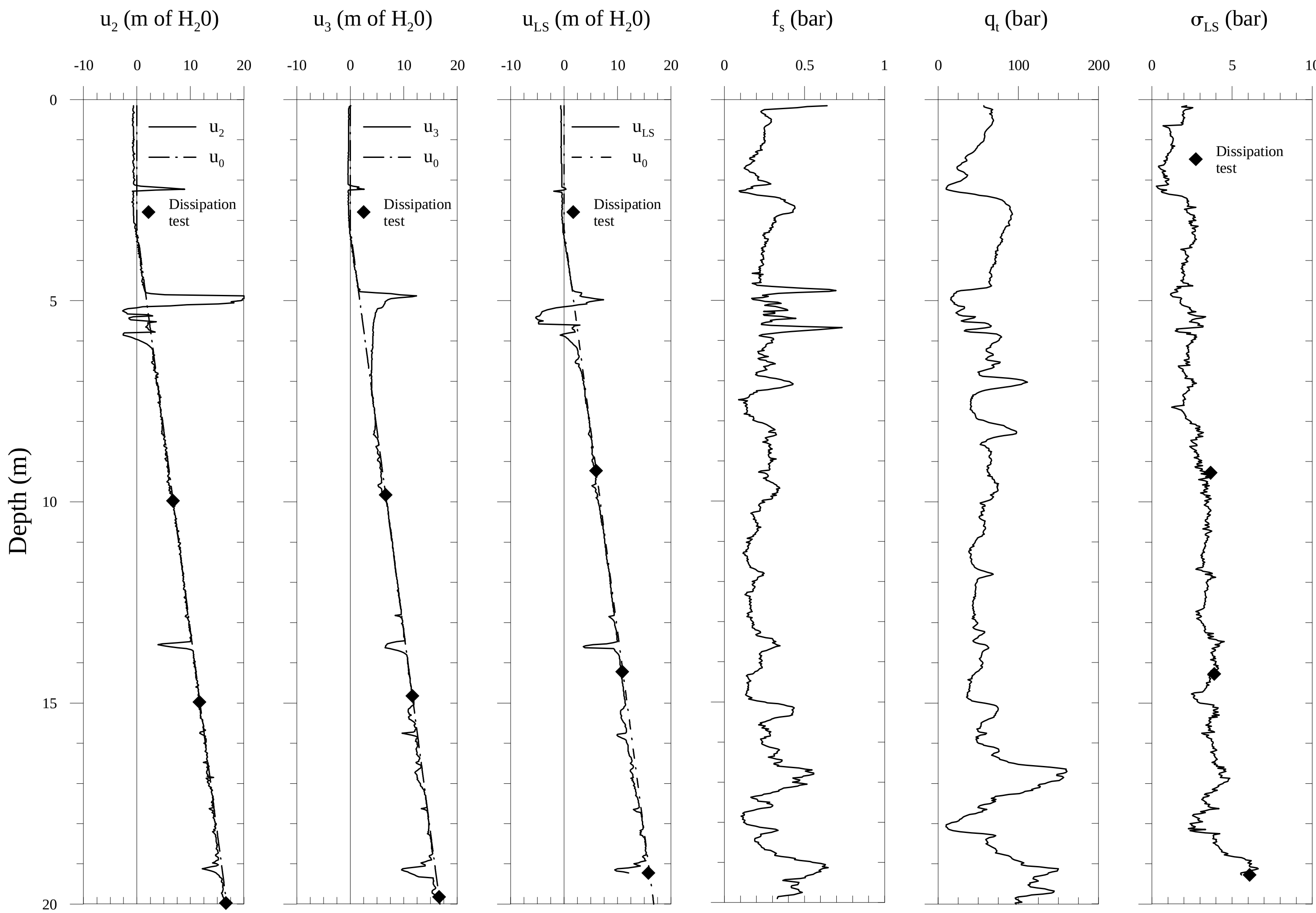

UBC

Sounding: LSC-04	γ_{av}= 18.50 kN/m³	W.T.= 3.20 m	Date: 18/06/2008
Location: Massey Tunnel	Max. depth: 20.00 m	Rig: UBC-CPT truck	Crew: IRC/MAS

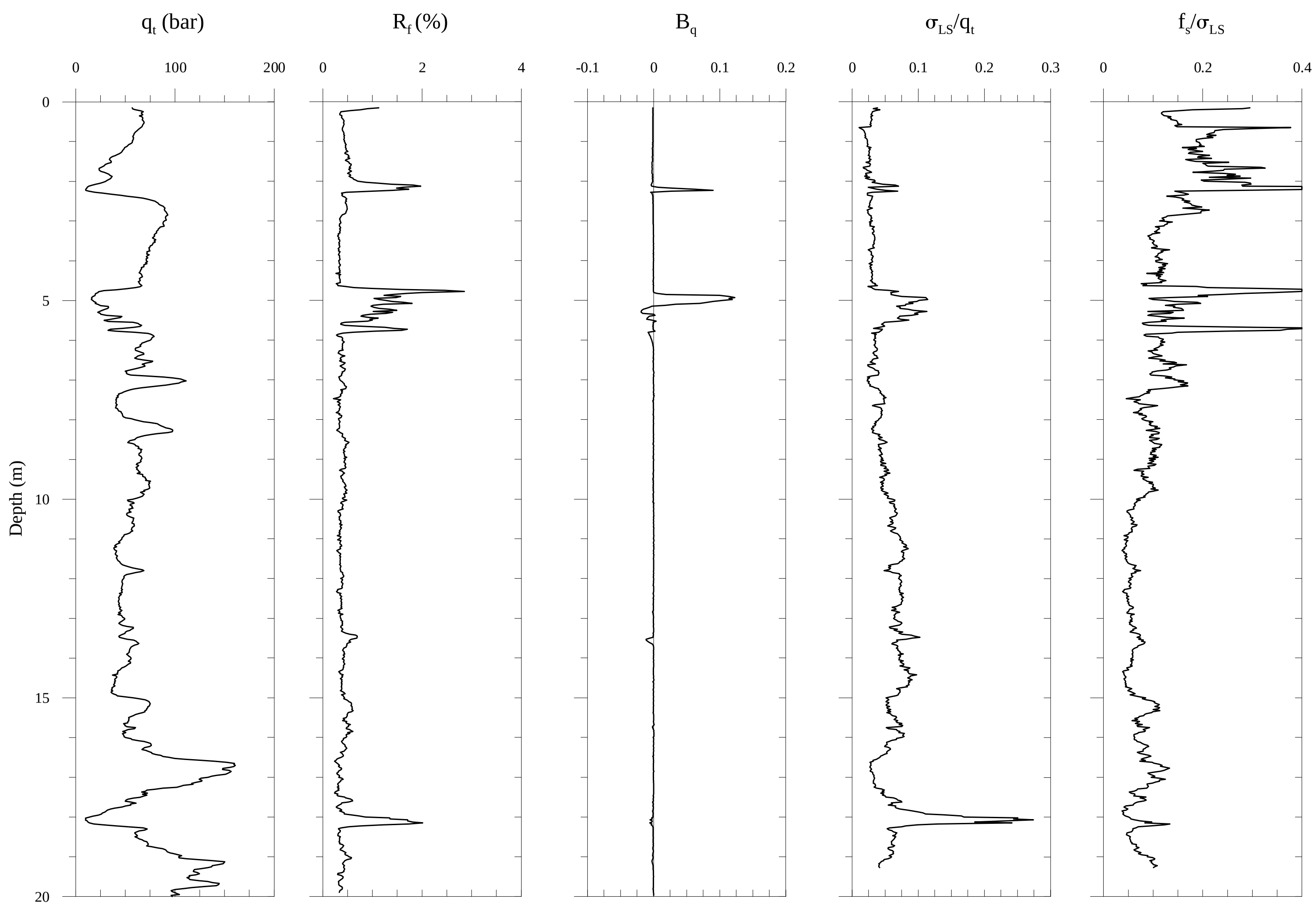

UBC

Sounding: LSC-05 | γ_{av} = 18.50 kN/m^3 | W.T.= 0.40 m | Date: 20/06/2008

Location: Patterson Park | Max. depth: 20.00 m | Rig: UBC-CPT truck | Crew: IRC/MAS

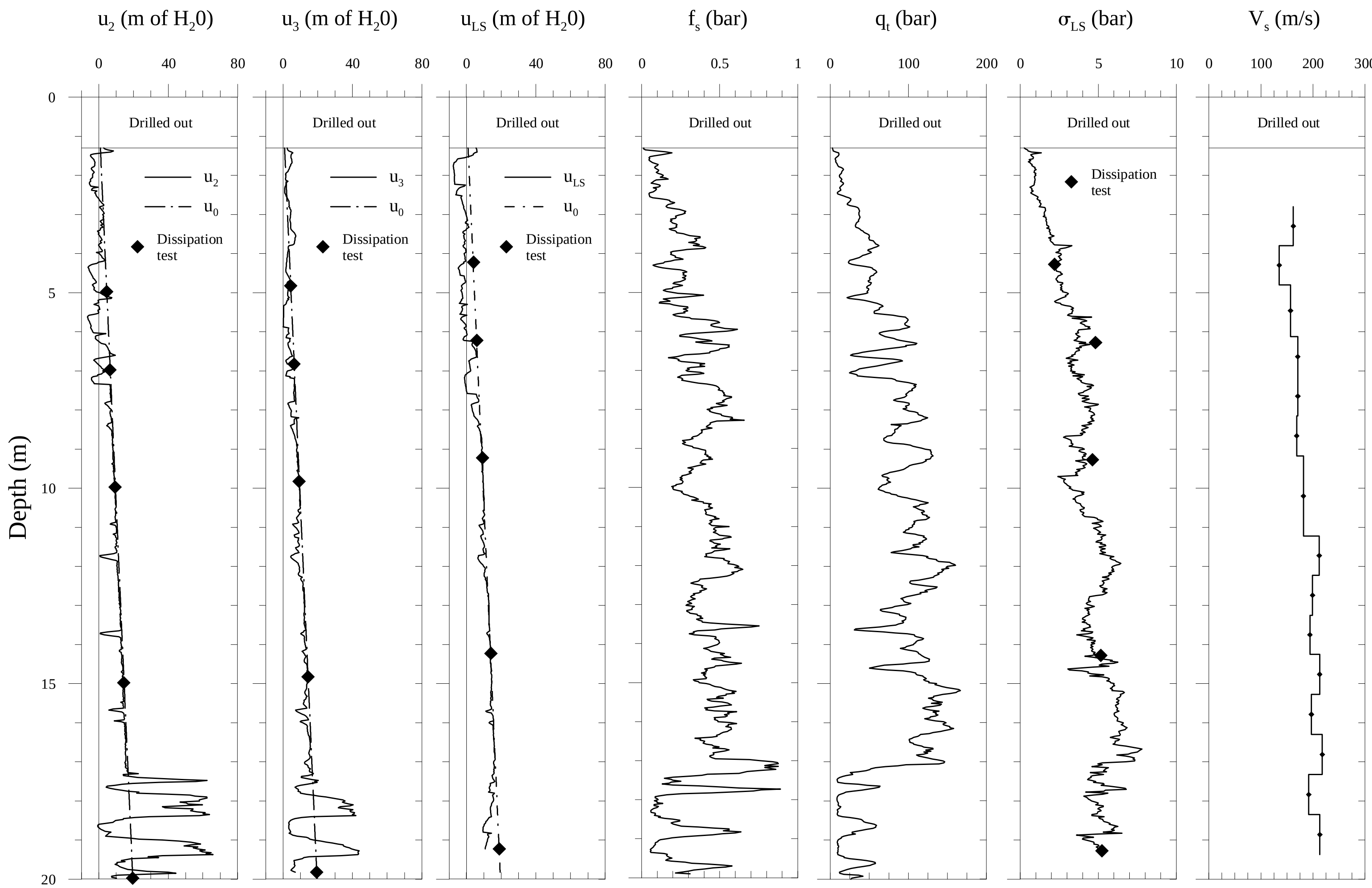

UBC

Sounding: LSC-05 | γ_{av} = 18.50 kN/m^3 | W.T.= 0.40 m | Date: 20/06/2008

Location: Patterson Park | Max. depth: 20.00 m | Rig: UBC-CPT truck | Crew: IRC/MAS

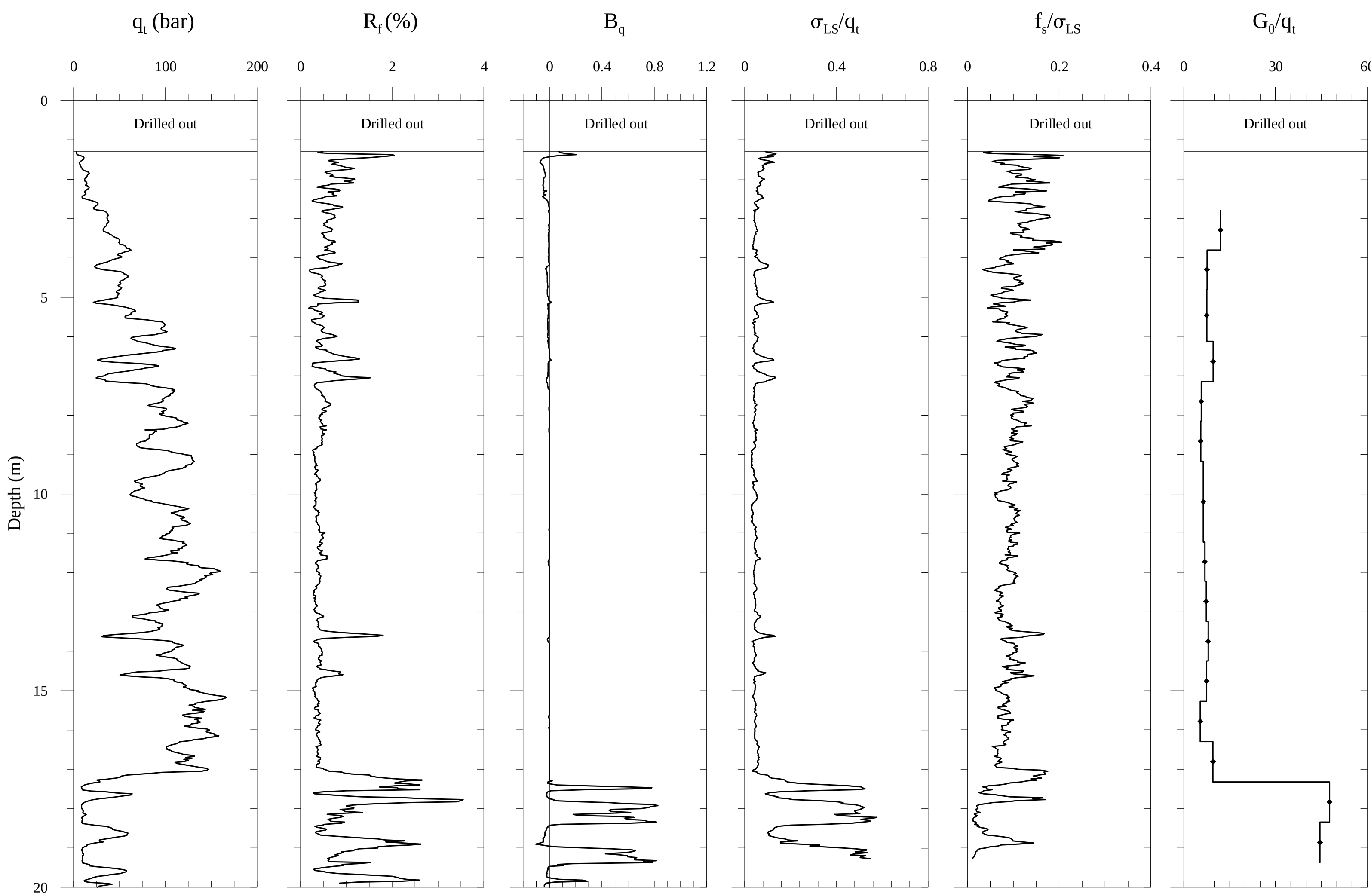

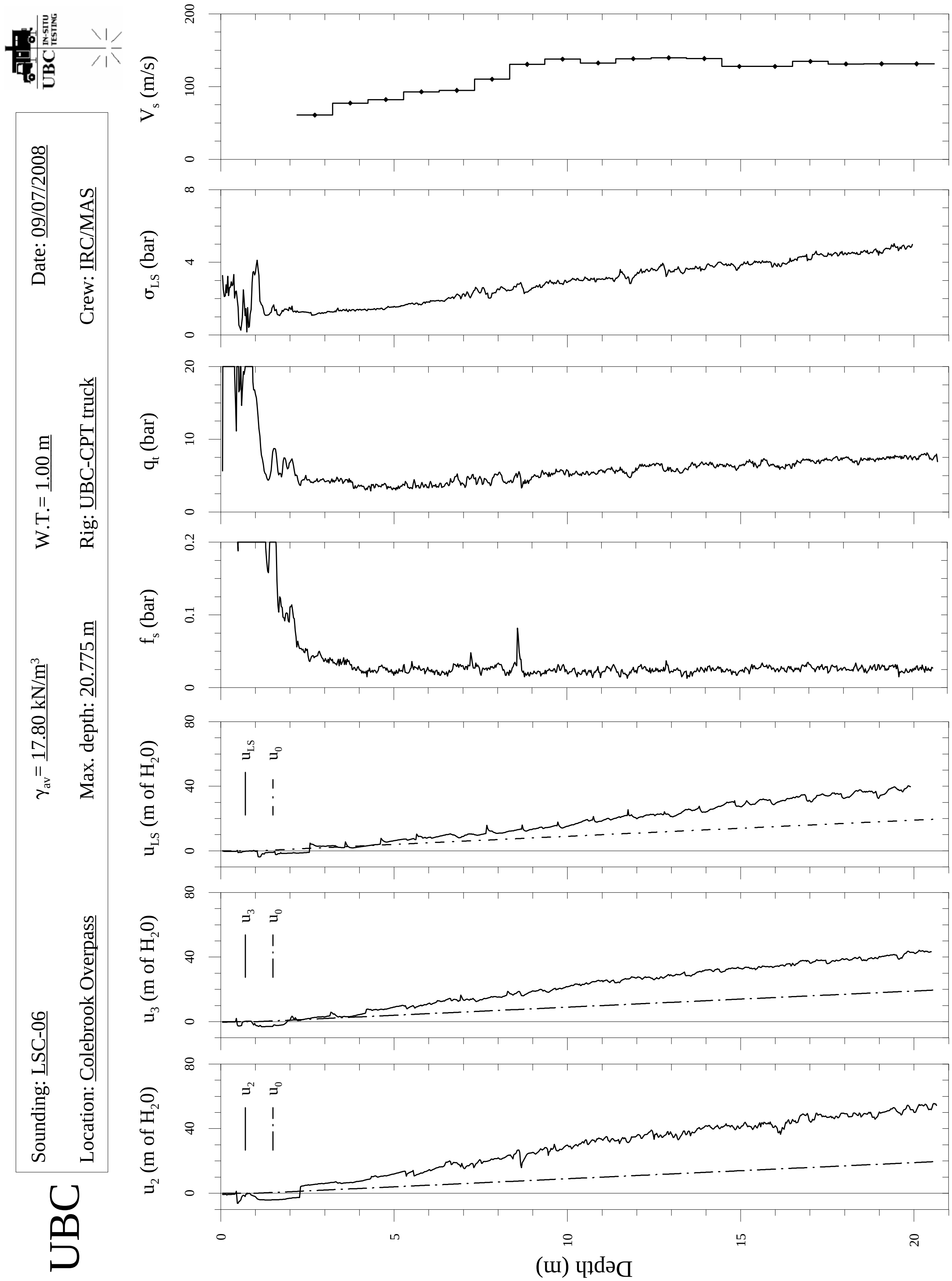
UBC
UBC IN-SITU TESTING
Sounding: LSC-06
Location: Colebrook Overpass
γ_{av} = 17.80 kN/m^3
Max. depth: 20.775 m
W.T.= 1.00 m
Rig: UBC-CPT truck
Date: 09/07/2008
Crew: IRC/MAS
u_2 (m of H_20)
u_3 (m of H_20)
u_{LS} (m of H_20)
f_s (bar)
q_t (bar)
σ_{LS} (bar)
V_s (m/s)
u_2
u_3
u_{LS}
u_0
Depth (m)
0
5
10
15
20
40
80
0.1
0.2
8
100
200

UBC

Sounding: LSC-06 | γ_{av}= 17.80 kN/m^3 | W.T.= 1.00 m | Date: 09/07/2008

Location: Colebrook Overpass | Max. depth: 20.775 m | Rig: UBC-CPT truck | Crew: IRC/MAS

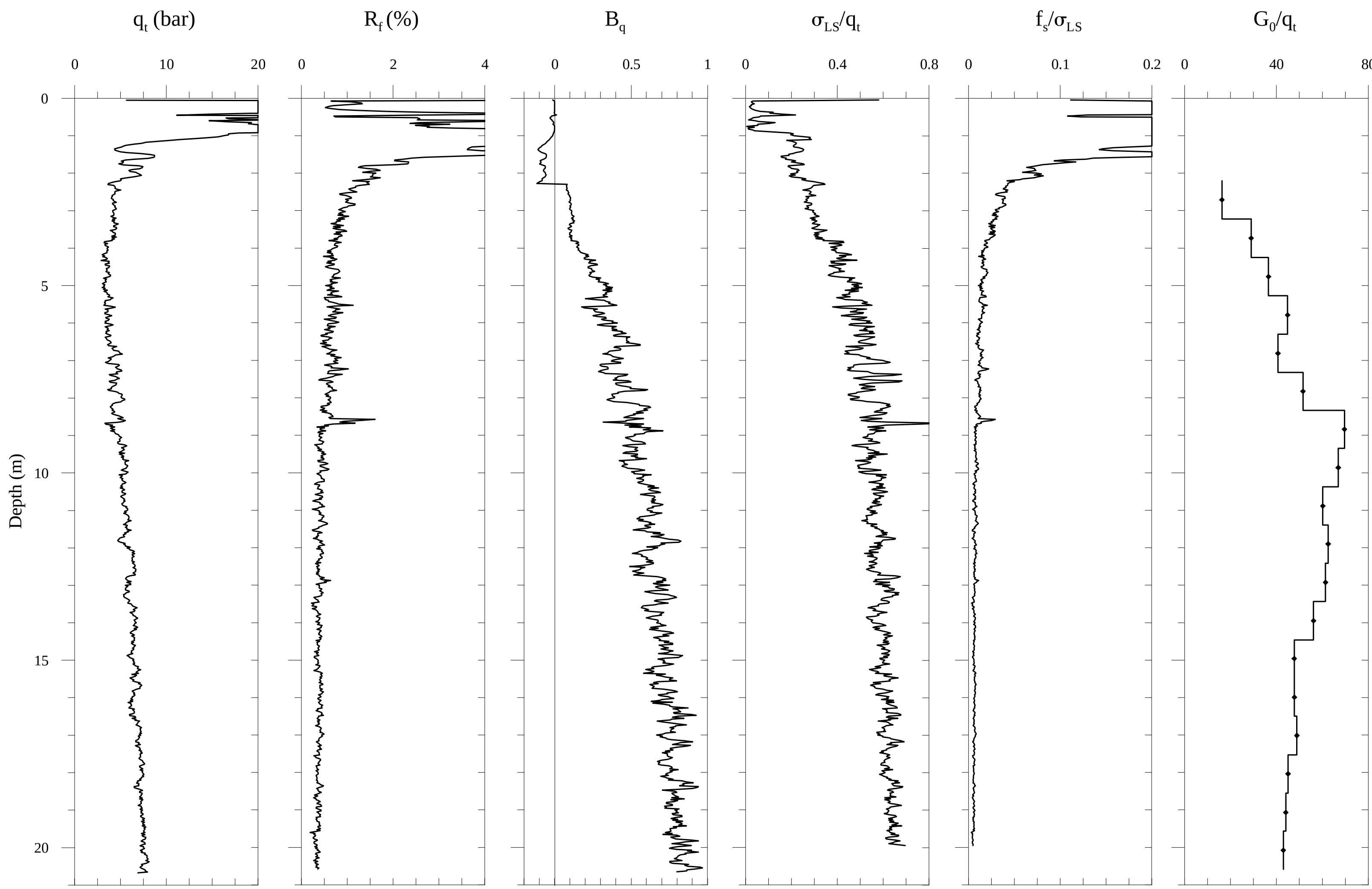

UBC

Sounding: LSC-07 | γ_{av}= 17.80 kN/m^3 | W.T.= 1.00 m | Date: 09/07/2008

Location: Colebrook Overpass | Max. depth: 20.775 m | Rig: UBC-CPT truck | Crew: IRC/MAS

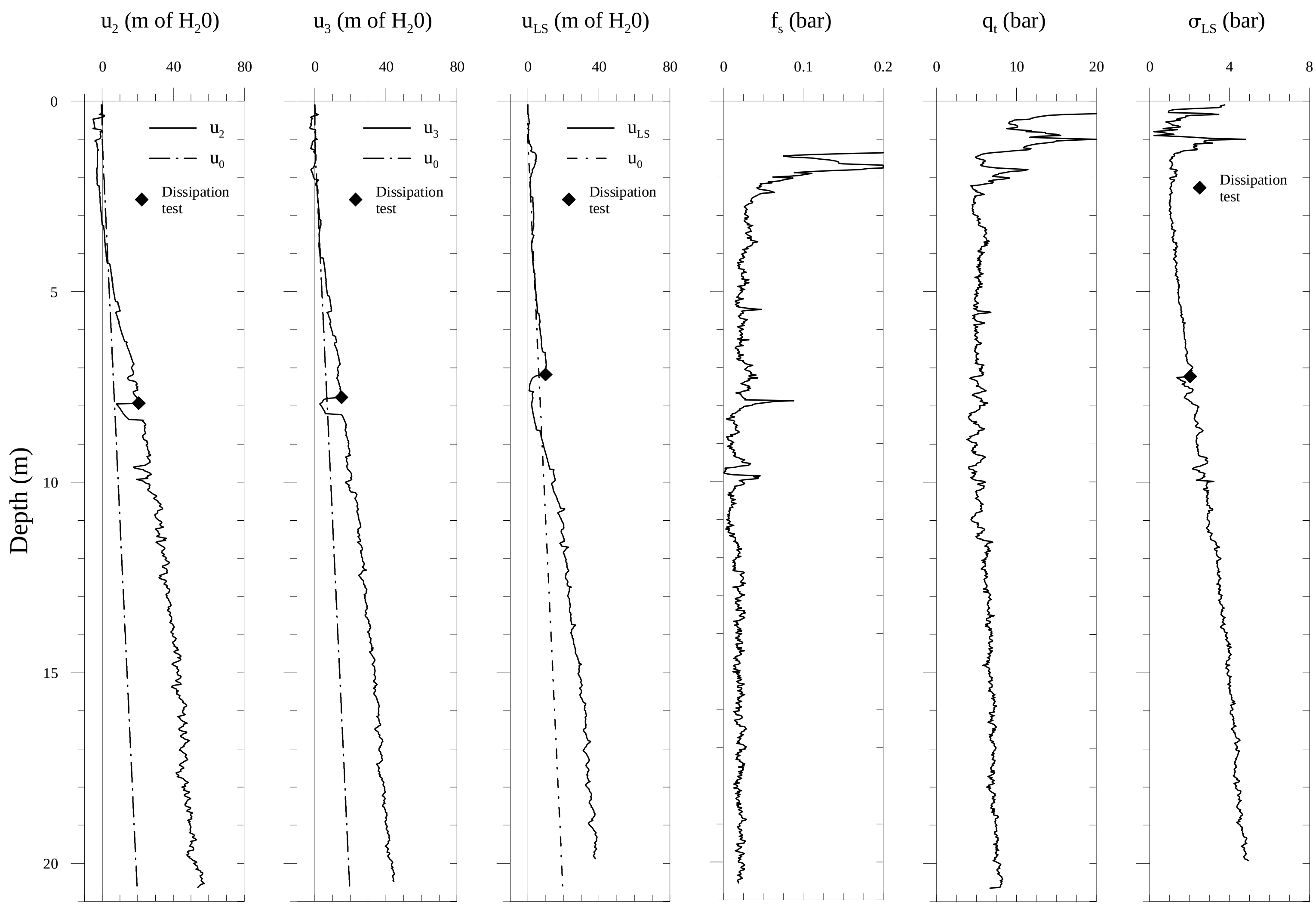

UBC

Sounding: LSC-07 | γ_{av}= 17.80 kN/m^3 | W.T.= 1.00 m | Date: 09/07/2008

Location: Colebrook Overpass | Max. depth: 20.775 m | Rig: UBC-CPT truck | Crew: IRC/MAS